SMART VIBRATION CONTROL OF FLUID STORAGE TANKS VIA MAGNETORHEOLOGICAL DAMPERS

By

Seyed Ehsan Aghakouchaki Hosseini

A thesis submitted to Auckland University of Technology
in partial fulfilment of the requirements for the degree of
Doctor of Philosophy

Supervised by
Associate Professor Sherif Beskhyroun

Department of Built Environment Engineering
School of Future Environments
Auckland University of Technology
New Zealand

April 2025

Abstract

Fluid storage tanks play a pivotal role in strategic industries, and hence their dynamic behaviour and damage possibilities have been the focus of attention of research communities for decades. Water supply and storage systems, wineries and dairy products industries, refineries, hospitals, and petrochemical industries are among the most important industries in which these structures are employed. The dynamic behaviour of these structures is very complicated in that it is involved with the fluid-structure interaction phenomenon. The simplified mechanical model is the most used technique for defining this complicated behaviour that has widely been utilised in the seismic design codes of many countries for the analysis and design of these tanks. This method provides the lowest computational cost at the expense of inflicting some inaccuracies on the structural response estimation of the fluid tank. Many different energy-dissipating and seismic protection devices have been investigated in the literature by many researchers for fluid storage tanks. However, the focus of all of these devices has been on the application of passive control devices such as base isolators or baffles, to name but a few. The volume of experimental investigations done in this field is not comparable to the theoretical research work. Also, compared to the amount of theoretical research on passive systems, less has been done on the application of active control systems for these structures. On the other hand, passive and active systems face some drawbacks in terms of adaptability,

robustness, and reliability in the event of power failure during severe seismic occurrences.

Semi-active control mechanisms combine the advantages of both of these systems and remove their drawbacks. Among different semi-active control systems innovated in the literature, magnetorheological (MR) dampers, due to their special characteristics, have found successful applications in various industries. These dampers require a very low power source ($0 - 3$ *or* $5V$), are fail-safe in that in the absence of a power source they turn into passive control systems and continue dissipating the external energy, having a wide operational temperature make them suitable for both internal and external applications. Applications of these dampers include civil structures and infrastructures, the automotive industry, prosthetic applications, and robotics, among others. Nonetheless, for the nonlinear hysteretic nature of these dampers, analysing their dynamics is more complicated than other control mechanisms.

In this research, first, a series of experimental investigations were conducted on a highly flexible full-scale flat-based stainless steel fluid tank to understand the dynamic behaviour of these structures. Then, a series of numerical investigations were applied to a legged flexible cylindrical stainless steel fluid tank equipped with an MR damper using different semi-active control designs. Finally, a series of numerical and comprehensive experimental tests were conducted over a rigid legged cylindrical stainless steel fluid tank with and without the application of MR dampers. Numerical and experimental tests were applied using seismic records of real ground motions that occurred in the past in different countries with different frequency contents. In the case of the rigid legged cylindrical tank, a new set of equations representing the dynamics of the rocking tank was developed to analyse its dynamic behaviour and control the fluid-tank system. Two software platforms were developed based on MATLAB and SIMULINK. The first software can be used for signal processing of the experimental results using the sensory

system and extracting the natural frequencies of the system. The second software can perform data acquisition and control system design over the system using the sensory system. To control the fluid-tank-MR system, different model-based designs optimised with Hunger Game Search as a new metaheuristic search tool were employed. However, real-world phenomena can hardly be put into precise closed-form formulae. Moreover, the complex behaviour of the dynamical system, time-varying characteristics and degradation of the system over time, and stochastic nature of the external excitations diminish the application of model-based control system designs. Here is when the data-driven control systems come into play. Online real-time semi-active data-driven adaptive control techniques have been developed and applied to these systems to make the application of MR dampers for making seismic-resilient fluid tanks as optimal as possible. Results of numerical and experimental investigations of equipping the fluid tank with MR dampers demonstrate the promising potential of these dampers over other systems for seismic response mitigation, retrofitting, and enhancing the structural responses of fluid tanks under the base excitations. Developed methods and techniques in this research have a low computational cost, reasonable accuracy, and proper performance, which makes them suitable for deployment on micro-controllers for making autonomous control devices to be applied to practical applications.

Keywords: Fluid storage tanks, Seismic-resilient structures, Smart vibration control, Magnetorheological dampers, Data-driven control

Contents

List of Tables

List of Figures

Attestation of Authorship

I hereby declare that this submission is my own work and that, to the best of my knowledge and belief, it contains no material previously published or written by another person nor material which to a substantial extent has been accepted for the qualification of any other degree or diploma of a university or other institution of higher learning.

Signature of candidate

Publications

Hosseini, S. E. A., Beskhyroun, S. (2023, March). Fluid storage tanks: A review on dynamic behaviour modelling, seismic energy-dissipating devices, structural control, and structural health monitoring techniques. In *Structures* (Vol. 49, pp. 537-556). Elsevier.

Hosseini, S. E. A., Beskhyroun, S. (2023, December). Seismic vibration control of fluid storage tanks using magnetorheological dampers. In Australasian Conference on the Mechanics of Structures and Materials (pp. 445-455). Singapore: Springer Nature Singapore.

Hosseini, S. E. A., Beskhyroun, S. (2024, October). Numerical investigations of seismic-resilient techniques for legged fluid storage tanks utilising magnetorheological dampers. In *Structures* (Vol. 68, p. 107090). Elsevier.

Hosseini, S. E. A., Beskhyroun, S. (2024, December). Dynamic performance investigations of a full-scale unanchored thin-walled steel fluid storage tank via shake table tests. In *Structures* (Vol. 70, p. 107548). Elsevier.

Acknowledgements

I want to express my sincere thanks and great gratitude to my dear supervisor, Associate Prof. Dr. Sherif Beskhyroun for his support, advice, encouragement, and guidance.

I deeply appreciate the Earthquake Commission (EQC), Wellington, New Zealand for the financial support to this project. I would also like to express my deep gratitude to all Auckland University of Technology (AUT) mentors, staff, and technicians. My special thanks to the Auckland Unversity of Technology (AUT) and the New Zealand government that offered me the opportunity and support to continue my studies for the fulfillment of the PhD degree. Thank you for your hospitality, kindness, and generosity. Even though I had many difficulties and ironic days, believing in this quote from Nietzsche "What Doesn't Kill You Makes You Stronger", helped me to be braver and gain new experiences in my life.

Chapter 1

Introduction

1.1 Background of the study

Fluid storage tanks are the lifeline to strategic industries. They are employed in many industries including petrochemicals, aerospace, wineries, hospitals, etc. These tanks are found in different geometrical shapes, are made of mainly stainless steel or reinforced concrete, are flat-based or legged, anchored or unanchored, ground-based or elevated. Depending on the material and thickness of the tank body, they could be categorized as rigid or flexible. Rigid and flexible stainless steel cylindrical legged fluid tanks find extensive applications in wineries, hospitals, petrochemicals, etc. Unanchored tanks are freely set on the ground while anchored tanks are fixed to the base commonly using anchor bolts. Under base excitations out of seismic events, large forces are absorbed by the anchor bolts which are subsequently transferred to the body of the tanks. On the other hand, unanchored tanks will face large uplift displacement. In both extreme ends of this spectrum, during past earthquakes in seismic-prone countries including New Zealand among others, different types of damage resulted in fluid tanks including elephant foot

buckling, diamond shape buckling, anchor pull-out, anchor buckling, base plate rupture, and damage to the top part of the tank body due to large sloshing of the liquid. Damages to fluid tanks will result in huge economic losses, failure in the industry itself, may result in fire, and will cause environmental hazards. The dynamic behaviour of these structures is very complicated as it involves fluid dynamics, structural dynamics, and the interaction between these two phenomena. Researchers have been conducting substantial research now for decades to understand the coupled fluid-structure dynamics of tanks under the base excitations and modify and improve the primary equations developed for these structures.

Different types of energy-dissipating devices have been proposed to protect fluid storage tanks seismically. Almost all of these devices have a passive mechanism, meaning that they are devices that cannot be adapted to the changes in future excitations, considering the fact that earthquakes have a stochastic and unpredictable nature. Base isolators and baffles are two of the most common devices in this category. A series of active control devices have been investigated for fluid tanks. These devices can adapt themselves to external excitation and can largely mitigate the vibrations of the structural system. However, they require considerable external power sources and their reliability and robustness are often matters of concern that could render the system out of the loop. Active baffles and piezoelectric patches could be named as instances of these mechanisms. Semi-active mechanisms are a combination of passive and active systems combining their advantages and removing the drawbacks of each. Intrinsically they are passive systems. Including some parts in these devices make them adaptive devices that resemble the behaviour of active systems. However, their main difference with active systems is that there would be no hydraulic jacks or similar devices in these systems to exert external forces on the equipped system. Thus, they do not require any substantial

external power source. Reliability and robustness are not any concerns for these systems either as they are fail-safe devices that could easily be transformed into passive devices and continue dissipating the external energy applied to the structure. Literature indeed lacks comprehensive theoretical or experimental investigations on the application of semi-active control mechanisms for seismic response reduction of fluid storage tanks. Variable dampers for making smart base isolation and magnetorheological (MR) dampers are examples of such mechanisms.

Control theory and its applications in different fields are interesting areas of science and engineering with a variety of applications in many industries. Control system designs could be divided into model-based and data-driven systems in a broader view. Model-based control laws are developed based on a mathematical representation of the dynamical system. These algorithms and control methods include some parameters to be designed. Optimisation techniques usually based on soft computing and metaheuristic approaches in the form of Artificial Intelligence (AI) tools are applied in abundance to optimally design the parameters of the controllers. Both the mathematical model of the mechanical system and control parameters are challenges on the way of model-based control designs. In that, there are many cases that there could not be expressed a closed-form mathematical model for the system to be controlled or the mathematical model could not fully represent a physical system in the real world and there are always inaccuracies. Moreover, the control system and the mechanical system to be controlled both have characteristics that will change and degrade over time. Thus, it could happen that a control system that is efficient now, may not be in the future. Data-driven control systems that rely on the data received from the sensory system expressing the behaviour of the system at the moment can efficiently tackle these problems and bottlenecks on the way model-based controls.

1.2 Research motivation

Based on the facts expressed above, it was motivated in this research to first understand the behaviour of fluid tanks under the base excitations. Then, considering the available energy-dissipating devices proposed in the literature and applied in practice for seismic protection of fluid tanks, and the potential of semi-active systems for improving the means towards achieving this aim, the application of MR dampers as smart devices was considered.

1.3 Aim and objective

The main aim of this thesis is to:

- To study the past and existing methods for dynamic behaviour modelling of fluid storage tanks, causes of their failure under earthquakes, and energy-dissipating devices for their seismic protection, and to prepare an actual state-of-the-art review.
- Investigating the dynamic performance of unanchored flexible flat-based stainless steel cylindrical fluid tanks under base excitations.
- Developing the dynamic representation of legged flexible cylindrical fluid tanks equipped with MR dampers as smart semi-active devices for their seismic response mitigation and conducting numerical investigations in this regard.
- Developing a set of equations that could represent the dynamic behaviour of rocking legged rigid cylindrical fluid tanks under base excitations.
- Numerical and experimental investigations of the rocking legged rigid cylindrical

fluid tanks equipped with MR dampers for seismic response attenuation and making seismic-resilient tanks.

- Developing three software platforms based on MATLAB and SIMULINK. The first one can be used for post-processing and data analysis of measured signals from different types of sensors in both time and frequency domains using advanced signal processing tools. The second could be used for data acquisition in real-time using the sensory system, over any type of structural system, visualization, and output saving the measurement data in real-time. The third one can be applied for simultaneous data acquisition and vibration control of structures using different model-based and data-driven control strategies.

1.4 Scope and delimitation of the study

The scope of this study is as follows:

- Review the available literature on fluid tanks, causes of their failure, and different devices for their seismic protection from past to present.
- Focus on circular cylindrical stainless steel fluid tanks.
- Manifest the dynamic performance of flat-based unanchored flexible cylindrical tanks via shake table tests and identify natural frequencies of such tanks.
- Examining the efficiency of MR dampers in seismic response mitigation of legged flexible cylindrical fluid tanks numerically.
- Developing a new set of equations of rocking legged rigid cylindrical fluid tanks.

- Developing a semi-active data-driven adaptive online control technique for controlling fluid tanks.
- Examining the efficiency of MR dampers in vibration mitigation of rigid legged cylindrical fluid tanks under rocking motions using model-based and data-driven control methods both numerically and experimentally.

1.5 Thesis structure

This thesis is presented in the following chapters:

- **Chapter 1 (Introduction):** The current chapter presents a generalized idea about this research work. It elaborates on the aim and objectives to be achieved in due process.

- **Chapter 2 (Literature Review):** This chapter provides insight into the previous and recent studies and their limitations on dynamic behaviour modelling of fluid tanks, vibration protection against earthquakes, vibration control systems, and structural health monitoring of these structures.

- **Chapter 3 (Research Methodology):** In this chapter the equation of motion of a circular cylindrical flat-based tank is presented. Then the dynamic equation of motion for a legged flexible cylindrical tank equipped with an MR damper is developed. Different control laws are presented along with a recently developed novel metaheuristic optimisation tool for designing parameters of model-based

controllers. A series of equations are developed to express the dynamic behaviour of rocking rigid legged cylindrical fluid tanks. Based on the developed equations, transfer functions are obtained for the vibration control of such tanks. Finally, data-driven control techniques are explained and a semi-active data-driven adaptive online control procedure is developed to control the rocking rigid legged cylindrical fluid tanks equipped with MR dampers.

- **Chapter 4 (Results and Discussion):** The dynamic performance of a full-scale thin-walled flat-based stainless steel cylindrical fluid tank is investigated experimentally using shake table tests. Signal processing analyses are done over the experimental results, natural frequencies are extracted, and comparisons are made with theoretical values. Numerical examinations over a legged flexible cylindrical stainless steel fluid tank equipped with an MR damper are done. The system is examined under the records of six earthquakes with different frequency contents and the efficiency of the damper in reducing the structural responses of the tank is proved. Finally, the numerical and experimental results of the tests over a rocking rigid legged cylindrical stainless steel fluid tank equipped with MR dampers under base excitations are presented to show the efficiency of these dampers in this mode of vibration of such tanks.

- **Chapter 5 (Conclusion):** The thesis is finalised with conclusions and achievements in this chapter and future recommendations are provided.

- **Appendix A:** Glossary

- **Appendix B:** Control procedures and digital filters

Chapter 2

Literature Review

2.1 Introduction

Fluid storage tanks are used for storage, distribution, or process of different kinds of fluids including water, oil, wine, wastes, liquefied natural gas (LNG), chemicals, diesel fuel tanks, medical liquids, etc. They are the lifeline of strategic industries such as refineries, wineries, hospitals, petrochemical, and nuclear plants, among others (Zhai & Feng, 2014; A. S. Veletsos, Shivakumar, Tang & Tang, 1990; Fischer, Liu & Varma, 2016). Such tanks have also been proposed for vibration mitigation of structures, termed as Tuned Liquid Dampers (TLDs) in various forms (Ibrahim, 2005; Konar & Ghosh, 2021). Fluid storage tanks in terms of their aspect ratios are categorized as either slender (aspect ratio =< 1) or broad (aspect ratio > 1). Materials used for fluid storage tanks are mainly stainless steel and concrete. Masonry tanks have also been reported in the literature but in very limited cases. In terms of installation, they are either buried, ground-based, elevated, or mounted over (supported by) a structural frame. Ground-based tanks are either flat-based or legged. In terms of support, they can be simply supported (unanchored) or anchored

using anchor bolts and required connections. Based on applications, they may be used for water storage and supply purposes, storage of oil, liquefied gas, medical liquids, and other chemicals in related industries, and finally for fermentation and storage of wine at wineries, to mention but a few. These structural systems, due to their importance, are the focus of more concerns compared to other civil engineering structures and infrastructures, hence requiring more attention in different aspects.

Steel liquid-storage tanks are categorized as acceleration-sensitive non-structural elements in FEMA 274 (Council, 1997) and the subject of Chapter C9, 'Vertical Liquid-Storage Tanks', in nuclear code ASCE/SEI 4-16 (ASCE, 2017). Industrial buildings and plants demand a higher level of seismic design considerations as any damage to them can cause large-scale socioeconomic and environmental impacts. Such plants most often include liquid storage tanks containing a variety of fluids that could be flammable, pollutant, etc., and be mounted over a steel frame/rack. Research on the coupling effects of a fluid-storage tank as a non-structural element supported by a structural frame or building system under seismic loads is quite scarce (Paolacci, Reza & Bursi, 2011; Paolacci, Reza, Bursi, Gresnigt & Kumar, 2013; Paolacci, Giannini & De Angelis, 2013). Detailed studies in this field by considering fluid storage tanks as secondary structures mounted over a supporting frame and evaluating the seismic responses of both the tank and the supporting structure have recently been conducted by Merino et al. (Vela, Brunesi & Nascimbene, 2018; Merino Vela, Brunesi & Nascimbene, 2019b, 2019a). The seismic performance of a liquid storage tank supported by an industrial steel moment-resisting frame and the tank-structure interaction was studied by Gabbianelli et al. (Gabbianelli, Perrone, Brunesi & Monteiro, 2022). The study in (Vela et al., 2018) derived floor acceleration spectra for a special concentrically braced frame that supports a cylindrical liquid-contained tank.

Early research on evaluating the dynamic response of fluid storage tanks under seismic excitations was started by pioneering works of Hoskins and Jacobsen (Hoskins & Jacobsen, 1934), Jacobsen (Jacobsen, 1949), Housner (Housner, 1954), Veletsos (A. S. Veletsos, 1974; A. Veletsos, 1984), Veletsos and Tang (A. S. Veletsos & Tang, 1987a), Kana (Kana, 1979), Haroun (Haroun, 1983, 1980), Haround and Abou-Izzeddine (Haroun & Abou-Izzeddine, 1992a, 1992b), Haroun and Ellaithy (Haroun & Ellaithy, 1985a), Haroun and Housner (Haroun & Housner, 1981b, 1982a, 1981a, 1982b), Haroun and Tayel (Haroun & Tayel, 1985), Malhotra (P. K. Malhotra, 1997), Malhotra and Veletsos (P. K. Malhotra & Veletsos, 1994c, 1994b, 1994a), Malhotra et. al (P. Malhotra, Veletsos & Tang, 1993; P. K. Malhotra, Wenk & Wieland, 2000), and Manos and Clough (Manos & Clough, 1985, 1982), among others. Important types of forces and stresses that are developed in fluid storage tanks during seismic ground motions are base shear, overturning moment, hoop stress, axial compressive stress, and bending stress. Two types of vibration modes have been introduced for these tanks, i.e. the flexural (beam/global bending/cantilever type) modes and cross-sectional (oval type) modes specified by circumferential and axial wave numbers. Meanwhile, the flexibility of the wall and foundation would amplify these stresses and forces accordingly and hence need to be included in calculations and design of tanks.

Dynamic analysis of fluid storage tanks is much more challenging and complicated than other civil engineering structures and infrastructures such as buildings and bridges due to various factors affecting the tank's dynamic behavior. These factors include interaction between the fluid and the tank wall, characteristics of the input excitation (frequency content, amplitude, and period), direction of the excitation, aspect ratio and geometry of the tank, material properties of the tank, type of supports, flexibility of the tank wall, and the underlying soil/foundation. Fluid-structure-soil interaction which adds

the flexibility of the underlying soil to the dynamic behavior and seismic response of tanks is a crucial topic in seismic response analysis of fluid storage tanks.

Stainless steel fluid storage tanks are used in a variety of applications and industries including wineries, dairy products industries, water storage purposes, and petrochemical industries, to name but a few. Related industries were heavily damaged financially during past earthquakes. Examples of past occurrences which resulted in massive losses are the 2010 Maul earthquake in Chile (González, Almazán, Beltrán, Herrera & Sandoval, 2013), the 2011 Christchurch (Rosewitz & Kahanek, 2014), the 2013 Marlborough (Morris, Bradley, Walker & Matuschka, 2013), and the 2016 Kaikōura (Dizhur et al., 2017) earthquakes in New Zealand, the 2012 Emilia earthquake in Italy (Brunesi, Nascimbene, Pagani & Beilic, 2015), the 2014 Napa earthquake in California (Fischer et al., 2016), and the 1989 Loma Prieta earthquake (Team et al., 1990), among others. Due to the huge inflicted losses caused by these events, it is imperative to understand the way these structures will behave realistically during seismic events. This will help modify the current analysis procedures for more accurate designs of these structures to avoid future catastrophes.

The main approaches that are applied for the analysis and design of these tanks are based on the equivalent mechanical models proposed in the literature. Mostly used techniques for this purpose include those presented by Housner (Housner, 1954, 1957a), Haroun (Haroun, 1983), Veletsos (A. S. Veletsos, 1984), and Malhotra (P. K. Malhotra et al., 2000), among others, which form the design basis of many seismic codes in different parts of the world including American Petroleum Institute (API) 650 (API, 2005), Eurocode 8, Part 4 (EN, 2006), and the New Zealand Society for Earthquake Engineering (NZSEE) (NZSEE, 2009). These simplified techniques were substantial efforts to express a highly complicated phenomenon in these structures which is the

fluid-structure interaction in a closed-form mathematical expression that could be easily applied for calculations. However, there are many approximate and simplified assumptions behind these mechanical models, the most important of which are irrotationality and small-amplitude surface fluid oscillations when formulating the Navier-Stokes equations. A comprehensive literature review conducted by the authors studied in detail a variety of dynamic modelling techniques proposed for these structural systems (Hosseini & Beskhyroun, 2023), different types of damages observed in past seismic events, different methodologies proposed in the literature for analysing the fluid tanks, the assumptions made for each technique, and the modified proposed models. Among the crucial factors that cause the violation of these assumptions and substantial differences between mathematical results and what occurs in practice, the below items can be mentioned:

- flexibility of the tank shell in thin-walled steel tanks (Nicolici & Bilegan, 2013; Chiba, 1993).
- the fixity conditions of the tank base plate to the ground or foundation (Ormeño, Larkin & Chouw, 2015).
- the rotational and chaotic behaviour of the surface water oscillations (Hernandez-Hernandez, Larkin, Chouw & Banide, 2020a).
- interaction between the underlying soil and the tank (Hernandez-Hernandez, Larkin & Chouw, 2021b).
- characteristics of the ground motion, including duration, mechanism, frequency content, and amplitude (Fang, Chen, Yan, Cao & Wang, 2013).
- second order (P-Δ) and material nonlinearities, as well as uncertainties in properties of the tank materials and geometry, contained liquid, and excitation (Kamarroudi,

Hosseini & Hosseini, 2021b; Khayat, Baghlani & Dehghan, 2022) and finally,

- fluid flow characteristics such as multi-phase flow and Coriolis effects (Kang, Yang & Jeon, 2019).

These approximations when formulating the mechanical models will result in inaccuracies in estimating the structural characteristics of fluid tanks including natural frequencies of the impulsive and convective modes which are the two dominant vibrational modes in these structures. Subsequently, the structural responses including uplift displacements, lateral accelerations and displacements, and internal stresses and strain would be underestimated.

Stainless-steel fluid storage tanks depending on the flexibility and thickness of their shell are categorised as rigid or thin-walled flexible and are commonly used for the storage of wine, water, dairy products, etc. These tanks are either legged or flat-based. In terms of connection to the ground or foundation, they could be anchored or unanchored. Studies have shown that these structures are one of the main elements of wineries that are vulnerable to damage even in regions that have a low seismic risk (Ogunmakinde, Egbelakin, Omotayo & Sojobi, 2023). Recently, some research efforts were dedicated to a better understanding of the seismic behaviour of fluid storage tanks and modifying initial simplified mechanical models, either numerically or experimentally (Hosseini & Beskhyroun, 2023). Compared to a considerable number of numerical investigations conducted on the dynamic behaviour modelling of fluid storage tanks in the literature less experimental investigation has been done. Recently a series of experimental tests and corresponding numerical validations have been performed over double-layer liquefied natural gas (LNG) storage tanks (D.-Y. Zhang & Wu, 2024; D.-Y. Zhang, Wu, Zhou & Gong, 2023). Liu et al. (W. Liu, Xiao, Zhou & Wang, 2023) investigated the effects of

fluid-structure interaction (FSI) and the validity of the small amplitude linearized fluid motions theory of the liquid surface in a liquefied natural gas (LNG) storage tank made of an inner steel cylindrical tank and an outer reinforced concrete tank. They reported significant discrepancies between their experimental results and those presented by the simplified mechanical model of Housner (Housner, 1957a) under seismic excitations. Compagnoni and Curadelli (Compagnoni & Curadelli, 2018) tested a flat-based steel cylindrical tank with a thickness of 1.5mm using shake table excitations for aspect ratios of 0.5, 1.0, and 1.5. They showed that the simplified mechanical model underestimates some of the fluid tank's responses while overestimating the other. Shake table tests over an aluminum tank were implemented for two cases of anchored and unanchored conditions by Ormeño et al. (Ormeño, Larkin & Chouw, 2012). This tank model had a shell and base thickness of 3mm. Shake table testing of a large-scale legged fluid storage tank with a shell thickness of 2mm was conducted by Yazdanian et al. (Yazdanian, Firouzsalari, Ingham & Dizhur, 2021). Shake table examinations over a legged stainless-steel cylindrical fluid tank were conducted by Reyes et al. (Reyes et al., 2022) to study the performance of the new isolation system. It is noteworthy that shell thickness in stainless-steel tanks plays a pivotal role in the flexibility of the coupled fluid-tank system, and hence the dynamic characteristics of the structure including natural frequencies and damping ratios. Moreover, damage assessments of fluid tanks in previous seismic events have shown that the thickness of the shell, aspect ratio, and the characteristics of the ground excitation are among the most important factors that substantially contribute to major fluid tank damages including diamond shape and elephant foot buckling damage types (Dizhur et al., 2017; Yazdanian, Ingham et al., 2021; Yazdanian, Ingham, Lomax, Wood & Dizhur, 2020; Hernandez-Hernandez, Larkin & Chouw, 2021a; Chiba, 1993).

Researchers have utilised different excitation methods for the vibrational analysis

of fluid storage tanks in literature. The contribution of the second convective mode in responses of rigid liquid storage tanks using wavelets was examined numerically in (Kalogerakou, Maniatakis, Spyrakos & Psarropoulos, 2017). Wavelet analysis was used for numerical seismic response evaluation of base-isolated liquid storage tanks (Uckan, Umut, Sisman, Karimzadeh & Askan, 2018). Sine and ricker wavelet excitation tests have been applied for shake table testing of an LDPE tank (Hernandez-Hernandez et al., 2021a). Pulse test by shake table was used for the same tank in (Hernandez-Hernandez, Larkin & Chouw, 2022) for free-vibration frequency determination of the fluid tank for rigid and flexible support conditions. Swept-sine excitation tests have been proved as simple and efficient means for natural frequency estimation of structures which offer robustness, rapidity, and stability, as well (Mituletu, Gillich & Maia, 2019; F. Wang & Song, 2019; Decuyper, De Troyer, Tiels, Schoukens & Runacres, 2020). They also have found successful applications for structural health monitoring purposes (F. Wang & Song, 2019; Sohn, Lim, DeSimio, Brown & Derriso, 2014).

In this chapter, a review of different dynamic modeling techniques proposed in the literature, from pioneering works up to the present, for analyzing the behavior of fluid storage tanks under seismic excitations is provided. Different analytical, semi-analytical, numerical, and probabilistic methods, fundamental assumptions for the behaviour of the liquid and tank, and available international codes for seismic resistant analysis and design of these systems have been discussed. A variety of energy-dissipating devices have been proposed in the literature and applied in industries for their vibration attenuation and structural control. Some of the explored structural health monitoring approaches and devices have been examined. Different types of damages observed in previous earthquakes have been studied. Even though considerable contributions have been made by many researchers, there are still many research areas to be investigated regarding

the dynamic modeling, seismic protection, and health monitoring of fluid storage tanks. Therefore, it has been tried to scrutinize the literature in this field and identify prominent aspects of analysis and design of these structures, current challenges, and future research opportunities.

2.2 Dynamic behaviour

A fluid storage tank is a coupled system and its dynamic behavior is governed by the interaction between motions of the fluid and the tank wall and bottom. The decisive part in investigating the dynamic responses of fluid storage tanks is the analysis of fluid-structure interaction which is a complex phenomenon and has been dealt with by numerous researchers through different approaches. The fluid domain is governed by fluid dynamics equations that are presented usually by Navier-Stokes, Laplace, and Bernoulli equations to obtain the hydrodynamic pressure distribution over the tank wall. Recently, the application of acoustic wave theory using the Helmholtz equation has been considered for investigating the seismically induced sloshing and hydrodynamic behavior of fluid storage tanks (Rawat, Mittal, Chakraborty & Matsagar, 2019). On the other hand, the tank's structure follows the structural dynamics rules. Hamilton's principle, Lagrangian approach, and the Donnell shell theory have been utilized for formulating dynamic equations of motion of the tank's body, among others.

A review on different analytical models for seismic analysis of fluid-storage tanks for both rigid and flexible base-supported cylindrical tanks can be found in (Yu & Whittaker, 2021) that compares the seismic responses of tanks using exact and approximate solutions presented in the literature. They have demonstrated the significance of considering exact methods as well as including wall flexibility effects in calculations. Another more general

review by Zingoni (Zingoni, 2015) discusses different effects of environmental loading such as wind and liquid pressures, seismic motions, and thermal effects on different kinds of fluid storage tanks. Horizontal and vertical cylindrical tanks in their review have been considered mostly from a shell structures perspective.

2.2.1 Analytical, semi-analytical, and numerical methods

From early attempts to evaluate the dynamic behavior of fluid storage tanks excited at their base, it was recognized that one part of the fluid which is close to the bottom of the tank moves in unison with the tank wall. This part of the fluid is called impulsive mass vibrating at a high-frequency range while the upper part of the fluid and the free surface encounters sloshing oscillations. The latter part is termed as convective mass contributing to vibrations of the liquid at the low-frequency range, in other words, having a long period of motion. Analytical approaches for dealing with the coupled fluid-structure equation of motion are based on solving the Laplace equation for velocity potential. Then some assumptions are considered for the characteristics of the fluid and its motion to obtain the hydrodynamic pressure distributions along the wall of the tank for these two masses.

Usually, a simplified mechanical model composed of lumped mass-spring-dashpot elements (Housner, 1957b, 1963b) or an equivalent pendulum model is used to obtain the dynamic equation of motion for the whole system and analyze its behavior. This equivalent mechanical model for analyzing the fluid-tank dynamic motion has been used in research studies in abundance. Seismic fragility assessments of tanks and tank-structure interaction analyses of structural frames supporting fluid storage tanks have been conducted using this approach (Vela et al., 2018; Merino Vela et al., 2019b, 2019a;

Gabbianelli et al., 2022). On the other hand, numerical approaches such as Finite Element (FE) based methods, Boundary Element (BE), Finite Difference (FD), Volume of Fluid (VOF), and Smooth Particle Hydrodynamics (SPH) have been applied to examine the coupled fluid-tank dynamic behavior (Vesenjak, Mullerschon, Hummel & Ren, 2004; Souto-Iglesias, Delorme, Pérez-Rojas & Abril-Pérez, 2006; Lakis, Bursuc & Toorani, 2009; Goudarzi & Sabbagh-Yazdi, 2012). For semi-analytical methods used in this regard, one can mention the work by Wang et al. (J. Wang, Lo & Zhou, 2012; W. Wang, Peng, Zhou & Zhang, 2016). Some other numerical methods proposed by researchers include coupled BE-FE (Shekari, Khaji & Ahmadi, 2009), coupled BE-FE-BE (Shekari, 2018), coupled Acoustic-Structural (CAS) and coupled Eulerian-Lagrangian (CEL) (Rawat et al., 2019), Arbitrary Eulerian-Lagrangian (ALE) (Longatte, Bendjeddou & Souli, 2003; Aquelet, Souli, Gabrys & Olovson, 2003; Souli & Zolesio, 2001), scaled boundary FE technique (Lin, Liu, Li & Hu, 2015), and finite-volume method (Goudarzi & Danesh, 2016), among others. In between, the Divergence theorem, Green-Gauss theorem, Green's function, and the Galerkin principle are used to solve the differential equations in the fluid domain. Rayleigh-ritz method, substructuring, and Galerkin method have been applied by several researchers as efficient analytical approaches to study the coupled fluid-structure system and characterize the sloshing and bulging modes and frequencies (Amabili, 1997, 1998; Y. W. Kim & Lee, 2005; Askari, Daneshmand & Amabili, 2011). Figure 2.1 shows different dynamical models proposed in the literature and the underlying fundamental assumptions used for developing such models, vibration modes, and stresses developed in fluid storage tanks under seismic vibrations.

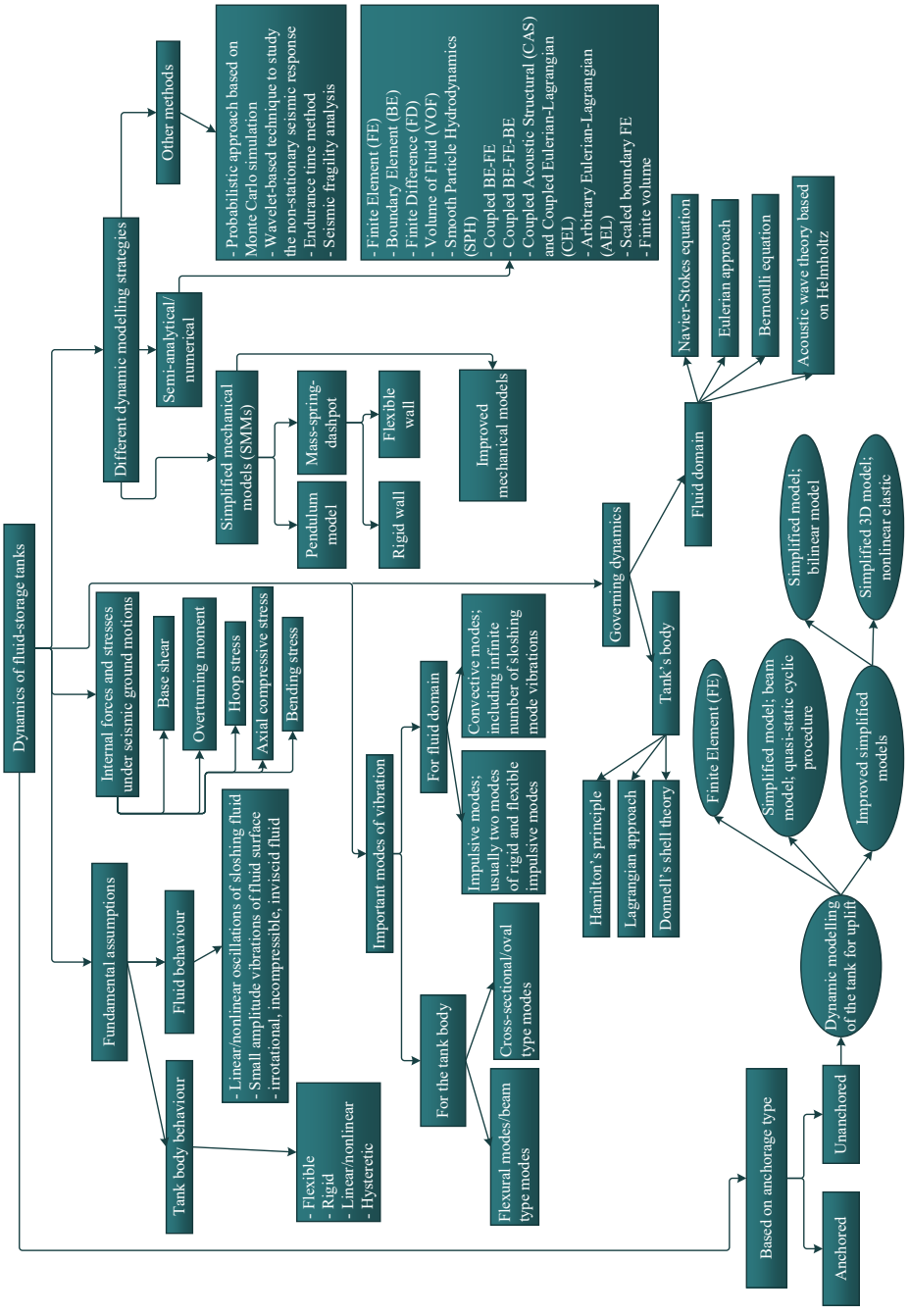

Figure 2.1: Fluid-storage tanks: Dynamic modeling, vibration modes, stresses, and fundamental assumptions

2.2.2 Probabilistic methods, uncertainties, and other methods

For other methods proposed by researchers for investigating seismically induced dynamic responses of fluid storage tanks, one can mention the work by Merino et al. (Merino, Brunesi & Nascimbene, 2020) which is a probabilistic approach based on a Monte Carlo (MC) simulation. Chatterjee and Basu (Chatterjee & Basu, 2004) used a wavelet-based technique to study the non-stationary seismic response of fluid storage tanks based on the equivalent mechanical model for tank-liquid system taking into account the foundation-soil flexibility. Endurance time method was proposed by Estekanchi and Alembagheri (Estekanchi & Alembagheri, 2012) as a time history analysis of the tank under artificial dynamic excitation which is intensified gradually to examine the systems' response under different intensity levels and monitor the damage indices. Seismic fragility analysis for base-isolated liquid storage tanks under non-stationary earthquakes using the equivalent mechanical model of Haroun and Housner (Haroun & Housner, 1981a) and the MC simulation for randomly generated seismic accelerations was used by Saha et al. (S. K. Saha, Matsagar & Jain, 2016). The purpose of this study was to investigate the probability of failure in fixed-based and base-isolated slender and broad tanks by conducting non-linear time history analyses. Stochastic seismic analysis of fixed-base, as well as base isolated tanks using elastomeric and sliding bearings, was studied by Safari and Tarinejad (Safari & Tarinejad, 2018). They conducted their evaluations in the frequency domain using Power Spectral Density Function (PSDF) under near-fault and far-fault earthquakes based on the equivalent mechanical model of Haroun (Haroun, 1983). Curadelli (Curadelli, 2013) conducted a stochastic seismic analysis over cylindrical base-isolated fluid storage tanks using the mechanical model of Haroun (Haroun, 1983) to study the influences of the isolation system parameters as well as the

soil conditions on the seismic performance of such tanks. This study also tried to deal with the uncertainties related to ground excitations using a Gaussian stationary random process stochastically consistent with a given design spectrum. Another stochastic seismic analysis in this field is the work of Saha et al. (S. Saha, Sepahvand, Matsagar, Jain & Marburg, 2013) which considered the parametric uncertainties in the isolator parameters and the base excitations, as well. They applied the generalized Polynomial Chaos method as well as the stochastic Galerkin approach to deal with uncertainties and implement stochastic analyses. They discussed that this method could promise efficiency and less computational effort at the same time with proven advantages over methods such as perturbation technique, MC, and Karhunen-Loéve (KL) (Xiu & Karniadakis, 2002, 2003; Sepahvand, Marburg & Hardtke, 2010, 2012).

2.2.3 Soil-structure-fluid interaction

Idealization of structural systems as fixed-based models and ignoring the effects of the soil on the structural responses is far from reality. Underlying soil can significantly impact the dynamic responses of structures under seismic loading. Depending on the dynamic properties of the soil and the structure, and frequency content of the excitation, the structural natural period would be affected, and hence the structural responses. Thus, soil-structure interaction (SSI) has been the focus of attention by many researchers for seismic analysis of structures from the pioneering works of (Lysmer & Kuhlemeyer, 1969; Jennings & Bielak, 1973; A. S. Veletsos & Meek, 1974; A. S. Veletsos & Nair, 1975; A. S. Veletsos & Tang, 1987b; A. S. Veletsos & Wei, 1971; Luco, 1976; Gazetas, 1983; Gazetas & Tassios, 1978). Induced significant effects, increased maximum inelastic displacement demands, and larger displacements in tall structures and those behaving

nonlinearly as a result of SSI effects have been demonstrated by several researchers (Bielak, 1978; Miranda & Bertero, 1994; Halabian & El Naggar, 2002; Mitropoulou, Kostopanagiotis, Kopanos, Ioakim & Lagaros, 2016; Ghannad & Jahankhah, 2007; Khoshnoudian & Ahmadi, 2015; Khoshnoudian, Ahmadi & Nik, 2013; Demirol & Ayoub, 2017; Demirol, Fragkos, Arulanantham & Ayoub, 2018; Hassani, Bararnia & Amiri, 2018; Shi, Song, Guo & Pan, 2022). Effect of soil on the transfer of seismic waves from ground to the fluid storage tanks will result in a more intricate phenomenon termed as soil-structure-fluid interaction (SSFI). From early works on dynamic modeling and seismic analysis of fluid storage tanks, consideration of SSFI effect on dynamic analysis of these strategic structures was felt substantial. Dynamic analysis results demonstrated amplification of hydrodynamic pressures over the tank wall, overturning moment, and base shear as a result of SSFI effect (Haroun & Abou-Izzeddine, 1992a, 1992b; Chatterjee & Basu, 2004; J. Sun et al., 2018; Livaoglu & Dogangun, 2007; el Mezaini, 2006; Lyu, Sun, Sun, Cui & Wang, 2020; Farajian, Khodakarami & Kontoni, 2017; Ma & Chang, 1993; Kirtas, Rovithis & Makra, 2020; Chatterjee & Basu, 2006; X. Meng et al., 2019). Lyu et al. (Lyu et al., 2020) developed a simplified mechanical model for horizontal fluid storage tanks under seismic ground motions considering the SSFI effect. Livaoglu and Dogangun (Livaoglu & Dogangun, 2007) studied the foundation embedment and considered the SSFI effect on the seismic behavior of elevated fluid storage tanks using the FE technique. They concluded that soft soil types considerably affect the seismic responses of such structures including roof displacement, sloshing heights, and base shear. Kirtas et al. (Kirtas et al., 2020) conducted tests on a real case study of an instrumented steel cylindrical water tank with H/R of 0.74. They compared their results with that of obtained from recommended formulae by seismic design codes such as Eurocode 8 (EN, 2006) and NZSEE (NZSEE, 2009) for tanks with H/R < 1. An agreement was concluded

between the recorded data and provisions of these codes in terms of rigid tank behavior which could be a possible mode for tanks with aspect ratios of less than one supported by flexible soil.

The study by Tsipianitis et al. (Tsipianitis, Tsompanakis & Psarropoulos, 2020) investigated the SSI effect on the dynamic response of fluid storage tanks. They applied the spring-mass analogy proposed by Erkmen (Erkmen, 2017) based on the FE technique and considered different aspect ratios, seismic ground excitations, and soil conditions to examine the increase or decrease of the dynamic responses of anchored and unanchored cylindrical tanks. Their results showed soft soil conditions cause the sliding and uplift of both slender and broad tanks to be increased. An experimental study by Ormeño et al. (Ormeño, Larkin & Chouw, 2019) evaluated the effect of soft soil on compressive stress levels of a PVC tank as a prototype of a steel tank. Their results demonstrated that in the majority of tests, a flexible base decreases the axial compressive stress values in the tank shell, and fundamental frequency of the tank whereas it amplifies the top displacement, wall acceleration, and rocking possibility of the tank. Nonlinear SSFI effect due to material and geometrical nonlinearities over structural responses of a low-density polyethylene tank was studied experimentally in (Hernandez-Hernandez et al., 2021b). The results of this study proved a close correlation between the aspect ratio of the tank, the frequency of the excitations, and the development of stresses and other structural responses in the fluid-contained tank over a flexible base.

2.2.4 Unanchored tanks and uplift effect

The main principles for modeling the dynamic behavior of fluid storage tanks for anchored or fixed-based tanks are applied to unanchored tanks as well. However, when

tanks are exposed to the uplift occurrence, dynamic equations of motion need to be modified to account for the rotation or rocking of the tank as a result of the uplift. First attempts to model the uplift behavior of tanks include the methodologies developed by Veletsos (A. Veletsos, 1984), Veletsos and Tang (A. S. Veletsos & Tang, 1987a), Haroun and Ellaithy (Haroun & Ellaithy, 1985b), Ishida and Kobayashi (Ishida & Kobayashi, 1988), and Malhotra and Veletsos who considered a nonlinear rotational spring at the bottom of the tank (P. K. Malhotra & Veletsos, 1994c, 1994b, 1994a). Other recently modified versions of dynamic modeling for uplift were presented by (Vathi & Karamanos, 2014b, 2014a, 2015, 2018) which model the relationship between the overturning moment and the rotation of the tank's base using a bilinear approach. The tapered beam model proposed by (Ahari, Eshghi & Ashtiany, 2009) represents a more realistic formulation for base plate rotation during the uplift of the tank. Research by Mir et al. (Mir, Yu & Whittaker, 2021) modified the procedure proposed by Veletsos and Tang (A. S. Veletsos & Tang, 1987a) by including base rotational displacements in the analytical model for obtaining pressure equation and the base moment. Results of their modified approach showed a very good agreement with that of obtained using FE analyses. Maheri et al. (Maheri, Karbaschi & Mahzoon, 2016) focused on natural and rocking mode frequencies of unanchored tanks and examined the partial uplift of the base plate during rotation.

Colombo and Almazan (J. Colombo & Almazán, 2019) proposed a simplified 3D dynamic model to analyze the uplift of fluid storage tanks using a nonlinear elastic model and examined the compressive axial and hoop stress distributions over the tank wall. Cortes and Prinz (Cortes & Prinz, 2017) employed the seismic fragility analysis to examine the probability of damage in large, unanchored steel tanks by introducing a mechanical model consisting of only the impulsive mass at the end of an elastic beam

element representing the tank shell which rests on a rigid link with horizontal and vertical springs at both ends. Their analysis evaluated two types of damages including shell buckling due to uplift and ultra-low cycle fatigue of the shell-to-base connections using their proposed method. Experimental investigations on the effects of uplift on the shell stress levels and other structural responses of unanchored tanks have recently been conducted by Ormeño et al. (Ormeño et al., 2019, 2012, 2015).

2.2.5 Standards and wall flexibility

International standards that govern the design procedures of fluid storage tanks include API 650 (API, 2005), Eurocode 8 Part 4 (EN, 2006), NZSEE (NZSEE, 2009; Priestley, 1986), ACI 350.3-06 (ACI, 2009), AWWA D-100 (AWWA, 2011), IITK-GSDM (IITK-GSDMA, 2007), UNI EN 14015 (EN, 2004), and AIJ (Japan, 2010). The equivalent mechanical model of the fluid-tank system based on the mass-spring-dashpot analogy forms the basis of the design approach of these standards. The mechanical equivalent model introduced by Housner (Housner, 1954) was a two-mass model, namely impulsive and convective, which did not consider the flexibility of the tank wall. Later, it was observed by numerous researchers that the flexibility of the wall significantly amplifies the dynamic responses of tanks. It was found by Veletsos (A. S. Veletsos, 1974) that the peak acceleration of the flexible tank can be even higher than the peak ground acceleration and used the added mass theory to represent the fluid domain in the tank's dynamic equations. Thus, the three-mass model by Haroun (Haroun, 1983) was proposed that took into account the flexibility of the tank wall. In fact, in the two-mass model by Housner (Housner, 1954) there were only two parts of the liquid, i.e. the rigid impulsive mass and the convective mass. However, in the three-mass model by Haroun (Haroun, 1983),

there are three masses: impulsive rigid mass connected rigidly to the tank wall, impulsive flexible mass (with spring and dashpot), and the convective mass. It is noteworthy that in most analytical techniques through the equivalent mechanical model only the first fundamental impulsive mode and the first fundamental convective modes are considered for simulations.

Most researchers considered only the first impulsive and convective modes for analyses. However, further research by means of shaking table tests conducted by Manos and Clough (Manos & Clough, 1982, 1983) and investigations by Veletsos (A. S. Veletsos, 1984) proved that more than one convective mode need to be considered for analysis and design. Thus, in some later research works, usually, up to three convective modes have been considered for seismic response evaluation of tanks. It should be mentioned that in the equivalent mechanical model, the impulsive mode and convective mode are considered decoupled for solving the dynamic equation of motion. The reason is the natural frequency of the convective mode is much lower than the impulsive one, hence enabling for decoupling of dynamic equations of motion for the two modes. Recently, a surrogate modeling technique using a single vertical beam-column element resting on rigid beam spokes with edge springs was proposed by Bakalis et al. (Bakalis, Fragiadakis & Vamvatsikos, 2017). They aimed to assess the seismic response of liquid storage tanks with results that are comparable with 3D FE models of the tanks considered in their study. Their model offered reasonable accuracy and good computational efficiency compared to the FE approach, empowering the method to be used for efficient performance-based design of tanks.

2.2.6 Improved mechanical models

There have been some research works on the applicability, validity, and accuracy of the equivalent mechanical model by comparing numerical and experimental results with that of obtained through detailed FE analyses. Goudarzi and Sabbagh-Yazdi (Goudarzi & Sabagh, 2009) investigated the accuracy of the mechanical model proposed by Malhotra (P. K. Malhotra et al., 2000) which is a modified version of the model proposed by Veletsos (A. Veletsos, 1976) and compared obtained numerical results with that of FE analysis conducted in ANSYS software. They found good agreements between the results of numerical analyses from the simplified mechanical model of Malhotra (P. K. Malhotra et al., 2000) and FE model. However, some discrepancies were also observed in terms of natural periods predicted by the simplified model, overturning moment, base shear, and maximum sloshing wave height (up to more than two times difference). The reason could be explained as neglecting non-linear sloshing behavior in the simplified model. It was also found that higher convective modes need to be considered in the simplified models as the maximum sloshing wave height is mainly affected by the period of the seismic record. Since, the convective mode has a considerably higher natural period of vibration, and hence would be amplified under long-period ground motions; the well-known concerning result would be the resonance sloshing. Compagnoni and Curadelli (Compagnoni & Curadelli, 2018) as complementary research to this work, conducted experimental and numerical investigations. In the numerical part, the results of the simplified model were compared with that of Lagrangian FE analysis using ANSYS software over ground-supported fluid storage tanks. Experiments were conducted over a steel cylindrical tank with one laser displacement sensor at the top of the tank and one accelerometer at the base to measure the motions of the shaking table. They found virtually similar fundamental

mode frequencies of the tank-liquid system for the considered three models. However, the simplified mechanical model provided underestimated maximum sloshing wave height and overestimated maximum base shear and overturning moment on the conservative side. The conclusion was the suggestion of the simplified mechanical model proposed by Malhotra (P. K. Malhotra et al., 2000) to be applied cautiously for preliminary designs.

Experimental shake table investigations were conducted by (Hernandez-Hernandez et al., 2021a) over a polyethylene tank containing water with different aspect ratios to examine the sufficiency of the equivalent mechanical model in terms of the maximum stress levels developed in the tank. This study considered the influence of the frequency content of excitation as well as maximum acceleration over the tank wall stress levels. Results proved that the equivalent mechanical model produces underestimated maximum hoop and axial stress levels in the wall of the tank. The reason can be described as the resonance phenomenon and chaotic and rotary sloshing of free surface liquid which have been ignored when deriving the equivalent mechanical model. Another experimental work by researchers in (Hernandez-Hernandez, Larkin, Chouw & Banide, 2020b) is another confirmation of this fact. Results of conducted tests demonstrated that rotary sloshing which occurred under excitation frequencies close to the first free vibration frequency of the tested tank increased the tank wall accelerations perpendicular to the excitation, and hoop and axial strain levels in the tank wall.

Li and Gou (Y.-C. Li & Gou, 2018) examined the traditional equivalent mechanical model of Graham and Rodriguez (Graham & Rodriguez, 1952) and Housner's model (Housner, 1957b) and compared the results for the sloshing mode of vibrations with that of their own proposed modified model. They concluded that the traditional model gives correct sloshing frequencies, equivalent masses, and spring constants. However, they found that the locations of equivalent masses were not correct. Also, they expressed that

Housner's model (Housner, 1957b) is based on physical intuition and is only suitable for vertical tanks with a flat bottom under horizontal excitation. Finally, they proposed a modified equivalent mechanical model for rigid tanks of arbitrary shapes applicable only to translational excitations. They regarded the linear behavior (small amplitude) of the liquid free surface oscillations in the velocity potential equation and Bernoulli's equation for deriving the hydrodynamic pressure. Sun et al. (Y. Sun, Zhou & Wang, 2019; Y. Sun, Zhou, Wang & Han, 2021) proposed an equivalent lumped parameter model for liquid sloshing in rigid cylindrical tanks with rigid annular baffles using the subdomain method. They applied the continuity conditions for velocity and pressure for modeling the continuous fluid domain and the substructure method for formulating their equivalent lumped model of the tank-liquid system. In (Y. Sun et al., 2019), they considered a rigid multi-tank system (each tank equipped with one rigid baffle) fixed to a rigid platform sliding without friction on a rigid foundation. While in (Y. Sun et al., 2021) they examined the case of a tank with multiple annular baffles base isolated using the lead rubber bearing (LRB) system. In both studies, the key and stepping-stone assumptions include the linearised sloshing theory, the rigidity of the tank wall and foundation, consideration of only horizontal excitations, and the ideal fluid (inviscid, irrotational, incompressible) behavior. They showed that the proposed model can provide results of satisfactory accuracy with a much smaller computational cost for complex fluid-structure systems. The proposed model took much less computational time compared to FE analyses conducted in ADINA (9s duration for the equivalent model using MATLAB versus 508s duration for computations using ADINA (Y. Sun et al., 2021)).

Another work in this field was established by Ebrahimian et al. (Ebrahimian, Noorian & Haddadpour, 2014). They proposed an equivalent model for rigid tanks of arbitrary geometry with multiple baffles using Green's second identity, the divergence theorem

in the boundary element model, and the Bernoulli equation. They ignored the damping effects in their calculations and compared their results with those of equivalent models for simple rectangular and cylindrical tanks. Another interesting work in the field of improved equivalent mechanical models for fluid storage tanks is that of Moradi et al. (Moradi, Behnamfar & Hashemi, 2018). They proposed a lumped parameter model for cylindrical concrete fluid storage tanks considering the wall flexibility. Their results showed a good agreement with that of ACI 350.3-06 (ACI, 2009). Also, they emphasized the removal of limitations for obtaining the proposed mechanical model compared to that of Haroun and Housner (Haroun & Housner, 1981b). They applied the Rayleigh-Ritz method instead of the approximate FE analysis in (Haroun & Housner, 1981b) and included the thickness of the tank's wall, partial fulfillment, and wall mass in their formulations.

Virella et al. (Virella, Godoy & Suárez, 2006) studied the impulsive vibration modes of anchored cylindrical liquid storage tanks with conical roofs and with height/diameter ratios from 0.4 to 0.95, subjected to horizontal ground excitations. They applied the added mass approach as well as the acoustic FE technique in their analyses. Results of their analyses showed that for H/D ratios of the tanks larger than 0.63, the fundamental modes follow that of the cantilever beam while for the H/D equal to 0.4 the bending mode is dominant. Also, it was shown that the added mass method compares very well with the more comprehensive acoustic FE technique in terms of fundamental periods and mode shapes.

2.2.7 Limitations of proposed models

It should be mentioned that one limitation of almost all studies reviewed in the literature above is the consideration of the underlying assumptions for formulating the velocity potential equation and the hydrodynamic pressure. The most important constraint among these assumptions is the hypothesis of linear oscillations of the sloshing fluid. However, further research showed that under seismic excitations, large amplitude sloshing vibrations occur which result in the nonlinearity of this kind of vibrations in the fluid (Goudarzi & Sabbagh-Yazdi, 2012). Therefore, the linearity of the sloshing liquid cannot be held valid anymore and can lead to the underestimated design of tanks (W. Chen, Haroun & Liu, 1996). It has been found by several researchers that the vertical component of the ground motion, especially when combined with the horizontal components, can considerably affect the seismic behavior of tanks and lead to the nonlinear sloshing behavior of the convective liquid (Haroun & Tayel, 1985; Kianoush & Chen, 2006; Ghaemmaghami & Kianoush, 2010; Yamada, Iemura, Noda & Shimada, 1987; J. K. Kim, Koh & Kwahk, 1996; Kamarroudi, Hosseini & Hosseini, 2021a). Investigations on the nonlinear sloshing phenomenon in liquid storage tanks under either unidirectional or a combination of horizontal and vertical ground excitations have been conducted using the computational fluid dynamics (CFD) analysis (Vakilaadsarabi, Miyajima & Murata, 2012; Godderidge, Tan, Earl & Turnock, 2007; Frandsen, 2004).

Most of the studies on the nonlinear behavior of the sloshing liquid did not fully consider the nonlinearity due to the mixture of fluid and air, realistic ground motions, and the validation of numerical studies by experimental results. More advanced research was conducted by Kang et al. (Kang et al., 2019) that examined this important phenomenon using CFD analysis and a shear stress transport (SST) model by considering continuity

and momentum equations for multi-phase flow, and the mass transfer between the phases. They validated their results by numerical studies using ANSYS CFX (Inc, 2016) and experimental data obtained by Baek et al. (Baek, Choi, Park, Kim & Kim, 2017) who conducted shake table tests over a circular cylindrical steel tank instrumented by hydraulic pressure gauges. The study by Kang et al. (Kang et al., 2019) was conducted over rigid tanks and proved that the vertical component of the seismic motions will change the amount of the maximum hydrodynamic pressure and its location on the circumference. It was also shown that the distribution of the hydrodynamic pressure along the wall will be affected due to Coriolis effects. Another important result of this study was that the frequency content of the considered excitations affected the convective and impulsive pressure energies differently. In this study, the effect of the flexibility of the tank wall was recommended to be considered in further studies. Table 2.1 below represents an overview of some of the dynamic modeling techniques applied to seismic vibration analysis of fluid storage tanks, the study approach, the type of considered excitation, and some remarks on the applied techniques.

Table 2.1: An overview of different dynamic modeling techniques proposed for the coupled fluid-tank system

Reference	Shape	Material	Wall flexibility	Modeling methodology	Structural behavior	Fluid behavior	Study approach	Excitation	Remarks
(Rawat et al., 2019)	3-D Cylindrical and rectangular	–	Rigid	–FEM; CAS and CEL –Analytical	Bi-linear rigid elements in FEM software	–Linear and non-linear wave theory for CAS and CEL – Linear wave theory for analytical	Numerical	Horizontal seismic; monodirectional; far field and near field earthquakes	It was concluded that the nonlinearity of sloshing wave displacement does not have a significant effect on the calculation of hydrodynamic pressure distribution over the wall of rigid tanks
(Hashemi, Saadatpour & Kianoush, 2013)	3-D Rectangular	Concrete	Flexible	Analytical; simplified mechanical model	Linear elastic	Linear wave theory	Numerical	Horizontal; monodirectional seismic	Proposes an analytical approach based on the Rayleigh-Ritz method and vibration modes of flexible plates to examine the seismic response of 3-D rectangular concrete tanks considering the flexibility of walls; based on the proposed method a mechanical model is proposed considering the flexibility of the tank walls; a simplified 2-D model for pressure distribution on the flexible wall is suggested to improve formulas in seismic design codes of fluid tanks

Continue on the next page

Table 2.1: An overview of different dynamic modeling techniques proposed for the coupled fluid-tank system

Reference	Shape	Material	Wall flexibility	Modeling methodology	Structural behavior	Fluid behavior	Study approach	Excitation	Remarks
(Mittal, Chakraborty & Matsagar, 2014)	3-D Cylindrical	Mild steel	Flexible	FEM; CEL	Bi-linear rigid elements in FEM software	Linear Mie–Grüneisen equation-of-state	Numerical	Blast loading	Uses the CEL method in FE analysis to investigate maximum hoop stress and shear stress in the tank wall under blast loading
(J. Wang et al., 2012)	3-D Cylindrical	–	Rigid	Semi-analytical; sub-domain	Linear behavior	Linear wave theory	Numerical	Horizontal harmonic and monodirectional seismic	Proposes a method to examine structural responses of multi-baffled rigid cylindrical tanks against horizontal excitations using the semi-analytical subdomain method; the method has a high accuracy and small computational cost compared to FE and BE methods

Continue on the next page

Table 2.1: An overview of different dynamic modeling techniques proposed for the coupled fluid-tank system

Reference	Shape	Material	Wall flexibility	Modeling methodology	Structural behavior	Fluid behavior	Study approach	Excitation	Remarks
(Shekari, 2018)	Rectangular	Concrete	Flexible and Rigid	FEM; BE-FE-BE	Linear elastic	Linear wave theory	Numerical	Horizontal monodirec-tional seismic	Investigates the three-dimensional problem of soil-structure-fluid interaction for base-isolated rectangular concrete tanks; shows that base-isolation reduces the earthquake effects by lengthening the structure's fundamental natural period in many earthquakes but has adverse effects for special cases of soil stiffness and shaking frequency
(Y. Sun et al., 2021)	3-D Cylindrical	–	Rigid	Semi-analytical; sub-domain	Linear	Linear wave theory; neglecting hydrodynamic damping	Numerical	Horizontal harmonic and bidirectional seismic	A novel lumped parameter model is proposed for rigid circular cylindrical tanks under horizontal excitations; the proposed model can provide results of satisfactory accuracy with much smaller computational cost for complex fluid-structure systems, compared to FE analyses

Continue on the next page

Table 2.1: An overview of different dynamic modeling techniques proposed for the coupled fluid-tank system

Reference	Shape	Material	Wall flexibility	Modeling methodology	Structural behavior	Fluid behavior	Study approach	Excitation	Remarks
(Ghaemmaghami & Kianoush, 2010)	2-D Rectangular	Concrete	Flexible	FEM	Linear	Linear wave theory	Numerical	Horizontal and vertical seismic	Vertical acceleration of ground motion was shown to have a less significant effect on the dynamic response of the liquid tank system when horizontal and vertical components of excitation are applied simultaneously
(Compagnoni & Curadelli, 2018)	3-D Cylindrical	Steel	Flexible	–FEM; Lagrangian – simplified mechanical model by Malhotra (P. K. Malhotra et al., 2000)	Linear	Linear wave theory	Numerical and experimental	Horizontal monodirec-tional seismic	Comparative study showed virtually similar fundamental mode frequency of the tank-liquid system for considered three models. However, the simplified mechanical model provided underestimated maximum sloshing wave height while overestimating maximum base shear and overturning moment on the conservative side

Continue on the next page

Table 2.1: An overview of different dynamic modeling techniques proposed for the coupled fluid-tank system

Reference	Shape	Material	Wall flexibility	Modeling methodology	Structural behavior	Fluid behavior	Study approach	Excitation	Remarks
(Kang et al., 2019)	Cylindrical	–	Rigid	CFD technique	Linear	Nonlinearity of the fluid motion	Numerical and experimental	Seismic; longitudinal, transverse, vertical, and their combined actions	Examines non-linear hydrodynamic pressure over the inner wall of the tank using CFD technique; studies the effect of the vertical ground motion over the hydrodynamic pressure of the tank; concluded that vertical ground motion significantly increases the hydrodynamic pressure on the inner wall; effects of water elevation and tank dimensions on the hydrodynamic pressure under combined vertical-horizontal seismic motion are investigated; the study considers multi-phase flow, mass transfer between phases, and Coriolis effects as a result of a combination of vertical and horizontal seismic motions

2.3 On the damping of the fluid-tank system

One of the key factors that considerably affects the seismic response of fluid storage tanks is the effect of damping on the dynamic responses of the coupled fluid-tank system. While some studies neglect the effect of damping in their calculations, others apply the same damping ratios proposed in similar studies over the seismic analysis of these structures. Proposed values for impulsive and convective damping ratios in pioneering works over fluid storage tanks form the basis of design procedures in the well-known standards including API 650 (API, 2005), Eurocode 8, Part 4 (EN, 2006), NZSEE (Priestley, 1986; NZSEE, 2009), ACI 350.3-06 (ACI, 2009), IITK-GSDM (IITK-GSDMA, 2007), UNI EN 14015 (EN, 2004), and AIJ (Japan, 2010).

Considering the impulsive mass in the tank moves in unison with the tank wall, it has been regarded that its damping ratio is governed by the damping characteristics of the tank wall which depends on the materials used for the tank. It has been observed in almost all studies conducted on the dynamic behavior of fluid storage tanks that the damping ratios of 2% for steel tanks and 5% for concrete tanks have been considered for the impulsive mass. The damping ratio for the convective fluid (sloshing liquid) has been considered as 0.5%. Classical Rayleigh damping has been used to construct the dynamic equation of motion in which α parameter accounts for the damping ratio of the convective mode of vibration and β represents the damping of the impulsive mode. All codes specify the convective damping ratio of 0.5%. API 650 (API, 2005) and ACI 350.3-06 (ACI, 2009) standards consider a damping ratio of 5% for the impulsive mode of vibration. Eurocode 8-4 (for the Serviceability Limit State) (EN, 2006) recommends 2% damping ratio for anchored and unanchored tanks on rigid foundation (Ozdemir, Souli & Fahjan, 2010). In contrast, NZSEE (Priestley, 1986; NZSEE, 2009) defines distinct damping levels for impulsive mode depending on the soil type, type of support, and direction of seismic loading (horizontal or vertical). It has been reported by Morris et al. (Morris et al., 2013) that NZSEE recommends a damping ratio of 3% for tanks with dominant impulsive mode and H/D of 1.5. In between, larger values of impulsive mode damping ratios of 4% for steel and 7% for concrete have been recommended by

Eurocode 8 for Ultimate Limit State. A damping ratio of 0% has been observed in the study by Scharf (Scharf, 1993).

Recently, the interesting and challenging research by Habenberger (Habenberger, 2015) investigated the effects of the geometry of the shell and viscosity of the fluid on the convective damping and justified numerically that all above recommended values of the convective damping are too optimistic. This study applied a one-dimensional shear flow to consider the tangential interaction conditions at the tank wall and bottom as well as the normal boundary conditions in the potential equations of an ideal fluid. It was proved that this shear flow results in the decrease of the mechanical energy of the liquid-tank system due to the friction on the tank wall and bottom as a result of the radial and circumferential fluid flow. This study showed that by decreasing the radius of cylindrical tanks the convective damping will increase which is due to an increase in the surface-to-volume ratio. This phenomenon was related to the transport of impulse by diffusion being faster than convection. Effects of the frequency of the input excitation, the tank size, and the viscosity of the fluid were signified in this study as well.

2.4 Types of damages observed in previous seismic events

Elephant foot buckling and diamond-shaped buckling are among the major and widely observed types of damage that have occurred to fluid storage tanks in previous earthquakes. However, depending on the type of supports, size of the tank and aspect ratio, type of enclosure (open top, flat roof, conical roof, etc.), and applications of the liquid storage tanks, other types of damage may occur as well. Seismic performance and damages that occurred to these systems during well-known previous earthquakes have been investigated in the literature. Examples of major past seismic events which caused severe damages to fluid-contained tanks include the 1960 earthquake in Chile (Steinbrugge & Flores A, 1963), the 1964 earthquake in Alaska (Hanson, 1973), the 1977 earthquake in San Juan, Argentina (Manos, 1991), the 1979 Imperial County earthquake, California (Gates, 1980), the 1980 Livermore earthquake, California (Niwa & Clough,

1982), the 1983 Coalinga earthquake, California (Manos & Clough, 1985), the 1984 Morgan hill earthquake, California (Swan, Miller & Yanev, 1985), the 1994 Northridge earthquake, California (Hall, Holmes & Somers, 1995), the 2014 Napa Valley earthquake, California (Fischer et al., 2016), the 2001 Bhuj earthquake in India (Jain, LETTIS, MURTY & Bardet, 2002), the 2010 Maule earthquake in Chile (González et al., 2013; E. F. Cruz & Valdivia, 2011; Zareian et al., 2012), the 2012 Emilia earthquake, Italy (Brunesi et al., 2015), the 2003 Tokachi-Oki earthquake, Japan (Hatayama, 2008), the 2008 Wenchuan earthquake, China (Krausmann, Cruz & Affeltranger, 2010), the 1999 Kocaeli earthquake, Turkey (Suzuki, 2002), the 2013 earthquake in Seddon, Cook Strait, New Zealand (Rosewitz & Kahanek, 2014), the 2013 Lake Grassmere earthquake, New Zealand (Morris et al., 2013), the 2016 Kaikōura earthquake, New Zealand (Dizhur et al., 2017), among others. Investigations of observed damages that occurred to these tanks and their dynamic behavior during such extreme events reveal the paramount importance of seismic protection and the exact dynamic modeling of these structures.

Damage observations during above mentioned earthquakes have disclosed several types of damages in liquid storage tanks including: 1) Elephant foot buckling, 2) Diamond shape buckling, 3) anchor bolt buckling, 4) bracket failure, 5) bolt elongation, 6) displaced anchor, 7) barrel insulation damage, 8) tank pounding by neighbouring tanks, 9) cone creasing, roof buckling and/or damage to roof and top zones of the tank, 10) catwalk indent, 11) brace buckling, 12) leg buckling, 13) base punching, 14) leg tilting, 15) global movement, 16) telescopic buckling, 17) anchor pull-out and slab damage, 18) ruptured anchor bolt, 19) leaning of the tank, 20) failure of the brace, 21) skirt damage, 22) loose bolt, 23) base knuckling (for tanks over plinths), and 24) damage to piping system (Fischer et al., 2016; Yazdanian, Ingham & Dizhur, 2019; Yazdanian, Ingham, Lomax et al., 2020; Yazdanian, Ingham, Kahanek et al., 2020; Yazdanian, Ingham & Dizhur, 2020). Such damages to fluid storage tanks as vital elements of industrial plants can cause adverse environmental impacts and substantial financial and human losses. It is noteworthy that damages observed at the top zone of the tank are mostly due to the suction caused by loss of the liquid, or the sloshing liquid impacting the upper part of the tank. The latter occurs in cases where the convective pressure is highly

considerable under certain seismic motions with frequencies that govern the frequency of the convective mode.

A review of different types of damages occurred to steel liquid storage tanks at wineries has shown that elephant foot buckling has been more common to broad tanks while diamond shape buckling has been observed more often in slender tanks (Fischer et al., 2016). Elephant foot buckling is caused by a combination of vertical compressive stresses and hoop tension stresses when they exceed the corresponding critical buckling stress and yield limit of the tank wall, respectively. Diamond shape buckling is developed as a result of large vertical compressive stresses. Investigations of damages during the 2013 Seddon earthquake in Cook Strait, New Zealand, have demonstrated that elephant foot buckling, diamond shape buckling, pounding damage by neighboring tanks, damage to catwalk connections, anchorage failure, and damage to the piping system, have been the most common types of damages (Fischer et al., 2016).

The presence of an opening or cutout in the tank wall for access purposes increases the propensity of the shell to buckling occurrence even with stiffening around the cutout area. Considerable stress concentrations around the opening and contribution of the cutout to significant shell buckling have been well presented in (Brunesi & Nascimbene, 2018). This research presented examples of damages that occurred to fluid storage tanks in relation to wall opening during the May 2012 Emilia earthquake (Brunesi et al., 2015). Large shell buckling was observed in the damaged tanks even in the presence of reinforcement for the cutout. Due to the significant role of opening in the shell buckling phenomenon, a series of research works were initiated to address strengthening techniques to improve the behavior of such tanks (Hilburger & Starnes Jr, 2005; Alsalah, Holloway & Ghazijahani, 2017; Ghazijahani, Jiao & Holloway, 2015). More detailed analyses were conducted by Brunesi and Nascimbene (Brunesi & Nascimbene, 2018) by considering the material and geometrical nonlinearities. They examined the influence of the opening's shape, size, position, and number in the shell over the buckling and post-buckling responses of cylindrical thin-walled steel liquid storage tanks using sophisticated FE models.

2.5 Seismic energy-dissipating devices for fluid tanks

As stated earlier in this chapter, one of the major contributors to the dynamic behavior of fluid storage tanks is the sloshing phenomenon in partially filled liquid storage tanks. Liquid sloshing highly affects the dynamic responses of fluid-contained tanks, can cause damage to the upper part of the tank and roof, may result in spillover, and could have catastrophic environmental consequences. This phenomenon can result in the instabilities of moving tanks and those excited at the base under earthquakes in civil and industrial sectors (Zama et al., 2012; Hatayama, 2008; Yazici & Cili, 2008). Thus, a major part of experimental and numerical approaches and control techniques in the field of fluid storage tanks have been dedicated to slosh dynamics and control. Such investigations and techniques will have a variety of applications in different industries from civil engineering to mechanical engineering, maritime industries, and aerospace, to name but a few. The flow chart in Figure 2.2 depicts different energy-dissipating devices and their variants investigated in literature for seismic protection and energy dissipation of fluid storage tanks, numerically and/or experimentally.

2.5.1 Base isolators

For seismic response mitigation of liquid storage tanks, some energy-dissipating devices have been proposed by researchers from the early research works in this field. Elastomeric bearings, lead rubber bearings (LRB) (also called N-Z system as it was first invented in New Zealand), high damping rubber bearings (HDRB), pure friction system, friction pendulum system (FPS), resilient-friction base isolator, and electric de France are among some of the applied base isolation systems used for seismic protection of liquid storage tanks (M. K. Shrimali & Jangid, 2002; Safari & Tarinejad, 2018; Paolacci, 2015). Elastomeric bearings, LRB, and FPS are among the widely used systems. Different variants of FPS systems include single friction pendulum bearings (SFPB), double friction pendulum bearings (DFPB), triple friction pendulum bearings (TFPB), and variable friction pendulum system (VFPS) (Tsipianitis & Tsompanakis, 2021; Panchal

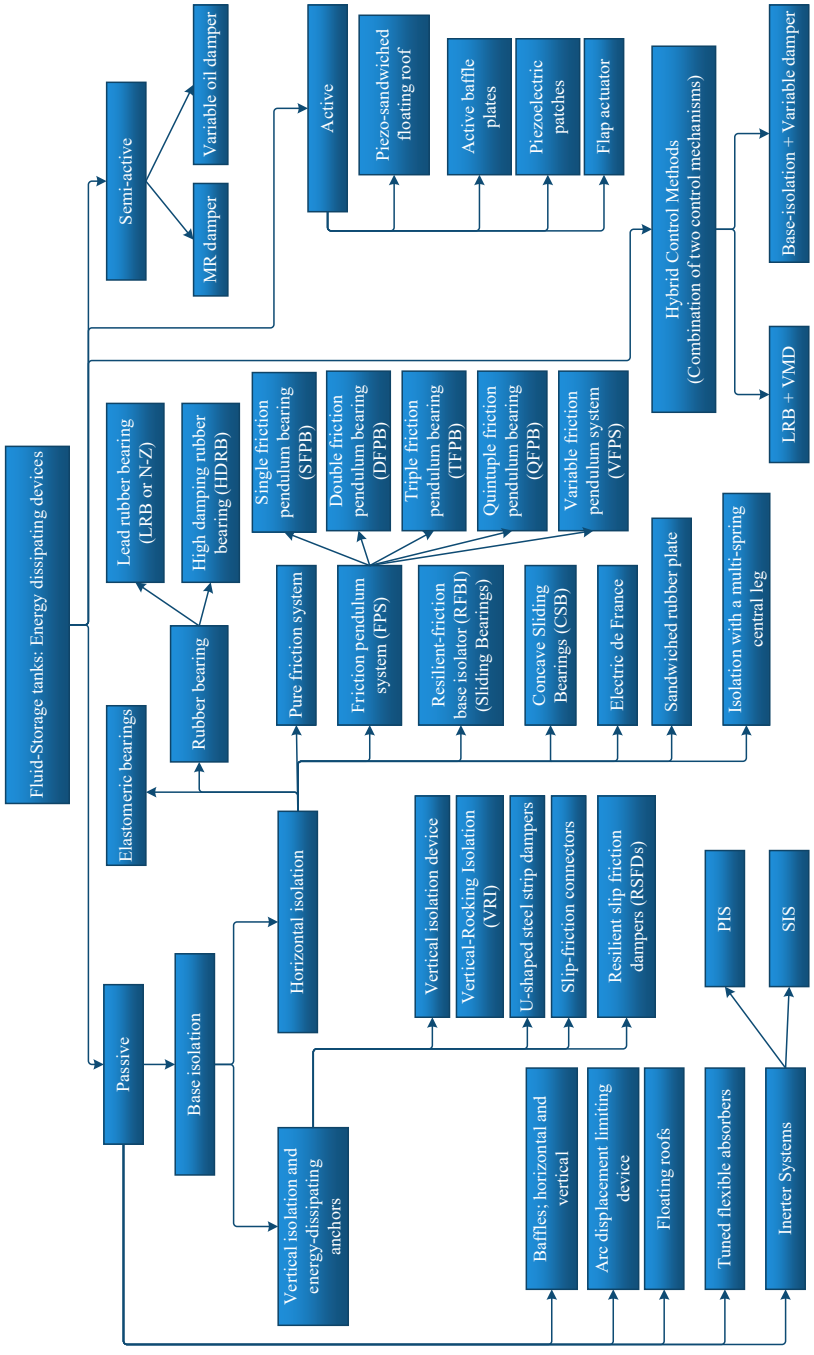

Figure 2.2: Different energy-dissipating devices proposed for vibration mitigation and seismic protection of fluid-storage tanks

& Jangid, 2008; Moeindarbari, Malekzadeh & Taghikhany, 2014). Studies on multiple sliding surfaces led to the extension of TFPB to a new type of friction pendulum bearing named quintuple friction pendulum bearing (QFPB) proposed by (Tsai, Lin & Su, 2010). More advanced studies on the behavior of QFPB were conducted by Lee and Constantinou (Lee & Constantinou, 2016) who suggested analytical models that could trace the behavior of this isolator under loading and unloading as well as geometrical and frictional configurations. A fragility analysis on base-isolated liquid-contained tanks using sliding bearings including SFPB, TFPB, and QFPB was conducted in (Tsipianitis & Tsompanakis, 2018b) with a focus on the isolators' displacements under near-fault ground excitations. Results of this study showed superior efficiency of QFPB in resisting large displacements compared to the other three friction base isolators.

The 1999 Koaceli earthquake in Itzmmit, Turkey, resulted in severe damages or collapses of LNG steel storage tanks resting on short reinforced concrete (RC) columns (Sezen, Livaoglu & Dogangun, 2008) at Habas pharmaceutics plant. The efficacy of FPS and HDRB systems in reducing the seismic response of such tanks were studied in (Paolacci, 2015) using the equivalent mechanical model and time history analyses. Both systems showed high efficiency in reducing base shear and stress levels in the tank wall. However, the FPS device presented a higher capability in reducing the sloshing displacements. Hence the application of sliding bearings was recommended rather than HDRB. Phan et al. (Phan et al., 2016) numerically investigated the efficiency of placing concave sliding bearings (CSB) between the tank base and the top of RC columns for vibration mitigation of the same type of tanks. They applied a 3D lumped mechanical model using OpenSEES (McKenna, Fenves & Scott, 2006) platform and conducted nonlinear dynamic and seismic fragility analyses. Results of their examinations showed the high efficiency of CSB system in reducing column drifts and meridional stress in the tank wall.

Base isolation has proved effective in the reduction of seismic response of liquid storage tanks. However, they do not have a significant effect on liquid sloshing and even can amplify it. Recently, some new devices have been invented such as arc displacement limiting devices (Cheng, Jing & Gong, 2017) proposed for concrete liquid storage

tanks as a step further to remove this drawback. It was deduced that this device could at the same time reduce the wall cracking failure mode. Hybrid control mechanisms through a combination of two different controlling mechanisms (passive+passive or passive+semi-active) have been proposed by some researchers to mitigate seismically induced vibrations in fluid storage tanks. Examples include the application of sliding bearings in combination with another energy-dissipating device like a variable oil damper (Iemura, Igarashi & Kalantari, 2004; Kalantari, 2017) or a viscous mass damper (Luo, Zhang & Weng, 2016) to enhance the efficacy of traditional sliding bearing systems. The major contribution of the hybrid control system proposed by Luo et al. (Luo et al., 2016) is to remove the deficiencies of base-isolation systems which may result in enlarging sloshing heights under certain seismic excitations by adding a Parallel Inerter System (PIS). The impact of different layouts for inerter systems including PIS and Series Inerter System (SIS) for vibration extenuation of fluid storage tanks was investigated by (R. Zhang, Zhao & Pan, 2018). A new type of isolation system made by sandwiching a thin rubber plate between two metal plates has also been proposed by Aoki et al. (Aoki, Bando, Watanabe & Suzuki, 2019). This device had an efficient effect on impulsive pressures under short-period seismic excitations, however, sloshing effects were not suppressed considerably.

Recently a new line of research has been started to improve the seismic response of liquid storage tanks equipped with seismic isolators using the application of Artificial Intelligence (AI) techniques. Examples include the application of a Genetic Algorithm for optimizing parameters of SFPB (Tsipianitis & Tsompanakis, 2018a). Application of several AI techniques including Cuckoo Search, Particle Swarm Optimization (PSO), Cuckoo Search-Bird Swarm Algorithm, and Enhanced Cuckoo Search has been regarded for enhancing the key parameters of SFPB and TFPB for seismic isolation of cylindrical steel fluid storage tanks (Tsipianitis & Tsompanakis, 2021).

2.5.2 Other energy-dissipating devices applied to fluid tanks

The sloshing phenomenon and its consequent damaging effects that occur in moving containers or base-excited fluid storage tanks are the main critical subjects of many industries. Some examples include the automobile industry, aerospace and marine vehicles, fluid-carrying trucks, nuclear plants, the petrochemical industry, oil refineries, hospitals, water supply systems, and wineries, etc. Thus, various passive control systems (Paolacci, Giannini & De Angelis, 2013) such as baffles (Hasheminejad, Mohammadi & Jarrahi, 2014) in different configurations (vertical or horizontal), tuned flexible absorbers (Gradinscak, Semercigil & Turan, 2011), floating roofs (De Angelis, Giannini & Paolacci, 2010), flexible active floating panel (Hasheminejad & Mohammadi, 2016; Hasheminejad, Mohammadi & Jamalpoor, 2020), and a floating roof equipped with viscous dampers (Ozsarac, Brunesi & Nascimbene, 2021) have been proposed by researchers. Application of viscous dampers along with a floating roof proposed by (Ozsarac et al., 2021) is a new energy-dissipating system for designing new fluid storage tanks as well as retrofitting existing ones equipped with floating roofs, specifically for broad tanks used in the oil industries. High-definition FE analyses using the commercial software LS-DYNA (Hallquist et al., 2007) were conducted in this study to account for fluid-structure interaction. Moreover, geometrical and material nonlinearities were considered in analyses as well.

Energy-dissipating anchorages are another category of seismic protection devices proposed by different researchers that allow a partial fixation of the tank and provide a trade-off between the uplift displacement and the axial compressive stress developed in the tank wall. Some instances of such devices are the U-shaped steel strip dampers (J. I. Colombo & Almazán, 2015), vertical isolation (Nikoomanesh, Moeini & Goudarzi, 2019), Vertical-Rocking Isolation (VRI) (Almazán, Cerda, Juan & López-García, 2007), slip-friction connectors (Ormeño, Geddes, Larkin & Chouw, 2015), and Resilient Slip Friction Dampers (RSFDs) (Sahami, Zarnani & Quenneville, 2020, 2021). U-shaped steel strip dampers have widely been used in Japan for energy dissipation of base-isolated structures (Oh, Song, Lee & Kim, 2012, 2013). This type of damper was

applied by Colombo and Almazán (J. I. Colombo & Almazán, 2015) for seismic energy dissipation of ground-based continuously supported slender and broad wine storage tanks. The aim was to avoid two types of damages in fluid storage tanks, namely low-cycle failure at the shell-to-base connection and rupture of the tank wall at the location of anchor bolts (González et al., 2013; Cortes, Nussbaumer, Berger & Lattion, 2011; Prinz & Nussbaumer, 2012a, 2012b). They conducted nonlinear static pushover analysis using ANSYS software as well as nonlinear time history analysis using the equivalent mechanical model of the liquid-tank system. Only the impulsive mass was considered for dynamic analyses under rocking and translational motions. Nikoomanesh et al. (Nikoomanesh et al., 2019) proposed a new type of isolation termed vertical isolation which isolates the tank vertically with potential benefits for rocking motion isolation of tanks. Slip-friction connectors which originally were developed as an energy-dissipating device for steel structures (Butterworth, 2000) were utilized by Ormeño et al. (Ormeño et al., 2015) to reduce the uplift displacement and axial compressive stresses in the tank wall. RSFDs which are based on partial constraining of fluid storage tanks have been proposed (Sahami et al., 2020, 2021) to restrain the uplift displacement of tanks and simultaneously mitigate the induced vertical forces.

In between, studies on seismic protection of stainless steel cylindrical legged fluid storage tanks are very scarce in the literature, whether numerically or experimentally. Such tanks are generally used in the wine industry, among others, and their seismic protection is of paramount importance. One can note the work by Almazán et al. (Almazán et al., 2007) in which they investigated and compared the effectiveness of lateral isolation and a VRI system on the seismic vibrations of legged thin-walled tanks usually applied in the wine industry. They concluded that the novel proposed VRI system offers promising features for response reduction of these tanks compared to traditional isolation systems. An interesting experimental investigation on seismic protection of a full-scale stainless steel cylindrical legged fluid storage tank was conducted by Colombo and Almazán (J. Colombo & Almazán, 2017). They compared the seismic behavior of the fixed-base tank with two isolation configurations, i.e. the flat sliding bearing system, and an isolation mechanism consisting of a multi-spring central leg. Their results showed

that the developed novel isolation system could offer enhanced capabilities compared to the flat sliding bearings in terms of lateral displacement reduction and the seismic force demand in the legs. Application of active baffle plates and actively controlled water tanks using piezoelectric patches for sensing and control have been studied by other researchers (Hernández & Santamarina, 2012; Mehrvarz, Najafi Ardekani, Khodaei & Jalili, 2019). Shrimali and Kasar (M. K. Shrimali & Kasar, 2012) studied the effect of MR dampers on the vibration attenuation of seismically excited connected tanks. An overview of different energy-dissipating devices examined in the literature for seismic protection of fluid storage tanks, controlling mechanisms and techniques, assumptions considered in modeling the dynamic behavior of the system, study approach, application, and some remarks for each method can be seen in Table 2.2.

Table 2.2: Overview of different energy dissipating devices applied for vibration mitigation of fluid storage tank systems

Reference	Energy-dissipating device	Control mechanism	Application	Control technique	Wall flexibility	Dynamic modeling	Structural behavior	Fluid behavior	Study approach	Remarks
(Shekari, 2018)	Base-isolation	Passive	Rectangular concrete water tank	–	Flexible and rigid	BE-FE-BE	Linear elastic	Linear wave theory	Numerical	The isolation system reduces the seismic effects in many earthquakes; however, the isolation effect is highly dependent on the characteristics of the ground motion. So, the base isolation may amplify or control the tank responses.
(Hernández & Santamarina, 2012)	An elastic vertical baffle plate	Active	3-D Rectangular steel water tank	Active vibration control (AVC)	Rigid	FEM	Linear elastic	Linear wave theory	Numerical	A model of a 3-D rectangular steel tank equipped with one vertical internal baffle plate in the middle to represent a water tank in one case and two horizontal plates in the other case to simulate a liquid fuel storage pool (LFSP).

Continue on the next page

Table 2.2: Overview of different energy dissipating devices applied for vibration mitigation of fluid storage tank systems

Reference	Energy-dissipating device	Control mechanism	Application	Control technique	Wall flexibility	Dynamic modeling	Structural behavior	Fluid behavior	Study approach	Remarks
(Mehrvarz et al., 2019)	Piezoelectric patches for sensing and control attached to one flexible side wall	Active	2-D Rectangular water tank	Boundary controller	Rigid wall at one end and flexible wall at the other end	Analytical and FEM	Linear elastic	Linear wave theory	Numerical	The operational range of applied voltage to the piezoelectric actuator is ±250 ν to simulate a real condition. Fluid and structural damping have not been considered in the dynamic modeling of the system. The system has been examined under an initial condition being a potential velocity in the center of the fluid. The controller proves a proper speed in mitigating vibrations.

Continue on the next page

Table 2.2: Overview of different energy dissipating devices applied for vibration mitigation of fluid storage tank systems

Reference	Energy-dissipating device	Control mechanism	Application	Control technique	Wall flexibility	Dynamic modeling	Structural behavior	Fluid behavior	Study approach	Remarks
(Hasheminejad et al., 2020)	Piezo-sandwiched floating roof panel	Active	3-D Rectangular water tank	Active damping control (ADC)	Rigid	Analytical and FEM	Linear	Linear wave theory	Numerical	The numerical model of a 3-D rectangular tank filled with water has been examined under a seismic-bidirectional event (Elcentro 1940), an oblique planar base excitation, and a distributed impulse floating roof excitation. The focus of the study is on the suppression of transient liquid sloshing in rectangular tanks with rigid walls. The study presents an analytical model for 3-D forced transient liquid sloshing in a rectangular tank with a floating roof.

Continue on the next page

Table 2.2: Overview of different energy dissipating devices applied for vibration mitigation of fluid storage tank systems

Reference	Energy-dissipating device	Control mechan-ism	Application	Control technique	Wall flexibility	Dynamic modeling	Structural behavior	Fluid behavior	Study approach	Remarks
(Iemura et al., 2004)	Base isolation, and base isolation in combination with a variable damper	Passive and Hybrid (passive + semi-active)	2-D Cylindrical	Pseudo negative stiffness (PNS)	Rigid	Equivalent mechanical model (Housner, 1963b)	Linear	Linear wave theory	Numerical	The numerical model examines the seismic responses of a tank model equipped with three control mechanisms; two base isolation mechanisms and a hybrid system. The model equipped with the hybrid system resulted in the least base shear of the tank and lower values of both accelerations and displacements. Application of semi-active PNS algorithm generates larger hysteresis loops and more energy dissipation.

Continue on the next page

Table 2.2: Overview of different energy dissipating devices applied for vibration mitigation of fluid storage tank systems

Reference	Energy-dissipating device	Control mechanism	Application	Control technique	Wall flexibility	Dynamic modeling	Structural behavior	Fluid behavior	Study approach	Remarks
(M. K. Shrimali & Kasar, 2012)	MR dampers	Semi-active	2-D Cylindrical	Lyapunov's direct approach	Rigid	Equivalent mechanical model (Housner, 1963b)	Linear	Linear wave theory	Numerical	The study uses the simplified mechanical model of Housner (Housner, 1963b) for the rigid fluid-tank model, the Modified Bouc-Wen model for the dynamic behavior of MR damper, and Lyapunov's direct approach for semi-active control.

2.6 Vibration control techniques for fluid tanks

Base isolation systems of different types have major effects on the impulsive mode while minor on the sloshing modes of vibration of tanks. Other passive systems like baffles and absorbers are known as largely used systems for slosh control in different sectors of industries for fluid storage tanks (Muto, Kasai & Nakahara, 1988; Modi & Munshi, 1998; Ikeda & Ibrahim, 2014). As a step further to remove drawbacks of passive systems like added complexity and weight to the overall system, active control systems have been introduced. Theoretical and experimental studies have been conducted for this purpose (Reid & Russell, 1985; Hara, 1994). Some instances of control techniques proposed in the literature for slosh control in fluid storage tanks include the Linear Quadratic Gaussian (LQG) controller (Venugopal & Bernstein, 1996), Proportional-Integral (PI) controller (Sira-Ramirez, 2002), sliding-mode control and Proportional-Integral-Derivative (PID) schemes (Bandyopadhyay, Gandhi & Kurode, 2009; Kurode, Spurgeon, Bandyopadhyay & Gandhi, 2012; Richter, 2010; Acarman & Ozguner, 2003), H∞ control (Yano & Terashima, 2001; Terashima & Schmidt, 1994), nonlinear feedback control based on Lyapunov theory and robotic control (Reyhanoglu & Hervas, 2013a, 2013b), nonlinear feedback Lyapunov control (Reyhanoglu & Hervas, 2012), infinite impulse response filter (Feddema et al., 1997), acceleration compensation based on the Waiter-Tray idea (S. J. Chen, Hein & Worn, 2007), input shaping (Terashima, Hamaguchi & Yamaura, 1996; Pridgen, Bai & Singhose, 2013; Terashima & Yano, 2001; Aboel-Hassan, Arafa & Nassef, 2009), hybrid-shaped technique for suppressing residual 3D slosh (Yano & Terashima, 2005; Yano, Toda & Terashima, 2001), and adaptive control (Adler, Lee & Saugen, 1991), among others.

Zang and Huang (Zang & Huang, 2014) used a command smoother as well as the combined input shaper and a low-pass filter (Singhose, Eloundou & Lawrence, 2010) to reduce the 3D slosh in a moving container while assuming small amplitude free surface vibrations of the liquid in a rectangular container. Simultaneous H∞ optimal controller for a coupled flexible fluid-structure model representing the dynamic behavior of a plane wing using piezoelectric actuators has been studied in (Robu, Baudouin, Prieur

& Arzelier, 2012). Finite dimensional approximation for the flexible plate, the linearised Bernoulli equation for the fluid, and the mass-pendulum mechanical approximation of the fluid-tank system have been regarded in this study. Another study on a similar model was conducted by Budinger et al. (Pommier Budinger, Richelot & Bordeneuve-Guibe, 2006) using Generalised Predictive Control and based on the Lagrangian FE approach. Hernández and Santamarina (Hernández & Santamarina, 2012) applied an optimal control technique based on the Active Vibration Control (AVC) to suppress the sloshing modes in a rectangular container with an internal plate based on the added mass theory and Reissner-Mindlin equations for the internal plate. Application of a flexible beam at one end of a rectangular partially filled tank with rigid baffles for vibration attenuation of a fluid storage tank was proposed by Mehrvarz et al. (Mehrvarz et al., 2019). In this study, piezoelectric sensors and actuators, a boundary controller based on Lyapunov function, and the piezoelectric voltage were applied for control purposes. They modeled the coupled equation of motion using the FE analysis, Hamilton principle, and the Green's first formula. Moreover, the Newtonian barotropic, inviscid, irrotational, and compressible fluid with low velocity and small amplitude free surface liquid oscillations are among the most important assumptions for formulations in this study. Also, it is noteworthy that the operating voltage of the piezoelectric actuator in this study was defined in the range of ±250 v to simulate a real condition. The boundary controller in this study was applied to avoid discretization of partial differential equations of the coupled fluid-structure system.

Hasheminejad and Mohammadi (Hasheminejad & Mohammadi, 2016) applied the active damping control (ADC) technique for mitigating the transient liquid slosh of rigid and flexible cylindrical tanks with a piezo-sandwich thin elastic circular floating plate. They implemented the linear potential theory, Kirchhoff's piezo-sandwich circular plate equations, Sander's classic thin shell model, and the classical Maxwell's equation of electrodynamics in their formulations. In this study, two AI techniques, i.e. multi-objective particle swarm optimization (MOPSO) and Non-dominated Sorting Genetic Algorithm (NSGA-II) have been used to obtain the control gains in a Proportional-Derivative (PD) control action and produce a feedback voltage for the piezo-actuator.

Results showed the superiority of the MOPSO approach in terms of convergence rate and computational effort compared to that of NSGA-II. A similar study using this control strategy was conducted on a rigid rectangular parallelepiped container under planar base excitation and bidirectional seismic events while a PI control action was applied for obtaining the input voltage to the piezo-actuator (Hasheminejad et al., 2020).

A semi-active control technique for suppression of the sloshing liquid motions was presented by Kobayashi and Koyama (Kobayashi & Koyama, 2010) for a rectangular closed vessel based on switching the air spring effect of gas chambers through a controllable valve. Iemura et al. (Iemura et al., 2004) applied the Pseudo Negative Stiffness (PNS) semi-active control algorithm for the application of a variable damper in combination with a linear elastic element as the base isolation to control a cylindrical liquid storage tank based on the equivalent mechanical model of Housner (Housner, 1963b). The rigid impulsive and the first convective modes were regarded in this study. They compared the results of the hybrid semi-active-passive scheme with two other passive cases including base isolation with linear elastic and nonlinear behavior. Results showed that the hybrid control strategy could effectively control both force and displacement contrary to the other two cases that decreased one parameter while increasing the other. Also, the hybrid system produced the least vibrational energy of the sloshing liquid (sum of the kinetic and strain energy of the convective mass) compared to the other two cases. Table 2.3 shows different vibration control strategies applied in the literature for the design of the vibration control for fluid storage tanks, the control mechanism implemented, application, dynamic modeling methodology, mode of study, the desired control objective, and a few remarks on each approach.

Table 2.3: Different vibration control schemes proposed for vibration mitigation of fluid in fluid containers and fluid-storage tanks

Reference	Control scheme	Control mechanism	Application	Dynamic modeling	Mode of study	Purpose of study	Remarks
(Venugopal & Bernstein, 1996)	Active feedback control based on LQG method	1-Surface pressure control based on acoustic waves and a speaker mounted on the top of the closed tank 2- Flap actuator at the surface of the fluid in an open-top tank	Rectangular tank	Analytical based on velocity potential of the fluid and continuity equation	Numerical	Mitigation of sloshing waves of liquid in the tank	Closed-loop performance was demonstrated numerically
(Sira-Ramirez, 2002)	Linear feedback control using a Generalised PI control method based on flatness-based controllers	–	Open containers carrying liquid	Analytical	Numerical	Liquid sloshing control in a moving container	Flatness-based controller assures controlling both horizontal movements and sloshing of the fluid surface waves

Continue on the next page

Table 2.3: Different vibration control schemes proposed for vibration mitigation of fluid in fluid containers and fluid-storage tanks

Reference	Control scheme	Control mechanism	Application	Dynamic modeling	Mode of study	Purpose of study	Remarks
(Acarman & Ozguner, 2003)	Sliding mode control	–	Fluid-carrying vehicles	Equivalent mechanical model – spring-mass-damper model for longitudinal sloshing and pendulum model for lateral sloshing	Numerical	To stabilize and attenuate fluid sloshing in liquid-carrying vehicles	The designed controller reduces the sloshing effects of the liquid in partly filled fluid-carrying vehicles
(Bandyopadhyay et al., 2009)	Sliding mode controller based on PID scheme	Active control mechanism using actuators	Acrylic cylindrical tank	Equivalent mechanical model; pendulum model for the fundamental mode of lateral sloshing	Numerical and Experimental	Suppressing lateral slosh of the liquid in a moving container	Experimental results show the efficiency of the proposed technique for slosh suppression using an effective observer for estimating states and control of the nonlinear system of slosh dynamics

Continue on the next page

Table 2.3: Different vibration control schemes proposed for vibration mitigation of fluid in fluid containers and fluid-storage tanks

Reference	Control scheme	Control mechanism	Application	Dynamic modeling	Mode of study	Purpose of study	Remarks
(Hernández & Santamarina, 2012)	Optimal control	Actively controlled baffle plates	3-D rectangular steel tank representing a water tank and a liquid fuel storage pool (LFSP)	Locking-free FEM	Numerical	Suppress of liquid slosh	In both cases the tank was considered filled with water; the optimal control technique for slosh control using an active vibration control algorithm was applied
(M. K. Shrimali & Kasar, 2012)	Lyapunov's direct approach	MR dampers	Connected liquid storage tanks	Equivalent mechanical model	Numerical	To control vibrations of fluid storage tanks by connecting them via MR dampers to avoid damage from adjacent tanks.	MR dampers have been considered schematically at the positions of impulsive and convective masses to control the vibrations of these two modes. It has been concluded that placing the damper at the location of the sloshing mass will produce more effective results

Continue on the next page

Table 2.3: Different vibration control schemes proposed for vibration mitigation of fluid in fluid containers and fluid-storage tanks

Reference	Control scheme	Control mechanism	Application	Dynamic modeling	Mode of study	Purpose of study	Remarks
(Zang & Huang, 2014)	Command smoothing technique	AC servomotors with encoders	3-D moving rectangular container	Analytical; velocity potential	Numerical and experimental	To control 3-D slosh dynamics of moving rectangular fluid containers under planar excitations	The command smoothing technique was used for suppressing 3-D slosh in moving rectangular liquid containers. Comparative studies between the proposed technique and the combined input shaper and low-pass filter showed more robustness and higher performance of the former method against sloshing frequency changes and reduction of transient and residual slosh vibrations
(Mehrvarz et al., 2019)	Boundary control technique	Piezoelectric patches for sensing and control attached to one flexible side wall	2-D Rectangular water tank	Analytical and FEM	Numerical	To control the fluid-structure vibrations	Piezoelectric transducers have been applied to control vibrations. Numerical results show fast response of the control system in mitigating vibrations

Continue on the next page

Table 2.3: Different vibration control schemes proposed for vibration mitigation of fluid in fluid containers and fluid-storage tanks

Reference	Control scheme	Control mechanism	Application	Dynamic modeling	Mode of study	Purpose of study	Remarks
(Hasheminejad et al., 2020)	Active damping control (ADC)	Piezo-sandwiched floating roof panel	3-D Rectangular water tank	Analytical and FEM	Numerical	Suppressing slosh responses of a 3D rectangular tank with a floating roof	A floating roof panel controlled in an active control scheme using piezoelectric actuators proved to suppress sloshing responses effectively compared to an uncontrolled floating panel

2.7 Structural health monitoring techniques for fluid tanks

Earthquakes are one of the major contributors to the Natech events (Natural Hazards Triggering Technological Disasters) which are described as technological accidents caused by natural hazards that can result in the release of hazardous materials (Mesa-Gómez, Casal & Muñoz, 2020; A. M. Cruz & Krausmann, 2013; Krausmann & Cruz, 2017). On the other hand, as mentioned earlier at the beginning of this review, fluid storage tanks are one of the most critical components in industrial plants and any damage to them can pose serious risks to human life and the reliability of the corresponding industries. Also, it was notified that these systems are categorized as acceleration-sensitive non-structural elements in FEMA 274 (Council, 1997) and are the subject of Chapter C9, 'Vertical Liquid-Storage Tanks' of the nuclear code ASCE/SEI 4-16 (ASCE, 2017). Substantial forces that govern the seismic design of these structures are the base shear and overturning moment due to large hydrodynamic pressures caused by the seismic ground accelerations. These forces will result in compressive, hoop, and bending stresses in the tank shell. To the best knowledge of the authors, contrary to the wide research conducted on a variety of structural health monitoring (SHM) techniques proposed and implemented for buildings and other infrastructure, either numerically or experimentally, much less has been done regarding the fluid storage tanks.

Fluid-structure interaction and the sloshing phenomenon in partially filled fluid storage tanks highly complicate the dynamic behavior of the whole system. In addition to this effect, the presence of fluid in the tank causes the parameters of the coupled system including mass, stiffness, and damping to change over time, leading to a time-varying system. Hence, the development of SHM techniques for these structures is an extra challenge. However, these techniques will assist in monitoring and predicting structural conditions and any current or potential future damages in these vital systems. Vibration-based damage detection techniques have been implemented in (Shaheen, Eltaly & Abd-Alla, 2013; Curadelli & Ambrosini, 2011; Zhou, Wu & Mevel, 2010) to remove

limitations of quasi-static monitoring in the detection of damages far away from the sensors by relying on global damage detection approaches. Fiber Optic sensors including Fiber Bragg Grating (FBG) and Fiber Segment Interferometry (FSI) represent promising, noninvasive, and robust types of sensors for the purpose of SHM for fluid storage tanks and the related industries (Salimbeni, De Angelis, Vezzari & Ciucci, 2022). Application of these types of sensors has been discussed in (Salimbeni et al., 2022) for SHM and seismic risk mitigation of fluid storage tanks, in particular liquid storage tanks with floating roofs. Other instances of implementation of these sensors for damage detection and SHM of CNG and composite tanks, steel pipes, and storage tanks can be found in (Glisic & Inaudi, 2004; Park, Kang, Bang, Park & Kim, 2006; Almahmoud, Shiryayev, Vahdati & Rostron, 2018). Distinguishing features of these sensors have turned them into a reliable alternative for SHM purposes for fluid storage tanks. These characteristics include robustness, multifunctionality, immunity to electromagnetic interference, insensitivity to erosion and oxidation, and ability to be continuously and remotely controlled under different operational and environmental conditions, etc. (Salimbeni et al., 2022). Thanks to these features, they have found many applications in a variety of strategic industries including oil and gas (Paolacci et al., 2021), among others. Therefore, authors in (Salimbeni et al., 2022) have discussed the application of these sensors for the detection of multiple main damages and occurrences common to fluid storage tanks, namely elephant foot buckling, diamond shape buckling, base uplift, anchor failure, and damages to the piping system, foundation of the tank, and the floating roof.

Rainieri et al. (Rainieri, Gargaro, Reynders & Fabbrocino, 2020) conducted experimental tests using accelerometers and proposed a modal-based SHM technique based on a covariance driven stochastic subspace identification approach. They considered the proposed method for fluid storage cylindrical steel tanks used in hospitals to detect damages at anchors. The bolt loosening was regarded as the type of damage in their studies while the operational (fluid level) conditions were considered as the influential factor in the damage detection procedure. It is worth mentioning that in this study the damping ratios of 1-2% for flexural modes and 0.1-0.2% for oval modes based on only fundamental circumferential waves, have been estimated. Numerical FE analyses were

applied using ANSYS. Obtained data were refined based on experimental results to assess the influence of the selected operational conditions on the dynamic responses of the tank. Zhou et al. (Zhou et al., 2010) used a similar approach based on statistical model-based subspace modal identification for damage detection in composite fuel storage tanks in the time domain. They considered the linear behavior of the system and the proportional damping in formulating the dynamic equation of motion. The input forces were taken as unmeasured non-stationary zero-mean Gaussian white noises. They used accelerometers in the experimental setup and applied high-frequency external excitations. The selection of excitation frequencies far from the natural frequencies of the fluid in this study made the authors able to consider the coupled system as a single linear dynamical model. Hence, it was possible to determine the eigenvalues and eigenvectors for the coupled system. Figure 2.3 displays some of the proposed or applied SHM techniques for damage detection of fluid storage tanks in the literature.

2.8 Summary

Based on this literature review, the below conclusions can be drawn:

- Different analytical, semi-analytical, and numerical approaches proposed in the literature for modeling the complex dynamic behavior of fluid storage tanks, from pioneering works up to the present, have been reviewed in this chapter. From the early attempts in this field, the simplified mechanical model of mass-spring-dashpot and/or the pendulum model have been proposed to represent this coupled dynamical system in the form of impulsive and convective modes. These models form the basis of analysis and design methods that are widely used in different standards for the seismic design of fluid storage tanks. In the first versions, only one impulsive mode considering the rigid shell and one convective mode were considered for analyses. However, further research and experiments proved that the flexibility of the tank shell (especially for steel tanks) and higher convective modes should be considered for more exact analysis and design of these tanks.

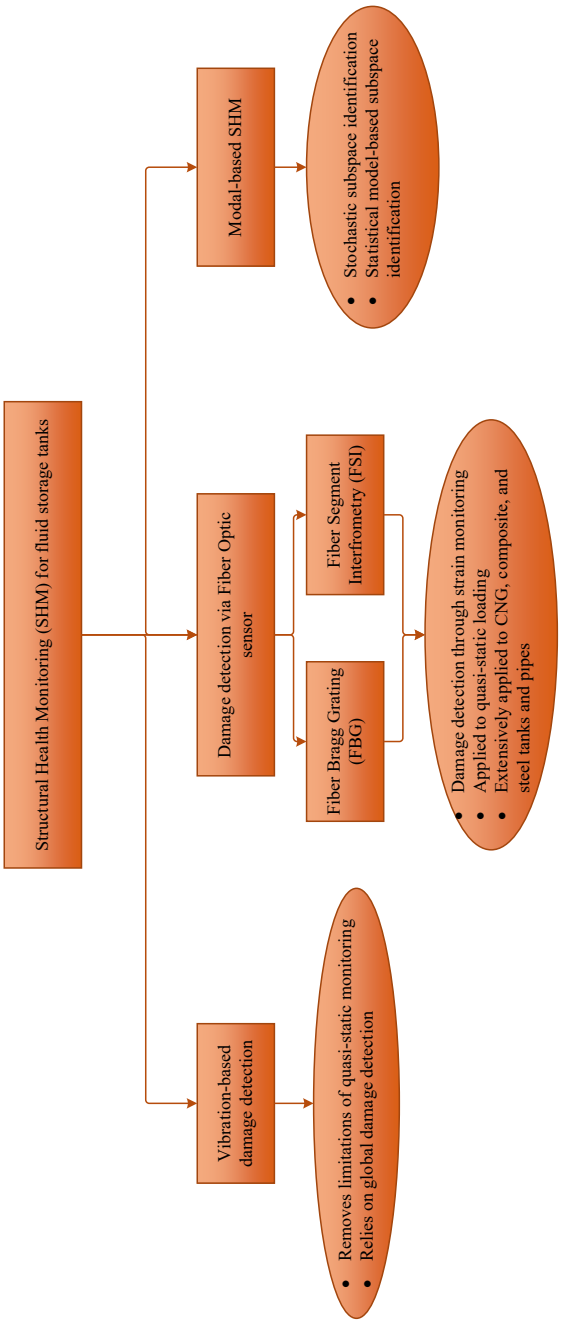

Figure 2.3: SHM techniques for fluid storage tanks

- Types of the tank's closure, i.e. no-closure (open top), conical, flat, and dome-type closure can affect the dynamic response of the tanks, differently. Evidently, the dynamical responses would be affected by the sloshing liquid and the convective pressure on the roof, which should be considered in the analysis and design of tanks. Some studies consider the roof as a single degree of freedom in formulating the dynamic equation of motion for the system.

- Studies have shown that the flexibility of the soil/foundation can considerably affect the dynamic responses of the tank. In this case, the rocking motion of the base/foundation with the appropriate stiffness and damping parameters of the underlying soil will enter the coupled equation of motion to consider the SSFI effects on the dynamic responses of the fluid storage tank.

- Based on the studies conducted in the literature, the combined vertical and horizontal components of the seismic event would generate higher vibrational effects in these structures. Therefore, it is required to evaluate the seismic responses of fluid storage tanks under these circumstances.

- Characteristics of the input excitations, including frequency and amplitude non-stationarity, the frequency content, and period can affect the seismic responses of fluid storage tanks, especially the sloshing mode of the fluid vibrations, in different ways.

- Accuracy, applicability, and validity of the proposed simplified mechanical model of fluid storage tanks have been studied by different researchers. Some researchers compared the obtained results of the simplified model with that of numerical results based on more detailed FE analyses using commercial software packages like ANSYS or ABAQUS or experimental findings. They deduced that the equivalent model shows good accuracy, however, they also observed some discrepancies and suggested that the equivalent model could be used cautiously for pre-design purposes. In between, some other researchers viewed the problem from other perspectives and proved that the first versions of the equivalent mechanical model

were based on physical intuition. These researchers obtained the modified mechanical models based on the fluid dynamics theory and compared their results with FE analyses. They proved a good accuracy for their proposed models while the model at the same time offered much less computational cost compared to FE approaches.

- Damping ratios considered for impulsive and convective modes of fluid vibrations have been overwhelmingly used as specific values in the literature. Proportional Rayleigh damping formulation has been applied in these works to form the damping matrix of the coupled system. Further research proved that these values do not have enough experimental justifications, especially for the sloshing mode. Considering the classical Rayleigh damping for coupled systems such as fluid-structure or soil-structure-fluid systems with significantly different levels of damping could be far from reality. Thus, further research in this field considering appropriate assumptions or identification methodologies for damping is required to analyze the behavior of the coupled system more precisely.

- Most studies on the seismic behavior of fluid storage tanks and even the proposed control techniques for the vibration control of these systems are based on the assumed linearised sloshing and irrotationality of the fluid behavior in the tank under excitations. However, further research proved that under certain seismic excitations these assumptions, especially the amplitude of the free surface liquid would not follow the linear theory anymore. Thus, the Coriolis effects, the nonlinearity of the sloshing oscillations, and turbulence can occur in the fluid domain and their negligence can adversely affect analyses.

- Analytical, semi-analytical, and numerical approaches for evaluating the seismic responses of fluid storage tanks including the base shear and overturning moment have been widely applied in the literature based on the simplified assumptions for the fluid motion. On the other hand, fewer experimental works have been conducted which shows the necessity of more experimental works in this field.

- Various types of damage to fluid storage tanks, even those designed according to

seismic codes, have been observed during previous earthquakes in different sectors of industries. This fact demonstrates that still there is a vital need for more precise methods for the analysis of fluid storage tanks. Efficient SHM techniques, seismic energy-dissipating devices, and appropriate control schemes need to be developed.

- During severe seismic events, the dynamic responses of fluid storage tanks will enter the inelastic region. Therefore, geometrical and material nonlinear dynamic analyses are to be conducted to account for the realistic dynamic behavior of these systems under extreme ground excitations. Evaluating the axial compressive stress in the shell which may result in two common types of damage, namely elephant foot buckling and diamond shape buckling needs to be considered in these circumstances.

- Compared to other sectors and industries, SHM techniques have less been established for damage detection and failure prediction of fluid storage tanks. Thus, there are considerable research opportunities in this field. Statistical model-based identification is one of the vibration-based SHM methods used for this purpose. However, this technique is environmentally and operationally sensitive which should be considered while using this approach for system identification and damage detection. It is noteworthy that for SHM techniques to be efficiently used for fluid storage tanks, different and common types of damage scenarios need to be considered.

- Extensive research on SHM techniques based on newly developed AI methodologies and wireless-based technologies with practical applications in damage detection and failure prediction of fluid storage tanks is required.

- Various energy-dissipating devices for seismic protection and vibration mitigation of fluid storage tanks have been investigated in the literature. Most of these devices are based on base isolation and passive control techniques. On the other hand, some active control mechanisms and very limited cases of semi-active control devices have been proposed. In either case, compared to numerical investigations,

fewer experimental examinations have been conducted to scrutinize the efficacy of each system in practical applications. Application of these devices for fluid storage tanks can enhance their seismic performance and mitigate their dynamic responses and internal stresses which may result in the failure of these systems. It is noteworthy that the structural parameters of fluid storage tanks including mass, stiffness, and damping change over time during dynamic excitations. Therefore, considering the time-varying dynamic properties of these structures for control design purposes will result in more precise evaluations.

- Application of SHM and structural control techniques for fluid storage systems can assure reliability, safety, and integrity of both existing tanks as well as new tanks during severe seismic actions. Either of these techniques offers great potential opportunities and advantages. However, a complete and fully reliable system would be the one that integrates both of them. This area demands substantial numerical and experimental examinations.

To sum up, fluid storage tanks are the lifeline to various industries and their reliability and stability can avert the occurrence of catastrophes under future seismic events. Reconnaissance of affected industries containing these structures after previous catastrophic earthquakes demonstrated that precise analysis and design of these structural systems is imperative. Therefore, this field requires more experimental and numerical studies, while considering realistic assumptions for the behavior of both the fluid and the tank shell, and characteristics of the input excitations. More extensive research using different SHM techniques and energy-dissipating devices is needed. Efficient control mechanisms and techniques that combine the benefits of both passive and active control systems are to be investigated more extensively. In between, the idea of integrated approaches for creating fully smart fluid storage tanks to ensure the stability of these systems during severe seismic ground motions will offer promising opportunities.

Chapter 3

Research Methodology

3.1 Introduction

To develop seismic-resilient fluid storage tanks and avoid damage to these structures during earthquakes different energy-dissipating devices have been proposed by researchers in the literature. A review of various mechanisms developed for this purpose can be found in (Hosseini & Beskhyroun, 2023). Vibration control systems and techniques have been targeted for decades to enhance the safety, reliability, and resiliency of engineering structures against undesirable vibrations, especially those caused by severe earthquakes. Passive control mechanisms offer reliability whereas they are not adaptable or versatile. On the other hand, active control systems, while removing drawbacks of passive systems, rely on considerable external power for their operation which could be a source of substantial concern during a disaster. Moreover, reliability and robustness are always matters of concern for active systems. Semi-active systems aim to combine the advantages of both passive and active systems while eliminating their weak points. Passive control devices for energy-dissipation and seismic protection of fluid storage tanks and industrial plants have been developed and applied to these structures in different forms now for decades (Paolacci, Giannini & De Angelis, 2013). Base isolators and their variants (M. K. Shrimali & Jangid, 2002), Horizontal and vertical baffles (Hasheminejad et al.,

2014), are amongst the most developed passive systems for fluid tanks. Active baffles (Hernández & Santamarina, 2012) and piezoelectric patches (Mehrvarz et al., 2019) can be named as instances of active devices proposed in this field. Semi-active control devices for vibration control and seismic protection of fluid-contained tanks and vessels have not been explored to the same extent as passive and active systems. Examples of such devices include variable dampers for making smart base isolation (Iemura et al., 2004), the semi-active mechanism proposed by Kobayashi and Koyama (Kobayashi & Koyama, 2010) based on the air spring effect of a gas chamber, and the application of Magnetorheological (MR) dampers by Shrimali and Kasar (M. K. Shrimali & Kasar, 2012). The study by Shrimali and Kasar (M. K. Shrimali & Kasar, 2012) considered the utilization of MR dampers between two adjacent tanks for the aim of seismic response reduction of connected liquid storage tanks. Authors believe that the effects of employing these dampers over the vibrational responses of these strategic structures under seismic base excitations have not been comprehensively examined.

In this chapter, first, a series of formulations representing the dynamic fluid-structure interaction in circular cylindrical base-supported fluid storage tanks are presented. Then a set of appropriate boundary conditions is considered and finally, the cyclic natural frequencies of convective and impulsive modes are expressed. Later in the next chapter, the experimental results of shake table tests conducted over an unanchored thin-walled stainless-steel circular cylindrical fluid tank are presented to better understand the dynamic performance of such tanks and their behaviour under actual ground motions. In the next section of this chapter dynamic behaviour modelling of a legged flexible circular cylindrical fluid tank equipped with an MR damper is formulated to numerically investigate the potential of this damper for developing seismic-resilient fluid tanks. In developing the dynamic equation of motion in this section, the configuration of implementing the MR damper was considered in a horizontal style connected rigidly between the tank legs and the ground. The connections of the tank's legs to the ground in this part were regarded as fixed. In the last part of this chapter, a vertical mode for implementation of the MR dampers for equipping a legged rigid circular cylindrical fluid tank is considered. This tank was considered in an unanchored condition rocking freely as a rigid body under

the base excitations. A new set of equations was developed to represent the dynamic behaviour of such a coupled MR-fluid-tank system. A set of numerical examinations was conducted to study the efficacy of MR dampers in mitigating the seismic responses of such a tank. In the next chapter, the experimental results of shake table tests done over a rigid legged cylindrical fluid tank equipped with MR dampers connected between the legs and the ground vertically to develop a rocking isolation system for fluid tanks based on smart dampers are presented.

3.2 Simplified mechanical model

A circular cylindrical base-supported fluid tank is considered as shown in Figure 3.1.

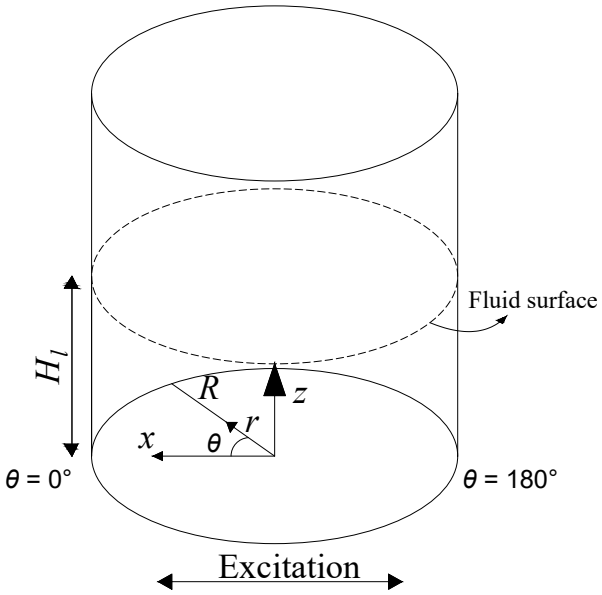

Figure 3.1: Fluid flow representation in a circular cylindrical container under base excitations

In Figure 3.1, *R* is the radius of the circular cylindrical fluid tank. Laplace's equation for an incompressible, inviscid, and irrotational fluid flow in the polar coordinates, r, θ, and z is expressed as in Equation (3.1) (A. S. Veletsos, 1984; Ibrahim, 2005),

$$\nabla^2\varphi(r,\theta,z,t) = 0 \tag{3.1}$$

where φ is the velocity potential of the fluid as a function of time and position, and H_l is the distance between the surface liquid and the base. This equation is expanded as Equation (3.2),

$$\frac{\partial^2\varphi}{\partial r^2} + \frac{1}{r}\frac{\partial\varphi}{\partial r} + \frac{1}{r^2}\frac{\partial^2\varphi}{\partial\theta^2} + \frac{\partial^2\varphi}{\partial z^2} = 0 \tag{3.2}$$

To solve this partial differential equation (PDE), a proper set of boundary conditions (BC's) should be considered. For an arbitrary point in space and time, the liquid velocity and the hydrodynamic pressure in a generalised ϵ-coordinate direction are stated as below,

$$\nu_\epsilon = -\frac{\partial\varphi}{\partial\epsilon} \tag{3.3}$$

$$P = \rho_l\frac{\partial\varphi}{\partial t} \tag{3.4}$$

where ρ_l is the mass density of the liquid in the tank. To solve the equation 3.3, three main BC's are to be considered as follows,

$$\begin{cases} BC1: & -\frac{\partial\varphi}{\partial z}|_{z=0} = 0 \\ BC2: & -\frac{\partial\varphi}{\partial r}|_{r=R} = \frac{\partial W}{\partial t} \\ BC3: & (\frac{\partial^2\varphi}{\partial t^2} + g\frac{\partial\varphi}{\partial z})|_{z=H_l} = 0 \end{cases} \tag{3.5}$$

where g is the gravitational acceleration. The first boundary condition (BC1) implies zero vertical velocity at the tank base while BC2 represents the radial velocity at the tank wall. The function W in BC2 is the radial deformation of the tank body and is a function of z, θ, and t. This function depends on several factors, the most important of which are the excitation characteristics and flexibility of the tank wall (A. S. Veletsos, 1984), among others. BC3 represents the linear sloshing theory of surface liquid vibrations.

Two modes of vibration for a fluid-tank system under base excitation can be identified, i.e. the impulsive mode and the convective mode. Convective mode represents vibrations of surface fluid which is independent of the wall flexibility while the impulsive mode reflects the vibrations of the fluid in the lower part of the tank and close to the base which highly depends on the flexibility of the wall. This implies that the velocity potential function of the fluid can be regarded as the sum of two parts of this function for impulsive (φ_{imp}) and convective (φ_{con}) modes as Equation (3.6) when represented in the cylindrical coordinates,

$$\varphi(r,\theta,z,t) = \varphi_{imp}(r,\theta,z,t) + \varphi_{con}(r,\theta,z,t) \tag{3.6}$$

3.2.1 Rigid tanks

To obtain a simplified mechanical model for rigid tanks, it is required to consider a set of appropriate boundary conditions and solve for the Equations (3.3 - 3.4) to obtain two lumped masses, i.e. the rigid impulsive mass and the convective mass, and their corresponding heights from the tank base. The procedure to obtain the closed-form mathematical equations for these parameters is explained in this section.

Rigid impulsive mode

Considering a rigid tank under the horizontal base accelerations of $\ddot{x}_g(t)$, the related BC's for the impulsive velocity potential are written as follows,

$$\begin{cases} BC4: & -\frac{\partial \varphi_{imp}}{\partial z}|_{z=0} = 0 \\ BC5: & -\frac{\partial \varphi_{imp}}{\partial r}|_{r=R} = \dot{x}_g(t)cos\theta \\ BC6: & \frac{\partial \varphi_{imp}}{\partial t}|_{z=H_l} = 0 \end{cases} \tag{3.7}$$

To solve for the impulsive component of the velocity potential through the method of separation of variables, the below equations for the velocity potential and the hydrodynamic pressure are considered,

$$\varphi_{imp} = \Psi_o(r,z) R\dot{x}_g cos\theta \tag{3.8}$$

$$P_{imp} = \Psi_o(r,z) \rho_l R\ddot{x}_g cos\theta \tag{3.9}$$

$$\Psi_o(r,z) = 2\frac{H_l}{R}\sum_{n=1}^{\infty}\frac{(-1)^{n+1} I_1(\alpha_n \frac{r}{H_l})}{\alpha_n^2 \dot{I}_1(\alpha_n \frac{R}{H_l})} cos(\alpha_n \frac{z}{H_l}) \tag{3.10}$$

$$\alpha_n = (2n-1)\frac{\pi}{2} \tag{3.11}$$

where $I_1[.]$ is the modified Bessel function of the first kind of order one, and $\dot{I}_1[.]$ is its first derivative. The wall pressure is obtained by setting $r = R$ in the Equation (3.10) and then substituting it in the Equation (3.9) for the impulsive hydrodynamic pressure as below,

$$P_{imp}|_{r=R} = \left[\Psi_o(r,z)|_{r=R}\right] \rho_l R\ddot{x}_g cos\theta \tag{3.12}$$

where ρ_l is the mass density of the contained fluid in the tank.

$$\Psi_o(r,z)|_{r=R} = (\frac{8}{\pi^2})(\frac{H_l}{R})\sum_{n=1}^{\infty}\frac{(-1)^{n+1}}{(2n-1)^2} \times \frac{I_1\left[(2n-1)\frac{\pi}{2}\frac{R}{H_l}\right]}{\dot{I}_1\left[(2n-1)\frac{\pi}{2}\frac{R}{H_l}\right]} \times cos\left[(2n-1)\frac{\pi}{2}\frac{z}{H_l}\right] \tag{3.13}$$

The lateral force exerted on the tank wall at any elevation z would be,

$$f(z,t) = \int_0^{2\pi} \left[P_{imp}|_{r=R}\right] R cos\theta \, d\theta \tag{3.14}$$

by setting,

$$\Psi_o(r,z)|_{r=R} = \psi_o(z) \tag{3.15}$$

the Equation 3.14 will reduce to below equation,

$$f(z,t) = \int_0^{2\pi} \rho_l R^2 \ddot{x}_g cos^2\theta \psi_o(z)\, d\theta \tag{3.16}$$

and the impulsive base shear which represents the total lateral force exerted on the tank wall along the total height of the tank would be as follows,

$$Q_{imp}(t) = \int_0^{2\pi} \int_0^{H_l} \rho_l R^2 \ddot{x}_g cos^2\theta \psi_o(z)\, dz\, d\theta \tag{3.17}$$

Following extensive mathematical manipulations, and defining the aspect ratio of the tank as $S = (H_l/R)$, the below expression is obtained for the base shear applied to the tank,

$$Q_{imp}(t) = M_l \sum_{n=1}^{\infty} A_n \ddot{x}_g(t) \tag{3.18}$$

where M_l is the total mass of the fluid in the tank, and A_n represents the below equation,

$$A_n = S\left[\frac{16}{\pi^3(2n-1)^3})\right] \frac{I_1\left[\frac{(2n-1)\pi}{2S}\right]}{\dot{I}_1\left[\frac{(2n-1)\pi}{2S}\right]} \tag{3.19}$$

By defining the rigid mass of the fluid in the tank as below,

$$M_o = M_l \sum_{n=1}^{\infty} A_n \tag{3.20}$$

the impulsive base shear at any time can be rewritten as follows,

$$Q_{imp}(t) = M_o \ddot{x}_g(t) \tag{3.21}$$

Based on the Equation (3.21), for a given maximum design acceleration in the region, a specific aspect ratio and radius of the tank, and the mass density of the contained fluid, one can obtain the maximum design base shear of the tank by solving for Equations (3.19 - 3.21). To acquire the expression for the effective height of the rigid impulsive mass from the tank base, the overturning moment at the tank base induced by the wall pressure should be calculated. This moment is expressed by the below equation,

$$M_{imp}(t) = \int_0^{H_l} f(z,t) z \, dz \tag{3.22}$$

by substituting the expression for $f(z,t)$ from the Equation (3.14) or (3.16), the overturning moment can be expressed as follows,

$$M_{imp}(t) = \rho_l R^2 \ddot{x}_g(t) \int_0^{2\pi} \int_0^{H_l} \psi_o(z) z cos^2\theta \, dz \, d\theta \tag{3.23}$$

Substituting the expression for $\psi_o(z)$ and the required mathematical manipulations, the above equation can be stated as the below expression,

$$M_{imp}(t) = \rho_l R^2 \pi H_l \ddot{x}_g(t) (\frac{8}{\pi^2 R}) \int_0^{H_l} \sum_{n=1}^{\infty} \frac{(-1)^{n+1}}{(2n-1)^2} \times \frac{I_1\left[\frac{(2n-1)\pi}{2S}\right]}{\dot{I}_1\left[\frac{(2n-1)\pi}{2S}\right]} cos\left[\frac{(2n-1)\pi z}{2H_l}\right] z \, dz \tag{3.24}$$

By applying extensive mathematical manipulations, the expression for the overturning moment can be reduced to the below equation,

$$M_{imp}(t) = M_l \ddot{x}_g(t) H_l \sum_{n=1}^{\infty} C_n \tag{3.25}$$

$$C_n = \left[1 - \frac{2 \times (-1)^{n+1}}{(2n-1)\pi}\right] A_n \tag{3.26}$$

Besides the M_{imp} which is the moment induced by the wall pressure, the pressure over the tank base creates an additional overturning moment which herein is shown by δM_{imp}. This moment can be calculated using the below formula,

$$\delta M_{imp}(t) = \int_{A_b} dM_{imp} \tag{3.27}$$

To expand on this formula and calculate the additional base moment, a set of formulae are considered as follows,

$$dM_{imp} = \left[P_{imp}|_{z=0}\right] r^2 cos\theta dr d\theta \tag{3.28}$$

$$P_{imp}|_{z=0} = \left[\Psi_o(r,z)|_{z=0}\right] \rho_l R\ddot{x}_g(t) cos\theta \tag{3.29}$$

$$\Psi_o(r,z)|_{z=0} = \psi_o(r) \tag{3.30}$$

Finally, the equation for calculating the δM_{imp} can be reduced to the below equation,

$$\delta M_{imp}(t) = R\rho_l \ddot{x}_g(t) \int_0^{2\pi} \int_0^R \psi_o(r) r^2 cos^2\theta \, dr \, d\theta \tag{3.31}$$

To solve the above equation and acquire a closed-form representation for the additional base moment extensive mathematical manipulations should be followed. Eventually, using the integral relation in Equation (3.32), the additional base moment can be calculated using equations (3.33 - 3.34).

$$\int_0^R r^2 I_1(\alpha_n r) \, dr = \frac{R^2}{\alpha_n} I_2(\alpha_n R) \tag{3.32}$$

$$\delta M_{imp}(t) = M_l H_l \ddot{x}_g(t) \sum_{n=1}^{\infty} B_n \tag{3.33}$$

$$B_n = \left[\frac{16(-1)^{n+1}}{\pi^3(2n-1)^3}\right] \frac{I_2\left[\frac{(2n-1)\pi}{2S}\right]}{\dot{I}_1\left[\frac{(2n-1)\pi}{2S}\right]} \tag{3.34}$$

where $I_2[.]$ is the modified Bessel function of the first kind of second order. To obtain a closed-form expression for the effective height of the rigid impulsive mass, herein shown as H_{ri}, and also the term that corrects for the differences due to the base pressure shown by δH_{ri}, the below relations are considered,

$$H_{ri} = \frac{M_{imp}(t)}{Q_{imp}(t)} \tag{3.35}$$

$$\delta H_{ri} = \frac{\delta M_{imp}(t)}{Q_{imp}(t)} \tag{3.36}$$

Considering the above relations and Equations (3.18), (3.25), and (3.33), the below equations are obtained for these heights,

$$H_{ri} = (\frac{M_l}{M_o}) H_l \sum_{n=1}^{\infty} C_n \tag{3.37}$$

$$\delta H_{ri} = (\frac{M_l}{M_o}) H_l \sum_{n=1}^{\infty} B_n \tag{3.38}$$

Therefore, when calculating the base moment including the effects of the base shear, especially for tanks with small aspect ratios, the effective height would be,

$$H_{ri}^{m} = H_{ri} + \delta H_{ri} \tag{3.39}$$

Convective mode

To obtain the corresponding equations for the convective components of the base shear and overturning moment a similar procedure as in the previous section with some differences is considered. Convective modes consist of several vibration modes that represent the oscillations of the fluid surface due to the base excitations. Thus, several convective lumped masses, their corresponding heights, and consequently natural frequencies would be revealed. To obtain the closed-form relations for these parameters, the steady-state response of the tank to a harmonic base excitation is considered. Hence, it is assumed that the tank is under a base excitation with the following function,

$$\ddot{x}_g(t) = \ddot{x}_{og} e^{i\omega t} \tag{3.40}$$

where $\ddot{x}_{og}$ is the amplitude of the excitation, ω is the circular frequency of the ground motion in (rad/s), and $i = \sqrt{-1}$ is the imaginary coordinate. Moreover, a set of appropriate BC's for the convective component of the fluid vibrations in the tank are considered

as below,

$$\begin{cases} BC7: & \frac{\partial \varphi_{con}}{\partial z}|_{z=0} = 0 \\ BC8: & \frac{\partial \varphi_{con}}{\partial r}|_{r=R} = 0 \\ BC9: & (\frac{\partial^2 \varphi_{con}}{\partial t^2} + g\frac{\partial \varphi_{con}}{\partial z})|_{z=H_l} = -(\frac{\partial^2 \varphi_{imp}}{\partial t^2} + g\frac{\partial \varphi_{imp}}{\partial z})|_{z=H_l} \end{cases} \tag{3.41}$$

Since at the fluid surface,

$$\frac{\partial \varphi_{imp}}{\partial t}|_{z=H_l} = 0 \tag{3.42}$$

BC9 can be represented as follows,

$$(\frac{\partial^2 \varphi_{con}}{\partial t^2} + g\frac{\partial \varphi_{con}}{\partial z})|_{z=H_l} = -g\frac{\partial \varphi_{imp}}{\partial z}|_{z=H_l} \tag{3.43}$$

A velocity potential function that satisfies the Equation (3.2) and the BC's stated in the Equations (3.41 - 3.43) can be regarded as follows,

$$\varphi_{con} = \sum_{j=1}^{\infty} \Lambda_j(r,z) \frac{1}{1-(\frac{\omega}{\omega_{cj}})^2} R(\frac{\ddot{x}_{og}}{i\omega}) e^{i\omega t} cos\theta \tag{3.44}$$

where $\Lambda_j(r,z)$ is defined as below,

$$\Lambda_j(r,z) = \frac{2J_1(\frac{\lambda_j r}{R})cosh(\frac{\lambda_j z}{R})}{(\lambda_j^2-1)J_1(\lambda_j)cosh(\lambda_j S)} \tag{3.45}$$

where ω_{cj}, $J_1(.)$, and λ_j in Equations (3.44) and (3.45), are the jth natural circular frequency of the convective mode, the Bessel function of the first kind of order one, and the jth root of the first derivative of the Bessel function of first kind of order one, i.e. $\dot{J}_1(.)$, respectively. Assuming small amplitude and linearized fluid motions at the fluid surface, the jth cyclic natural frequency of the convective mode is obtained according to Equation (3.46),

$$\omega_{cj} = \sqrt{\lambda_j \frac{g}{R} \tanh(\lambda_j S)} \tag{3.46}$$

where S is the aspect ratio of the fluid tank. The values of the first three roots of ${J_1}'$, i.e. λ_1, λ_2, and λ_3 are 1.8412, 5.3314, and 8.5363, respectively and g is the gravitational acceleration.

The convective component of the hydrodynamic pressure would be as follows,

$$P_{con}(r,\theta,z,t) = \rho_l \frac{\partial \varphi_{con}}{\partial t} \tag{3.47}$$

$$P_{con}(r,\theta,z,t) = \rho_l R \ddot{x}_{og} e^{i\omega t} cos\theta \sum_{j=1}^{\infty} \Lambda_j(r,z) \frac{1}{1-(\frac{\omega}{\omega_{cj}})^2} \tag{3.48}$$

Following a similar procedure as in the previous section, the convective component of the base shear would be,

$$Q_{con}(t) = \int_0^{2\pi} \int_0^{H_l} \left[P_{con}(r,\theta,z,t)|_{r=R}\right] R cos\theta \, dz \, d\theta \tag{3.49}$$

Substituting the relations for $P_{con}(r,\theta,z,t)|_{r=R}$, $\Lambda_j(r,z)$, and extensive mathematical manipulations, the convective base shear is represented in a closed-form expression as below,

$$Q_{con}(t) = \ddot{x}_{og} e^{i\omega t} \sum_{j=1}^{\infty} \frac{M_{cj}}{1-(\frac{\omega}{\omega_{cj}})^2} \tag{3.50}$$

where M_{cj} is the mass of the jth convective mode and is stated according to the below equation,

$$M_{cj} = M_l \left[\frac{2}{\lambda_j(\lambda_j^2-1)S}\right] tanh(\lambda_j S) \tag{3.51}$$

Correspondingly, the convective component of the base moment due to the wall pressure would be,

$$M_{con}(t) = R \int_0^{2\pi} \int_0^{H_l} \left[P_{con}(r,\theta,z,t)|_{r=R}\right] z cos\theta \, dz \, d\theta \tag{3.52}$$

Substituting for the convective hydrodynamic pressure and solving the integral results in

the below closed-form equation for the base moment due to the wall pressure,

$$M_{con}(t) = \ddot{x}_{og} e^{i\omega t} \sum_{j=1}^{\infty} \frac{M_{cj} H_{cj}}{1 - (\frac{\omega}{\omega_{cj}})^2} \tag{3.53}$$

where the H_{cj} is the height of the jth convective mass from the tank base and is formulated as below,

$$H_{cj} = [1 - \frac{1}{\lambda_j S} tanh(0.5\lambda_j S)] H_l \tag{3.54}$$

Similarly, the additional overturning base moment due to the base pressure, and the correcting term for the height of the jth convective mass from the base, considering this additional moment are formulated as follows (A. S. Veletsos, 1984),

$$\int_0^R r^2 J_1(\frac{\lambda_j r}{R}\, dr = (\frac{R^3}{\lambda_j^2}) J_1(\lambda_j) \tag{3.55}$$

$$\delta M_{con}(t) = \ddot{x}_{og} e^{i\omega t} \sum_{j=1}^{\infty} \frac{M_{cj} \delta H_{cj}}{1 - (\frac{\omega}{\omega_{cj}})^2} \tag{3.56}$$

$$\delta H_{cj} = \frac{R\Delta_j}{sinh(\lambda_j S)} \tag{3.57}$$

$$\Delta_j = \frac{1}{\lambda_j} \tag{3.58}$$

Similar to the concept of the total impulsive overturning moment in the previous section, the height of the jth convective mass from the base to calculate the convective component of the overturning moment due to both the wall and base pressures would be represented as below,

$$H_{cj}^m = H_{cj} + \delta H_{cj} \tag{3.59}$$

3.2.2 Flexible tanks

For flexible tanks, the same formulations as in the case of rigid tanks apply to the convective mode. However, the velocity potential equation for the impulsive mode highly relates to the flexibility of the wall. Shell flexibility, the flexibility of the base, the thickness of the shell, the direction of ground excitations (horizontal or vertical), and the base fixity condition are among the factors that affect the boundary conditions required for solving the impulsive velocity potential function. This will subsequently affect the closed-form formulas for structural characteristics of the tank including cyclic natural frequencies, masses, and heights of equivalent lumped masses have been examined by different researchers using various methods such as finite element method, Rayleight-Ritz method, etc. (Haroun & Ellaithy, 1985a; Haroun & Abou-Izzeddine, 1992a, 1992b; A. Veletsos, 1974). Recently efforts by various researchers were made to modify the originally proposed equation in this regard (Moradi et al., 2018; Kazemiyan et al., 2019; Kamarroudi et al., 2021b; Rezaiee-Pajand, Mirjalili & Kazemiyan, 2023; Wu, Yu & Gu, 2023). Here, the fundamental impulsive cyclic natural frequency for a flexible tank is obtained from Equation (3.60) (NZSEE, 2009; Haroun & Housner, 1981b),

$$f_{i1} = \frac{C}{2\pi}\frac{1}{H_l}\sqrt{\frac{E_t g}{\gamma_t}} \tag{3.60}$$

where E_t is Young's modulus of elasticity of the tank material, g is the gravitational acceleration, γ_t is the density of water, H_l is the height of liquid in the tank, and C is a dimensionless parameter, called "Frequency Parameter" which depends on several factors including aspect ratio (S), the ratio of the thickness of the wall to the radius of the tank ($\frac{t_w}{R}$), E_t, γ_t, and Poisson's ratio of the tank material (ν) (A. S. Veletsos, 1984). This parameter can be found through charts presented in (A. S. Veletsos, 1984; NZSEE, 2009; Haroun & Housner, 1981b) and is represented as below,

$$C = \omega_{i1} H_l \sqrt{\frac{\rho_t}{E_t}} \tag{3.61}$$

which ω_{i1} is the fundamental impulsive circular natural frequency of the tank-water system. The height of the impulsive mass depends on both the aspect ratio (S) and the ratio of the wall thickness to the radius ($\frac{t_w}{R}$) of the tank and has been presented in graphs for the design of tanks (Haroun & Housner, 1981b; NZSEE, 2009).

3.3 Vibration control of fluid tanks

Vibration control systems and techniques have been targeted for decades to enhance the safety, reliability, and resiliency of engineering structures against undesirable vibrations, especially those caused by severe earthquakes. Passive control mechanisms offer reliability whereas they are not adaptable or versatile. On the other hand, active control systems, while removing drawbacks of passive systems, rely on considerable external power for their operation which could be a source of substantial concern during a disaster. Moreover, reliability and robustness are always matters of concern for active systems. Semi-active systems aim to combine the advantages of both passive and active systems while eliminating their weak points. Application of a semi-active variable stiffness damper in combination with two passive systems including Elastomeric Rubber Bearing (ERB) and Lead Rubber Bearing (LRB) also called N-Z system (Robinson & Tucker, 1977; X. Chen & Li, 2020) for seismic protection of a horizontally curved bridge has been examined in (Kataria & Jangid, 2016). Passive control devices for energy-dissipation and seismic protection of fluid storage tanks and industrial plants have been developed and applied to these structures in different forms now for decades (Paolacci, Giannini & De Angelis, 2013). Base isolators and their variants (Rawat & Matsagar, 2022; Safari & Tarinejad, 2018; Tsipianitis & Tsompanakis, 2021), Horizontal and vertical baffles (Hasheminejad et al., 2014; Y. Sun et al., 2021), are amongst the most developed passive systems for fluid tanks. Active baffles (Hernández & Santamarina, 2012) and piezoelectric patches (Mehrvarz et al., 2019) can be named as instances of active devices proposed in this field. Semi-active control devices for vibration control and seismic protection of fluid-contained tanks and vessels have not been explored to the same extent

as passive and active systems. Examples of such devices include variable dampers for making smart base isolation (Iemura et al., 2004), the semi-active mechanism proposed by Kobayashi and Koyama (Kobayashi & Koyama, 2010) based on the air spring effect of a gas chamber, and the application of Magnetorheological (MR) dampers by Shrimali and Kasar (M. K. Shrimali & Kasar, 2012). The study by Shrimali and Kasar (M. K. Shrimali & Kasar, 2012) considered the utilization of MR dampers between two adjacent tanks for the aim of seismic response reduction of connected liquid storage tanks. Authors believe that the effects of employing these dampers over the vibrational responses of these strategic structures under seismic base excitations have not been comprehensively examined.

Legged steel fluid storage tanks are widely used in different industries including the wineries, dairy products industries, petrochemicals, etc. for storage of oil, water, and other chemicals (J. Colombo & Almazán, 2017; Ogunmakinde et al., 2023; J. Colombo, Wilches & Leon, 2022). In this paper, the application of MR dampers for vibration attenuation of legged ground-supported fluid storage tanks against seismic actions is investigated. Two cases are considered including a flexible legged tank and a rigid legged tank. In the first case, the connections of the legs to the base are considered fixed and the tank shell is regarded as flexible. In this case, an MR damper is rigidly connected between the top of one of the legs and the ground in a horizontal direction to perform the energy dissipation. In the second case, the tank is set up freely on the ground while four MR dampers, each installed beside one of the legs and the base dissipate the rocking motion of the tank under seismic base excitations. Using the simplified mechanical model proposed in the literature (Haroun, 1983; A. S. Veletsos, 1984; Haroun & Housner, 1981b; M. Shrimali & Jangid, 2004; Zhu, Tang & Luo, 2023) and seismic design codes (NZSEE, 2009) for the dynamic behaviour of fluid tanks, the equation of motion for the coupled fluid-tank system incorporating the MR damper(s) is formulated in each case. To model the nonlinear hysteretic behaviour of MR dampers, the modified Bouc-Wen model (Spencer Jr, Dyke, Sain & Carlson, 1997; Dominguez, Sedaghati & Stiharu, 2008; Mohebbi, Dadkhah & Rasouli Dabbagh, 2018; Lavassani et al., 2022) is employed. To perform a semi-active vibration control technique to the

considered fluid-tank systems, a series of control strategies, comprising three traditional classical control techniques and one modern data-driven adaptive approach are adopted. Selected classical control strategies include the H2/Linear Quadratic Gaussian (H2/LQG) (Fallah & Taghikhany, 2013; Mohebbi et al., 2018; Zafarani & Halabian, 2018, 2020; Wani & Tantray, 2022), the Proportional-Integral-Derivative (PID) (F. Meng, Liu & Liu, 2020; Şahin et al., 2021), and the Fractional order PID (FOPID) (Maiti, Acharya, Chakraborty, Konar & Janarthanan, 2008; Tepljakov et al., 2019; Lavassani et al., 2022) which have demonstrated desirable performances in variety of control applications. When using classical control approaches, each controller has some parameters that need to be designed appropriately to achieve a desirable control action and satisfy the control objective. Here, an optimisation technique termed Hunger Game Search (HGS) (Yang, Chen, Heidari & Gandomi, 2021) which has proved promising features in the literature has been employed to design the parameters of the adopted classical control techniques. Furthermore, to perform the optimisation process more effectively, for each controller an appropriate objective function is defined based on which the optimisation of parameters are conducted. To apply a modern data-driven control approach, an adaptive direct data-driven PID controller has been utilised. Due to the nature of the semi-active control mechanism the calculated active control force cannot be commanded, a secondary control technique is required to adjust the required voltages to the MR damper. To this aim, the clipping control algorithm (Dyke, Spencer Jr, Sain & Carlson, 1996; Kamalzare, Johnson & Wojtkiewicz, 2015; Mohebbi et al., 2018; Abdeddaim, Djerouni, Ounis, Athamnia & Farsangi, 2022) has been regarded.

3.3.1 Magnetorheological Dampers

MR dampers are based on smart MR fluid with adaptable properties. Physical properties such as the viscosity of such a fluid can be changed in a few milliseconds (Dyke et al., 1996; Z. Zhang & Peng, 2020) upon the application of a magnetic field. Thus, the interactive force produced by the damper can be rapidly controlled and adapted according to the force required at each time step to counteract the applied external force on the

system. These dampers are fail-safe as in case of any malfunction in the control system they are turned into passive devices (passive-off mode) and still can continue damping the vibrations. Special features of these dampers such as a wide operational temperature range, and high achievable yield stresses, to name but a few, have enabled this possibility to apply them in a variety of interior and exterior applications for seismic and vibration mitigation of civil structures and infrastructures as well as other industrial applications (Ahamed, Choi & Ferdaus, 2018). Performance of an MR damper as a variable damper for seismic protection of highway bridges has been discussed in (Madhekar & Jangid, 2009). Chen et al. investigated the performance of MR dampers in smart base isolation systems using real-time hybrid tests (P.-C. Chen, Tsai & Lin, 2014). Prakash and Jangid studied the results of coupling an MR damper with a nonlinear isolation system called Unbonded Fiber-Reinforced Elastomeric Isolator (UFREI) over the structural response mitigation of a full-scale three-story benchmark building (Prakash & Jangid, 2022).

3.3.2 Dynamic behaviour modelling of MR damper

MR damper force is calculated based on the modified Bouc-Wen hysteresis dynamic representation of the behaviour of this damper. According to this dynamic modelling, the force produced by the damper is formulated using Equations (3.62 - 3.67) (Spencer Jr et al., 1997),

$$f_{MR} = \alpha z + c_0(\dot{x}_M - \dot{y}) + k_0(x_M - y) + k_1(x_M - x_0) \tag{3.62}$$

$$\dot{z} = -\gamma|\dot{x}_M - \dot{y}|z|z|^{(n-1)} - \beta(\dot{x}_M - \dot{y})|z|^n + A(\dot{x}_M - \dot{y}) \tag{3.63}$$

$$\dot{y} = \frac{1}{c_0 + c_1}\left[\alpha z + c_0\dot{x}_M + k_0(x_M - y)\right] \tag{3.64}$$

$$\alpha(\tau) = \alpha_a + \alpha_b\tau \tag{3.65}$$

$$c_1(\tau) = c_{1a} + c_{1b}\tau \tag{3.66}$$

$$c_0(\tau) = c_{0a} + c_{0b}\tau \tag{3.67}$$

where α_a, α_b, c_{1a}, c_{1b}, c_{0a}, c_{0b}, μ, k_0, k_1, A, β, γ, x_0, and n are the 14 parameters associated with the modified Bouc-Wen model, and x_M and $\dot{x}_M$ are the displacement and velocity of the MR damper. τ is a first-order filter with a time constant $1/\mu$, expressed in the form of a transfer function in the s-domain in the Equation (3.68) that is applied over the decided voltage v to the damper,

$$\tau(s) = \frac{\mu}{s + \mu} \tag{3.68}$$

where the constant μ is given in the next chapter, Table 4.5, representing the parameters of the considered MR damper in the control process design. This filter in the z-domain is given in Appendix B, Equation (B.4).

3.3.3 Dynamic modelling of coupled system; flexible legged tanks

The schematic of a flexible legged circular cylindrical fluid storage tank equipped with an MR damper connected rigidly in a horizontal direction between the tank base and the ground through one of its legs, as shown in Figure 3.2 is considered. This tank has been regarded as made of stainless steel material for both the shell and the legs. Legs are made of tubular cross-sections. Dimensions and profiles of the tank and legs with their cross sections can be found in this figure. The connections of the legs to the base have been considered fixed. This tank is filled with water up to a height of H_l. The equivalent mechanical representation of the physical MR damper-tank-fluid system is shown in Figure 3.3.

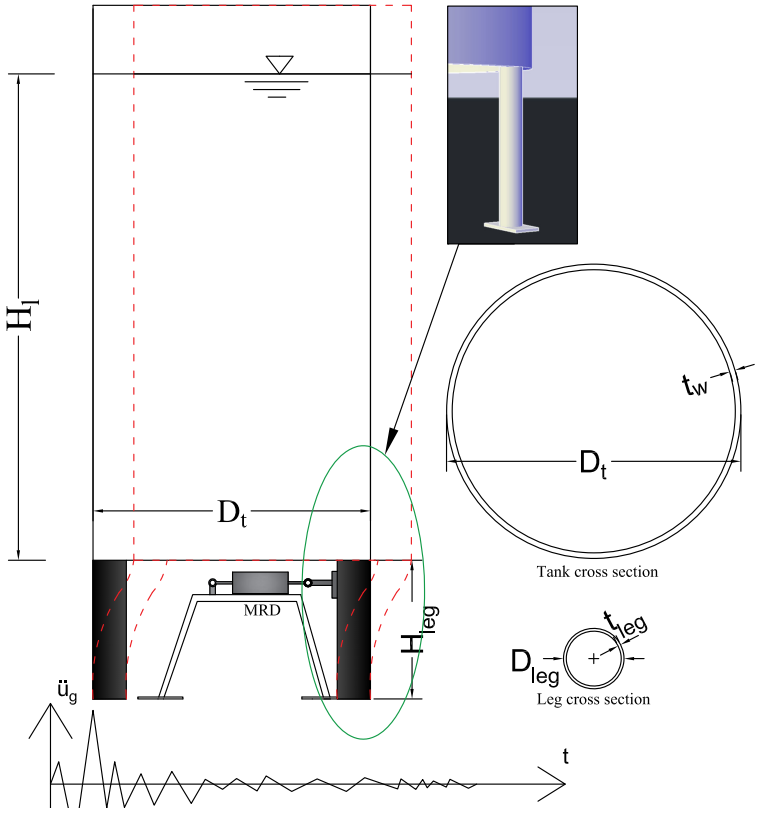

Figure 3.2: Shematic of MRD-fluid-tank system

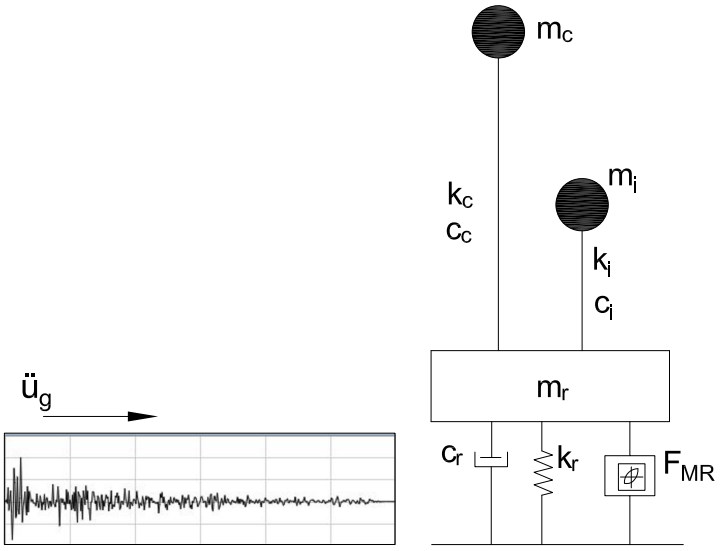

Figure 3.3: Mechanical representation of the MRD-fluid-tank system

Assuming the tank body will not enter the material nonlinearity region while undergoing vibrations, the dynamic equation of motion for the coupled fluid-tank-MR damper system shown in Figure 3.3 is written according to Equation (3.69),

$$M\ddot{U}(t) + C\dot{U}(t) + KU(t) = \xi F_{MR} - M\lambda\ddot{u_g}(t) \tag{3.69}$$

where, M, C, and K are the mass, damping, and stiffness matrices, F_{MR} and $\ddot{u_g}$ are the MR damper force and ground acceleration, ξ and λ are position vectors, and the vectors $\ddot{U}$, $\dot{U}$ and U are acceleration, velocity, and displacement vectors of lumped masses shown in Figure 3.3, respectively. These matrices and vectors are defined as follows,

$$\begin{gathered} M = \begin{bmatrix} m_r & 0 & 0 \\ 0 & m_i & 0 \\ 0 & 0 & m_c \end{bmatrix}, C = \begin{bmatrix} c_r + c_i + c_c & -c_i & -c_c \\ -c_i & c_i & 0 \\ -c_c & 0 & c_c \end{bmatrix}, \\ K = \begin{bmatrix} k_r + k_i + k_c & -k_i & -k_c \\ -k_i & k_i & 0 \\ -k_c & 0 & k_c \end{bmatrix} \end{gathered} \tag{3.70}$$

$$\ddot{U} = \begin{bmatrix} \ddot{u_r} \\ \ddot{u_i} \\ \ddot{u_c} \end{bmatrix}, \dot{U} = \begin{bmatrix} \dot{u_r} \\ \dot{u_i} \\ \dot{u_c} \end{bmatrix}, U = \begin{bmatrix} u_r \\ u_i \\ u_c \end{bmatrix}, \xi = \begin{bmatrix} -1 \\ 0 \\ 0 \end{bmatrix}, \lambda = [1]_{3\times1} \tag{3.71}$$

In this representation, the tank shell has been considered flexible, and only the first impulsive and the first convective modes are considered. Mass, damping, and stiffness of these modes are shown as m_i, m_c, c_i, c_c, k_i, k_c, while m_r is the fluid mass that moves rigidly with the tank shell. The c_r and k_r represent the damping and stiffness associated with the tank legs. The u_r, u_i, and u_c are displacements of the rigid mass, impulsive mass, and convective mass, respectively. To obtain the structural parameters of the coupled tank-fluid system the small amplitude linearised fluid surface vibrations theory is considered. These parameters are written as follows (Haroun, 1983; A. S. Veletsos,

1984; Haroun & Housner, 1981b),

$$m_{i1} = \gamma_{i1} m_l \tag{3.72}$$

$$m_{c1} = \left[\frac{2m_l}{(\lambda_1^2 - 1)\lambda_1 S}\right] tanh(\lambda_1 S) \tag{3.73}$$

$$m_l = \pi R_t^2 H_l \rho_w \tag{3.74}$$

$$\omega_{i1} = \frac{\phi}{H_l}\sqrt{\frac{E_t g}{\gamma_t}} \tag{3.75}$$

$$\omega_{c1} = \sqrt{\lambda_1 \frac{g}{R_t} \tanh(\lambda_1 S)} \tag{3.76}$$

$$S = \frac{H_l}{R_t} \tag{3.77}$$

$$k_{i1} = m_{i1}\omega_{i1}^2 \tag{3.78}$$

$$k_{c1} = m_{c1}\omega_{c1}^2 \tag{3.79}$$

$$c_{i1} = 2\zeta_{i1} m_{i1}\omega_{i1} \tag{3.80}$$

$$c_{c1} = 2\zeta_{c1} m_{c1}\omega_{c1} \tag{3.81}$$

The rigid mass is formulated as the below equation,

$$m_r = m_l - (m_{i1} + m_{c1}) \tag{3.82}$$

Assuming the rigid mass as shown in Figure 3.3 displaces rigidly and the columns connecting the rigid mass to the ground behave as clamped-clamped columns representing a shear behaviour, the stiffness of the columns is written as below,

$$k_r = \frac{12E_tI_{leg}}{H_{leg}^3} \tag{3.83}$$

for the thin tubular cross-section of the legs,

$$I_{leg} = \pi R_{leg}^3 t_{leg} \tag{3.84}$$

while the circular frequency of the vibration of the columns and their corresponding damping coefficient according to the structural dynamics can be conveniently written as follows,

$$\omega_r = \sqrt{\frac{k_r}{m_r}} \tag{3.85}$$

$$c_r = 2\zeta_r m_r \omega_r \tag{3.86}$$

where λ_1 is the first root of the first derivative of the Bessel function of the first kind of order one (J_1) and is equal to 1.8412. E_t is the modulus of elasticity of the tank and legs' material, ρ_w is the mass density of the fluid (water), γ_t is the density of the tank material, H_l is the height of the liquid in the tank, g is the gravitational acceleration, S is the aspect ratio, R_t is the radius of the tank, R_{leg} is the radius of the tank's legs, H_{leg} is the height of legs, t_w is the thickness of the tank wall, t_{leg} is the thickness of the tank's legs, ϕ is the Frequency Parameter, and m_l is the total mass of the fluid in the tank. The frequency parameter depends on several factors, most importantly aspect ratio (S), the ratio of the thickness of the wall to the radius of the tank ($\frac{t_w}{R_t}$), and material properties of the tank. Charts have been presented in the literature and seismic design codes for fluid storage tanks to calculate this parameter (A. S. Veletsos, 1984; NZSEE, 2009; Haroun & Housner, 1981b). The m_{i1} and m_{c1} are the masses of the first impulsive and the

first convective modes, and k_{i1}, k_{c1}, c_{i1}, c_{c1}, ζ_{i1}, ζ_{c1}, ω_{i1}, ω_{c1} are the stiffness, damping coefficients, damping ratios, and circular natural frequencies of these modes, respectively. The ζ_r, and ω_r represent the damping ratio and the natural circular frequency of the legs connecting the rigid mass of the tank to the ground. The parameters ϕ and γ_{i1} as functions of S for the case of $(\frac{t_w}{R_t})$ = 0.004 can be conveniently obtained from the below equations (M. Shrimali & Jangid, 2004),

$$\phi = 0.037085 + 0.084302S - 0.05088S^2 + 0.012523S^3 - 0.0012S^4 \tag{3.87}$$

$$\gamma_{i1} = -0.15467 + 1.21716S - 0.62839S^2 + 0.14434S^3 - 0.0125S^4 \tag{3.88}$$

Equations (3.87-3.88) and their variants presented in the literature, are in fact derived from the interpolation of data based on the charts presented in (Haroun, 1983; P. K. Malhotra et al., 2000).

The state-space representation of Equation (4.1) can be formulated according to Equation (3.89) which represents a sixth-order dynamical system,

$$\dot{X} = AX + Bu^* \tag{3.89}$$

where the state and control input matrices A and B are defined as follows,

$$A = \begin{bmatrix} 0 & 1 & 0 & 0 & 0 & 0 \\ -\frac{k_r+k_i+k_c}{m_r} & -\frac{c_r+c_i+c_c}{m_r} & \frac{k_i}{m_r} & \frac{c_i}{m_r} & \frac{k_c}{m_r} & \frac{c_c}{m_r} \\ 0 & 0 & 0 & 1 & 0 & 0 \\ \frac{k_i}{m_i} & \frac{c_i}{m_i} & -\frac{k_i}{m_i} & -\frac{c_i}{m_i} & 0 & 0 \\ 0 & 0 & 0 & 0 & 0 & 1 \\ \frac{k_c}{m_c} & \frac{c_c}{m_c} & 0 & 0 & -\frac{k_c}{m_c} & -\frac{c_c}{m_c} \end{bmatrix}, B = \begin{bmatrix} B_1 & B_2 \end{bmatrix} \tag{3.90}$$

$$B_1 = \begin{bmatrix} 0 \\ -\frac{1}{m_r} \\ 0 \\ 0 \\ 0 \\ 0 \end{bmatrix}, B_2 = \begin{bmatrix} 0 \\ -1 \\ 0 \\ -1 \\ 0 \\ -1 \end{bmatrix} \tag{3.91}$$

while the vectors of states and the control inputs are expressed as,

$$X = \begin{bmatrix} x_1 \\ x_2 \\ x_3 \\ x_4 \\ x_5 \\ x_6 \end{bmatrix} = \begin{bmatrix} u_r \\ \dot{u_r} \\ u_i \\ \dot{u_i} \\ u_c \\ \dot{u_c} \end{bmatrix}, u^* = \begin{bmatrix} f_{MR} \\ \ddot{u_g} \end{bmatrix} \tag{3.92}$$

It is assumed that the absolute accelerations of the system through accelerometers at the locations of rigid mass, impulsive mass, convective mass, as well as the displacement of the rigid mass are measured. Regarding the mentioned measurements, the output equation for the controlled system is formulated according to Equation (3.93),

$$Y = C^* X + Du^* + \epsilon \tag{3.93}$$

where Y is the output vector and ϵ is the measurement noise. The measurement and direct transition matrices, C^* and D are obtained from Equations (3.94-3.95),

$$C^* = \begin{bmatrix} -\frac{k_r+k_i+k_c}{m_r} & -\frac{c_r+c_i+c_c}{m_r} & \frac{k_i}{m_r} & \frac{c_i}{m_r} & \frac{k_c}{m_r} & \frac{c_c}{m_r} \\ \frac{k_i}{m_i} & \frac{c_i}{m_i} & -\frac{k_i}{m_i} & -\frac{c_i}{m_i} & 0 & 0 \\ \frac{k_c}{m_c} & \frac{c_c}{m_c} & 0 & 0 & -\frac{k_c}{m_c} & -\frac{c_c}{m_c} \end{bmatrix}, D = \begin{bmatrix} D_1 & D_2 \end{bmatrix} \tag{3.94}$$

$$D_1 = \begin{bmatrix} -\frac{1}{m_r} \\ 0 \\ 0 \end{bmatrix}, D_2 = \left[0\right]_{3\times 1} \tag{3.95}$$

3.3.4 Dynamic modelling of coupled system; rigid legged tanks

In this section, the equation of motion for a rigid legged circular cylindrical tank under the base seismic excitations is developed. To the best knowledge of the author, this set of equations to represent the dynamic behaviour of such tanks has not been explored in the literature before. Owing to the fact that the tank is rigid and under the base excitations, it will be subject to rocking motions. When tanks under the base excitations undergo vertical displacements at their sides which technically is called "uplift", the equations of motion for the dynamic behaviour of the tank become even more complicated than the case that it experiences only lateral vibrations. These equations will be highly dependent on the flexibility of the tank and especially the tank's base plate uplift behaviour. A review of the research works done in the literature in this field has already been discussed in section 2.2.4. In the case of rigid tanks, when the tank experiences uplift under the base excitations, it will in fact be subject to rocking motions as a rigid body. The set of equations developed for such tanks in this section has been inspired by the seminal works of pioneers and researchers who studied the rocking motion of rigid blocks (Housner, 1963a; Hogan, 1992; Vlachakis, Giouvanidis, Mehrotra & Lourenço, 2021; Casapulla, Giresini & Lourenço, 2017; Peña, Prieto, Lourenço, Campos Costa & Lemos, 2007; Y. Liu, Páez Chávez, Brzeski & Perlikowski, 2021). Hence, the idea of rocking rigid structures has been extended to the application of rigid tanks to develop the required equations and then use them for the purpose of the vibration control of the coupled system. Due to the rigidity of the tank, the whole fluid-tank system can be modeled as a single lumped mass under a rocking motion. Thus, using the equations presented for rigid tanks in section 3.2.1, the equivalent mass, mass moment of inertia, and height of the lumped mass to the base are calculated. Then based on the idea of the rocking motion of rigid bodies, the equation of motion for the rigid legged tank is developed. MR

damper forces are then incorporated in the developed equation of motion for the system and finally, a transfer function from the input base excitation to the output rotation of the system is acquired. Using the obtained transfer function different control techniques are then developed to examine the performance of the added smart dampers a vertical rocking isolation system for vibration mitigation of fluid storage tanks. To the aim of developing the equation of motion for the considered rigid legged tank, the schematic of the system equipped with MR dampers and the equivalent lumped mass system have been illustrated in Figures 3.4 and 3.5, respectively. The cross-section of the tank cylinder and the leggs are as shown in Figure 3.6.

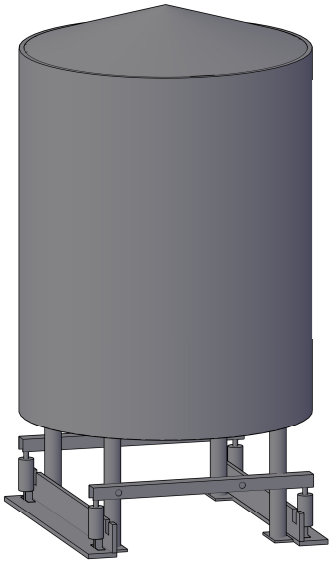

Figure 3.4: 3-D Schematic of the rigid legged circular cylindrical tank equipped with MR dampers under uni-directional base excitaions

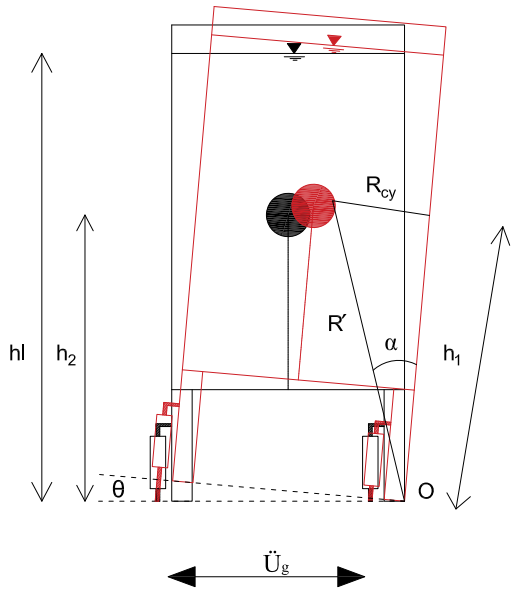

Figure 3.5: Rigid body rocking motion of a rigid legged circular cylindrical tank under uni-directional base excitations

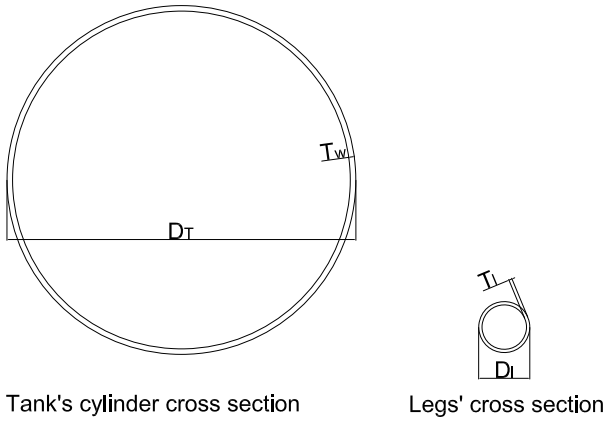

Figure 3.6: Cross section of the tank's cylinder and legs

The equation of motion of the system without MR dampers is written as follows,

$$I'\ddot{\theta} + m'gR'sin(\alpha - \theta) = -m'R'\ddot{U}_g(t) \tag{3.96}$$

$$I' = I_{tot} + m'h'R' \tag{3.97}$$

$$R' = \sqrt{R_{cy}^2 + h_1^2} \tag{3.98}$$

$$m' = m_{eff-liq} + m_{tank} \tag{3.99}$$

$$h' = \frac{m_{eff-liq}h_{eff-liq} + m_{tank}\left[\frac{h_{cy}}{2} + h_{leg}\right]}{m_{eff-liq+m_{tank}}} \tag{3.100}$$

$$I_{tot} = I_F + I_{cy} \tag{3.101}$$

$$I_{cy} = m_{tank}\left[\frac{h_{cy}^2}{12} + \frac{R^2}{4}\right] \tag{3.102}$$

$$I_F = A_s I_s \tag{3.103}$$

$$I_s = m_F\left[\frac{h_l^2}{12} + \frac{Rcy^2}{4}\right] \tag{3.104}$$

In the above equations, θ is the angle of the rigid body rotation, I' the mass moment of inertia of the system, I_F the mass moment of inertia of the fluid inside the tank, I_s the mass moment of inertia of a solidified liquid inside a cylindrical container, I_{cy} the mass moment of inertia of the tank cylinder, R_{cy} the radius of the cylinder, h_{cy} the height of the tank cylinder, h_l the height of the liquid in the tank, h_{leg} the height of the legs, $m_{eff-liq}$ the effective equivalent lumped mass of the rigid fluid tank equal to M_o according to

Equation (3.20), m_{tank} the mass of the tank without the contained fluid, m_F the mass of the fluid inside the tank, $h_{eff-liq}$ is the height of the equivalent lumped mass for a rigid fluid tank according to Equation (3.37), and A_s is a factor that can be conveniently be obtained from charts presented in the literature for calculating the equivalent mass moment of inertia of fluid inside cylindrical containers (Ibrahim, 2005). A rotational damping term is defined as below,

$$C_\theta = \zeta_\theta m' R'^2 \sqrt{\frac{g}{R'}} \tag{3.105}$$

Adding the rotational damping term to Equation (3.96) and then dividing by the term R' will result,

$$\frac{I'}{R'^2}\ddot{\theta} + \zeta_\theta m' \sqrt{\frac{g}{R'}}\dot{\theta} + m'\frac{g}{R'}sin(\alpha - \theta) = -\frac{m'}{R'}\ddot{U}_g(t) \tag{3.106}$$

By defining the "Rocking Frequency Parameter" of the rigid tank as,

$$P' = \sqrt{\frac{g}{R'}} \tag{3.107}$$

and considering the below approximation for small amounts of θ,

$$sin(\alpha - \theta) \approx sin\theta \approx \theta \tag{3.108}$$

Equation (3.106) can be rewritten as below,

$$\frac{I'}{R'^2}\ddot{\theta} + \zeta_\theta m' P'\dot{\theta} + m' P'^2\theta = -\frac{m' P'^2}{g}\ddot{U}_g(t) \tag{3.109}$$

Considering a legged tank-fluid system in a practical three-dimensional application, including the applied control mechanism beside each leg of the tank, and incorporating the corresponding control force in the equation of motion, Equation (3.109) would turn into the below equation,

$$\frac{I'}{R'^2}\ddot{\theta} + \zeta_\theta m' P'\dot{\theta} + m' P'^2\theta = -\frac{m' P'^2}{g}\ddot{U}_g(t) - \frac{4R}{R'^2}U_{cont}(t) \tag{3.110}$$

The above system can be regarded as a multi-input single-output system with ground motion as the disturbance to the system while the objective of the control force is to minimize the effects of the input disturbances and maintain the stability of the system. Taking the Laplace transform from both sides of Equation (3.110), considering zero initial conditions, gives,

$$\theta(s)\left[\frac{I'}{R'^2}s^2 + \zeta_\theta m'P's + m'P'^2\right] = -\frac{m'P'^2}{g}U_g(s) - \frac{4R}{R'^2}U_{cont}(s) \tag{3.111}$$

Thus, the transfer functions from inputs $\ddot{U}_g(t)$ and $\ddot{U}_{cont}(t)$ to the output $\theta(t)$, respectively, would be,

$$H_1(s) = \frac{\theta(s)}{-U_g(s)} = \frac{\frac{m'P'^2}{g}}{\left[\frac{I'}{R'^2}s^2 + \zeta_\theta m'P's + m'P'^2\right]} \tag{3.112}$$

$$H_2(s) = \frac{\theta(s)}{-U_{cont}(s)} = \frac{\frac{4R}{R'^2}}{\left[\frac{I'}{R'^2}s^2 + \zeta_\theta m'P's + m'P'^2\right]} \tag{3.113}$$

Using the transfer functions above, a control strategy can be employed to design the control force and satisfy the control objectives. To fulfill the control objectives and minimise the effects of the input disturbance (ground motion) on the considered rigid legged cylindrical tank, two control strategies have been applied. A description of the employed control strategies will be discussed in the next section.

3.3.5 H2/LQG control technique

The H2/Linear Quadratic Gaussian (H2/LQG) control scheme which minimizes the H_2 norm of the closed-loop system is an optimal and robust control strategy that has proved efficient in structural vibration control applications (Y. Wang & Dyke, 2006; Fallah & Taghikhany, 2013; Mohebbi et al., 2018; Zafarani & Halabian, 2018, 2020; Wani & Tantray, 2022; Prakash & Jangid, 2022). Based on the selected control scheme, the

desired optimal control force would be obtained using Equation (3.114),

$$U_{LQG} = -K_{LQR}\tilde{X} \tag{3.114}$$

where $\tilde{X}$ is the vector of estimated states using the Kalman-Bucy filter (Sorenson, 1966; Baltieri & Buckley, 2020; Ji, Lyu, Pan, Wei & Wei, 2022), and K_{LQR} is the state feedback gain matrix which minimizes the infinite horizon linear quadratic cost function with output weighting stated in Equation (3.115),

$$J = \lim_{T\to\infty} \frac{1}{T} E \int_0^T (Y^T Q Y + U_{LQG}^T R U_{LQG})\, dt \tag{3.115}$$

In this equation, Q and R are weighting matrices that weight selected measured responses of the system and control force, respectively. Solving for P and Θ in the reduced-matrix Riccati Equations (3.116) and (3.119) gives the gain matrices K_{LQR} of the Linear Quadratic Regulator (LQR) and the K_{LQG} of Kalman filter gain as in Equations (3.118) and (3.120), respectively,

$$A^T P + PA + C^{*T} Q C^* - (PB + C^{*T} Q D_1)(D_1^T Q D_1 + R)^{-1}(B_1^T P + D_1^T Q C^*) = 0 \tag{3.116}$$

$$R_s = D_1^T Q D_1 + R \tag{3.117}$$

$$K_{LQR} = R_s^{-1}(B^T P + D_1^T Q C^*) \tag{3.118}$$

$$A\Theta + \Theta A^T - (C^*\Theta)^T (C^*\Theta) + B_2 \Lambda B_2^T = 0 \tag{3.119}$$

$$K_{LQG} = \Theta C^{*T} \tag{3.120}$$

where Λ represents the power ratio of the process noise to the measurement noise given by,

$$\Lambda = \frac{P(\ddot{u}_g \ddot{u}_g)}{P(\epsilon\epsilon)} \tag{3.121}$$

where $P(\ddot{u}_g \ddot{u}_g)$ and $P(\epsilon\epsilon)$ are the average power of the signal and noise, respectively. The observer-controller transfer function of the system is represented in the closed form of Equation (3.122),

$$K_{Ob-Co}(s) = K_{LQR}(sI - (A - K_{LQG}C^*))^{-1} \begin{bmatrix} K_{LQG} & B_1 - K_{LQG}D_1 \end{bmatrix} \tag{3.122}$$

where B_1 and D_1 are the first columns of matrices B and D, respectively. The Matrix Q was regarded to equally weigh the accelerations of the lumped masses while the parameter R weighs the control effort. The weighting matrix Q, the parameter R, and the Λ are written as follows,

$$Q = \begin{bmatrix} Q_f & 0 & 0 \\ 0 & Q_f & 0 \\ 0 & 0 & Q_f \end{bmatrix}, R = R_f \tag{3.123}$$

where the parameters Q_f and R_f are optimally designed using the HGS optimisation approach and an adopted objective function. For the H2/LQG-COC-HGS controller, the objective function in the optimisation process of finding the controller's parameters is defined as follows,

$$Obj = \begin{cases} Min\{u_i\}, & |U_{LQG}| < f_{MR,Max} \\ Min\{\ddot{u}_i\}, & |U_{LQG}| \geq f_{MR,Max} \end{cases} \tag{3.124}$$

Considering the value of the desired control force compared to the capacity of the MR damper, the objective function Obj switches between minimising the displacement or acceleration of the impulsive mass to avoid applying excessive damping forces that could

increase the accelerations of the system unnecessarily.

3.3.6 PID control strategy

The PID control strategy is one of the widely applied control techniques for various applications. This control strategy has proved to be simple, robust, effective, and applicable to a broad class of industrial systems (Sreenivasappa & Udaykumar, 2010; Zand, Sabouri, Katebi & Nouri, 2021). This technique has been used for control design of industrial processes (Dubey, Goud & Sharma, 2022), robotic manipulators (H. Zhang, Trott & Paul, 1990; Shaban, Sayed & Abdelhamid, 2019), biomedical applications (Slate & Sheppard, 1982; Marchetti, Barolo, Jovanovic, Zisser & Seborg, 2008), electric drives and power applications (Glickman, Kulessky & Nudelman, 2004), and mechanical and civil engineering structures (F. Meng et al., 2020; Şahin et al., 2021), to name but a few.

The PID control force in the parallel form is written as below,

$$U_{PID}(t) = K_P \left[e(t) + \frac{1}{T_i} \int_0^t e(t)\, dt + T_d \frac{de(t)}{dt} \right] \tag{3.125}$$

where $e(t)$ is the error function defined as the difference between the output and the reference. The Laplace transform of the above equation would be as follows,

$$U_{PID}(s) = U_P(s) + U_I(s) + U_D(s) \tag{3.126}$$

and the controller gain would be,

$$K_{PID}(s) = K_P + \frac{K_P}{T_i}\left(\frac{1}{s}\right) + K_P T_d s \tag{3.127}$$

Considering the below relations,

$$K_I = \frac{K_P}{T_I}, K_D = K_P T_d \tag{3.128}$$

Equations (3.125) and (3.127) can be rewritten as Equation (3.129) and (3.130), respectively,

$$U_{PID}(t) = K_p e(t) + K_i \int_0^t e(t)\,dt + K_d \frac{de(t)}{dt} \tag{3.129}$$

$$K_{PID}(s) = K_P + K_I(\frac{1}{s}) + K_D s \tag{3.130}$$

where K_p, K_i, K_d, T_i, T_d, and $e(t)$ are the proportional gain, integral gain, derivative gain, integral time constant, derivative time constant, and the error between the reference and the output, respectively. Since the process usually contains noise, a low-pass filtered derivative instead of the pure derivative is applied. In this case, the control force in Equation (3.126) would be reformulated as follows,

$$U_{PID}(s) = U_P(s) + U_I(s) + U_{D-LPF}(s) \tag{3.131}$$

where the filtered derivative term would be in the below form,

$$U_{D-LPF} = K_D \left[\frac{s}{T_f s + 1} \right] \tag{3.132}$$

where T_f is the filter time constant.

3.3.7 FOPID controller

Fractional controllers that are indeed based on the fractional calculus were developed for controlling dynamical systems (Oustaloup, Sabatier & Moreau, 1998). Fractional order PID (FOPID) introduced by Podlubny (Podlubny, 1999) is indeed a generalised form of PID controller which depending on the values of the parameters could reduce to different forms of Proportional (P), Proportional-Integral (PI), Proportional-Derivative (PD), PID, and finally the general form of $PI^{\lambda_s}D^{\mu_s}$. FOPID controllers through having non-integer orders for the derivation and integration processes try to enhance the performance of the PID controllers (Maiti et al., 2008; Tepljakov et al., 2019; Lavassani et al., 2022). In this

controller, contrary to the PID controller, a generalised operator which is the extended form of integration and differentiation is applied. The fractional order calculus is defined by the below equation,

$$D_t^{\Phi} = \begin{cases} \frac{d^{\Phi}}{dt^{\Phi}} & \Phi > 0 \\ 1 & \Phi = 0 \\ \int_0^t (d\tau)^{\Phi} & \Phi < 0 \end{cases} \tag{3.133}$$

Therefore, based on this control law The control force is formulated as,

$$U_{FOPID}(t) = K_P e(t) + K_I D^{-\lambda_s} e(t) + K_D D^{\mu_s} e(t) \tag{3.134}$$

and the controller gain can be obtained from the below equation,

$$K_{FOPID}(s) = K_P + \frac{K_I}{s^{\lambda_s}} + K_D s^{\mu_s}, (\lambda_s, \mu_s > 0) \tag{3.135}$$

where λ_s and μ_s are the non-integer orders of the integration and derivation processes, respectively.

3.3.8 Error-based objective function

When designing or optimising the PID and FOPID control parameters one efficient methodology is to use some error criteria instead of the error function itself (Kumar, Sampath, Praneeth & Kumar, 2021). Different error performance indices have been proposed in the literature for this purpose including Integral of time-weighted absolute error (ITAE), Integral of squared error (ISE), Integral of absolute error (IAE), Integral of time-weighted squared error (ITSE), Integral of squared time-weighted squared error (ISTSE), and Integral of squared time-weighted error (ISTE) (Daful, 2018; Maiti et al., 2008; Rao, Santosh et al., 2020; Kumar et al., 2021; Joseph, Dada, Abidemi, Oyewola & Khammas, 2022). In this study, the ITAE error-based performance index criterion which has proved powerful features including smaller overshoots and oscillations, less settling time, no steady-state error, and computational efficiency (Maiti et al., 2008; Kumar et

al., 2021), is adopted as the objective function for the optimisation process of the HGS algorithm. This error criterion is defined as follows,

$$ITAE = \int_0^\infty t|e(t)|\,dt \tag{3.136}$$

Since among the three lumped masses, the acceleration of the impulsive mass is the greatest, hence the error function for both PID-COC-HGS and FOPID-COC-HGS controllers is defined as the difference between the reference and the impulsive mass acceleration as below,

$$e(t) = \ddot{u}_{ref} - \ddot{u}_i \tag{3.137}$$

$$\ddot{u}_{ref} = 0 \rightarrow e(t) = -\ddot{u}_i \tag{3.138}$$

3.3.9 Hunger Game Search optimisation

A variety of optimisation techniques have been proposed in the literature for the purpose of selecting the optimal and best values of parameters that affect the minimum value of a cost or objective function in engineering problems (Falcone, Lima & Martinelli, 2020; Harirchian et al., 2021; Flah, Nunez, Ben Chaabene & Nehdi, 2021). Most of the optimisation strategies used in the literature so far mainly focused on two major ideas, i.e. evolution and swarm intelligence. Examples of such tactics include the Genetic Algorithm (GA) (Katoch, Chauhan & Kumar, 2021), Particle Swarm Optimisation (PSO) (Shami et al., 2022), Ant Colony Optimisation (ACO) (Nayar, Gautam, Singh & Mehta, 2021), Harris Hawk Optimiser (HHO) (Heidari et al., 2019), Grey Wolf Optimiser (GWO) (Mirjalili, Mirjalili & Lewis, 2014), etc. The Hunger Game Search (HGS) recently developed by Yang et al. (Yang et al., 2021) is indeed a general-purpose optimisation approach which is a population-based method. This dynamic technique is based on hunger as the most crucial desire in all animals for decision-making. It follows some logical rules called “games”, has a simple structure, has proved promising features

including stability and competitive performance, and has been validated for benchmark and IEEE CEC2014 functions (Yang et al., 2021). Considering the main concept of this method, three rules (games) are applied as follows (Yang et al., 2021),

$$\overrightarrow{X(i+1)} = \begin{cases} \text{Game 1} : search\ based\ on\ \overrightarrow{X(i)} \\ \text{Games 2 and 3} : search\ based\ on\ \overrightarrow{X_b} \end{cases} \tag{3.139}$$

where t is the current iteration. In $Game\ 1$ there is a set of instructions for finding the food without any teamwork and only based on each individual's location ($\overrightarrow{X(i)}$) and does not include any cooperative communication. On the other hand, Games 2 and 3 are based on cooperation between search agents for finding the food using some functions termed "weights of hunger", and the best individual's location ($\overrightarrow{X_b}$) in each iteration. These games and their weights are represented using mathematical rules and fitness functions for the search methodology for the location of agents to guarantee the optimal solution. The mathematical details of this technique can be found in (Yang et al., 2021) and are not discussed here for brevity.

3.3.10 Semi-active controller

Finally, the control signal using the secondary controller would be acquired using Equation (3.140) (Dyke et al., 1996; Kamalzare et al., 2015; Mohebbi et al., 2018; Abdeddaim et al., 2022),

$$v_{MR} = V_{max,MR} H\{(U_{Cont} - f_{MR}) f_{MR}\} \tag{3.140}$$

where $V_{max,MR}$ is the maximum voltage that can be commanded to the damper which depends on the capacity and specifications of the damper, $H\{.\}$ is the Heaviside function, and U_{Cont} is the desirable control force decided by the selected control laws and strategies. A modified version of the clipping algorithm stated in Equation (3.140) selects any values between 0 and $V_{max,MR}$. This technique is written as follows (Yoshida & Dyke, 2004; Pohoryles & Duffour, 2015; Pei, Peng & Qiu, 2022; Brandão & Miguel, 2023),

$$\upsilon_{MR} = V_{d,MR} H\{(U_{Cont} - f_{MR}) f_{MR}\} \tag{3.141}$$

where $V_{d,MR}$ is decided from the below equation,

$$V_{d,MR} = \begin{cases} V_{max,MR}, & |U_{Cont}| > f_{max,MR} \\ \frac{V_{max,MR}}{f_{max,MR}} |U_{Cont}|, & |U_{Cont}| \leq f_{max,MR} \end{cases} \tag{3.142}$$

where $f_{max,MR}$ is the maximum capacity of the MR damper.

The block diagram of the control system design would be as shown in Figure 3.7.

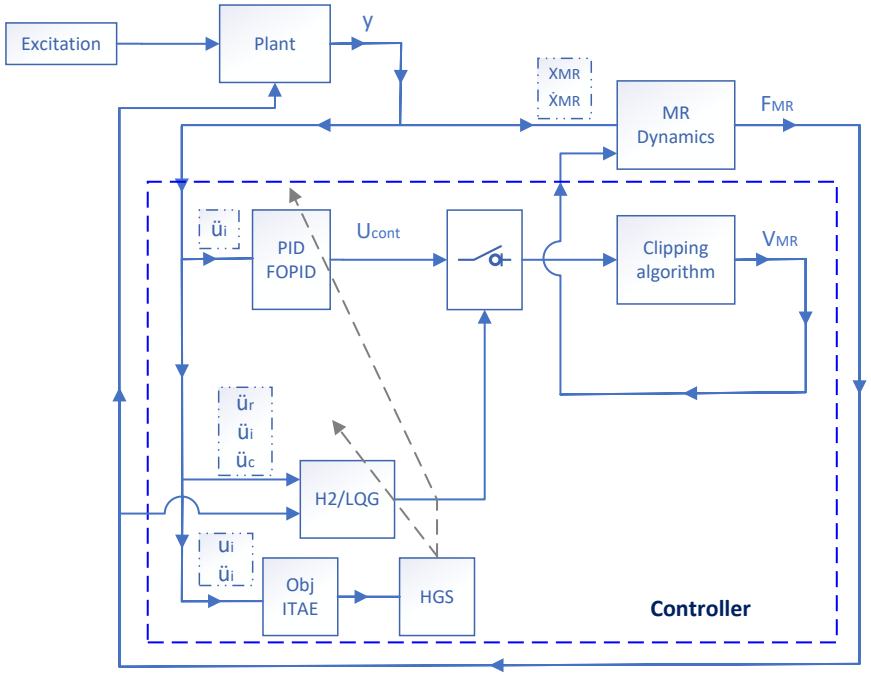

Figure 3.7: Schematic of the control design block diagram for semi-active control of the flexible legged cylindrical fluid tank

3.3.11 Energy dissipation control strategy

This control strategy is in fact a variation of the decentralised bang-bang control technique (Jansen & Dyke, 2000; Şahin et al., 2021; Y. Zhang, Xu, Du & Wang, 2023). In this

technique, only the measurements of the damper's force and velocity are required. This strategy benefits from a very simple formula and ensures the command voltage is at its maximum value when the dampers' force is dissipating energy and is at its minimum when the force is not dissipating. The Lyapunov function representing the total energy of the structure is written as below,

$$\Upsilon = \frac{1}{2} X_{str}^{T} K_{str} X + \frac{1}{2} \dot{X}_{str} M_{str} \dot{X}_{str} \tag{3.143}$$

where X_{str}, $\dot{X}_{str}$, M_{str}, and K_{str}, are the displacement and velocity vector, mass, and stiffness of the structural system. Having the MR damper connected between the ground and the system, to maximise the rate of change of the energy dissipation, the below control law is applied which directly affects the energy of the system,

$$\upsilon_{MR} = V_{max,MR} H\{(-\dot{X}_{MR}^{T}) f_{MR}\} \tag{3.144}$$

where $\dot{X}_{MR}^{T}$ is the transpose of the relative velocity of the MR damper. The advantage of this technique in the current application is when the damper is connected between the ground the tank's base or legs only the absolute velocity of the damper is needed. This measurement can be obtained through applying a proper transfer function to the measurements of the accelerometers' data.

3.3.12 Online data-driven adaptive PID control strategy

In practice, many systems in the real world have much more complicated dynamics and behaviour that cannot be modelled using closed-form representations. Even if the the system's dynamic behaviour can be modelled there would be other challenges such as a high computational burden of a substantially complex formula for multi-physics problems such as fluid tanks for a feasible control application. Additionally, issues including nonlinearities in the system's behaviour, degradation of the system's properties over time, the system's time-varying properties under the applied excitations, and input and output signals' physical constraints, among others, render the application

of first-principles-based classical control design impractical and inefficient (Y. Li & Hou, 2014; Bu, Wang, Hou & Qian, 2018; Asadi, Farsangi, Bijami, Amani & Lee, 2021). To overcome these difficulties and enhance the performance of the control system, especially in the long run, a new class of control designs termed Data-Driven Control (DDC) systems come into play. These techniques are divided into two main categories of indirect or model-based DDC and direct or model-free methods (Markovsky, Huang & Dörfler, 2023). In indirect methods, first based on the observed data a model using system identification techniques is identified for the system under control. Then, based on the identified model, the controller is designed. However, in the direct methods, the system identification step is skipped and the observed data are directly mapped to the desired control action for the system. A variety of different direct and indirect DDC methods have been studied in the literature (Hou & Wang, 2013; Brunton & Noack, 2015; Tang & Daoutidis, 2022). Model-free Adaptive Control (MFAC), Iterative Feedback Tuning (IFT), Virtual Reference Tuning (VRF), Iterative Learning Control (ILC), DDC methods based on Behavioral Systems Theory, can be named among others (Hou & Wang, 2013; Markovsky et al., 2023). As discussed before in subsection 3.3.6, the PID control technique is a widely used strategy in most control applications in industry. This control method may have been the first technique applied in the world of DDC (Ziegler & Nichols, 1942; Hou & Wang, 2013). Here, a data-driven technique based on the PID control strategy is used to control the rigid cylindrical legged tank described in subsection 3.3.4. Experimental tests over this tank have been conducted in the Structural Engineering Laboratory of Auckland University of Technology. The results of these tests will be described in detail in the next chapter and this subsection is dedicated to the theoretical description of the applied technique.

In this study, a semi-active online direct DDC method based on an adaptive PID control scheme is developed to control the rigid cylindrical legged tank. In this scheme, the online data from sensors are received at each time step. Then, based on a set point as the reference and a transfer function of the plant as the model reference, two error values are calculated at each time step. As discussed earlier, in direct DDC methods instead of identifying the plant, the observed data are directly used to design the controller.

Therefore, in the adopted control scheme here, the parameters of the PID controller are identified at each time step based on the observed data to satisfy the control objective. Different identification methods have been introduced in the literature to adaptively estimate the controller parameters, including fuzzy logic (Naik, Gupta & Fernandez, 2020), Predictive Neural Network (Mohamed, Metwally, El-Sayed & Selem, 2019), Chebyshev Neural Network (Govindharaj & Mariappan, 2020), and Monte Carlo based techniques (Öztürk & Kahraman, 2019; Fan et al., 2019), among others. Here, an adaptation mechanism using the Recursive Least Squares (RLS) is employed to minimise a cost function based on the estimation error (Fahmy, Badr & Rahman, 2014, 2018; Al-Bargothi, Qaryouti & Jaber, 2019). This technique offers promising features including robustness against faults when the system undergoes substantial changes, simplicity of the algorithm for application and modifications for different systems, and small memory requirements (Ghamari, Mollaee & Khavari, 2021). The adaptation mechanism estimates the parameters of the PID controller online for the next step of the control action. Finally, the calculated control force is sent to the clipping algorithm to decide the input voltage to the MR damper. The schematic of the control design block diagram is shown in Figure 3.8.

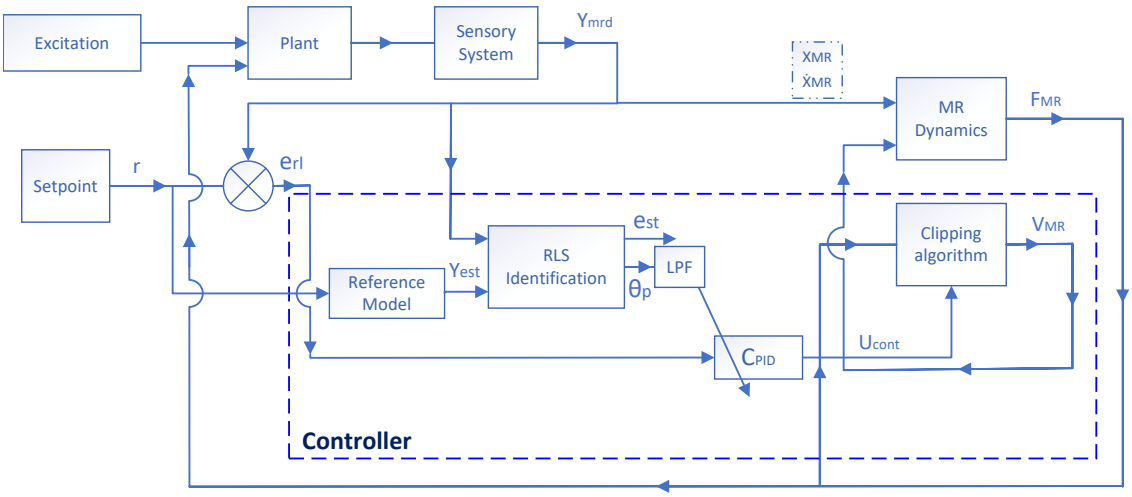

Figure 3.8: Schematic of the control design block diagram for semi-active control of the rigid legged cylindrical fluid tank

In Figure 3.8, Plant is the sysme to be controlled in this study, i.e. the fluid tank, adaptation mechanism to update the parameters of the adaptive PID (APID) controller online using the observed data from sensors is the RLS identification process, Reference Model is the transfer function of the system developed in section 3.3.4, i.e. $H_1(s)$ or $H_2(s)$ which work as the reference model for the DDC control system here, e_{rl} and e_{st} are the real error between received data from the sensors and the estimated error between the observed data and estimated response of the system, respectively, U_{cont} is the online DDC-APID control, r is the reference, Y_{mrd} and Y_{est} are the measured and estimated responses of the plant, respectively, X_{MR} and $\dot{X}_{MR}$ are the displacement and velocity of the MR damper, θ_p is the vector of identified parameters of the PID controller from the adaptation mechanism, LPF is a Low Pass Filter over these parameters, and F_{MR} and V_{MR} are the MR damper calculated force and the decided voltage to the damper based on the Clipping algorithm for the next time step in the online control process of teh system. Therefore, the author terms this control methodology as an Online Data-Driven Adaptive PID-Clipping control (ODDAPIDC) methodology developed for semi-active control of rigid legged cylindrical fluid storage tanks equipped with MR dampers in this study.

3.3.13 Recursive least squares adaptive PID control technique

In this technique, a tracking error is defined as the difference between the real output of the plant (measured by the sensory system) and the estimated output from the model reference. The RLS strategy tries to converge this error to zero asymptotically. Here this tracking error is written as below,

$$\zeta_{RLS}(t) = Y_{mrd}(t) - Y_{est}(t) \rightarrow 0 \tag{3.145}$$

$$Y_{mrd}(t) = r(t) - e_{rl}(t) \tag{3.146}$$

$$Y_{est}(t) = H_M(s)r(t) \tag{3.147}$$

Therefore, to satisfy Equation (3.145),

$$H_M(s)r(t) = r(t) - e_{rl}(t) \tag{3.148}$$

where $H_M(s)$ is the transfer function of the model reference. Considering a PID control gain with a filtered derivative action that counteracts the undesirable noise amplification as follows,

$$C_{PID}(s) = K_P(s) + K_I(s)\frac{1}{s} + K_D\frac{s}{T_f(s)+1} \tag{3.149}$$

it is obtained,

$$U_{cont}(s) = C_{PID}(s)e_{rl}(s) \tag{3.150}$$

which in discrete time and the z-domain would be,

$$U_{cont}(z) = C_{PID}(z)e_{rl} \tag{3.151}$$

Writing Equation (3.148) and multiplying both sides of it by the controller gain $C_{PID}(z)$ yields,

$$C_{PID}(z)H_M(z)r = C_{PID}(z)(r - e_{rl}) \tag{3.152}$$

Using Equation (3.152) and some mathematical manipulations, the tracking error of the RLS technique for the current approach can be written as below,

$$\zeta_{RLS} = U_{cont} - C_{PID}(z)(1 - H_M(z))r \tag{3.153}$$

Having the tracking error, the cost function of RLS is regarded as follows to satisfy the convergence of the plant output to the desired one,

$$J_{RLS}(k) = \frac{1}{N}\sum_{i=0}^{N-1} \zeta_{RLS}^T(k-i)\zeta_{RLS}(k-i) \tag{3.154}$$

The controller gain $C_{PID}(z)$ is rewritten as bellow,

$$C_{PID}(z) = \Theta_{PID}^T \Phi_{PID}(z) \tag{3.155}$$

where Θ_{PID}^T are the controller parameters to be identified at each time step using the RLS technique,

$$\Theta_{PID}^T = \begin{bmatrix} K_P & K_I & K_D \end{bmatrix} \in \mathbb{R} \tag{3.156}$$

and $\Phi_{PID}(z)$ using the backward Euler method can be formulated as (Goodwin & Sin, 2014; Mansour, 2011; Solvang, 2019),

$$\Phi_{PID}(z) = \begin{bmatrix} 1 & \frac{\tau_s z}{z-1} & \frac{z-1}{(T_f+\tau_s)z-T_f} \end{bmatrix}^T \tag{3.157}$$

where τ_s and T_f are the sampling time and filtered-derivative time constant, respectively. Substituting Equation (3.155) into Equation (3.153) and defining,

$$\Phi_{PID,rf} = \Phi_{PID}(z)(1 - H_M(z))r \tag{3.158}$$

the equation of the tracking error in a step-wise manner can be written as,

$$\zeta_{RLS}(k) = U_{cont}(k) - \Theta_{PID}^T(k-1)\Phi_{PID,rf}(k) \tag{3.159}$$

Finally, the estimated parameters of the controller using the RLS technique, i.e. the $\Theta_{PID}(k)$, are passed through a Low Pass Filter (LPF) to account for rapid changes in the plant's characteristics (Fahmy et al., 2018). The transfer function of this filter in the z-domain is written as follows,

$$H_{LPF}(z) = \frac{\beta_f}{z + \beta_f - 1}, \qquad 0 \leq \beta_f \leq 1 \tag{3.160}$$

where β_f is a positive constant that is selected as a sufficiently small value, resulting in more signal smoothing over time. It is important to mention that incorporating Equation (3.159) in the cost function of the RLS algorithm will result in the process of estimation and updating the controller's parameters online in an adaptive manner at each time step by the Θ_{PID} factor, depending on the previous one. To ensure the stability of the control technique, asymptotic convergence of the tracking error to zero, and avoiding the disturbing effects of the parametric variations in both the identification process and the system itself, the RLS algorithm using the forgetting factor strategy is applied (Fahmy et al., 2018; Ghamari et al., 2021). Using this approach,

$$\Theta_{PID}^T(k) = \Theta_{PID}^T(k-1) + K_{RLS}(k)\left[U_{cont}(k) - \Theta_{PID}^T(k-1)\Phi_{PID,rf}(k)\right] \tag{3.161}$$

K_{RLS} is the adaptation gain vector of the RLS technique that is formulated according to the below equation,

$$K_{RLS}(k) = \frac{\Phi_{PID,rf}^{T}(k)P_{RLS}(k-1)}{\Lambda_{RLS} + \Phi_{PID,rf}^{T}P_{RLS}(k-1)\Phi_{PID,rf}}, \quad 0 < \Lambda_{RLS} < 1 \tag{3.162}$$

In the above equation, P_{RLS} is the covariance matrix and Λ_{RLS} is the forgetting factor. The covariance matrix is written as follows,

$$P_{RLS}(k) = P_{RLS}(k-1) - K_{RLS}(k)P_{RLS}(k-1)\Phi_{PID,rf} \tag{3.163}$$

Using the developed formulations, techniques, and approaches in this chapter, numerical simulations, and experimental results are presented in the next chapter to examine the efficiency of the the MR damper on the dynamic behaviour of the legged fluid tank under the base excitations.

3.4 Summary

In this chapter, first, the dynamic behaviour modelling of the coupled fluid-tank system using Laplace's equation for a circular cylindrical tank was described in polar coordinates. A series of appropriate boundary conditions and the linearised sloshing theory were employed to solve the velocity potential equation. Closed-form representations for the mass and height of the impulsive and convective modes and the frequency of vibrations for the convective mode in the rigid case were obtained. As the complexity of equations for the flexible case increases even more, for this case the frequency of vibrations of impulsive mode were described using the seismic design codes. Equations related to the convective mode for flexible tanks remain unchanged. Due to the simplicity, appropriate accuracy, and low computational cost of the simplified mechanical model for fluid tanks especially for applications with control system designs and micro-controllers, this model was used to develop the equation of motion of a fluid tank equipped with MR dampers. The dynamic behaviour of the damper was described using the modified Bouc-Wen model. Two cases of fluid tanks equipped with MR dampers were considered. In the first

case, a flexible legged circular cylindrical liquid tank equipped with one MR damper installed rigidly between the legs and the ground in a horizontal configuration was regarded. In this case, it was assumed that connections of the legs to the ground are fixed. Equation of motion in both standard form and state-space representation was developed. Finally, based on measurements of only acceleration data points for the rigid, impulsive, and convective modes which provide a practical point of view for real-life applications, the output vector was formulated. In the second scenario, a rigid legged circular cylindrical tank equipped with four MR dampers, each installed vertically beside on of the legs, was considered. In this case, the tank was assumed to be freely set on the ground with rocking motion allowed. Equation of motion in this scenario with inspiration from the rocking behaviour of rigid blocks and then combining this idea with only one vibration mode for the coupled tank-liquid system (impulsive mode) was developed. Closed-form representations for the equivalent dynamic system were obtained, and eventually, the transfer functions from input ground motion disturbance and control force to the output rocking angle of the liquid tank were acquired. Different classical model-based control techniques including H2/LQG, PID, and FOPID were considered. A metaheuristic optimisation method using HGS recently developed in the literature was employed for optimally designing the parameters of these controllers. A modern online data-driven control approach based on the adaptive PID control technique and the Clipping methodology using the robust RLS approach, termed as ODDAPIDC was formulated which works based on online data from the sensory system in real-time. All the control techniques were combined with the semi-active Clipping algorithm to decide the voltage to the damper at each time instant.

In the next chapter, the experimental investigations over a thin-walled flexible circular cylindrical stainless steel tank are presented and the frequency of vibrations using the advanced signal processing tools are obtained to compare and contrast with the simplified mechanical model for a better understanding of behaviour of these structures. Later, the numerical and experimental investigations for both scenarios of the legged cylindrical liquid tank equipped with MR damper(s) are presented to examine the efficacy of the investigated smart dampers in seismic response attenuation and their potential for seismic

retrofitting of these strategic structures.

Chapter 4

Results and Discussion

4.1 Introduction

This chapter is discussed in three main parts. First, the experimental results of a flat-based thin-walled stainless steel circular cylindrical liquid tank over a shake table are presented. Different signal processing analyses are conducted over the measurements from the sensory system. In this part, the main objective is to extract the natural frequencies of the coupled fluid-tank system and compare them with the theoretical formulations based on the equivalent mechanical model. This comparison shows how close the practical and theoretical frequencies of the system are. Moreover, the damping ratios of each mode, the effects of the excitation frequency over the detected frequencies and peak absolute accelerations of the tank body and axial strains, the amplification of the transmitted accelerations from base to the body, and the variation of axial strains along the height of the tank body are examined.

In the second part of the chapter, the results of numerical investigations over a legged flexible thin-walled stainless steel circular cylindrical liquid tank equipped with one MR damper are presented. In this case, one MR damper is considered to be connected rigidly in a horizontal configuration between the top of the legs and the ground.

Numerical investigations were conducted using SIMULINK-MATLAB platform. Different model based control techniques described in the previous chapter were utilised to control the coupled system based on the mechanical model of the three-mode system (rigid-impulsive-convective). The system was examined under different Far-Fault and Near-Fault ground motions and for three different aspect ratios as the most important operational condition in fluid tanks to study the MR damper's efficacy and the performance of each control technique in mitigating the relative lateral displacements and absolute accelerations of the system.

Finally, in the last part of this chapter, the results of the experimental investigations over a legged rigid stainless steel circular cylindrical liquid tank equipped with four MR dampers via shake table tests are presented. Different ground motions with different PGA scales were applied and the system was controlled using the installed MR dampers. Each MR damper was installed rigidly in a vertical configuration beside each leg of the tank. A software platform using SIMULINK-MATLAB was developed which performs simultaneous data acquisition and control over the system. Using this platform, the measured data are received through the National Instruments Data Acquisition (DAQ) hardware and then based on the developed control algorithms a voltage signal is calculated and commanded to the damper. The received and commanded data are visualised and saved in real-time. Different model-based as well as the developed adaptive data-driven control techniques in the previous chapter were applied to control the system. The obtained results then were analysed to demonstrate the performance of the MR damper in reducing the seismic responses of the fluid tank using the developed flexible rocking isolation based on the smart dampers.

A software platform based on MATLAB was developed for data analysis of the DAQ measurements from the sensory system in the laboratory as shown in Figure 4.1. This software has different capabilities including the most important signal processing tools, stacking plots for comparison purposes, applying different types of filters such as low pass, band pass, and high pass filters, windowing, damping estimation of each modal frequency of the system, etc.

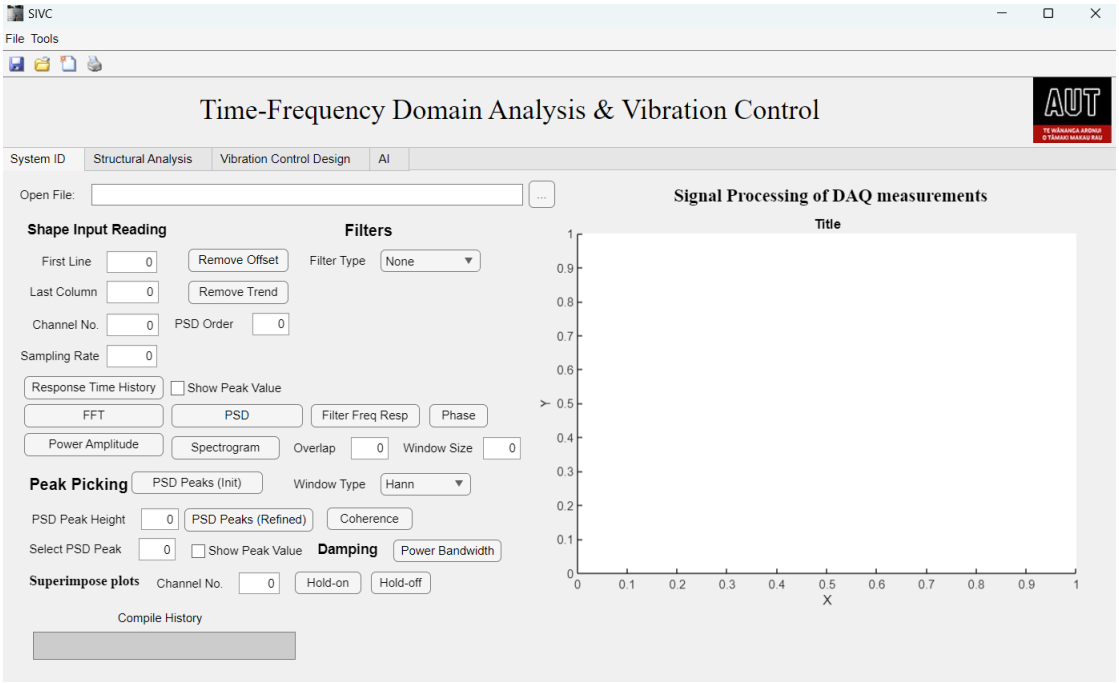

Figure 4.1: Developed software platform based on MATLAB for signal processing analyses of Data Acquisition measurements from the sensory system

4.2 Experimental investigations of a flat-based thin-walled fluid tank

4.2.1 Installations, Dimensions, and supporting frame

The investigated fluid storage tank was set over the unidirectional shake table in the Structural Engineering Laboratory of the Auckland University of Technology (AUT) as seen in Figures 4.2 and 4.3. The shake table platform is a unidirectional table with dimensions of 4000 mm by 2896 mm and a maximum horizontal stroke of ± 200 mm, run by the Shore Western controller. The maximum payload of the table is 1 ton and it is capable of producing accelerations up to $2g$. As there were no connections from the tank base to the table, a supporting frame was provided as shown in Figure 4.3. This

supporting frame consists of steel columns and beams, timber beams, and a timber plate underneath the tank to avoid any kind of damage to the shake table and other apparatus in case of overturning, buckling, or puncture of the shell or base that could cause flow of water over the table. This tank was made of stainless steel of grade 304, had a capacity of 1000 liters, and a height, diameter, and thickness equal to 1900 mm, 850 mm, and 0.5 mm, respectively. The tank was filled in three stages up to 50%, 70%, and 85% of its capacity with water to conduct tests.

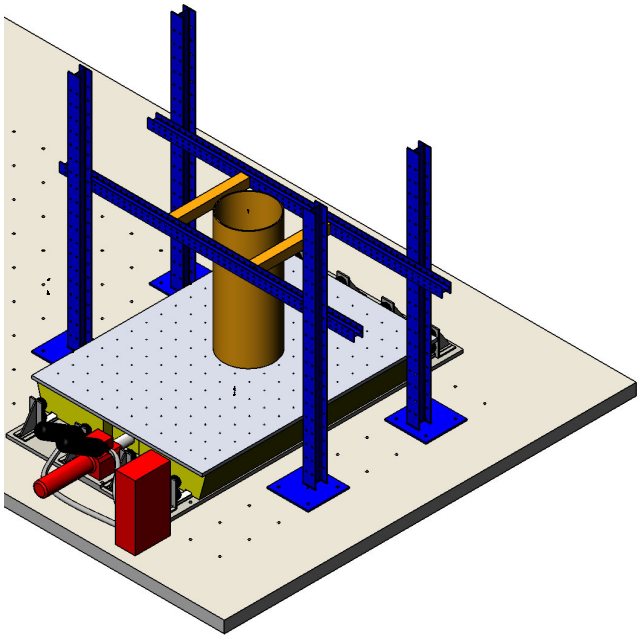

Figure 4.2: Isogeometric perspective of the experimental set-up using SOLIDWORKS

Figure 4.3: Physical model of the tank and the supporting frame

4.2.2 Instrumentation

The fluid storage tank was instrumented according to Figure 4.4. Different types of sensors including accelerometers, strain gauges, draw wires, and LVDTs were employed to measure structural responses of the system. These measurements include lateral accelerations and displacements of the shell, axial strains in the shell, and uplift of the tank base. Data acquisition was provided using the National Instruments Data Acquisition (NI DAQ) system for receiving and logging signals from the sensors. One accelerometer was attached to the shake table to measure the table's acceleration time history. Ultra-low-noise signal conditioned accelerometers with applications in structural monitoring, modal analysis, and vibration and shock monitoring were used for measurements. The employed accelerometers had operating temperature ranges of -55° to +125°C with 5000g shock protection, incorporated gas damped MEMS elements, and provided integral temperature compensation with dynamic ranges from ±2 to ±100g.

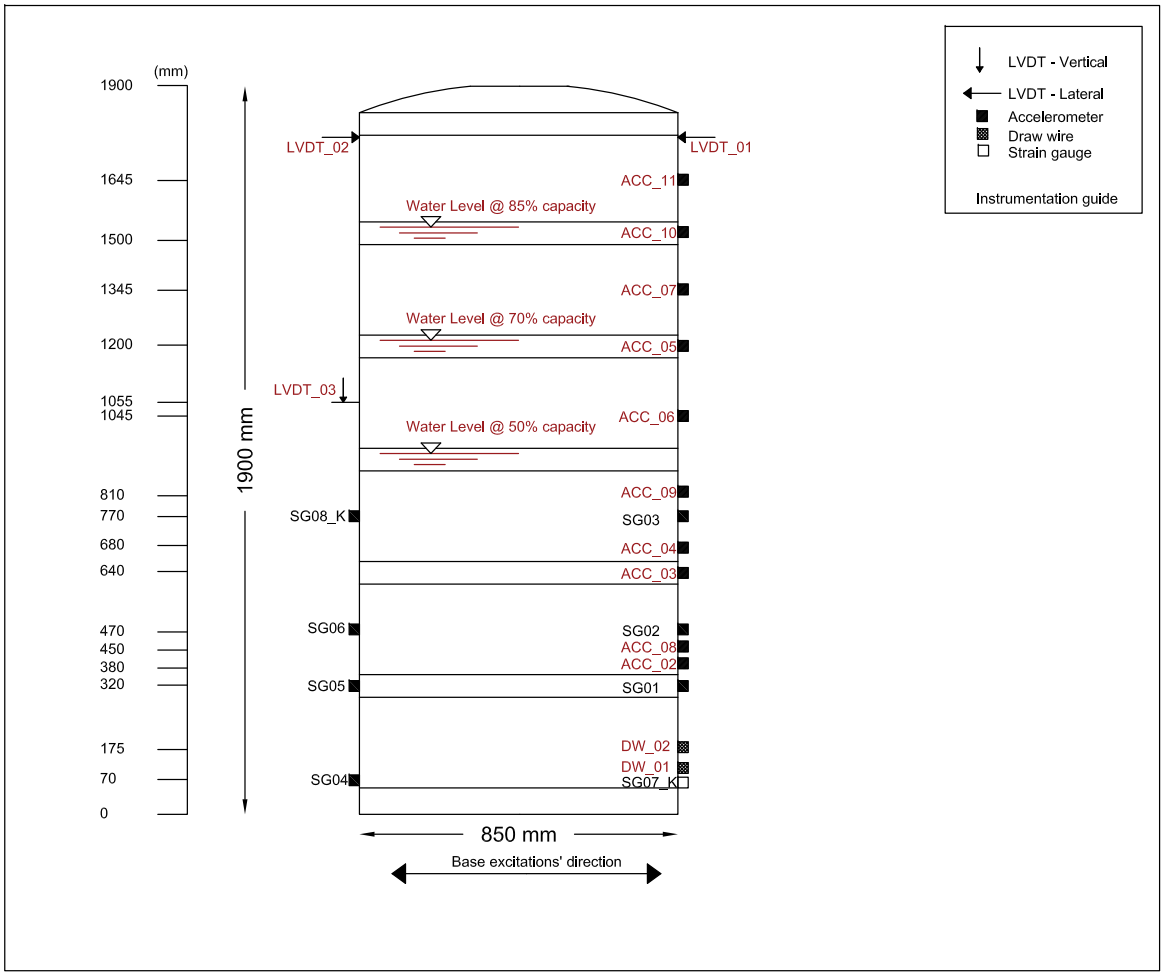

Figure 4.4: Instrumentation of the fluid tank

4.2.3 Base excitation tests

Two types of excitation were applied to the shake table including swept-sine tests and displacement time histories of five past historic ground motions. A total of 101 tests were conducted which consisted of 39 swept-sine tests and 62 seismic ground motion tests. More precise details of the conducted tests and base excitations can be found through Tables (4.1-4.3).

4.2.4 Swept-sine tests

Swept-sine excitation tests have demonstrated high performance and efficiency in vibration tests and structural health monitoring techniques in terms of simplicity, rapidity, robustness, and repeatability (Mituletu et al., 2019; F. Wang & Song, 2019; Decuyper et al., 2020; Sohn et al., 2014). A swept-sine excitation with a linear frequency rate can be mathematically represented as Equation (4.1),

$$A(t) = A_{amp} \sin\left[2\pi\left(f_0 t + \frac{\beta t^2}{2}\right) + \varphi_0\right] \tag{4.1}$$

$$\beta = \frac{f_f - f_0}{T} \tag{4.2}$$

where A_{amp} is the amplitude of the swept-sine, f_0 is the initial frequency, f_f is the final frequency, T is the sweep duration, β is the sweep rate, and φ_0 is the initial phase.

In this study, each swept-sine test had a different frequency band, duration, and amplitude. The swept-sine tests were of linear type for Frequency Sweep with constant amplitude. Each test was applied with a specific constant amplitude. Some of the tests were repeated up to three times to account for uncertainties and noise influences. The swept-sine tests were conducted for three different capacities of the tank, i.e. 50%, 70%, and 85% equivalent to aspect ratios of 2.1, 2.8, and 3.5, respectively. Accordingly, the frequency band of the swept-sine was regulated to target the natural frequencies of the system at specific ranges. The higher the values of the frequency band of the swept-sine test, the lower the displacement amplitude of the sweep was applied.

It was found that both the frequency values of the excitation and its amplitude have considerable influences on the vibratory behaviour of the system. However, the influence of the frequency values of excitation in exciting the fluid-tank system was found more influential than the displacement amplitude. When the frequency of the excitation matched the resonant frequency of the system in each test, the tank started to vibrate terrifically due to its very low thickness. Therefore, as the dynamic behaviour of the tank was monitored visually in each test, it was managed to regulate the displacement

amplitude of the next sweep test according to its frequency band values to avoid any unexpected damage and finish the test successfully. For some tests when it was found safe, for the same frequency band of the sweep the amplitude value was increased in the next test to examine its effect in the responses of the tank. Reversely, in some tests, the sweep amplitude was decreased and the same test was repeated. The duration of tests were selected as 60 sec, 120 sec, 240 sec and 300 sec. When targeting a specific frequency of the system, the time duration was increased and the same test was repeated to provide more data points and allow for more accurate and comparative data analyses. A total number of 39 swept-sine tests were conducted over the fluid storage tank. Details of the swept-sine tests have been provided in Table 4.1.

Table 4.1: Characteristics of the swept-sine tests

Observation No.	**Tank Capacity** (%)	**Aspect ratio**	**Frequency band** (Hz)	**Amplitude** (mm)	**Duration** (Sec)	**Repetition** ($No.$)
1	50	2.1	0.1-2.0	5	60	3
2	50	2.1	0.1-2.0	5	120	3
3	50	2.1	0.1-3.0	4	120	1
4	50	2.1	1.0-4.0	1	120	1
5	50	2.1	1.0-4.0	3	120	1
6	50	2.1	2.0-5.0	1	120	1
7	50	2.1	3.0-6.0	0.5	120	1
8	50	2.1	3.0-8.0	0.3	240	1
9	50	2.1	4.0-5.0	0.5	120	1
10	50	2.1	4.0-5.0	0.5	240	1
11	50	2.1	4.0-9.0	0.2	240	1
12	50	2.1	4.0-10.0	0.2	300	1
13	50	2.1	4.0-11.0	0.2	300	1
14	50	2.1	5.5-6.5	0.5	240	1
15	50	2.1	6.0-7.5	0.5	240	1

Continue on the next page

Table 4.1: Characteristics of the swept-sine tests

Observation No.	**Tank Capacity** (%)	**Aspect ratio**	**Frequency band** (Hz)	**Amplitude** (mm)	**Duration** (Sec)	**Repetition** ($No.$)
16	70	2.8	0.1-6.0	0.2	300	3
17	70	2.8	0.1-11.0	0.2	300	3
18	70	2.8	5.0-11.0	0.2	300	3
19	85	3.5	0.1-4.0	0.2	240	1
20	85	3.5	0.1-4.0	0.3	240	2
21	85	3.5	3.0-6.0	0.3	240	1
22	85	3.5	3.0-6.0	0.2	240	2
23	85	3.5	5.0-8.0	0.2	300	1
24	85	3.5	5.0-8.0	0.3	300	1
25	85	3.5	6.0-12.0	0.2	300	1
26	85	3.5	6.0-12.0	0.3	300	1

4.2.5 Seismic ground motion tests

Seismic records of five past devastating earthquakes including 1979 ElCentro, 1999 Kocaeli, 1995 Kobe, 1990 Manjil, and 2011 Christchurch were used for these types of tests. Records of the selected ground motions were obtained from the Pacific Earthquake Engineering Research Center (PEER), Next Generation Attenuation (NGA-West2) database for historical earthquake records (Ancheta et al., 2014), (https://ngawest2.berkeley.edu/). Each record was scaled using SeismoSignal (Seismosoft, 2022) to Peak Ground Acceleration (PGA) values of 0.05g, 0.1g, 0.15g, 0.2g, 0.25g, and 0.3g. Displacement time histories in millimeters units were used for each scaled ground motion and were given to the shake table to produce the excitations. A time step of 0.02 sec was used for producing time histories using the shake table. Details of each ground motion including event name, station, year, fault type, mechanism, moment magnitude (M_w), and PGA

have been presented in Table 4.2. Details of conducted ground motion tests can be found in Table 4.3. All ground motion tests were applied when the tank was up to 85% capacity full and each test was repeated up to three times.

Table 4.2: Details of the earthquake records used for seismic ground motion tests of the fluid storage tank

Event	**Station**	**Year**	**Fault type**	**Mechanism**	M_w	**PGA** (g)
Imperial Valley	ElCentro	1979	Near-fault, Pulse-like	Strike-Slip	6.53	0.449
Kocaeli	Atakoy	1999	Far-field	Strike-Slip	7.51	0.168
Kobe	KJMA	1995	Near-fault, Pulse-like	Strike-Slip	6.9	0.834
Manjil	Abbar	1990	Far-filed	Strike-Slip	7.37	0.497
Christchurch	Cathedral College	2011	Near-fault	Reverse Oblique	6.2	0.478

Table 4.3: Characteristics of the ground motion tests

Ovservation No.	**Ground motion**	**Tank Capacity** $(\%)$	**Aspect ratio**	**PGA** (g)	**Repetition** $(No.)$
1	Christchurch	85	3.5	0.05	3
2	Christchurch	85	3.5	0.10	3
3	Christchurch	85	3.5	0.15	3
4	Christchurch	85	3.5	0.20	3
5	Christchurch	85	3.5	0.25	3
6	Christchurch	85	3.5	0.30	3
7	ElCentro	85	3.5	0.05	3
8	ElCentro	85	3.5	0.10	3

Continue on the next page

Table 4.3: Characteristics of the ground motion tests

Ovservation No.	**Ground motion**	**Tank Capacity** (%)	**Aspect ratio**	**PGA** (g)	**Repetition** ($No.$)
9	Kobe	85	3.5	0.05	3
10	Kobe	85	3.5	0.10	3
11	Kobe	85	3.5	0.15	3
12	Kobe	85	3.5	0.20	3
13	Kobe	85	3.5	0.25	3
14	Kocaeli	85	3.5	0.05	3
15	Kocaeli	85	3.5	0.10	3
16	Kocaeli	85	3.5	0.15	3
17	Manjil	85	3.5	0.05	3
18	Manjil	85	3.5	0.10	3
19	Manjil	85	3.5	0.15	3
20	Manjil	85	3.5	0.20	3
21	Manjil	85	3.5	0.25	3

4.2.6 Experimental results

A sampling rate of 200 Hz with a Nyquist frequency of 100 Hz was used for data acquisition for swept-sine and ground motion tests. Acquired data were analysed in frequency and time-frequency domains based on FFT, PSD, CPSD, FRF, and STFT (Spectrogram) analyses using the Signal Processing Toolbox of MATLAB R2023a. These analyses were applied to obtain the natural frequencies and damping ratios of the detected vibrational modes. Furthermore, they were employed to investigate the effect of the frequency content of the input excitation over structural responses of the system including shell accelerations and strain values. Details of conducted data analysis to achieve the aims of this research are elucidated in the below sub-sections.

4.2.7 Swept-sine tests; Natural frequencies and damping ratios

In total, 39 swept-sine tests with different frequencies ranging from 0.1 Hz to 12 Hz and amplitudes from 0.2 mm up to 5 mm, as described in detail for each test in Table 4.1, were applied to the tank. Frequency domain and time-frequency domain analyses were conducted over time-history measurements of sensors attached to the tank. The PSD, FFT, and STFT or Spectrogram were calculated for time-history measurements of accelerations, displacements, and strains recorded by the respective sensors. Using the applied analyses, natural frequencies of different modes of the vibrations of the coupled fluid-tank system were detected.

Damping ratios

The half power bandwidth (-3dB rule) method (Papagiannopoulos & Hatzigeorgiou, 2011; Casiano, 2016; Silvestri et al., 2022) was used to calculate the damping ratio (ζ) of each detected mode of vibration, and a quality (amplification) factor (Q) was calculated corresponding to each damping ratio. The relationship between the amplification factor, the damping ratio, and the bandwidth are as defined in Equations (4.3) and (4.4) (Papagiannopoulos & Hatzigeorgiou, 2011; Casiano, 2016) below,

$$Q = \frac{1}{2\zeta} \tag{4.3}$$

$$Q \approx \frac{\omega_p}{\omega_2 - \omega_1} \tag{4.4}$$

where, ω_p is the peak frequency in Hz, and (ω_2 - ω_1) is the bandwidth in Hz corresponding to positions where peak power amplitude (A_{max}) drops for 3dB which corresponds to positions of the $\frac{\sqrt{2}}{2}$ A_{max}. The power amplitude graphs of accelerometers No. 2 and 3 for the aspect ratios of 2.1 and 3.8 which represent the locations of impulsive mass for these aspect ratios and the damping ratios for frequencies 9 Hz and 9.5 Hz have been calculated using the half-power bandwidth as illustrated in Figure 4.5 (a, b), respectively. Damping ratios of 0.5% and 3% have been widely used in literature and seismic design

codes of fluid storage tanks for the convective and impulsive modes, respectively. The half-power bandwidth analysis conducted over power amplitude graphs of signal measurements at different natural frequencies detected different damping ratios mostly in the range of 0.3%-3%. The damping ratios of 0.3% at the location of the convective mass and 0.4% at the location of accelerometer channel No. 2, both for the centre frequency of 9.5 Hz and the aspect ratio of 3.5, have been calculated. These values fall near the recommended value of 0.5% for the first convective mode. A damping ratio of 2.56% at the location of accelerometer channel No. 11 for the centre frequency of 27.70 Hz and the aspect ratio of 3.5 was observed. This experimentally observed damping ratio is a well-matched value to the advised damping ratio of 3% in seismic codes and the literature for analysis and design of stainless steel fluid tanks.

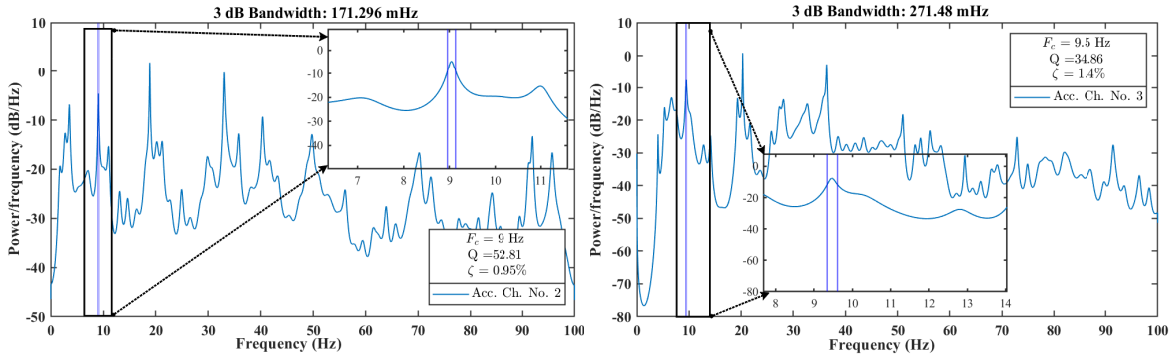

(a) Impulsive mass for S = 2.1

(b) Impulsive mass for S = 2.8

Figure 4.5: Power amplitude graph and the calculated damping ratio using half-power bandwidth

4.2.8 Fundamental natural frequencies of the system

Evaluated natural frequencies and comparisons between theoretical and experimental results have been illustrated in Table 4.4. In this table, the detected experimental and calculated theoretical natural frequencies have been presented for each aspect ratio (S) examined in this research. For the theoretical modes, only the first convective and the

first impulsive modes according to Equations (3.74) and (3.75) have been considered, respectively. To calculate the fundamental impulsive frequency of the tank-water system, E_t and γ_t for the material of the tank were considered as 200 GPa, and 7850 (kg/m^3), respectively.

Examining the experimental results demonstrated that the closest match between the theoretical and experimental convective frequency could be attributed to the aspect ratio of 2.1 that resulted in a frequency of 1.85 Hz which matches the second convective mode frequency f_{c2} according to Equation (3.46). For the theoretical impulsive mode of the coupled system, the best matches were found for the aspect ratios of 2.8 and 3.5 for the experimentally detected natural frequencies of 56.30 and 41.66 Hz, respectively. These frequencies match the calculated fundamental impulsive natural frequencies of the fluid tank via Equation (3.60). Other observed frequencies from the experimental results were 2.85 Hz for the aspect ratio of 2.1, and 73.30 Hz for the aspect ratio of 3.5. It may be concluded that for the impulsive mode of the system, the higher the aspect ratio the closer the theoretical value to the experimental results. This could be attributed to the fact that the high values of the aspect ratio cause the system to behave more like a flexural beam which corresponds to the theory used for formulating the mathematical model. The discrepancies found between the theoretical and experimentally detected natural frequencies of the coupled fluid-tank system could be attributed to the chaotic, rotational, and highly nonlinear vibrations of the fluid in the tank that violate the simplified hypotheses considered when formulating the SMM of these structures. Figure 4.6 (a, b) shows the PSD graphs versus frequency in Hz illustrated for the acceleration time-history of a series of accelerometers for the aspect ratios of S = 2.1 and S = 2.8. Observations of fluid surface vibrations during swept-sine tests which demonstrate the nonlinear, rotational, and chaotic fluid surface vibrations have been illustrated in Figure (4.7). Based on the experimental results obtained for the natural frequencies of the fluid tank system, it seems that consideration of higher sloshing modes will result in more exact calculations for the analysis and design of fluid storage tanks.

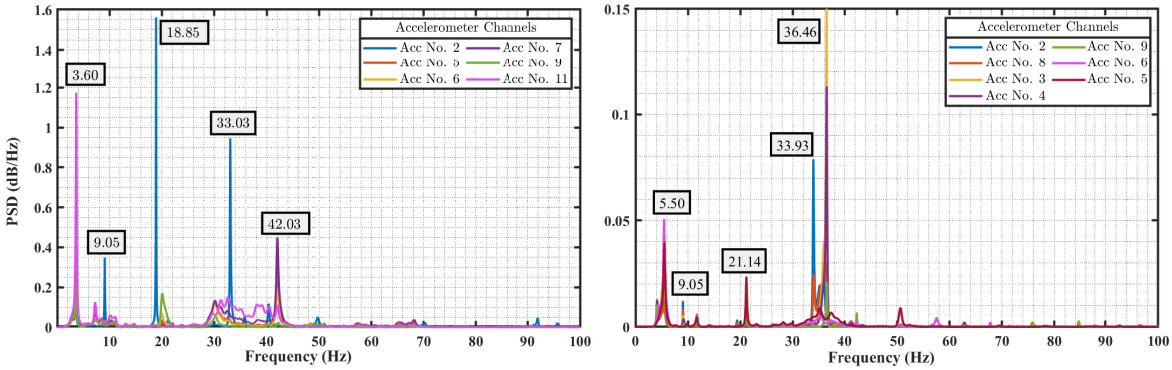

(a) S = 2.1 (b) S = 2.8

Figure 4.6: Power spectral density graph for a series of accelerometer channels: (a) Swept-sine [1-4] Hz, 3 mm amp, 120 s, (b) Swept-sine [0.1-6] Hz, 0.2 mm amp, 300 s

Table 4.4: Evaluated experimental and theoretical natural frequencies of the thin-walled steel fluid-tank system

S	**Experimentally detected modes** (Hz)											**Theoretical modes** (Hz)		
	1	**2**	**3**	**4**	**5**	**6**	**7**	**8**	**9**	**10**	**11**	f_{c1}	f_{c2}	f_{i1}
2.1	**1.85**	3.60	5.60	7.20	9.80	14.30	20.20	33.10	35.90	42.50	70.04	1.037	**1.77**	78.11
2.8	–	4.02	5.52	6.50	9.80	14.30	20.30	32.60	36.40	42.30	**56.30**	1.038	1.77	**55.02**
3.5	–	3.70	5.50	6.90	9.60	14.80	19.60	32.70	35.60	**41.66**	77.10	1.038	1.77	**41.51**

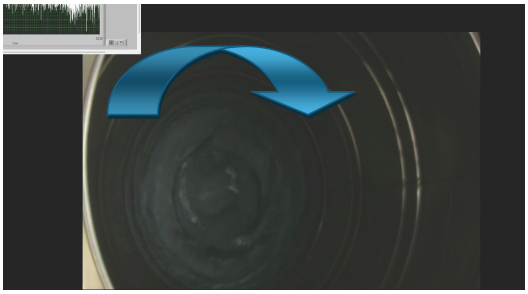

Rotational fluid surface vibrations

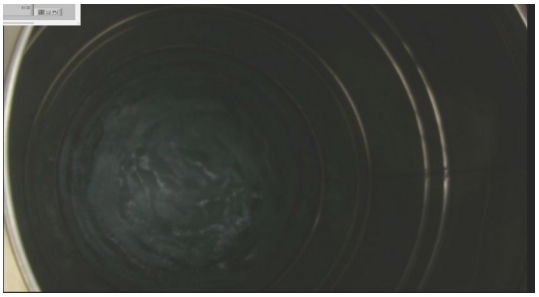

Planar nonlinear fluid surface vibrations

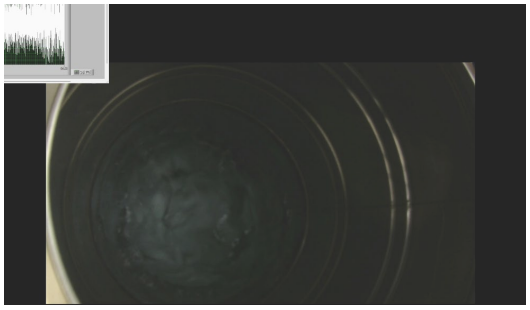

Chaotic fluid surface vibrations

Figure 4.7: Observations of fluid surface vibrations during swept-sine excitation tests under different flow conditions including nonlinear, rotational, and chaotic fluid flows

4.2.9 Effects of the swept-sine excitation frequency

In this section, the effects of the input excitation's frequency content, amplitude, and duration on the structural responses of the tank-water system including accelerations and axial strains are examined.

4.2.10 Examining the effects over accelerations

Herein, the effects of the swept-sine excitation frequency band over the acceleration time history responses of accelerometer channels No. 2 and 3 for the aspect ratio of 2.1 and 2.8, representing the locations of the impulsive mass for these aspect rations, respectively, in the frequency and time-frequency domains have been studied. The PSD graph of the accelerometer channel No. 2 for the aspect ratio of 2.1 has been depicted in Figure 4.8 (a, b), while Figure 4.9 illustrates the STFT graph of accelerometer channel No. 3

for the aspect ratio of 2.8. Two swept-sine signals with the same duration but different amplitudes and frequency bands were considered for the aspect ratio of 2.1 in Figure 4.8 (a) containing a frequency window of [17-20.5] Hz in this graph which shows how the amplitude of the PSD is magnified for a frequency of 18.8 Hz when the frequency of the swept is increased from [1-4] Hz to the [2-5] Hz even with a lower amplitude. In Figure 4.8 (b), a frequency of around 33 Hz was the focus of attention. The two swept-sine signals with the same amplitude and duration but different frequency bands have been applied. The frequency window of [30-36] Hz shows that the higher amplitude of the PSD graph occurs under the swept-sine signal with the frequency band of [6-7.5] Hz.

The one-sided spectrograms using the STFT method for accelerometer channel No. 3 for the aspect raio of 2.8 have been calculated and represented in Figure 4.9 (a, b). A kaiser window of length 200 samples with a shape factor of β = 5, equivalent to a leakage of l = 87.5%, 200 Discrete Fourier Transform (DFT) points, and 100 samples (50%) of overlap between adjoining points were used for calculating the STFT of the signals (Boashash, 2016). As seen in Figure 4.9 (a, b), the same frequency range which falls in the frequency band of the input excitation signal shows the strongest beams of light. For the case of the input signal with the frequency band of [5-11] Hz, the expanding beams of light are more obvious and could be interpreted as activating more natural frequencies of the system.

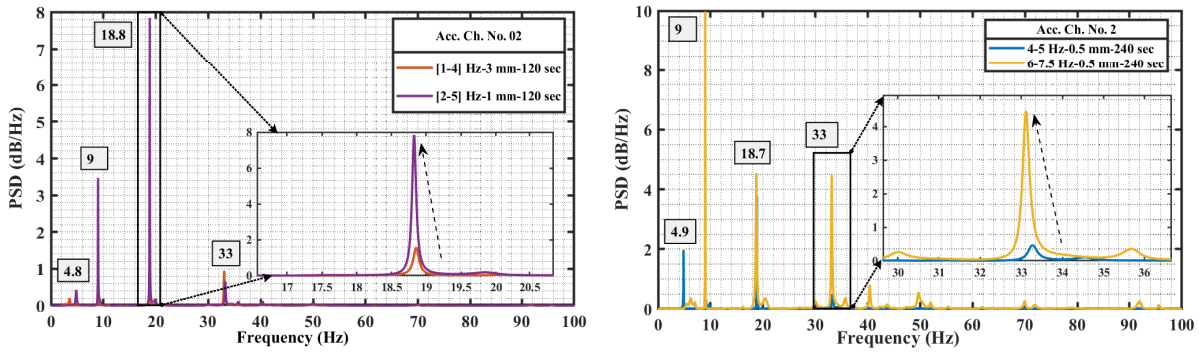

(a) f = 18.8 Hz (b) f = 33 Hz

Figure 4.8: Power spectral density graph of accelerometer channel No. 2 (location of impulsive mass) for tests with S = 2.1: (a) Swept-sine tests [1-4] Hz, 3 mm amp, 120 s and [2-5] Hz, 1 mm amp, 120 s, (b) Swept-sine tests [4-5] Hz, 0.5 mm amp, 240 s and [6-7.5] Hz, 1 mm amp, 120 s

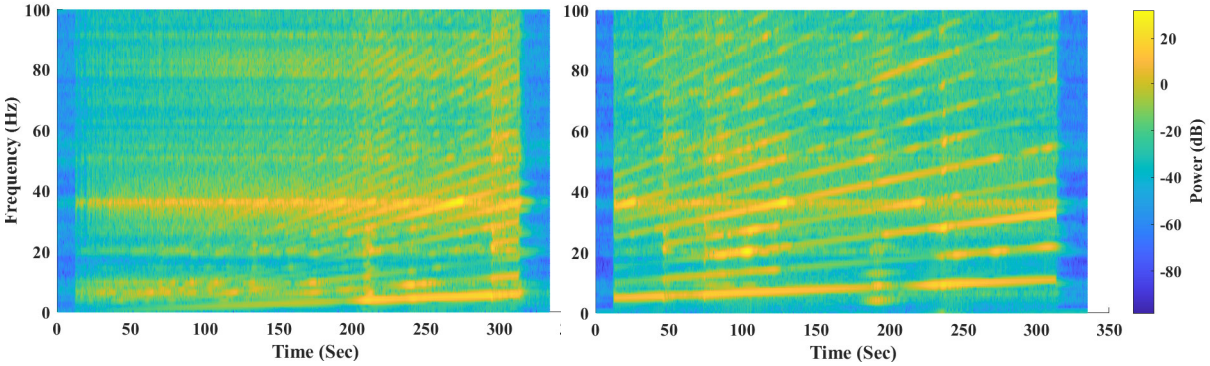

(a) Swept-sine 0.1-6 Hz (b) Swept-sine 5-11 Hz

Figure 4.9: Spectrogram of accelerometer channel No. 3 (location of impulsive mass) for tests with S = 2.8: (a) Swept-sine test [0.1-6] Hz, 0.2 mm amp, 300 s (b) Swept-sine test [5-11] Hz, 0.2 mm amp, 300 s

4.2.11 Considering the effects over axial strains

Two swept-sine signal tests with the frequency bands of [0.1-4] and [6-12] Hz, with the same amplitude of 0.3 mm, and durations of 240 and 300 Sec, respectively, are considered. The spectrogram of channel No. 21 which represents the strain gauge No. 4 attached to the tank shell, very close to the base (at a distance of 70 mm), in response to these excitations for the aspect ratio of S = 3.5 has been depicted in Figure 4.10(a,b). As seen in these figures the same frequency bands of the input excitation have been activated in the corresponding spectrograms of the strain gauge channels under consideration through showing themselves as the brightest rays of light. In Figure 4.10(b) for the excitation with the frequency band of [6-12] Hz activation of more natural frequencies is evident.

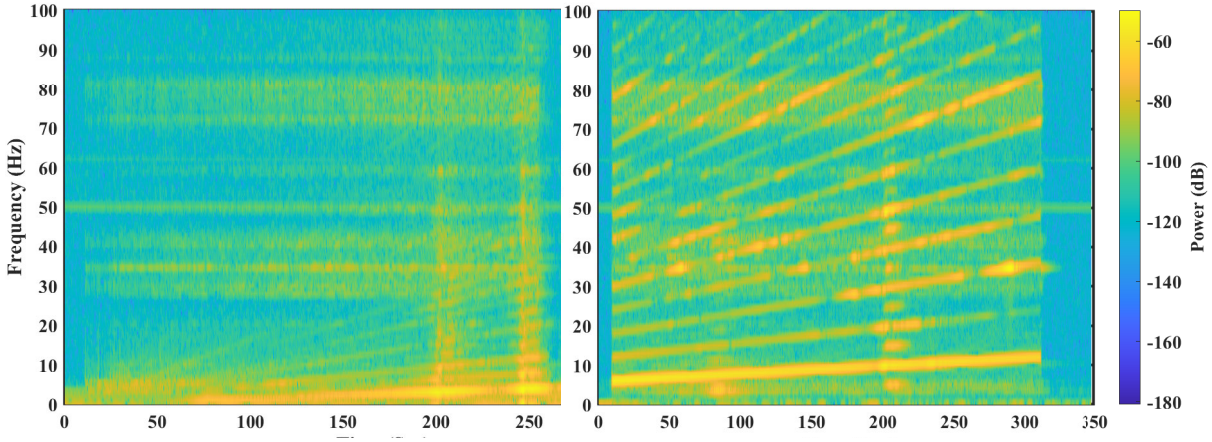

(a) Swept-sine 0.1-4 Hz (b) Swept-sine 6-12 Hz

Figure 4.10: Spectrogram of strain gauge No. 4 (70 mm from the base) for tests with S = 3.5: (a) Swept-sine test [0.1-4] Hz, 0.3 mm amp, 240 s (b) Swept-sine test [6-12] Hz, 0.3 mm amp, 300 s

4.2.12 Ground motion tests

In this section, the effects of different near-fault and far-fault seismic ground motions with different frequency contents considered in this study over the structural responses of

the steel fluid storage tank have been examined. Considered ground motions which were described in detail in section 3.2 and Table 4.2 were scaled according to Table 4.3 and were applied to the shake table when the tank was full up to 85%. As discussed before this level of water in the tank is equal to the aspect ratio of 3.5. The effects of these ground motions at different scales of PGA over a series of signals have been studied. These signals include measurements of strain gauges at the bottom and mid-height of the tank body as well as accelerometers at different levels of height. Amplification of accelerations transmitted to the tank shell at the positions of calculated impulsive and convective masses as well as fluid surface have been calculated and presented in graphs. A comparative study of the effects of the considered ground motions, all at the same PGA level of 0.1 G, over the acceleration amplifications and strains developed in the shell has been presented. The FFT diagram of these ground motions has been depicted in Figure 4.11. The CPSD analysis from the input base excitation acceleration time history (Channel No. 12) to the output shell acceleration at the location of the convective mass (Channel No. 7) has been presented in Figure 4.12. The CPSD analysis was conducted using the Welch (Welch, 1967) method and a Bartlett window with 50% overlap between the adjoining segments. It is inferred from this graph that the Manjil 0.1 G ground motion has the dominant effect over the acceleration time history of the shell at the location of the convective mass over most of the frequency components. The FRF analysis of this earthquake between the same Input/Output channels, representing the magnitude, phase, and coherence, using a Hanning window with 50% overlap between the adjoining segments has been illustrated in Figure 4.13.

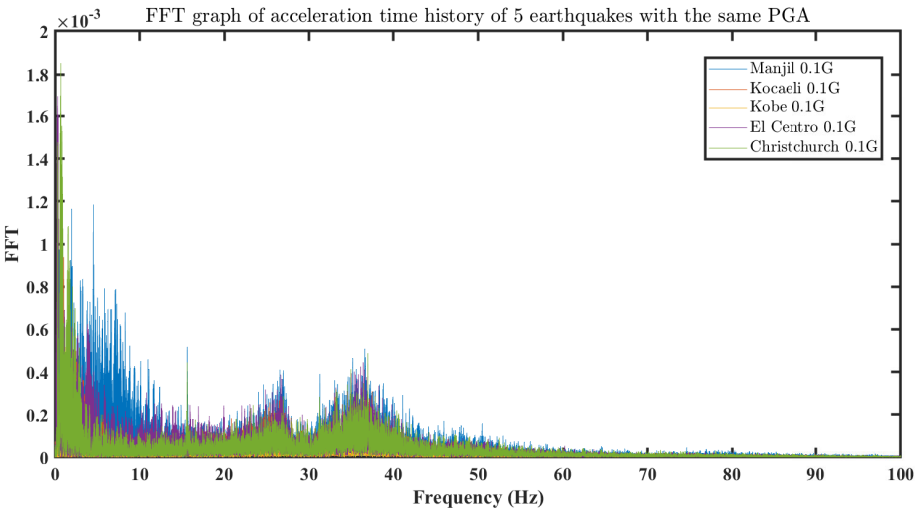

Figure 4.11: FFT of the acceleration time history of shake table under five earthquakes with the same PGA of $0.1G$ for S = 3.5

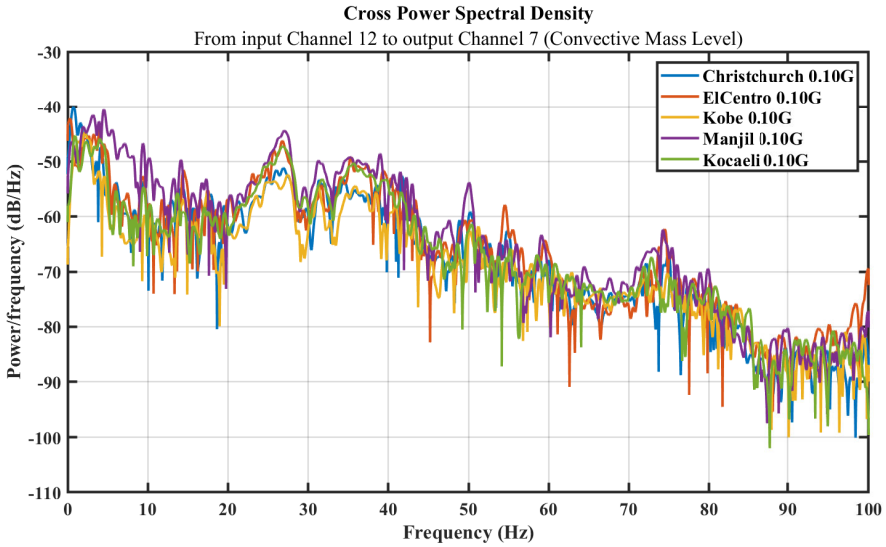

Figure 4.12: Comparative evaluation of Cross Power Spectral Density (CPSD) from input base excitation (Accelerometer Channel No. 12) to output Accelerometer Channel No. 07 (location of convective mass) for S = 3.5 under different earthquakes of PGA = $0.1G$

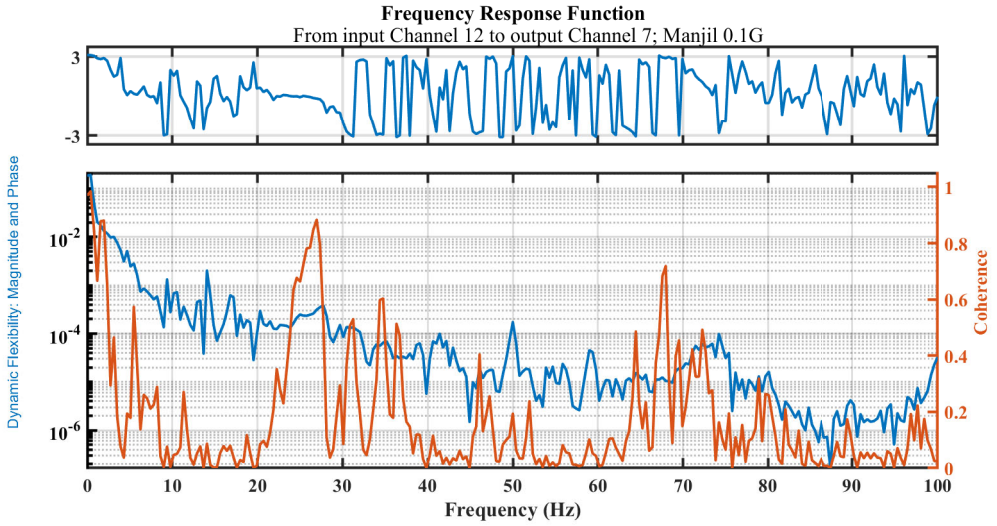

Figure 4.13: Frequency Response Function (FRF) from input base excitation (Accelerometer Channel No. 12) to output Accelerometer Channel No. 07 (location of convective mass) for S = 3.5 under Manjil earthquakes of PGA = 0.1G

4.2.13 Transmitted acceleration and axial strain in the shell

To examine the effects of the frequency content of the input ground motions on the tested fluid storage tank, the acceleration amplification factor at different heights of the system is calculated and examined according to the below equation (Chopra, 2001; Thomson & Dahleh, 1997; J. Li, Chen & Chen, 2007; W. Liu et al., 2023),

$$Q_{acc}|_d = \frac{max(|\ddot{u}_d(t)|)}{PIA} \tag{4.5}$$

where, $Q_{acc}|_d$ is the amplification factor of acceleration at a distance of d from the base of the tank, $\ddot{u}_d(t)$ is the acceleration time history of a point over the tank body at a distance of d from the base, and PIA is the absolute value of the peak input acceleration to the system. Acceleration amplification factors for accelerometer channel Nos. 02, 03, 09, 05, 07, 10, and 11 with distances of 0.38 m, 0.64 m, 0.81 m, 1.2 m, 1.3 m, 1.5 m, and 1.65 m, respectively, under the Manjil 1990 earthquake at different PGA scales

have been depicted in Figure 4.14 (a). The height of the first convective mass according to the Equation (3.76) for 85% capacity of the tank (S = 3.5), with the water at a level of 1.5 m from the base, is calculated as 1.3 m which corresponds to the location of the accelerometer No. 07. For this water level in the tank, the height of the impulsive mass based on the graphs represented for the design of fluid tanks (Haroun & Housner, 1981b; NZSEE, 2009) is calculated as 0.83 m which corresponds to the location of accelerometer channel No. 9. Accelerometer No. 10 is located exactly at the location of surface liquid. A comparison of variations of acceleration amplification factors at different heights of the shell under different earthquakes, all scaled to the same PGA level of 0.1 g, has been illustrated in Figure 4.14 (b). This figure shows that the Manjil earthquake has caused the dominant acceleration amplification factors at almost all levels. Amplification factors shown in these figures for accelerometer channel No. 10 at the surface fluid reflect higher values than that of accelerometer channel No. 07. This confirms the fact that the acceleration responses of the tank body at different heights are governed by the surface fluid vibrations.

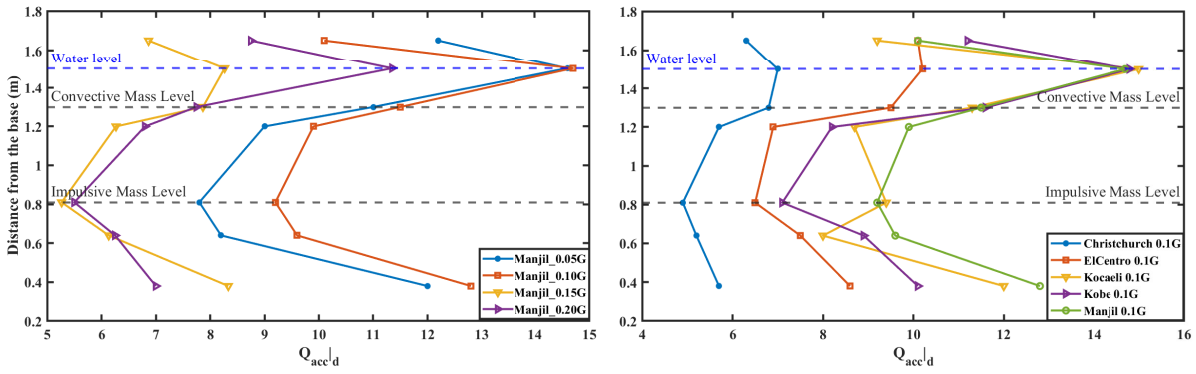

(a) Different PGA scales of Manjil earthquake

(b) Different earthquakes all at the PGA of $0.1G$

Figure 4.14: Acceleration amplification factor at different heights of the tank body for S = 3.5: (a) under different scales of the Manjil 1990 earthquake (b) under five earthquakes all at the PGA of $0.1G$

The variations of axial strain values over the shell body for strain gauge channel Nos. 21, 18, and 19 at distances of 70 mm, 320 mm, and 470 mm, respectively, under

different PGA scales of the Majil 1990 earthquake, have been shown in Figure 4.15 (a). A comparison of variations of axial strain values at different heights of the shell under different earthquakes all at the PGA level of $0.1G$ has been represented in Figure 4.15 (b). As seen in these figures the highest level of strain under all earthquakes occurs at the position of strain gauge channel No. 21 which is located 70 mm from the base of the tank. This fact justifies the reason for the common elephant foot buckling phenomenon that happens around the base as a result of high-stress concentrations. The response time histories of strain gauge channels No. 21 and 18 which are the strain gauges at distances of 70 mm (strain gauge No. 4) and 320 mm (strain gauge No. 1) from the base, under the Kobe 1995 earthquake at the PGA scale of $0.1g$ have been shown in Figure 4.16 (a) and (b), respectively. The strain values at the base of the tank in Figure 4.16 (a) show high levels of compression in the shell with an unsymmetrical trend. However, The strain values recorded by the strain gauge No. 1 at the height of 320 mm as shown in Figure 4.16 (b), represent a symmetrical behaviour of the compression and tension strains.

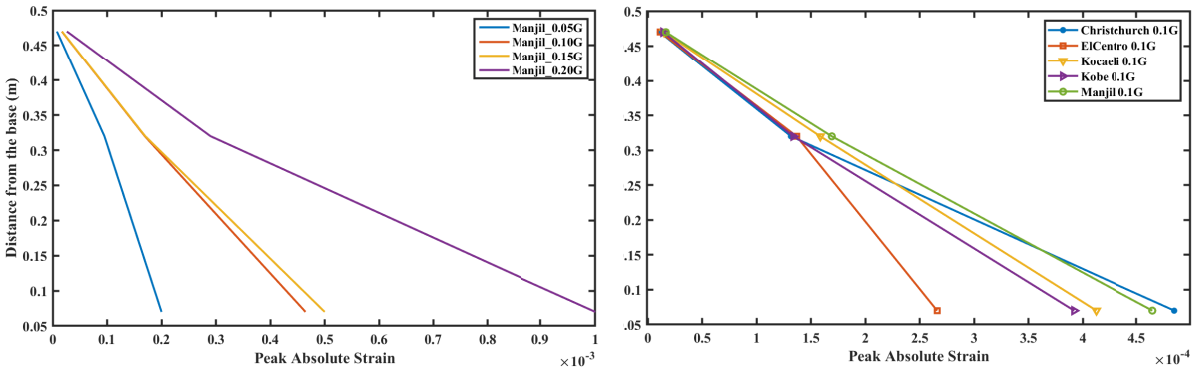

(a) Different PGA scales of Manjil earthquake

(b) Different earthquakes all at the PGA of $0.1G$

Figure 4.15: Variation of absolute axial strain values on the tank shell along the height for S = 3.5: (a) under different scales of the Manjil 1990 earthquake (b) under five earthquakes all at the PGA of $0.1G$

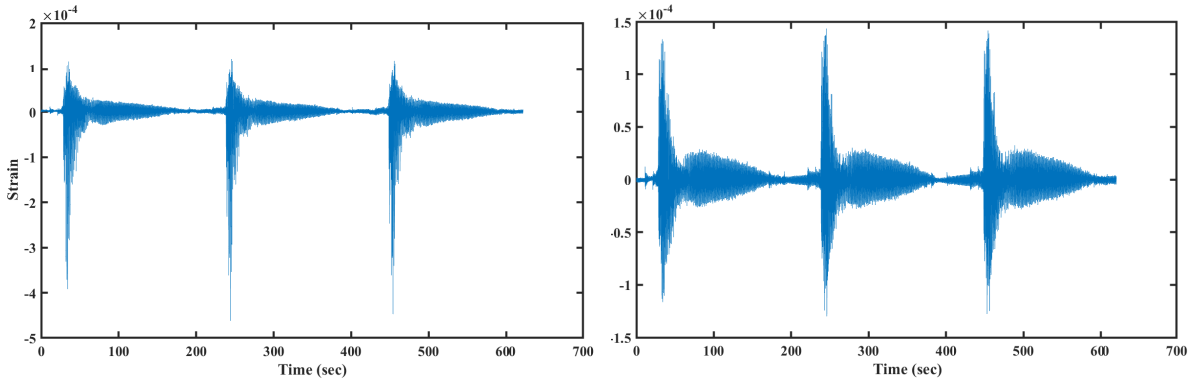

(a) Strain gauge No. 4 (b) Strain gauge No. 1

Figure 4.16: Response time histories of strain gages No. 1 and 4 under the Kobe $0.1G$ earthquake for S = 3.5 (three runs of the test): (a) at a distance of 70 mm from the base (b) at a distance of 320 mm from the base

4.3 Numerical investigations of a legged flexible tank-MR

To investigate the efficacy of MR dampers in vibration mitigation of the model fluid-tank system shown in Figure 3.2, represented in Chapter 3, section 3.3.3, an example of a stainless-steel circular cylindrical tank with a height of 1500 mm, a radius of 425 mm, and a shell thickness of 1.7 mm is considered. Legs are stainless-steel pipes with a thickness of 2 mm, height of 795 mm, and radius of 50 mm. Other specifications of the tank are modulus of elasticity, E_t = 200 GPa, poison's ratio ν = 0.3, density of steel, ρ_s = 7850 kg/m^3, and density of water, ρ_w = 1000 kg/m^3. Damping ratios of 2% and 0.5% have been considered for the tank shell material and the convective modes of fluid vibrations. The damping ratio for legs has been regarded as similar to that of the shell body. This fluid-tank system has been modeled by considering the first fundamental impulsive mode and the first fundamental convective mode to represent the fluid-structure interaction between the tank shell and the fluid domain. The parameter Λ for the noise

process of the H2/LQG control technique was selected as 50.

The considered MR damper in this study has a capacity of around 2.45 kN, and the input voltage to the damper is regarded in the range of 0 to 5 V. The MR damper model regarded in this study is RD-8041-1 (long stroke). The parameters of the modified Bouc-Wen model for the MR damper are considered as presented in Table (4.5) which have been experimentally obtained and verified in previous investigations (Gao, 2012). The fluid-tank-MR system has been studied under four seismic events, three Far-Fault, and three Near-Fault, as shown along with their characteristics in Table (4.6). In this table, M_w is the moment magnitude of the earthquake, PGA is the Peak Ground Acceleration in g (gravitational acceleration), and DF is the dominant frequency of the record in Hz. The frequency content of the selected input ground motions to examine the performance of the equipped fluid tank with the MR damper is shown in Figure 4.17. In this figure, $|P1(f)|$ is the single-sided amplitude spectrum of the signal versus the Nyquist frequencies, in the frequency domain $f(Hz)$, calculated using the signal processing toolbox of MATLAB R2023b. The coupled tank-liquid-MR damper system was analysed under uncontrolled and five different control strategies, including three semi-active and two passive control strategies. A description of the applied control techniques and their designed parameters using the HGS optimisation method for each ground motion and aspect ratio have been presented in Table (4.7).

Table 4.5: Parameters of the Bouc-Wen model of the MR damper

Parameter	**Value**	**Parameter**	**Value**
α_a	1921.141 (N/m)	k_0	1940.405 (N/m)
α_b	5882.51 $(N/V.m)$	k_1	1.751268 (N/m)
c_{1a}	2089.263 $(N.s/m)$	A	155.32
c_{1b}	14384.918 $(N.s/V.m)$	β	36332.07 (m^{-2})
c_{0a}	651.4718 $(N.s/m)$	γ	36332.07 (m^{-2})
c_{0b}	1043.7559 $(N.s/V.m)$	x_0	0.00 (m)
μ	60 (s^{-1})	n	2

Table 4.6: Characteristics of the selected input ground motions

Event	**Year**	**Fault type**	M_w	**PGA(g)**	**DF(Hz)**
El Centro	1940	Far-Fault	6.9	0.348	7.32
Hachinohe	1968	Far-Fault	7.8	0.229	1.83
Kobe	1995	Near-Fault	6.9	0.833	7.26
Northridge	1994	Near-Fault	6.7	0.842	3.17
Manjil	1990	Far-Fault	7.37	0.497	9.58
Tabas	1978	Near-Fault	7.35	0.854	6.35

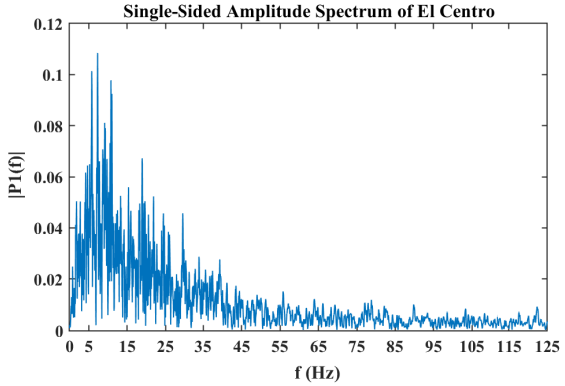

(a) ElCentro

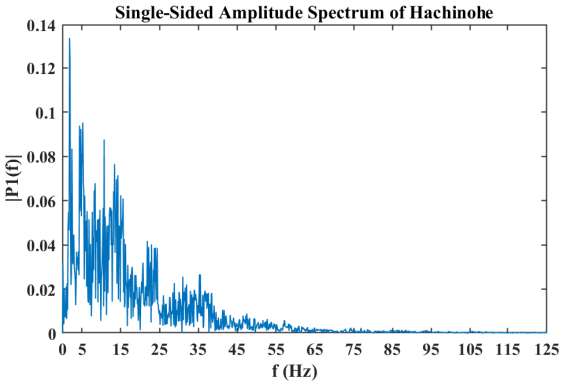

(b) Hachinohe

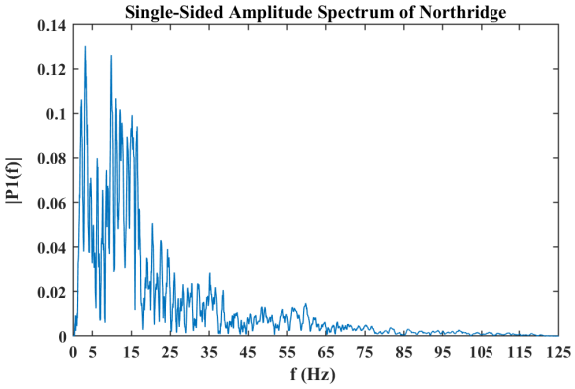

(c) Northridge

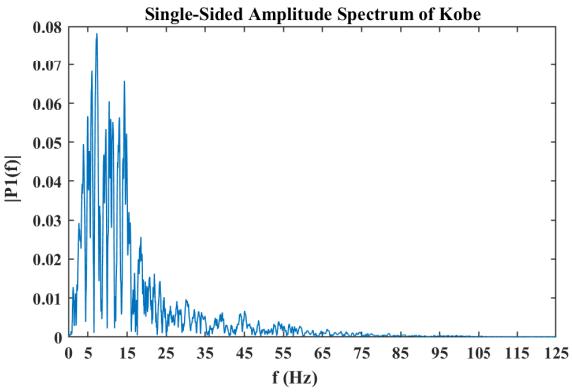

(d) Kobe

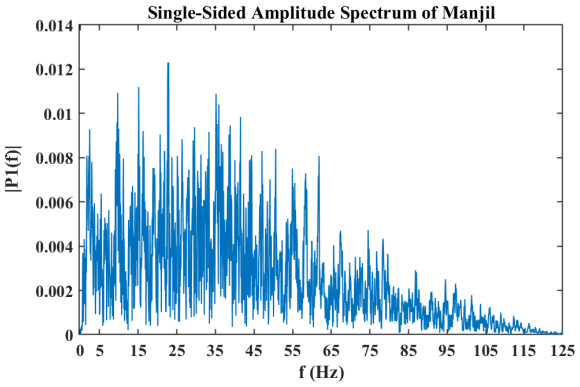

(e) Manjil

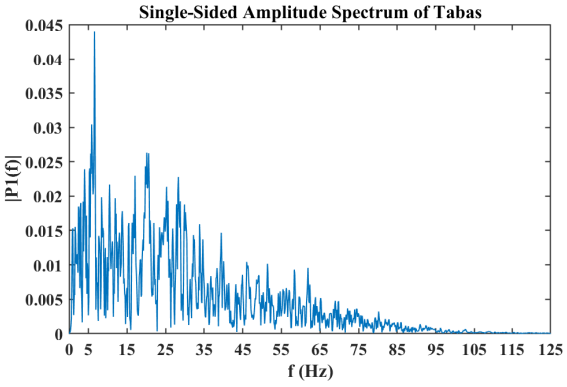

(f) Tabas

Figure 4.17: Frequency content of the selected Far-Fault and Near-Fault ground motions

Table 4.7: Optimal parameters of the selected semi-active controllers

Controller	Objective	Parameters	Range	El Centro	Hachinohe	Kobe	Northridge	Manjil	Tabas
S = 1.00 ($Broad\,tank$)									
PID-COC-HGS	ITAE	K_P	$[0\ 25000] \in \mathbb{R}$	25000	25000	0.00	19483	1891.90	11587
		K_I	$[0\ 25000] \in \mathbb{R}$	23033.60	24419	0.00	0.00	24989	24318
		K_D	$[0\ 10^4] \in \mathbb{R}$	2691.50	1857	9345.50	631.60	7913.60	5986.50
FOPID-COC-HGS	ITAE	K_P	$[0\ 10^4] \in \mathbb{R}$	10000	0.00	336.70	9464.50	9077.20	9631.40
		K_I	$[0\ 10^4] \in \mathbb{R}$	868.20	4501.50	4186.90	1.146	5951.10	2545.90
		K_D	$[0\ 10^4] \in \mathbb{R}$	6416.60	10000	1527.80	10000	1397	7481.10
		λ_s	$[0\ 2] \in \mathbb{R}$	0.00	0.96	0.83	2.00	1.30	0.10
		μ_s	$[0\ 2] \in \mathbb{R}$	0.56	0.50	0.59	0.47	0.64	0.59
H2/LQG-COC-HGS	Obj	Q_f	$[0\ 1] \in \mathbb{R}$	0.7813	0.9279	0.7883	0.8853	0.4172	0.5386
		R_f	$[10^{-1}\ 10^{-16}] \in \mathbb{R}$	$10^{-3.77}$	10^{-4}	$10^{-8.76}$	$10^{-3.57}$	$10^{-3.91}$	$10^{-3.81}$

Continue on the next page

Table 4.7: Optimal parameters of the selected semi-active controllers

Controller	Objective	Parameters	Range	El Centro	Hachinohe	Kobe	Northridge	Manjil	Tabas
S = 2.00 ($Slender\ tank$)									
PID-COC-HGS	ITAE	K_P	$[0\ 25000] \in \mathbb{R}$	25000	22011	14604	15499	25000	25000
		K_I	$[0\ 25000] \in \mathbb{R}$	2228.50	1663	23119	2818	389.84	0.00
		K_D	$[0\ 10^4] \in \mathbb{R}$	1369.60	2272	899.94	882.84	2550.30	3120
FOPID-COC-HGS	ITAE	K_P	$[0\ 10^4] \in \mathbb{R}$	0.00	1781.30	9505.70	1428.70	4005.10	10000
		K_I	$[0\ 10^4] \in \mathbb{R}$	7852.94	0.00	2662.30	10000	1427.40	4020.90
		K_D	$[0\ 10^4] \in \mathbb{R}$	6434	5134.50	9968.70	3547.90	1418.20	9008.80
		λ_s	$[0\ 2] \in \mathbb{R}$	1.01	0.1211	2.00	1.29	0.75	2.00
		μ_s	$[0\ 2] \in \mathbb{R}$	0.44	0.4895	0.53	0.46	0.51	0.53
H2/LQG-COC-HGS	Obj	Q_f	$[0\ 1] \in \mathbb{R}$	0.6053	0.8036	0.7388	1.00	0.7959	0.8279
		R_f	$[10^{-1}\ 10^{-16}] \in \mathbb{R}$	$10^{-4.67}$	$10^{-4.47}$	$10^{-4.63}$	$10^{-4.36}$	$10^{-4.45}$	$10^{-4.49}$

Continue on the next page

Table 4.7: Optimal parameters of the selected semi-active controllers

Controller	**Objective**	**Parameters**	**Range**	**El Centro**	**Hachinohe**	**Kobe**	**Northridge**	**Manjil**	**Tabas**
			S = 3.00 ($Slender\ tank$)						
PID-COC-HGS	ITAE	K_P	$[0\ 25000] \in \mathbb{R}$	24260	17193	16061	17687	25000	25000
		K_I	$[0\ 25000] \in \mathbb{R}$	284	8411	0.00	14203	11464	2180
		K_D	$[0\ 10^4] \in \mathbb{R}$	825	659	814.60	758.70	997.66	1215.50
FOPID-COC-HGS	ITAE	K_P	$[0\ 10^4] \in \mathbb{R}$	9998.50	2208.70	59.62	5591.30	7845.02	3373.10
		K_I	$[0\ 10^4] \in \mathbb{R}$	2265	8119.80	4908.52	0.00	4799.40	10000
		K_D	$[0\ 10^4] \in \mathbb{R}$	10000	5916.10	7922.06	7930.80	7899.20	9055.10
		λ_s	$[0\ 2] \in \mathbb{R}$	1.20	1.06	0.00	2.00	0.45	0.93
		μ_s	$[0\ 2] \in \mathbb{R}$	0.47	0.46	0.50	0.46	0.47	0.48
H2/LQG-COC-HGS	Obj	Q_f	$[0\ 1] \in \mathbb{R}$	0.3104	0.9490	1.00	0.020	0.0447	0.3344
		R_f	$[10^{-1}\ 10^{-16}] \in \mathbb{R}$	$10^{-5.42}$	$10^{-4.71}$	$10^{-4.75}$	$10^{-6.64}$	$10^{-6.27}$	$10^{-5.32}$

Numerical simulations have been conducted using SIMULINK and MATLAB R2023b to calculate the vibrational responses of the system under the considered ground motion. Results have been compared for different scenarios of the control strategies and aspect ratios as the main operational condition to evaluate the efficacy of the added damper to the fluid tank system. These scenarios include the uncontrolled case, the controlled system with three different control techniques including H2/LQG-COC-HGS, PID-COC-HGS, and FOPID-COC-HGS controllers, as well as two other scenarios in which the MR damper has been regarded merely as a passive device that requires no control signal to be commanded at each time step. These passive modes are the Passive-off and the Passive-on modes in which the voltage to the damper has been held at 0 V and the maximum level of 5 V throughout the control process, respectively. Table (4.8) shows the peak structural responses of the system under these scenarios. In this table, $\ddot{u}_{r,i,c}$ represent the peak absolute accelerations of each mass, $u_{r,i,c}$ are the peak relative displacements, f_{MR}^{max} is the peak generated force by the MR damper corresponding to each control strategy, f_{i1} the first cyclic impulsive frequency, and f_{c1} is the first cyclic convective frequency.

Table 4.8: Peak responses of the tank-liquid-MR damper system under the selected ground motions for different control techniques and aspect ratios

Response	Control technique	El Centro	Hachinohe	Kobe	Northridge	Manjil	Tabas
S = 1.00 $(Broad\ tank)$, f_{i1} = 154.68Hz, f_{c1} = 1.01Hz							
$u_r(cm)$	Uncontrolled	0.0122	0.0032	0.0124	0.0125	0.0278	0.0364
	PID-COC-HGS	0.0036	0.0018	0.0069	0.0096	0.0129	0.0107
	FOPID-COC-HGS	0.0037	0.0018	0.0069	0.0097	0.0127	0.0105
	H2/LQG-COC-HGS	0.0048	0.0020	0.0083	0.0110	0.0128	0.0148
	Passive On	0.0036	0.0018	0.0069	0.0094	0.0127	0.0103
	Passive Off	0.0091	0.0030	0.0104	0.0112	0.0236	0.0299
$\ddot{u}_r(cm/s^2)$	Uncontrolled	1226.42	360.01	1321.62	1270.56	2809.24	3633.07
	PID-COC-HGS	474.68	243.17	850.88	1233.20	1543.45	1300.54
	FOPID-COC-HGS	475.71	243.20	854.12	1238.99	1529.63	1336.64
	H2/LQG-COC-HGS	614.34	265.80	921.37	1221.14	2414.51	2152.96
	Passive On						
	Passive Off						

Continue on the next page

Table 4.8: Peak responses of the tank-liquid-MR damper system under the selected ground motions for different control techniques and aspect ratios

Response	Control technique	El Centro	Hachinohe	Kobe	Northridge	Manjil	Tabas
		474.31	243.71	854.90	1219.82	1524.81	1279.12
		920.48	307.76	1128.63	1218.65	2381.67	3004.52
$u_i(cm)$	Uncontrolled	0.0136	0.0036	0.0139	0.0139	0.0311	0.0407
	PID-COC-HGS	0.0042	0.0021	0.0078	0.0110	0.0147	0.0122
	FOPID-COC-HGS	0.0042	0.0021	0.0079	0.0111	0.0145	0.0120
	H2/LQG-COC-HGS	0.0054	0.0023	0.0092	0.0123	0.0144	0.0168
	Passive On	0.0041	0.0021	0.0079	0.0108	0.0144	0.0118
	Passive Off	0.0102	0.0033	0.0116	0.0125	0.0263	0.0333
$\ddot{u}_i(cm/s^2)$	Uncontrolled	1336.81	377.08	1380.08	1371.16	3093.86	4025.24
	PID-COC-HGS	519.87	250.11	856.70	1312.34	1712.28	1442.77
	FOPID-COC-HGS	521.07	250.11	860.39	1318.87	1696.88	1428.78
	H2/LQG-COC-HGS						
	Passive On						
	Passive Off						

Continue on the next page

Table 4.8: Peak responses of the tank-liquid-MR damper system under the selected ground motions for different control techniques and aspect ratios

Response	Control technique	El Centro	Hachinohe	Kobe	Northridge	Manjil	Tabas
		578.55	262.06	933.95	1295.41	1521.22	1846.36
		519.95	250.59	861.22	1294.46	1698.13	1409.04
		1009.19	320.23	1165.60	1298.88	2636.32	3261.32
$u_c(cm)$	Uncontrolled	1.03	1.12	1.44	2.18	3.21	6.66
	PID-COC-HGS	1.03	1.12	1.44	2.18	3.21	6.66
	FOPID-COC-HGS	1.03	1.12	1.44	2.18	3.21	6.66
	H2/LQG-COC-HGS	1.03	1.12	1.44	2.18	3.21	6.66
	Passive On	1.03	1.12	1.44	2.18	3.21	6.66
	Passive Off	1.03	1.12	1.44	2.18	3.21	6.66
$\ddot{u}_c(cm/s^2)$	Uncontrolled	41.66	45.23	58.16	88.29	130.09	269.45
	PID-COC-HGS	41.68	45.24	58.08	88.49	129.62	268.84
	FOPID-COC-HGS						
	H2/LQG-COC-HGS						
	Passive On						
	Passive Off						

Continue on the next page

Table 4.8: Peak responses of the tank-liquid-MR damper system under the selected ground motions for different control techniques and aspect ratios

Response	Control technique	El Centro	Hachinohe	Kobe	Northridge	Manjil	Tabas
		41.68	45.24	58.08	88.49	129.62	268.84
		41.69	45.24	58.08	88.42	129.65	268.85
		41.68	45.24	58.08	88.48	129.62	268.84
		41.69	45.24	58.09	88.25	129.77	268.85
$f_{MR}^{max}(N)$	Uncontrolled	–	–	–	–	–	–
	PID-COC-HGS	193	62	193	427	526	462
	FOPID-COC-HGS	191	61	196	419	535	468
	H2/LQG-COC-HGS	92	37	102	254	288	343
	Passive On	195	63	199	438	549	482
	Passive Off	21	5.9	16	25	60	72
S = 2.00 ($Slender\ tank$), f_{i1} = 78.59Hz, f_{c1} = 1.04Hz							

Continue on the next page

Table 4.8: Peak responses of the tank-liquid-MR damper system under the selected ground motions for different control techniques and aspect ratios

Response	Control technique	El Centro	Hachinohe	Kobe	Northridge	Manjil	Tabas
$u_r(cm)$	Uncontrolled	0.0380	0.0134	0.0385	0.0452	0.0932	0.1200
	PID-COC-HGS	0.0106	0.0065	0.0246	0.0272	0.0296	0.0572
	FOPID-COC-HGS	0.0106	0.0065	0.0247	0.0284	0.0298	0.0565
	H2/LQG-COC-HGS	0.0135	0.0091	0.0254	0.0263	0.0356	0.0691
	Passive On	0.0106	0.0065	0.0247	0.0263	0.0293	0.0540
	Passive Off	0.0318	0.0127	0.0356	0.0369	0.0733	0.0951
$\ddot{u}_r(cm/s^2)$	Uncontrolled	1363.31	479.48	1406.91	1616.96	3379.97	4181.78
	PID-COC-HGS	455.74	306.10	1058.28	1136.27	1231.60	2311.71
	FOPID-COC-HGS	457.16	305.66	1061.00	1168.77	1240.19	2286.06
	H2/LQG-COC-HGS	546.57	367.01	1039.32	1043.78	1350.58	2587.02
	Passive On	454.57	304.43	1064.52	1122.80	1221.42	2211.42
	Passive Off						

Continue on the next page

Table 4.8: Peak responses of the tank-liquid-MR damper system under the selected ground motions for different control techniques and aspect ratios

Response	Control technique	El Centro	Hachinohe	Kobe	Northridge	Manjil	Tabas
		1124.50	458.21	1313.20	1316.54	2591.94	3420.14
$u_i(cm)$	Uncontrolled	0.0444	0.0156	0.0449	0.0527	0.1100	0.1400
	PID-COC-HGS	0.0128	0.0078	0.0292	0.0325	0.0355	0.0679
	FOPID-COC-HGS	0.0128	0.0078	0.0293	0.0338	0.0359	0.0672
	H2/LQG-COC-HGS	0.0159	0.0107	0.0300	0.0310	0.0420	0.0813
	Passive On	0.0127	0.0078	0.0293	0.0316	0.0353	0.0642
	Passive Off	0.0372	0.0148	0.0416	0.0431	0.0855	0.1100
$\ddot{u}_i(cm/s^2)$	Uncontrolled	1538.54	543.81	1571.15	1826.05	3760.97	4755.60
	PID-COC-HGS	524.11	321.69	1120.89	1293.56	1463.17	2620.47
	FOPID-COC-HGS	524.31	320.18	1123.97	1324.45	1473.48	2593.95
	H2/LQG-COC-HGS	598.70	406.05	1125.38	1148.26	1576.60	2963.13
	Passive On						
	Passive Off						

Continue on the next page

Table 4.8: Peak responses of the tank-liquid-MR damper system under the selected ground motions for different control techniques and aspect ratios

Response	Control technique	El Centro	Hachinohe	Kobe	Northridge	Manjil	Tabas
		523.29	322.44	1126.11	1277.89	1467.39	2502.39
		1302.25	520.28	1462.24	1503.49	2975.21	3897.05
$u_c(cm)$	Uncontrolled	1.03	0.94	1.63	2.18	3.47	6.19
	PID-COC-HGS	1.03	0.94	1.63	2.18	3.47	6.19
	FOPID-COC-HGS	1.03	0.94	1.63	2.18	3.47	6.18
	H2/LQG-COC-HGS	1.03	0.94	1.63	2.18	3.47	6.18
	Passive On	1.03	0.94	1.63	2.18	3.47	6.14
	Passive Off	1.03	0.94	1.63	2.18	3.48	6.15
$\ddot{u}_c(cm/s^2)$	Uncontrolled	44.02	40.01	69.38	92.57	148.23	263.58
	PID-COC-HGS	43.51	40.00	69.39	93.21	147.23	262.23
	FOPID-COC-HGS	43.50	40.00	69.37	93.15	147.24	262.21
	H2/LQG-COC-HGS						
	Passive On						
	Passive Off						

Continue on the next page

Table 4.8: Peak responses of the tank-liquid-MR damper system under the selected ground motions for different control techniques and aspect ratios

Response	Control technique	El Centro	Hachinohe	Kobe	Northridge	Manjil	Tabas
		43.49	40.00	69.40	93.08	147.41	262.04
		43.50	40.00	69.38	93.22	147.27	260.33
		43.78	40.06	69.55	92.72	147.94	260.66
$f_{MR}^{max}(N)$	Uncontrolled	–	–	–	–	–	–
	PID-COC-HGS	444	250	805	911	1110	1496
	FOPID-COC-HGS	443	251	804	796	1111	1514
	H2/LQG-COC-HGS	303	181	541	584	751	1165
	Passive On	449	249	810	984	1126	1486
	Passive Off	62	23	66	71	121	145
S = 3.00 ($Slender\ tank$), f_{i1} = 45.99Hz, f_{c1} = 1.04Hz							
$u_r(cm)$	Uncontrolled	0.0489	0.0506	0.0782	0.0782	0.0889	0.1300
	PID-COC-HGS						
	FOPID-COC-HGS						
	H2/LQG-COC-HGS						
	Passive On						

Continue on the next page

Table 4.8: Peak responses of the tank-liquid-MR damper system under the selected ground motions for different control techniques and aspect ratios

Response	Control technique	El Centro	Hachinohe	Kobe	Northridge	Manjil	Tabas
		0.0223	0.0230	0.0404	0.0431	0.0459	0.0896
		0.0224	0.0229	0.0404	0.0433	0.0457	0.0899
		0.0253	0.0319	0.0452	0.0508	0.0601	0.1000
		0.0218	0.0228	0.0402	0.0433	0.0456	0.0892
		0.0423	0.0475	0.0677	0.0701	0.0862	0.1200
$\ddot{u}_r(cm/s^2)$	Uncontrolled	991.93	1026.61	1571.34	1561.33	1734.08	2505.27
	PID-COC-HGS	522.75	565.66	970.35	1128.05	1046.30	1982.51
	FOPID-COC-HGS	524.37	560.66	972.06	1132.00	1041.52	1989.16
	H2/LQG-COC-HGS	564.46	740.47	992.28	1249.49	1291.23	2260.33
	Passive On	514.79	558.64	968.66	1134.23	1044.94	1971.56
	Passive Off	869.76	971.76	1361.92	1434.88	1720.87	2389.75

Continue on the next page

Table 4.8: Peak responses of the tank-liquid-MR damper system under the selected ground motions for different control techniques and aspect ratios

Response	Control technique	El Centro	Hachinohe	Kobe	Northridge	Manjil	Tabas
$u_i(cm)$	Uncontrolled	0.0636	0.0659	0.1000	0.1000	0.1200	0.1600
	PID-COC-HGS	0.0306	0.0313	0.0537	0.0580	0.0622	0.1200
	FOPID-COC-HGS	0.0308	0.0312	0.0538	0.0583	0.0620	0.1200
	H2/LQG-COC-HGS	0.0336	0.0423	0.0590	0.0669	0.0795	0.1400
	Passive On	0.0300	0.0310	0.0535	0.0584	0.0617	0.1200
	Passive Off	0.0550	0.0620	0.0882	0.0914	0.1100	0.1600
$\ddot{u}_i(cm/s^2)$	Uncontrolled	1225.83	1277.95	1964.78	1971.29	2230.01	3179.72
	PID-COC-HGS	695.39	693.06	1113.67	1248.05	1352.41	2506.66
	FOPID-COC-HGS	696.48	687.51	1113.91	1252.55	1355.83	2513.61
	H2/LQG-COC-HGS	693.18	866.87	1157.63	1346.19	1625.76	2738.26
	Passive On	680.47	684.38	1108.57	1260.25	1356.24	2489.80
	Passive Off						

Continue on the next page

Table 4.8: Peak responses of the tank-liquid-MR damper system under the selected ground motions for different control techniques and aspect ratios

Response	Control technique	El Centro	Hachinohe	Kobe	Northridge	Manjil	Tabas
		1064.36	1205.96	1712.66	1779.60	2164.26	3050.08
$u_c(cm)$	Uncontrolled	1.02	0.94	1.64	2.18	3.48	6.18
	PID-COC-HGS	1.02	0.94	1.64	2.19	3.48	6.18
	FOPID-COC-HGS	1.02	0.94	1.64	2.18	3.48	6.18
	H2/LQG-COC-HGS	1.02	0.94	1.64	2.18	3.48	6.18
	Passive On	1.03	0.94	1.64	2.18	3.48	6.18
	Passive Off	1.02	0.94	1.64	2.18	3.47	6.19
$\ddot{u}_c(cm/s^2)$	Uncontrolled	44.42	41.77	69.79	95.55	148.73	263.62
	PID-COC-HGS	43.58	40.77	69.77	94.63	147.69	263.24
	FOPID-COC-HGS	43.43	40.79	69.78	94.63	147.69	263.28
	H2/LQG-COC-HGS	43.52	41.14	69.85	94.88	147.89	263.41
	Passive On						
	Passive Off						

Continue on the next page

Table 4.8: Peak responses of the tank-liquid-MR damper system under the selected ground motions for different control techniques and aspect ratios

Response	Control technique	El Centro	Hachinohe	Kobe	Northridge	Manjil	Tabas
		43.65	40.76	69.88	94.62	147.66	263.23
		44.21	41.61	69.63	95.41	148.14	263.34
$f_{MR}^{max}(N)$	Uncontrolled	–	–	–	–	–	–
	PID-COC-HGS	809	766	1207	1255	1379	1850
	FOPID-COC-HGS	814	766	1203	1235	1381	1849
	H2/LQG-COC-HGS	534	592	842	810	1089	1357
	Passive On	803	765	1207	1266	1380	1957
	Passive Off	67	73	96	98	120	140

It can be seen from Table (4.8) that the MR damper has reduced the vibrational response of the fluid tank system in all considered control scenarios. Reductions in responses of the convective mass are not considerable which could be justified by the very different vibrational properties (frequency and stiffness) of this mode from the impulsive and rigid modes. In fact, even though the damper has caused a substantial decrease in the structural responses of the rigid and impulsive modes, the significant difference between the stiffness and the damping of the convective mode from the other two modes has caused the damper to have little effects on its vibrational responses. It is noteworthy that the far too different vibrational properties of the convective mass cause its structural responses to be far away less affected by the responses of the other two modes even without having the damper in place which is evident from Table (4.8). It should be noted that for the three aspect ratios of S = 1, 2, and 3, the impulsive mass contributes to between 57% - 73% of the total mass of the system, and hence its vibrational responses are the governing ones for the analysis and design purposes.

To evaluate the performance of the applied control strategies in reducing the seismic structural responses of the coupled fluid-tank-MR system, four performance indices ($PI's$), termed as PI_1 to PI_4 are defined. These $PI's$ represent the ratios of the peak absolute structural responses in the controlled case to the uncontrolled one. These $PI's$ are considered as follows,

$$PI_1 = \frac{Max|u_{r,co}|}{Max|u_{r,uco}|} \tag{4.6}$$

$$PI_2 = \frac{Max|\ddot{u}_{r,co}|}{Max|\ddot{u}_{r,uco}|} \tag{4.7}$$

$$PI_3 = \frac{Max|u_{i,co}|}{Max|u_{i,uco}|} \tag{4.8}$$

$$PI_4 = \frac{Max|\ddot{u}_{i,co}|}{Max|\ddot{u}_{i,uco}|} \tag{4.9}$$

where $u_{r,i,co}$, $\ddot{u}_{r,i,uco}$, are the controlled and uncontrolled rigid and impulsive relative

displacements and absolute accelerations, respectively. These performance indices have been calculated for the considered ground motions, control strategies, and each aspect ratio as shown in Table (4.9).

Table 4.9: Performance indices for the applied control strategies to the fluid-tank-MR system

Performance Index	Control technique	El Centro	Hachinohe	Kobe	Northridge	Manjil	Tabas
			S = 1.00 $(Broad\ tank)$				
PI_1	PID-COC-HGS	0.2951	0.5625	0.5565	0.7680	0.4637	0.2931
	FOPID-COC-HGS	0.3033	0.5625	0.5565	0.7760	0.4568	0.2890
	H2/LQG-COC-HGS	0.3934	0.6250	0.6694	0.8800	0.4587	0.4069
	Passive On	0.2951	0.5625	0.5565	0.7520	0.4546	0.2840
	Passive Off	0.7459	0.9375	0.8387	0.8960	0.8477	0.8211
PI_2	PID-COC-HGS	0.3870	0.6755	0.6438	0.9706	0.5494	0.3580
	FOPID-COC-HGS	0.3879	0.6755	0.6463	0.9752	0.5444	0.3679
	H2/LQG-COC-HGS	0.5009	0.7383	0.6972	0.9611	0.8587	0.5927
	Passive On	0.3867	0.6770	0.6469	0.9600	0.5427	0.3520
	Passive Off	0.7505	0.8549	0.8540	0.9591	0.6151	0.7844
PI_3	PID-COC-HGS	0.3088	0.5833	0.5612	0.7914	0.4729	0.2997
	FOPID-COC-HGS						
	H2/LQG-COC-HGS						
	Passive On						
	Passive Off						

Continue on the next page

Table 4.9: Performance indices for the applied control strategies to the fluid-tank-MR system

Performance Index	Control technique	El Centro	Hachinohe	Kobe	Northridge	Manjil	Tabas
		0.3088	0.5833	0.5683	0.7986	0.4663	0.2958
		0.3971	0.6389	0.6619	0.8849	0.4621	0.4122
		0.3015	0.5833	0.5683	0.7770	0.4641	0.2907
		0.7500	0.9167	0.8345	0.8993	0.8452	0.8200
	PID-COC-HGS	0.3889	0.6633	0.6208	0.9571	0.5534	0.3584
	FOPID-COC-HGS	0.3900	0.6633	0.6234	0.9619	0.5485	0.3549
PI_4	H2/LQG-COC-HGS	0.4328	0.6950	0.6767	0.9448	0.4917	0.4587
	Passive On	0.3889	0.6646	0.6240	0.9441	0.5489	0.3501
	Passive Off	0.7549	0.8492	0.8446	0.9473	0.8523	0.8101
			S = 2.00 $(Slender\ tank)$				
	PID-COC-HGS	0.2789	0.4851	0.6390	0.6018	0.3170	0.4909
	FOPID-COC-HGS	0.2789	0.4851	0.6416	0.6238	0.3197	0.4845
PI_1	H2/LQG-COC-HGS						
	Passive On						
	Passive Off						

Continue on the next page

Table 4.9: Performance indices for the applied control strategies to the fluid-tank-MR system

Performance Index	Control technique	El Centro	Hachinohe	Kobe	Northridge	Manjil	Tabas
		0.3553	0.6791	0.6597	0.5819	0.3826	0.5915
		0.2789	0.4851	0.6416	0.5819	0.3140	0.5373
		0.8368	0.9478	0.9247	0.8164	0.7858	0.8753
PI_2	PID-COC-HGS	0.3343	0.6384	0.7522	0.7027	0.3644	0.5528
	FOPID-COC-HGS	0.3353	0.6375	0.7541	0.7228	0.3669	0.5266
	H2/LQG-COC-HGS	0.4010	0.7654	0.7387	0.6455	0.4127	0.6197
	Passive On	0.3334	0.6349	0.7566	0.6944	0.3747	0.6130
	Passive Off	0.8248	0.9556	0.9334	0.8142	0.7809	0.8782
PI_3	PID-COC-HGS	0.2883	0.5000	0.6503	0.6167	0.3271	0.4990
	FOPID-COC-HGS	0.2883	0.5000	0.6526	0.6414	0.3264	0.4932
	H2/LQG-COC-HGS	0.3581	0.6859	0.6682	0.5882	0.3878	0.5958
	Passive On	0.2860	0.5000	0.6526	0.5996	0.3248	0.5474
	Passive Off						

Continue on the next page

Table 4.9: Performance indices for the applied control strategies to the fluid-tank-MR system

Performance Index	**Control technique**	**El Centro**	**Hachinohe**	**Kobe**	**Northridge**	**Manjil**	**Tabas**
		0.8378	0.9487	0.9265	0.8178	0.7864	0.8736
PI_4	PID-COC-HGS	0.3407	0.5915	0.7134	0.7084	0.3890	0.5510
	FOPID-COC-HGS	0.3408	0.5888	0.7154	0.7253	0.3918	0.5459
	H2/LQG-COC-HGS	0.3891	0.7467	0.7163	0.6288	0.4203	0.6209
	Passive On	0.3401	0.5929	0.7167	0.6998	0.3893	0.6089
	Passive Off	0.8464	0.9567	0.9307	0.8234	0.7907	0.8775
S = 3.00 $(Slender\ tank)$							
PI_1	PID-COC-HGS	0.4560	0.4545	0.5166	0.5512	0.5170	0.7113
	FOPID-COC-HGS	0.4581	0.4526	0.5166	0.5537	0.5166	0.7134
	H2/LQG-COC-HGS	0.5174	0.6304	0.5780	0.6496	0.6782	0.8167
	Passive On	0.4458	0.4506	0.5141	0.5537	0.5148	0.7042
	Passive Off	0.8650	0.9387	0.8657	0.8964	0.9733	0.9501

Continue on the next page

Table 4.9: Performance indices for the applied control strategies to the fluid-tank-MR system

Performance Index	Control technique	El Centro	Hachinohe	Kobe	Northridge	Manjil	Tabas
PI_2	PID-COC-HGS	0.5270	0.5510	0.6175	0.7225	0.6034	0.7913
	FOPID-COC-HGS	0.5286	0.5461	0.6186	0.7250	0.6007	0.7936
	H2/LQG-COC-HGS	0.5691	0.7213	0.6315	0.8003	0.7432	0.9014
	Passive On	0.5190	0.5442	0.6165	0.7265	0.6031	0.7842
	Passive Off	0.8768	0.9466	0.8667	0.9190	0.9877	0.9505
PI_3	PID-COC-HGS	0.4811	0.4750	0.5370	0.5800	0.5381	0.7296
	FOPID-COC-HGS	0.4843	0.4734	0.5380	0.5830	0.5385	0.7317
	H2/LQG-COC-HGS	0.5283	0.6419	0.5900	0.6690	0.6903	0.8253
	Passive On	0.4717	0.4704	0.5350	0.5840	0.5361	0.7220
	Passive Off	0.8648	0.9408	0.8820	0.9140	0.9735	0.9509
PI_4	PID-COC-HGS	0.5673	0.5423	0.5668	0.6331	0.6065	0.7883
	FOPID-COC-HGS	0.5682	0.5380	0.5669	0.6354	0.6098	0.7905
	H2/LQG-COC-HGS						
	Passive On						
	Passive Off						

Continue on the next page

Table 4.9: Performance indices for the applied control strategies to the fluid-tank-MR system

Performance Index	**Control technique**	**El Centro**	**Hachinohe**	**Kobe**	**Northridge**	**Manjil**	**Tabas**
		0.5655	0.6783	0.5892	0.6829	0.7307	0.8571
		0.5551	0.5355	0.5642	0.6393	0.6099	0.7791
		0.8683	0.9437	0.8717	0.9028	0.9746	0.9525

Examining the structural responses in Table (4.8) and the performance indices in Table (4.9) shows that for the aspect ratio of 1 the highest reductions in the structural responses including the lateral displacements and absolute accelerations of the rigid and impulsive mass in the controlled case occur under the Tabas earthquake followed by the El Centro earthquake. However, for the aspect ratio of 2 the least responses of the controlled system are achieved under the El Centro earthquake followed by the Manjil earthquake. For the aspect ratio of 1, depending on the applied control technique, reductions up to around 71% in the lateral displacements of the rigid and impulsive mass and up to 65% in the absolute accelerations of these masses have been achieved. For the aspect ratio of 2, these reductions are further increased by a few percentage points. For the considered ground motions except for the Tabas earthquake, by increasing the aspect ratio from 1 to 2, further reductions in the peak lateral displacements and absolute accelerations of the rigid and impulsive masses in the case of Passive On and semi-active control strategies can be found. For all aspect ratios and under all the applied ground motions, the responses of the impulsive mass in the uncontrolled case, are higher than that of the rigid mass. Utilising the MR damper as the smart control mechanism and the semi-active control techniques applied in this study considerably reduce the structural responses of these two masses. The lateral displacements and absolute accelerations of the rigid and impulsive mass of the controlled system closely follow each other. For the aspect ratio of 3, the reductions in the lateral displacements and absolute accelerations of the rigid and impulsive mass under all seismic events and the employed control techniques become much closer to each other. For this aspect ratio, reduction percentage points in the lateral displacements of the rigid and impulsive mass using different semi-active control strategies and under the applied ground motions range between 54.7% for the rigid mass under the Hachinohe earthquake using the FOPID-COC-HGS to 17.5% for the impulsive mass under the Tabas earthquake using the H2/LQG-COC-HGS control technique. For all control techniques, applied earthquakes, and considered aspect ratios of the fluid tank, the least reductions in the controlled case occur under the Northridge earthquake for the aspect ratio of 1 which is reflected in PI_2 index. Decreases in the peak lateral displacements and absolute accelerations of the rigid and impulsive masses almost follow the same trends

and reduction percentage points. Among the considered semi-active control strategies, PID-COC-HGS and FOPID-COC-HGS have contributed to the most reductions in the structural responses, followed by Passive On mode. However, reductions in the case of Passive On would be at the expense of having the voltage commanded through the whole process. As apparent from the results of Tables (4.8) and (4.9) and shown in Figures (4.18 - 4.29) the PID-COC-HGS and FOPID-COC-HGS control techniques have made the most reductions in the structural responses and surpassed the H2/LQG-COC-HGS. These two control strategies almost make the same reduction percentage points in the peak responses. The designed H2/LQG-COC-HGS control strategy has produced the least MR damper force of around 47%-78% of the corresponding force in the case of the Passive On control strategy for all three aspect ratios for each ground motion. This technique has achieved comparable reductions with a maximum difference of around 23% with other semi-active control techniques, shown in PI_2 for the aspect ratio of 1.

Depending on the aspect ratio, the control scheme, and the applied ground motion, the MR damper has reduced the peak relative displacements of the rigid and impulsive masses up to 72% and a reduction percentage point for the peak absolute accelerations of these masses up to 67% has been achieved. Under the Northridge earthquake, by increasing the aspect ratio of the fluid-tank-MR damper system up to 3, more reductions in the structural responses, comparable to other earthquakes, are observed. For the aspect ratio 1, PI_1 to PI_4 of the control techniques under the Hachinohe and Kobe earthquakes are very close to each other while the performance indices of El Centro and Tabas follow the same trend. For the aspect ratio of 2, similar performance indices can be seen under the Kobe and Northridge for most of the semi-active control techniques. The frequency of the first convective mode by increasing the aspect ratio from 1 to 3 does not change significantly (from 1.01 Hz to 1.04 Hz). However, the frequency of the first impulsive mode changes substantially from 154.68 Hz for the aspect ratio of 1 to 45.99 Hz for the aspect ratio of 3. For the aspect ratio of 3, comparable performance indices for most control techniques and under different earthquakes can be seen except for the Tabas earthquake.

In fluid storage tanks, the base shear and overturning moments contribute to the main

causes of damage to these structures under the base excitations. According to Equations (4.10) and (4.11) the maximum of the base shear and overturning moment using the square root of the sum of squares (SRSS) are related to the peak accelerations of the rigid, impulsive, and convective masses (A. S. Veletsos, 1984; Haroun & Housner, 1981b),

$$Q^b{}_{max} = \sqrt{(m_c S_{a,c})^2 + (m_i S_{a,i})^2 + ((m_i - m_r)\ddot{u}_g^{max})^2} \tag{4.10}$$

$$M^o{}_{max} = \sqrt{(m_c h_c S_{a,c})^2 + (m_i h_i S_{a,i})^2 + ((m_i h_i - m_r h_r)\ddot{u}_g^{max})^2} \tag{4.11}$$

where, $Q^b{}_{max}$ and $M^o{}_{max}$ are the maximum base shear and overturning moment, $S_{a,c}$ and $S_{a,i}$ are the spectral accelerations of the fundamental convective and impulsive masses, h_c and h_i are the height of the corresponding masses from the base, respectively, and $\ddot{u}_g^{max}$ is the PGA of the ground motion. It is therefore concluded that the achieved reductions in the peak absolute accelerations of these masses can result in significant reductions of the system's base shear and overturning moments, thus reducing the damage risks in these structures.

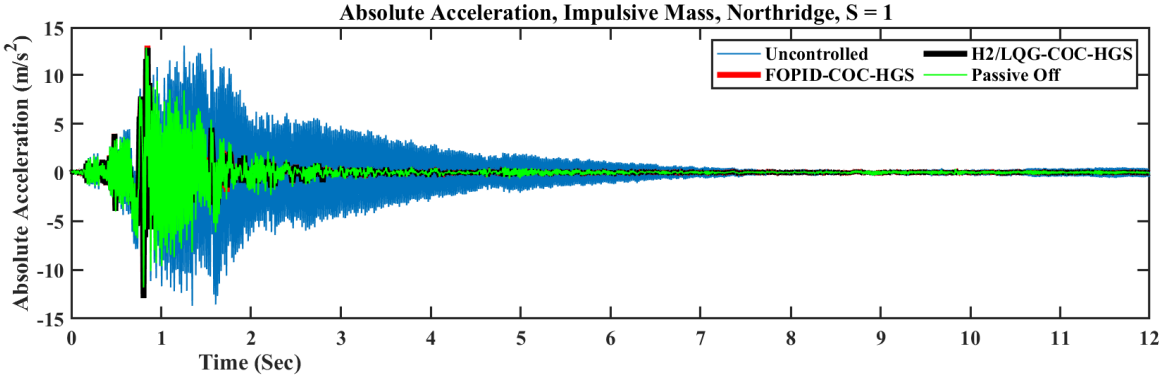

Figure 4.18: Absolute acceleration time history of the impulsive mass under the Northridge earthquake, S = 1.00

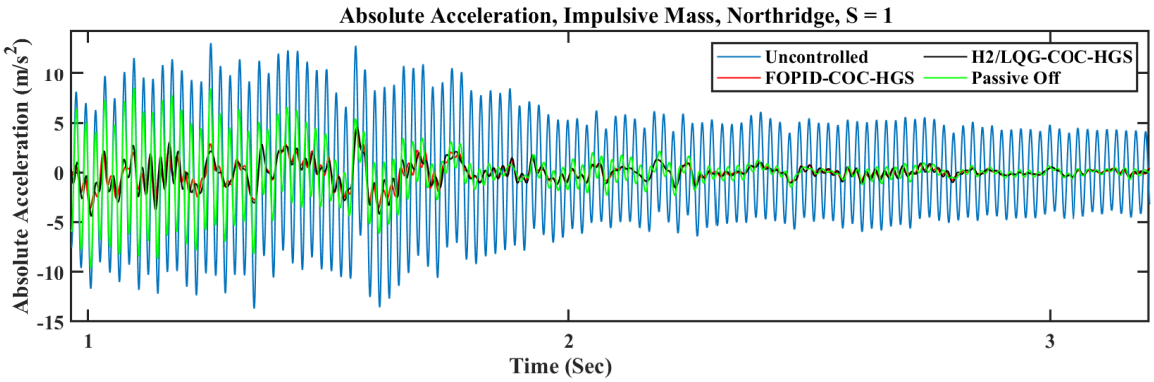

Figure 4.19: Absolute acceleration time history of the impulsive mass under the Northridge earthquake, $S = 1.00$, close-up

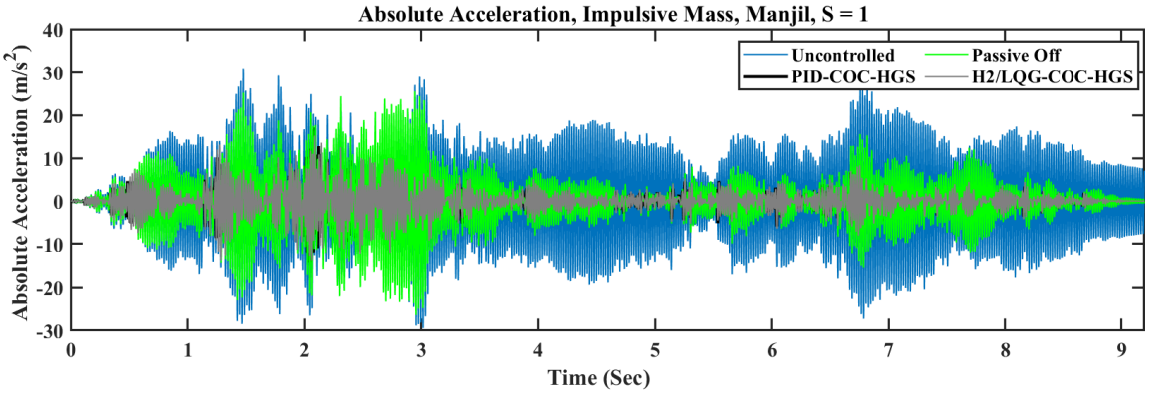

Figure 4.20: Absolute acceleration time history of the impulsive mass under the Manjil earthquake, $S = 1.00$

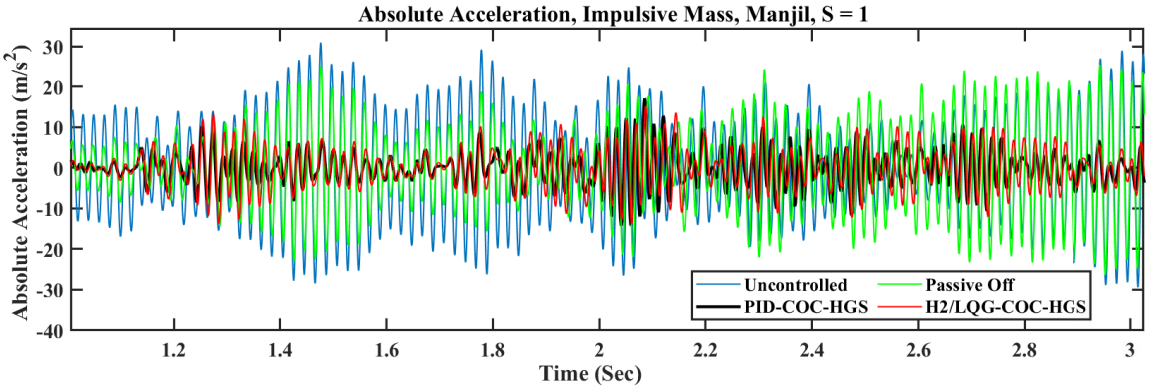

Figure 4.21: Absolute acceleration time history of the impulsive mass under the Manjil earthquake, S = 1.00, close-up

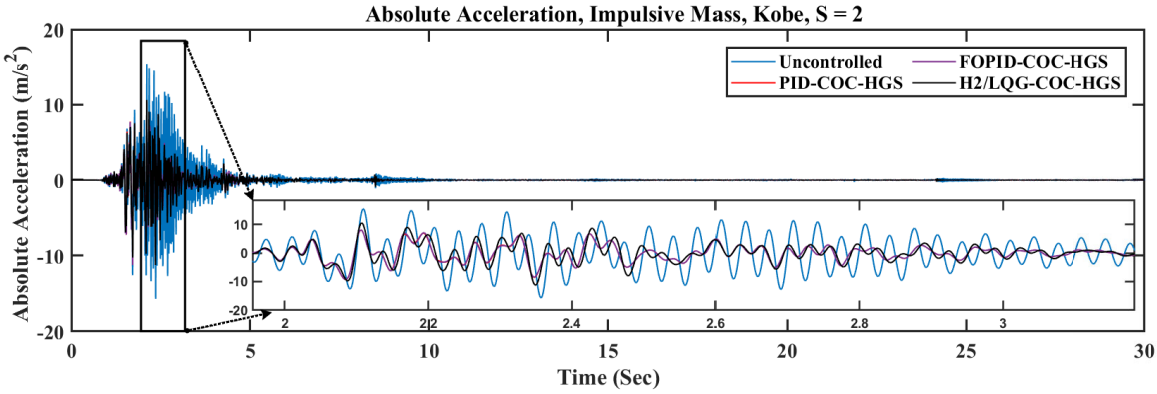

Figure 4.22: Absolute acceleration time history of the impulsive mass under the Kobe earthquake, S = 2.00

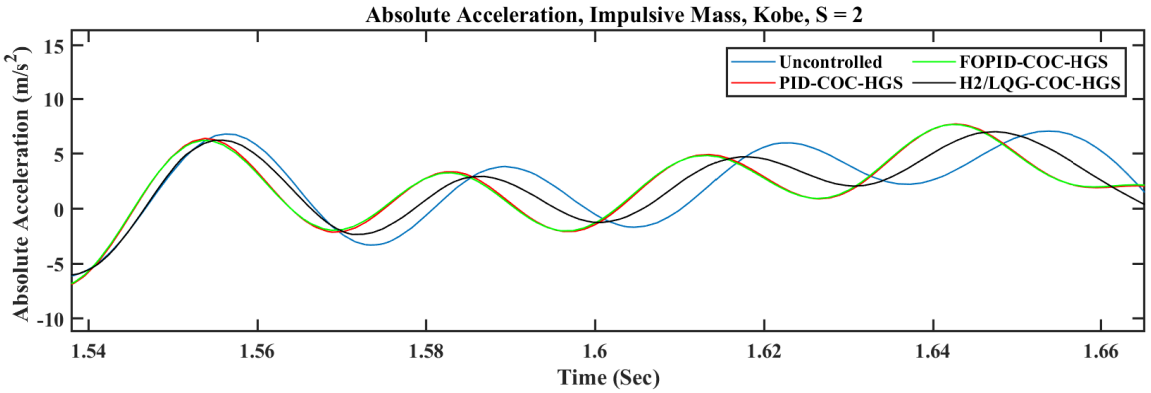

Figure 4.23: Absolute acceleration time history of the impulsive mass under the Kobe earthquake, S = 2.00, close-up

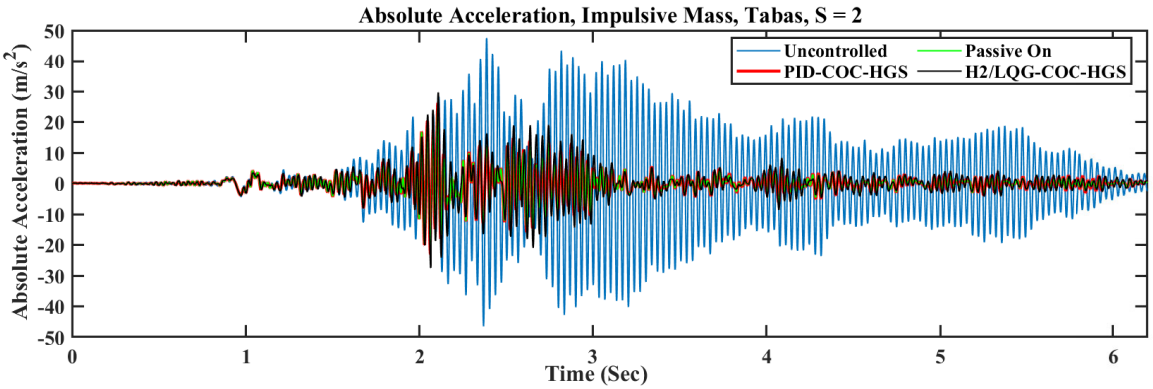

Figure 4.24: Absolute acceleration time history of the impulsive mass under the Tabas earthquake, S = 2.00

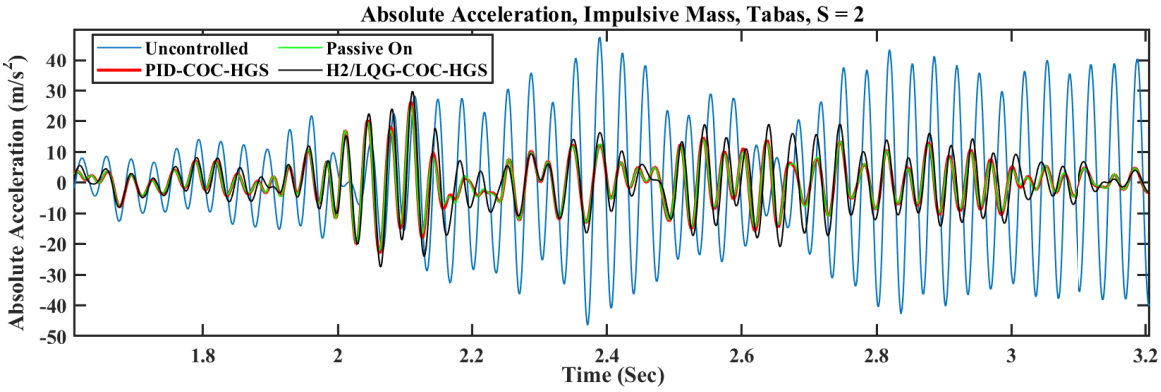

Figure 4.25: Absolute acceleration time history of the impulsive mass under the Tabas earthquake, S = 2.00, close-up

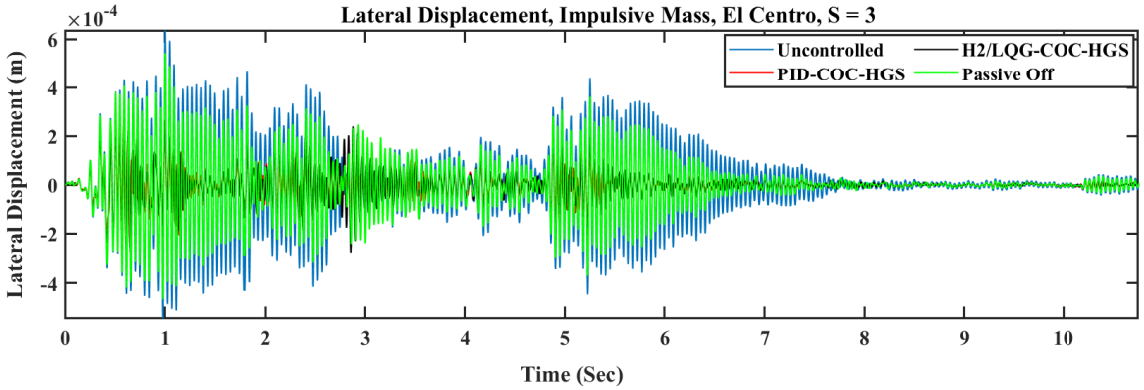

Figure 4.26: Lateral displacement time history of impulsive mass under El Centro earthquake, S = 3.00

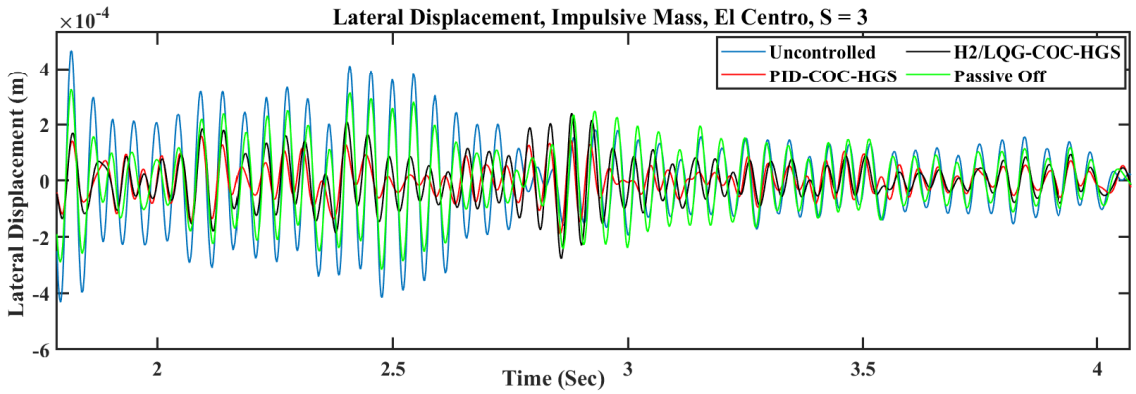

Figure 4.27: Lateral displacement time history of impulsive mass under El Centro earthquake, S = 3.00, close-up

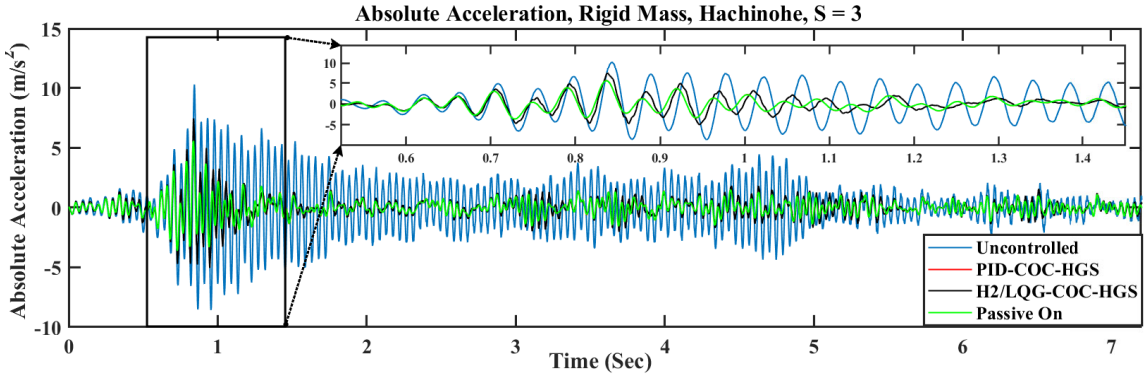

Figure 4.28: Absolute acceleration time history of rigid mass under Hachinohe earthquake, S = 3.00

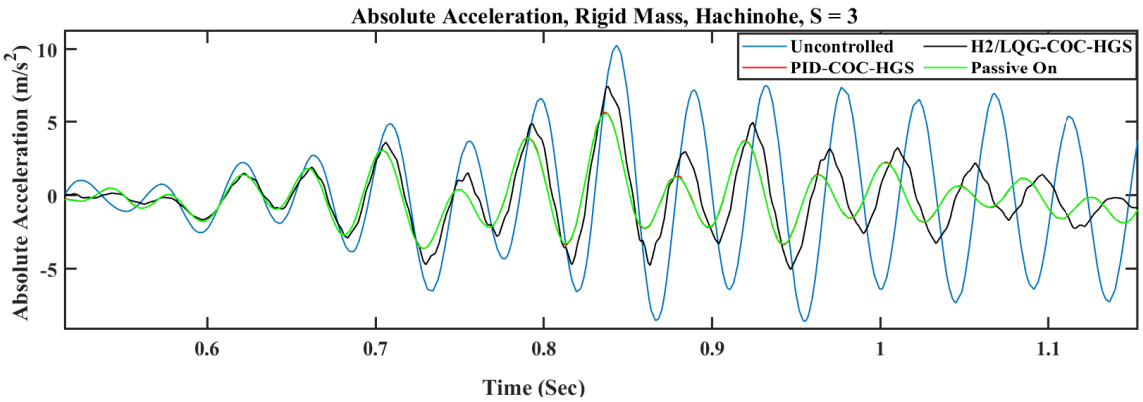

Figure 4.29: Absolute acceleration time history of rigid mass under Hachinohe earthquake, S = 3.00, close-up

4.4 Experimental and numerical investigations of a legged rigid tank-MR

This section presents the experimental results of shaking table tests over a legged rigid stainless steel circular cylindrical liquid tank equipped with four MR dampers under rocking motions. Details of these tests and data analysis of the experimental results are described in the below sub-sections. Geometrical specifications of this tank are given in Table 4.10.

Table 4.10: Geometrical and hydrodynamic characteristics of the rigid legged circular cylindrical fluid tank

Parameter	**Value**	**Parameter**	**Value**
h_{total}	1332 (mm)	A_n	0.8015
h_{leg}	400 (mm)	B_n	0.4294
$h_{cylinder}$	932 (mm)	C_n	0.3442
M_{total}	580 (Kg)	$h_{eff-liq}$	400 (mm)
D_{leg}	47.95 (mm)	R'	571.7 (mm)
$D_{cylinder}$	779.86 (mm)	I_F	9829700 $(kg.mm^2)$
S	2.33	I_s	49148300 $(kg.mm^2)$

4.4.1 Experimental setup for the tank-liquid-MR damper system

A rigid legged stainless steel circular cylindrical liquid tank was set up freely over the shake table in the Structural Engineering Laboratory of the Auckland University of Technology (AUT). This tank was filled with water. The characteristics of this table were already mentioned in the sub-section 4.2.1. The fluid tank and the MR damper were installed over the shake table in two scenarios. In the first scenario, the tank was installed over the shake table without the MR dampers connected to its legs. This tank was tested for a series of swept-sine as well as the selected ground motions with different PGA scales. The purpose of the swept-sine tests was to detect the natural frequencies of the legged rigid circular cylindrical stainless steel fluid tank while the aim of testing for ground motions was to compare results with the controlled tank. In the second scenario, the same tank was equipped with four MR dampers, each installed beside one of the legs. Again the tank was tested under the same ground motions. Finally, the results

of the vibration responses of the system including the uplift displacements of the tank, uplift relative accelerations of the legs, and the lateral absolute accelerations of the tank body in two cases were compared to examine the efficacy of the dampers in attenuating the seismic responses of the tank under the base excitations. Figures 4.30-4.34 show the details of the installation setup in two cases of the fluid tank with and without MR dampers.

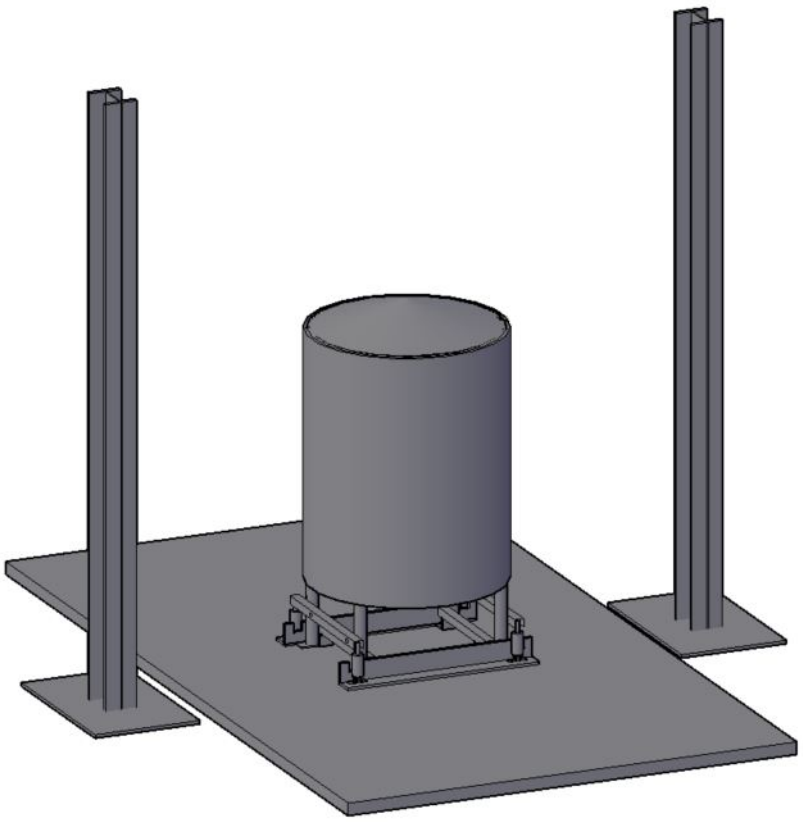

Figure 4.30: Isogeometric view of the fluid tank-MR system

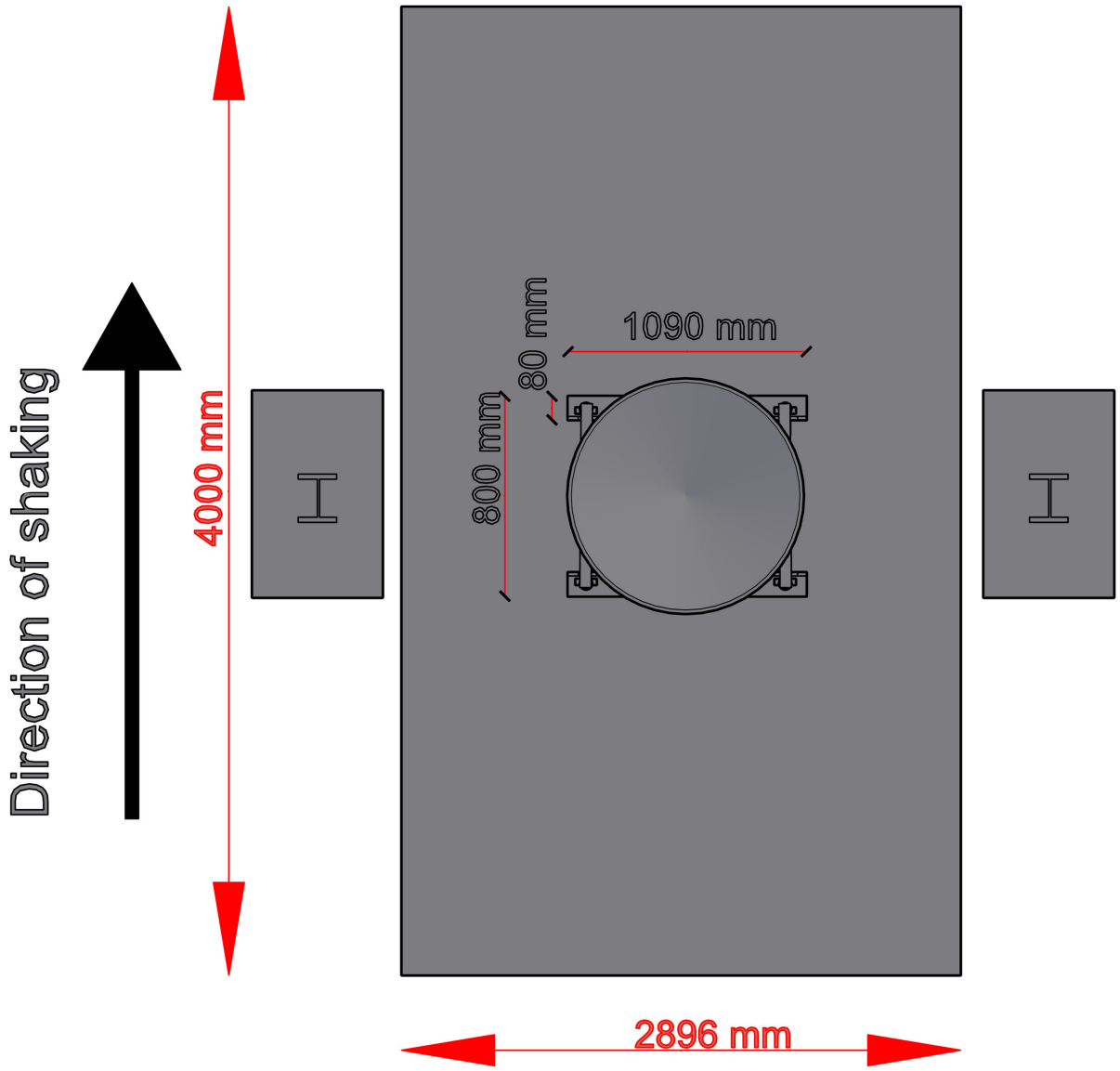

Figure 4.31: Plan view of the shake table, fluid tank connections, and supporting columns

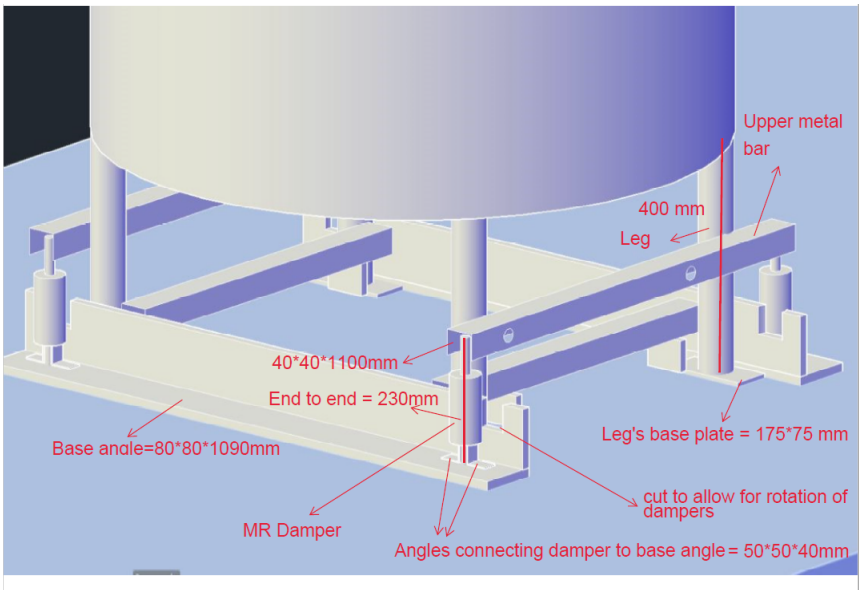

Figure 4.32: Details of the setup

Figure 4.33: Experimental setup of the tank without MR dampers

Figure 4.34: Experimental setup of the tank with MR dampers

4.4.2 Instrumentation of rigid fluid tank-MR system

The fluid tank was instrumented using different sensors including accelerometers and LVDT's, and MR dampers as shown in Figure 4.35. The instrumentation panel with details of the sensors are shown in Figure 4.36. To command the calculated voltage at each time step using the control algorithm to the damper a Pulse Width Modulator (PWM) control box was designed by the technicians of the Auckland University of Technology (AUT) as seen in Figure 4.37. Moreover, a software platform based on SIMULINK-MATLAB was developed for data acquisition and online control of the system based on the control techniques developed in Chapter 3. The block diagram for this software has been illustrated in Figure 4.38 and Figure 4.40 depicts a screenshot of this software. This software has different capabilities, including data acquisition from the sensory system for different types of sensors, online control using different control techniques which can easily be switched, real-time output saving, and data visualisation. Eight accelerometers, Acc 01 to Acc 08 were utilised. Acc 01 to Acc 03 were connected

to the bottom, mid-height, and top of the tank, respectively, to measure the lateral accelerations of the fluid tank. Acc 04 to Acc 07 were connected beside each leg very close to the position of each MR damper and LVDT to measure the upward accelerations of the legs. LVDT 01 to LVDT 04 were installed to measure the uplift displacements of the legs and MR 01 to MR 04 were installed beside the legs to control the system. Moreover, four PWM control boxes were applied to transmit the analog output from the DAQ and command the control voltage signal to the MR dampers. The National Instruments Data Acquisition (NI DAQ) hardware was employed for receiving and logging the analog input signals from the sensors and sending the analog output voltage command signal to the dampers. A sampling rate of 50 Hz was used for the process of simultaneous data acquisition and control.

The PWM boxes have the below I/O characteristics:

I/O delay: 5 ms

Rise time: 3.8 ms

Settling time: 9.4 ms

Two main control schemes were applied. In the first scheme shown in Figure 4.38 real-time data from LVDT's are used for the process of feedback in the control process. Many different control methods were employed using this scheme to examin the performance of the controlled system. Since, in practical applications, utilising LVDT's is not possible and only accelerometers are employed, in the second and final scheme data from accelerometer measurements are used. These data are passed through designed High Pass Filters and discrete integrators (Spencer Jr, Dyke & Deoskar, 1998; Jansen & Dyke, 2000; Thong, Woolfson, Crowe, Hayes-Gill & Jones, 2004; Abir, Longo, Morantz & Shore, 2016; Zheng, Dan, Cheng & Xia, 2019; F. Liu, Gao & Chang, 2021; Ribeiro, de Castro & Meggiolaro, 2021; W. Li, Hancock, Yang, Wang & Meng, 2022) to estimate the dynamic displacement and velocity in real time. Discrete-time integration was conducted using the trapezoidal method in SIMULINK. The details of the applied digital High Pass Filter have been given in Appendix B. Figure 4.39 shows the process of estimating

dynamic displacement from acceleration data in real time, schematically. Voltages sent to the PWM control boxes from the control design to be transmitted to the MR dampers were bounded in the range of $0 - 3\ V$.

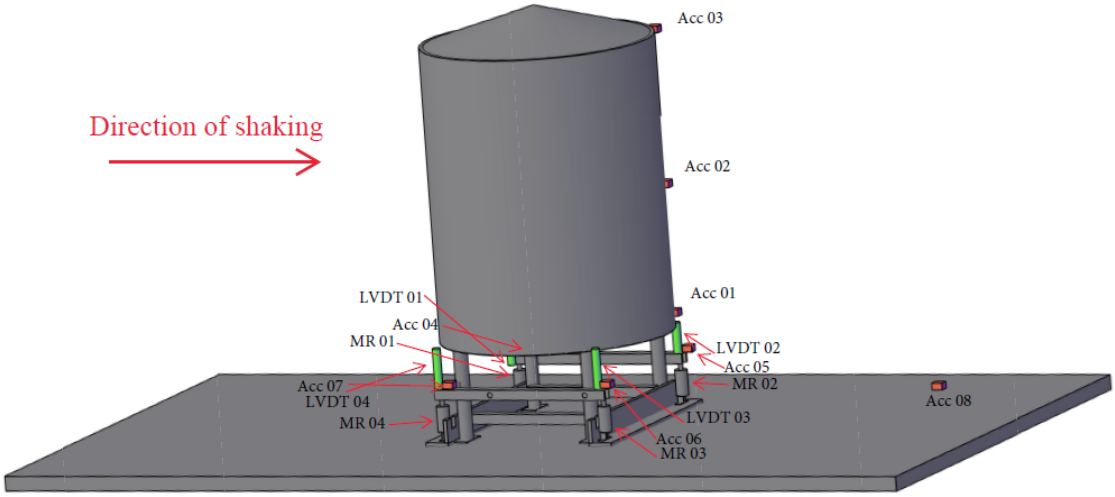

Figure 4.35: An iso-geometric view of the instrumentation of the rigid fluid tank-MR damper for data acquisition and control

Instrumentation Panel

Item_No	Sensor	Channel_ID	Module	Device	Measurement Type	Units	Terminal Config	Input Range	Coupling	Remarks
1	Acc 01	ai1	PXI1Slot2	PXIe-4302	Voltage	g	SENR	-10 to +10 Volts	DC	
2	Acc 02	ai2	PXI1Slot2	PXIe-4302	Voltage	g	SENR	-10 to +10 Volts	DC	
3	Acc 03	ai3	PXI1Slot2	PXIe-4302	Voltage	g	SENR	-10 to +10 Volts	DC	
4	Acc 04	ai4	PXI1Slot2	PXIe-4302	Voltage	g	SENR	-10 to +10 Volts	DC	
5	Acc 05	ai5	PXI1Slot2	PXIe-4302	Voltage	g	SENR	-10 to +10 Volts	DC	
6	Acc 06	ai6	PXI1Slot2	PXIe-4302	Voltage	g	SENR	-10 to +10 Volts	DC	
7	Acc 07	ai7	PXI1Slot2	PXIe-4302	Voltage	g	SENR	-10 to +10 Volts	DC	
8	Acc 08	ai8	PXI1Slot2	PXIe-4302	Voltage	g	SENR	-10 to +10 Volts	DC	Shake Table Accelerometer
9	DC LVDT_01	ai0	PXI1Slot6	PXIe-4302	Voltage	mm	SENR	-10 to +10 Volts	DC	
10	DC LVDT_02	ai1	PXI1Slot6	PXIe-4302	Voltage	mm	SENR	-10 to +10 Volts	DC	
11	DC LVDT_03	ai2	PXI1Slot6	PXIe-4302	Voltage	mm	SENR	-10 to +10 Volts	DC	
12	DC LVDT_04	ai3	PXI1Slot6	PXIe-4302	Voltage	mm	SENR	-10 to +10 Volts	DC	
13	MR_01	ao0	PXI1Slot3_4	PXIe-4322	Voltage	v		-16 to +16 Volts		
14	MR_02	ao1	PXI1Slot3_4	PXIe-4322	Voltage	v		-16 to +16 Volts		
15	MR_03	ao2	PXI1Slot3_4	PXIe-4322	Voltage	v		-16 to +16 Volts		
16	MR_04	ao3	PXI1Slot3_4	PXIe-4322	Voltage	v		-16 to +16 Volts		

Figure 4.36: Instrumentation panel of the rigid fluid tank-MR damper for data acquisition and control

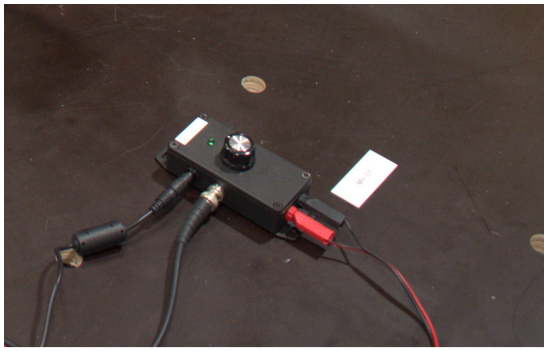

Figure 4.37: Pulse Width Modulator (PWM) control box developed for commanding voltage to the MR dampers

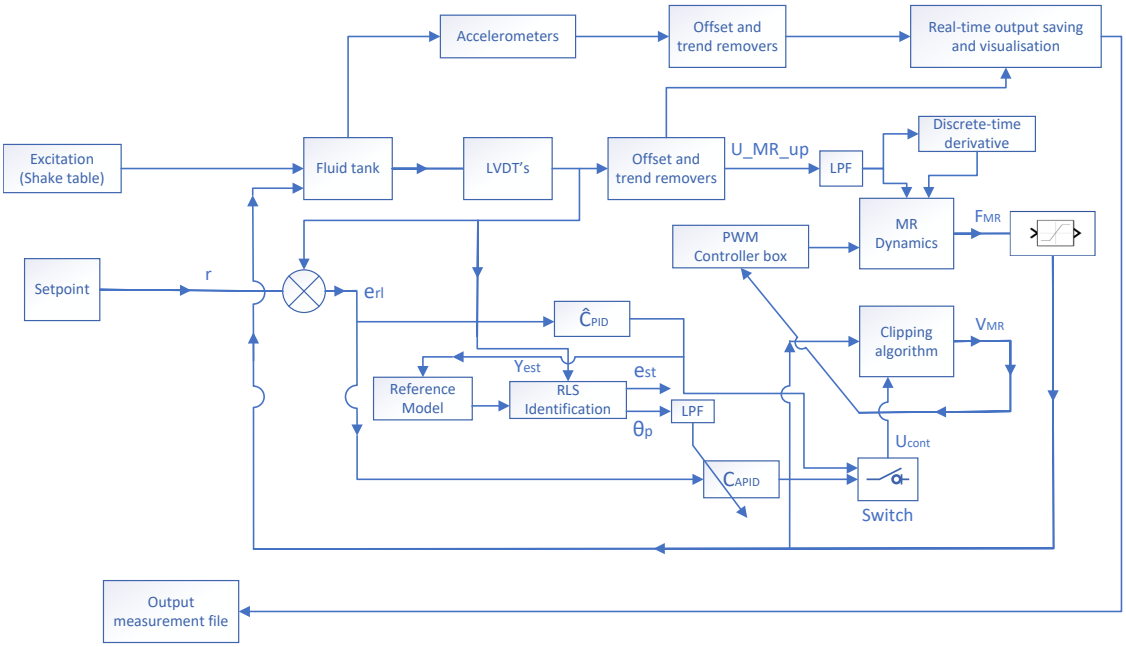

Figure 4.38: Data acquisition and online control system block diagram

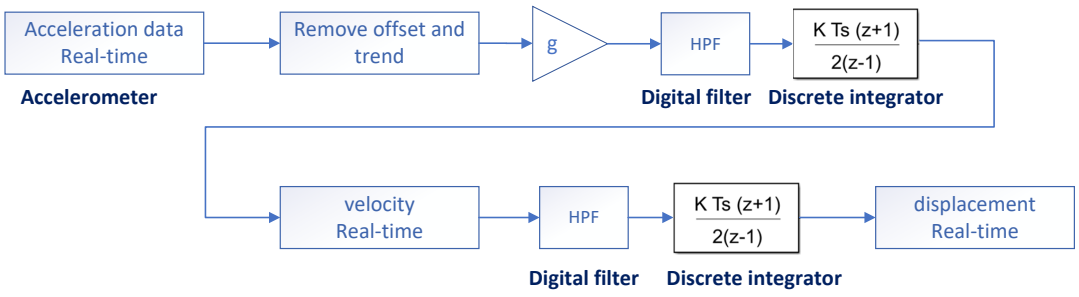

Figure 4.39: Real-time dynamic displacement estimation from accelerometer's measurements

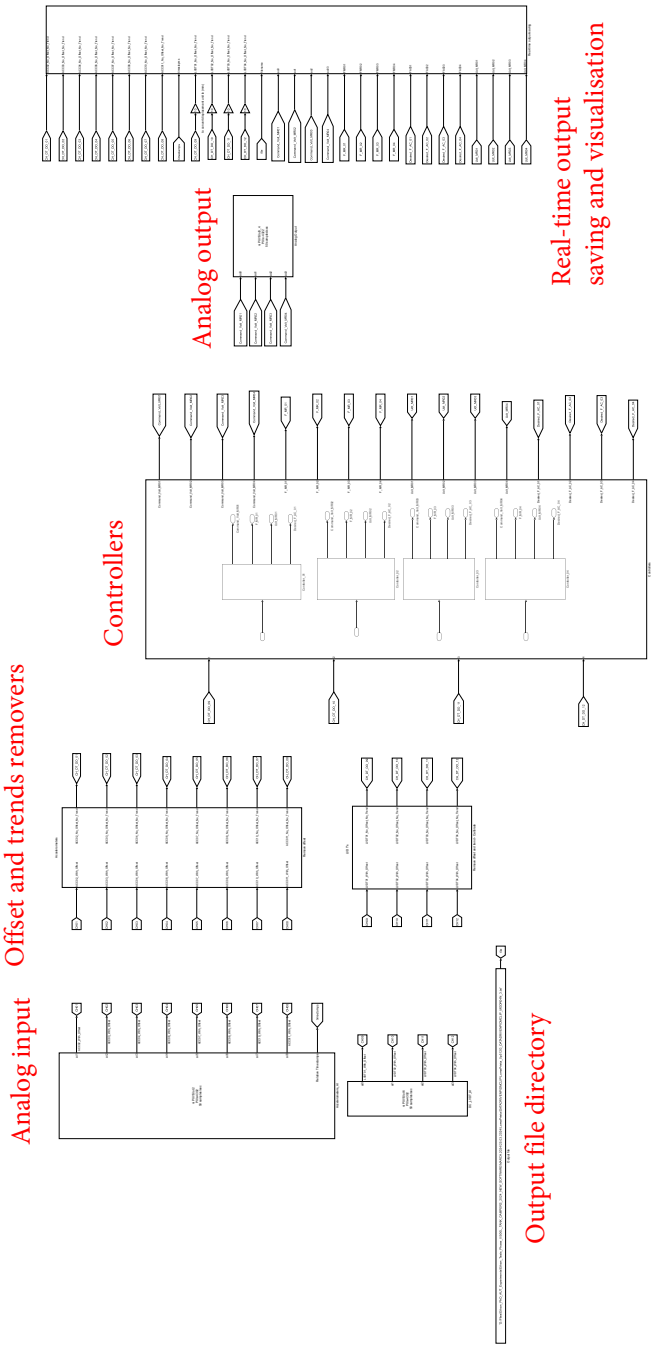

Figure 4.40: Developed software for simultaneous data acquisition and online control based on SIMULINK-MATLAB

4.4.3 Swept-sine tests over unanchored legged rigid fluid tank

A number of 26 swept-sine tests based on the same formulae described in sub-section 4.2.4 were conducted over the unanchored legged rigid fluid tank to examine its natural frequencies. Details of these tests can be found in Table (4.11).

Table 4.11: Characteristics of the swept-sine tests over the unanchored legged rigid fluid tank

Observation ($No.$)	**Frequency band** (Hz)	**Amplitude** (mm)	**Duration** (Sec)	**Repetition** ($No.$)
1	0.1-2.0	5	60	1
2	0.1-3.0	5	120	1
3	0.1-3.5	5	300	1
4	0.1-4.5	3	300	1
5	0.1-5.5	1	300	1
6	0.5-4.5	2	300	1
7	1.0-2.5	5	300	1
8	1.0-3.0	5	120	1
9	1.0-4.0	5	120	1
10	1.0-5.0	2	300	1
11	1.0-11.0	0.2	300	1
12	1.5-2.5	5	300	1
13	1.5-4.5	3	300	1
14	1.5-4.5	5	300	1
15	2.0-3.5	3	300	1
16	2.0-4.0	2	120	1
17	2.0-4.0	3	240	1
18	2.0-5.0	2	120	1
19	3.0-4.5	3	300	1
20	3.0-8.0	0.5	120	1
21	4.0-6.0	0.5	300	1

Continue on the next page

Table 4.11: Characteristics of the swept-sine tests over the unanchored legged rigid fluid tank

Observation ($No.$)	**Frequency band** (Hz)	**Amplitude** (mm)	**Duration** (Sec)	**Repetition** ($No.$)
22	4.5-5.5	2	300	1
23	4.0-11.0	0.2	120	1
24	4.0-11.0	0.5	120	1
25	6.5-8.5	0.2	300	1
26	8.5-11.5	0.2	300	1

4.4.4 Ground motion tests over legged rigid fluid tank-MR

The seismic records of seven past prominent earthquakes including the 1979 El Centro, the 1999 Kocaeli, the 1990 Manjil, the 1995 Kobe, the 1989 Loma Prieta, and the 2011 Christchurch, and the 1978 Tabas were used for experimental examinations. Records of the selected ground motions were obtained from the Pacific Earthquake Engineering Research Center (PEER), Next Generation Attenuation (NGA-West2) database for historical earthquake records (Ancheta et al., 2014), (https://ngawest2.berkeley.edu/). Each record was scaled using SeismoSignal (Seismosoft, 2022) to specific Peak Ground Acceleration (PGA) values. Displacement time histories in millimeters units were used for each scaled ground motion and were given to the shake table to produce the excitations. A time step of 0.02 sec was used for producing time histories using the shake table. Details of each ground motion including the event name, station, year, fault type, mechanism, magnitude (M_w), and PGA have been presented in Table 4.12. Characteristics of the ground motion tests have been represented in Table 4.13. The legged rigid fluid tank has been controlled under different scales of the selected ground motions and for various control techniques as shown in this table. The applied control methods consist of two passive modes including the Passive Off and Passive On, and different semi-active techniques including the energy dissipation method and a series of many other different techniques. Details of

the applied control methods, model and model reference transfer functions, controller parameters, and different applied digital filters can be found in Appendix B. 92 tests over the uncontrolled tank and 383 tests over the controlled tank using the MR dampers were conducted. In addition, around 150 trial tests were conducted to adjust and regulate the control system and design.

Table 4.12: Details of the earthquake records used for seismic ground motion tests of the fluid storage tank

Event	**Station**	**Year**	**Fault type**	**Mechanism**	M_w	**PGA** (g)
Imperial Valley	El Centro	1979	Near-fault, Pulse-like	Strike-Slip	6.53	0.449
Kocaeli	Atakoy	1999	Far-field	Strike-Slip	7.51	0.168
Manjil	Abbar	1990	Far-filed	Strike-Slip	7.37	0.497
Loma Prieta	APEEL 2E Hayward Muir Sch	1989	Far-fault	Reverse-Oblique	6.93	0.171
Kobe	KJMA	1995	Near-fault, Pulse-like	Strike-Slip	6.9	0.834
Christchurch	Cathedral College	2011	Near-fault	Reverse Oblique	6.2	0.478
Tabas	Tabas	1978	Near-Fault	Reverse	7.35	0.854

Table 4.13: Characteristics of the ground motion tests for the legged rigid fluid tank-MR

Ovservation $(No.)$	**Ground motion**	**PGA** (g)	**Control method**	**Repetition** $(No.)$
Uncontrolled system tests				
1	Christchurch	0.05	–	1

Continue on the next page

Table 4.13: Characteristics of the ground motion tests for the legged rigid fluid tank-MR

Ovservation ($No.$)	**Ground motion**	**PGA** (g)	**Control method**	**Repetition** ($No.$)
2	Christchurch	0.10	–	1
3	Christchurch	0.15	–	1
4	Christchurch	0.20	–	1
5	Christchurch	0.25	–	1
6	Christchurch	0.30	–	1
7	Christchurch	0.35	–	1
8	Christchurch	0.38	–	4
9	Christchurch	0.42	–	6
10	Christchurch	0.438	–	9
11	El Centro	0.05	–	1
12	El Centro	0.10	–	1
13	El Centro	0.11	–	1
14	Kobe	0.05	–	1
15	Kobe	0.10	–	1
16	Kobe	0.15	–	1
17	Kobe	0.20	–	1
18	Kobe	0.25	–	1
19	Kobe	0.30	–	1
20	Kobe	0.35	–	1
21	Kobe	0.42	–	1
22	Kobe	0.49	–	2
23	Kobe	0.525	–	8
24	Kobe	0.56	–	7
25	Kocaeli	0.05	–	1
26	Kocaeli	0.10	–	1
27	Kocaeli	0.15	–	1
28	Kocaeli	0.21	–	1

Continue on the next page

Table 4.13: Characteristics of the ground motion tests for the legged rigid fluid tank-MR

Ovservation ($No.$)	**Ground motion**	**PGA** (g)	**Control method**	**Repetition** ($No.$)
29	Kocaeli	0.25	–	2
30	Manjil	0.05	–	1
31	Manjil	0.10	–	1
32	Manjil	0.15	–	1
33	Manjil	0.20	–	1
34	Manjil	0.25	–	1
35	Manjil	0.30	–	1
36	Manjil	0.35	–	1
37	Manjil	0.385	–	1
38	Tabas	0.35	–	1
39	Tabas	0.40	–	1
40	Loma Prieta	0.171	–	1
41	Loma Prieta	0.22	–	1
42	Loma Prieta	0.31	–	1
43	Loma Prieta	0.341	–	1
44	Loma Prieta	0.426	–	5
45	Loma Prieta	0.512	–	13
Controlled system tests				
1	Christchurch	0.05	Passive Off	9
2	Christchurch	0.10	Passive Off	4
3	Christchurch	0.15	Passive Off	5
4	Christchurch	0.20	Passive Off	5
5	Christchurch	0.25	Passive Off	4
6	Christchurch	0.30	Passive Off	7
7	Christchurch	0.35	Passive Off	7
8	Christchurch	0.38	Passive Off	6
9	Christchurch	0.42	Passive Off	2

Continue on the next page

Table 4.13: Characteristics of the ground motion tests for the legged rigid fluid tank-MR

Ovservation ($No.$)	**Ground motion**	**PGA** (g)	**Control method**	**Repetition** ($No.$)
10	Christchurch	0.438	Passive Off	2
11	Christchurch	0.05	Passive On	12
12	Christchurch	0.10	Passive On	7
13	Christchurch	0.15	Passive On	5
14	Christchurch	0.20	Passive On	5
15	Christchurch	0.25	Passive On	2
16	Christchurch	0.30	Passive On	4
17	Christchurch	0.35	Passive On	4
18	Christchurch	0.38	Passive On	5
19	Christchurch	0.42	Passive On	2
20	Christchurch	0.438	Passive On	3
21	Christchurch	0.05	Energy dissipation	3
22	Christchurch	0.10	Energy dissipation	3
23	Christchurch	0.15	Energy dissipation	2
24	Christchurch	0.20	Energy dissipation	2
25	Christchurch	0.25	Energy dissipation	3
26	Christchurch	0.30	Energy dissipation	4
27	Christchurch	0.35	Energy dissipation	2
28	Christchurch	0.38	Energy dissipation	2
29	Christchurch	0.42	Energy dissipation	2
30	Christchurch	0.438	Energy dissipation	3
31	Christchurch	0.15	PIDCLIP01	1
32	Christchurch	0.30	PIDCLIP01	2
33	Christchurch	0.35	PIDCLIP01	2
34	Christchurch	0.38	PIDCLIP01	3
35	Christchurch	0.42	PIDCLIP01	3
36	Christchurch	0.438	PIDCLIP01	3

Continue on the next page

Table 4.13: Characteristics of the ground motion tests for the legged rigid fluid tank-MR

Ovservation ($No.$)	**Ground motion**	**PGA** (g)	**Control method**	**Repetition** ($No.$)
37	Christchurch	0.30	PIDCLIP02	2
38	Christchurch	0.35	PIDCLIP02	2
39	Christchurch	0.38	PIDCLIP02	2
40	Christchurch	0.42	PIDCLIP02	3
41	Christchurch	0.438	PIDCLIP02	2
42	Christchurch	0.438	PIDCLIP03	3
43	Christchurch	0.438	PIDCLIP04	3
44	Christchurch	0.438	PIDCLIP05	2
45	Christchurch	0.438	PIDCLIP06	4
46	Christchurch	0.438	PIDCLIP07	3
47	Christchurch	0.438	PIDCLIP08	3
48	Christchurch	0.438	PIDCLIP09	4
49	Christchurch	0.438	PIDCLIP10	4
50	Christchurch	0.438	PIDCLIP11	5
51	Christchurch	0.438	PIDCLIP12	3
52	Christchurch	0.438	ODDAPIDC01	7
53	Christchurch	0.438	ODDAPIDC02	8
54	Christchurch	0.438	ODDAPIDC03	4
55	Christchurch	0.438	ODDAPIDC04	4
56	Christchurch	0.438	ODDAPIDC05	4
57	Christchurch	0.438	PIDMCLIP01	3
58	Christchurch	0.438	PIDMCLIP02	4
59	Christchurch	0.438	PIDMCLIP03	4
60	Christchurch	0.438	PIDMCLIP04	5
61	Christchurch	0.438	PIDMCLIP05	4
62	Christchurch	0.438	ODDAPIDC06	4
63	Christchurch	0.438	ODDAPIDC07	4

Continue on the next page

Table 4.13: Characteristics of the ground motion tests for the legged rigid fluid tank-MR

Ovservation ($No.$)	**Ground motion**	**PGA** (g)	**Control method**	**Repetition** ($No.$)
64	Christchurch	0.438	ODDAPIDMC01	4
65	Christchurch	0.438	ODDAPIDMC02	4
66	Christchurch	0.438	ODDAPIDMC03	4
67	Christchurch	0.438	ODDAPIDMC04	4
68	Christchurch	0.438	ODDAPIDMC05	4
69	Kobe	0.525	Passive On	4
70	Kobe	0.525	Passive Off	4
71	Kobe	0.525	Energy dissipation	4
72	Kobe	0.525	PIDCLIP05	3
73	Kobe	0.525	PIDCLIP06	4
74	Kobe	0.525	PIDCLIP09	3
75	Kobe	0.525	PIDCLIP10	3
76	Kobe	0.525	PIDCLIP11	3
77	Kobe	0.525	PIDMCLIP01	3
78	Kobe	0.525	PIDMCLIP02	2
79	Kobe	0.525	PIDMCLIP03	3
80	Kobe	0.525	PIDMCLIP04	2
81	Kobe	0.525	PIDMCLIP05	3
82	Kobe	0.525	ODDAPIDC01	2
83	Kobe	0.525	ODDAPIDC02	3
84	Kobe	0.525	ODDAPIDC05	2
85	Kobe	0.525	ODDAPIDC06	2
86	Kobe	0.525	ODDAPIDC07	2
87	Kobe	0.525	ODDAPIDMC01	3
88	Kobe	0.525	ODDAPIDMC02	2
89	Kobe	0.525	ODDAPIDMC03	2
90	Kobe	0.525	ODDAPIDMC04	3

Continue on the next page

Table 4.13: Characteristics of the ground motion tests for the legged rigid fluid tank-MR

Ovservation ($No.$)	**Ground motion**	**PGA** (g)	**Control method**	**Repetition** ($No.$)
91	Kobe	0.525	ODDAPIDMC05	3
92	Loma Prieta	0.512	Passive On	3
93	Loma Prieta	0.512	Passive Off	3
94	Loma Prieta	0.512	Energy dissipation	3
95	Loma Prieta	0.512	PIDCLIP05	2
96	Loma Prieta	0.512	PIDCLIP06	2
97	Loma Prieta	0.512	PIDCLIP09	2
98	Loma Prieta	0.512	PIDCLIP10	2
99	Loma Prieta	0.512	PIDCLIP11	3
100	Loma Prieta	0.512	PIDMCLIP01	2
101	Loma Prieta	0.512	PIDMCLIP03	3
102	Loma Prieta	0.512	PIDMCLIP05	3
103	Loma Prieta	0.512	ODDAPIDC01	2
104	Loma Prieta	0.512	ODDAPIDC02	3
105	Loma Prieta	0.512	ODDAPIDC05	3
106	Loma Prieta	0.512	ODDAPIDC06	3
107	Loma Prieta	0.512	ODDAPIDMC02	3
108	Loma Prieta	0.512	ODDAPIDMC03	2
Acceleration feedback controlled system tests				
109	Christchurch	0.438	PIDCLIP10	3
110	Kobe	0.525	PIDCLIP10	3
111	Kobe	0.56	PIDCLIP10	3
112	Loma Prieta	0.512	PIDCLIP10	5

4.4.5 Experimental results of swept-sine tests over rigid legged tank

Analysing the signals from the accelerometer time-history measurements of the swept-sine tests over the rigid legged tank using the signal processing toolbox of MATLAB via the developed software by the author is shown in Figures 4.41-4.43. These figures represent the PSD, single-sided amplitude spectrum, and spectrogram (STFT) graphs, respectively, for the accelerometer sensors attached to the tank's body which measure the lateral acceleration. Three major natural frequencies of 3.9, 10.2, and 14.2 Hz for this rigid tank were detected by analysing the accelerometer signals.

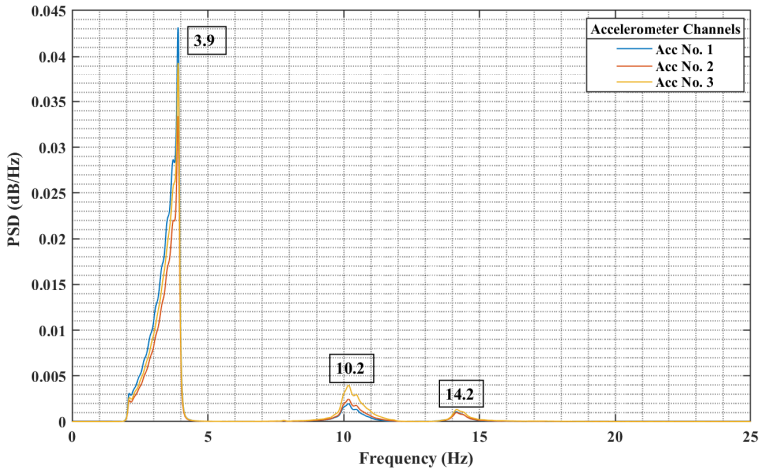

Figure 4.41: Power spectral density graph of rigid legged tank – Swept-sine test, 2-4 Hz frequency range, 2 mm amplitude, and 120 s duration

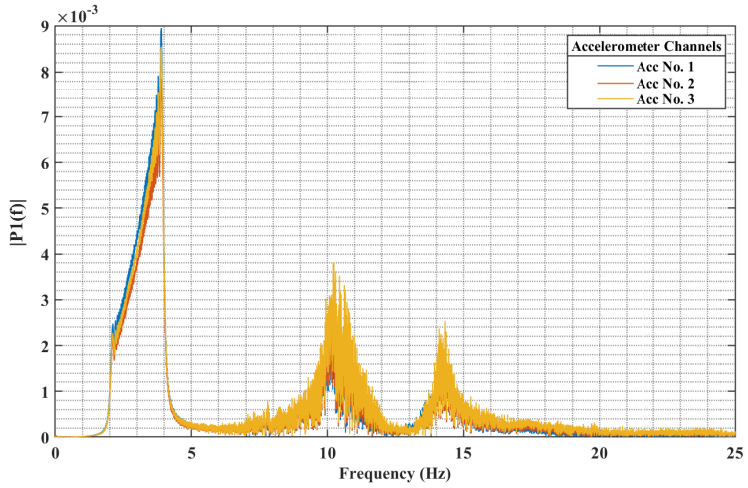

Figure 4.42: Single-sided amplitude spectrum graph of rigid legged tank – Swept-sine test, 2-4 Hz frequency range, 2 mm amplitude, and 120 s duration

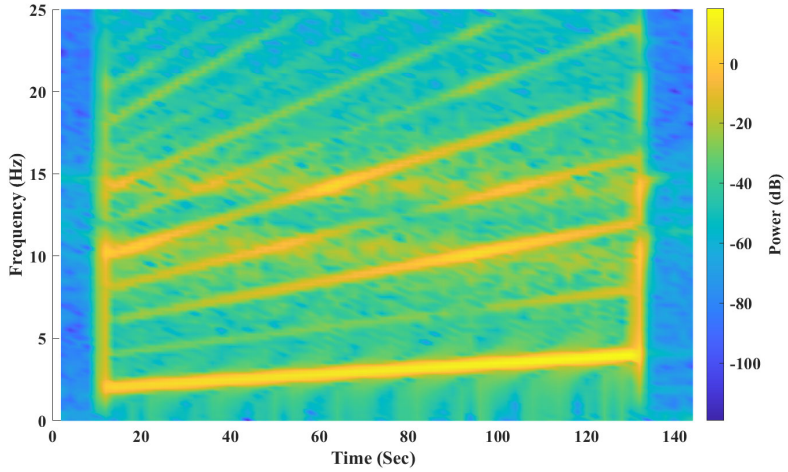

Figure 4.43: Spectrogram (STFT) graph of rigid legged tank – Swept-sine test, 2-4 Hz frequency range, 2 mm amplitude, and 120 s duration

4.4.6 Experimental and numerical results of the rigid legged tank-MR

Using the formulae developed in section 3.3.4 for the dynamic behaviour of a rocking rigid legged cylindrical tank, numerical simulations for the uncontrolled and controlled system utilising MR dampers were conducted using SIMULINK - MATLAB. Numerical results were polluted with White Gaussian Noise (WGN) with a signal-to-noise ratio (SNR) of 1 dB to simulate the practical applications in the presence of noise. Numerical results were compared to experimental ones to examine the performance of the developed equations and the conducted simulations. Comparisons between the numerical and experimental results for both cases of controlled and uncontrolled systems under the Christchurch $0.438g$ have been illustrated in Figures 4.46-4.47. In total, a series of 29 controllers were applied to the system, two of which being the passive controllers, i.e. the Passive On and Passive Off and the remaining 27 controllers include the semi-active model-based and online data-driven adaptive controllers. Experimental results of the uncontrolled system versus the controlled system, as well as the results of different controllers, under different ground motion tests, have been illustrated in Figures 4.48-4.59. The results of the uncontrolled system and controlled system using the acceleration feedback technique under the Christchurch $0.438g$ and Kobe $0.56g$ have been illustrated in Figures 4.60 and 4.63, respectively. The comparison between the estimated uplift based on the developed method in this research and the measured one under the Loma Prieta $0.512g$ and Kobe $0.525g$ have been expressed in Figures 4.61 and 4.62, respectively. The control system design implementation was achieved using the developed software platform via SIMULINK which receives signals from the National Instruments Data Acquisition (NI-DAQ) system, analyses and processes them using the developed control procedures, and commands them to the PWM boxes. The non-parametric frequency responses of the uncontrolled and controlled system using different semi-active controllers from input base excitation to the output uplift of the tank were estimated by the Spectral Analysis (SPA) approach via the Blackman-Tukey method (Ljung, 1998) using the Hann windowing. The non-parametric frequency response function using the Blackman-Tukey

is obtained using the below function,

$$\hat{G}_N(e^{i\omega}) = \frac{\hat{\Phi}_{in/out}(\omega)}{\hat{\Phi}_{in}(\omega)} \tag{4.12}$$

where $\hat{\Phi}_{in}(\omega)$ and $\hat{\Phi}_{in/out}(\omega)$ are the Fourier transforms of the covariance and cross-covariance from input to output signals, respectively.

These analyses were conducted using the System Identification toolbox of MATLAB R2023b to observe the effect of added control mechanism on the frequency behaviour of the system. Bode diagrams of the estimated frequency responses of the uncontrolled and controlled system using different semi-active controllers have been depicted in Figures 4.64-4.66. Parameters of one of the tested online adaptive data-driven controllers in real-time have been illustrated in Figures 4.67-4.68. Experimental results of peak uplift displacements of the tank under different PGA scales of the Christchurch 2011 earthquake have been presented in Table 4.15. In the presented figures and tables for the results, channel $CH10$ represents the $LVDT02$ sensor measuring the uplift displacements of the tank which were found to be the largest among that of other displacement sensors. After examining the experimental results of some primary tests, ground motions with certain PGA scales were found to create enough uplift displacements in the system for the MR dampers to come into action and start dissipating the external energy. Thus, these ground motions which include Christchurch $0.438g$, Kobe $0.525g$, and Loma Prieta $0.512g$ were set as the focus of controlled system tests. Experimental results of the peak uplift displacements of the uncontrolled and controlled system for the applied controllers have been listed in Table 4.16. Tests under the Kobe $0.56g$ were conducted only for the semi-active control design using acceleration feedback. Moreover, to easily compare the performance of various controllers examined for the system to mitigate the uplift displacements of the tank under the base excitation, a performance index in this regard is defined as follows,

$$PI_{upl} = \frac{Max|U_{co}^{upl}|}{Max|U_{uco}^{upl}|} \tag{4.13}$$

where, U_{co}^{upl} and U_{uco}^{upl} are the uplift displacements of the rigid tank in controlled and uncontrolled cases, respectively. Table 4.17 shows the calculated performance indices of the applied controllers for conducted tests presented in Table 4.16. Since at the beginning of the tests, there were uncertainties and little knowledge about the true behaviour of the system, some trial controllers including PIDCLIP01 – PIDCLIP04 were applied to examine the performance of the controlled system under the Christchurch $0.438g$. However, these controllers were not continued for later tests. Also, acceleration feedback design control systems were tested only using the semi-active controller PIDCLIP10. It is noteworthy that in some of the figures representing the experimental results of tests using different controllers or comparative figures between uncontrolled system and controlled system using different techniques, there are time differences between different plots. These differences are due to inevitable different start and stop times for measurements of the sensors at each test during the experiments. Besides the Christchurch earthquake for which tests were conducted for all controllers, for other earthquakes controlled system design tests were implemented selectively among different techniques.

Figure 4.44: Experimental tests of the tank without MR dampers under applied ground motions - Christchurch 2011

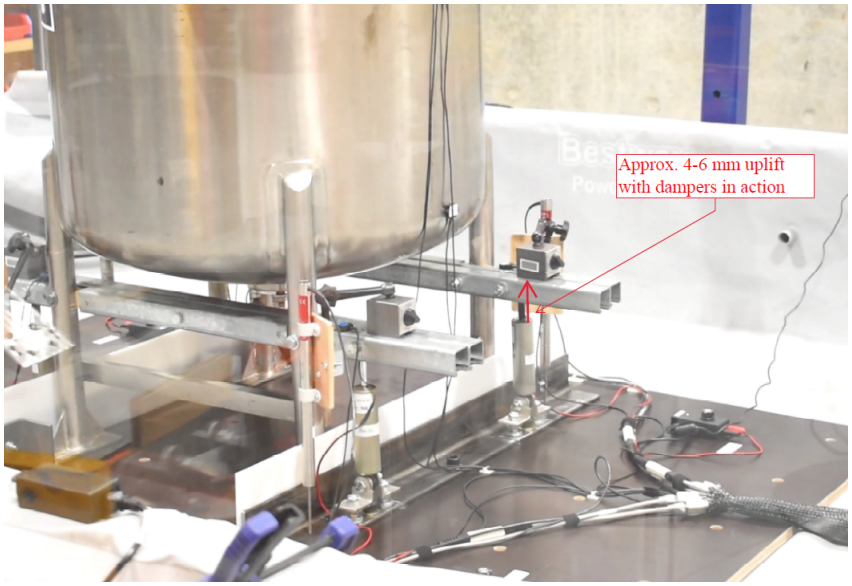

Figure 4.45: Experimental tests of the tank with MR dampers under applied ground motions - Christchurch 2011

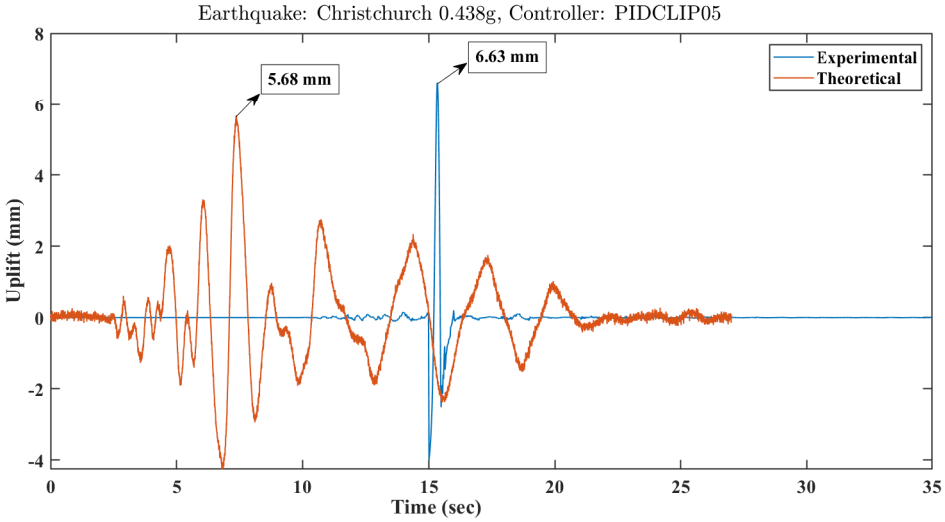

Figure 4.46: Experimental and theoretical uplift displacement comparison of the tank with MR dampers under the Christchurch 2011, 0.438 g for controller PIDCLIP05

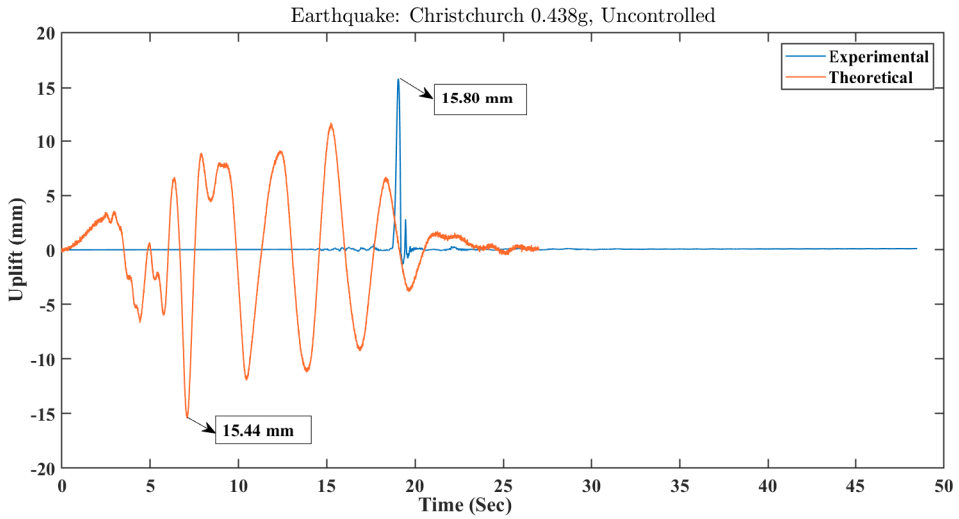

Figure 4.47: Experimental and theoretical uplift displacement comparison of the tank without MR dampers (uncontrolled system) under the Christchurch 2011, 0.438 g

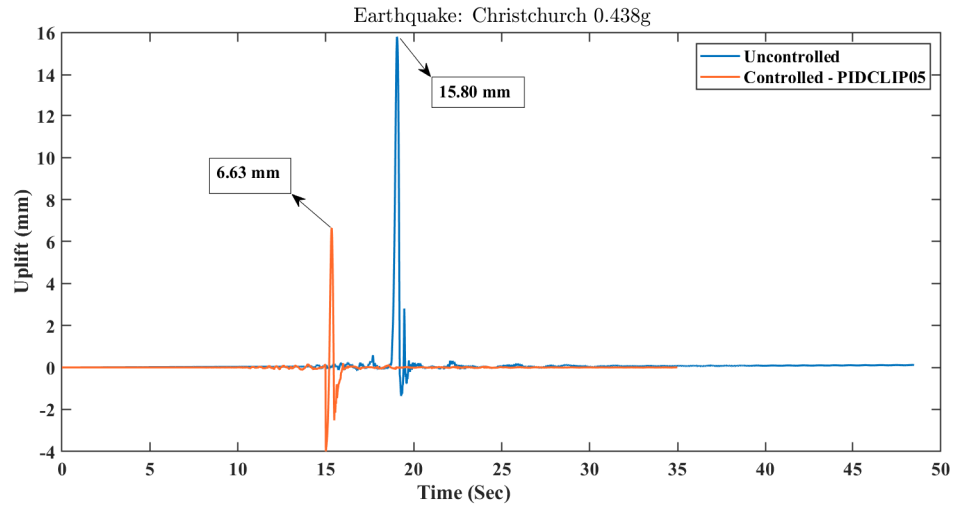

Figure 4.48: Uplift displacement comparison between experimental results of the controlled system using PIDCLIP05 controller and the uncontrolled tank under the Christchurch 2011, 0.438 g

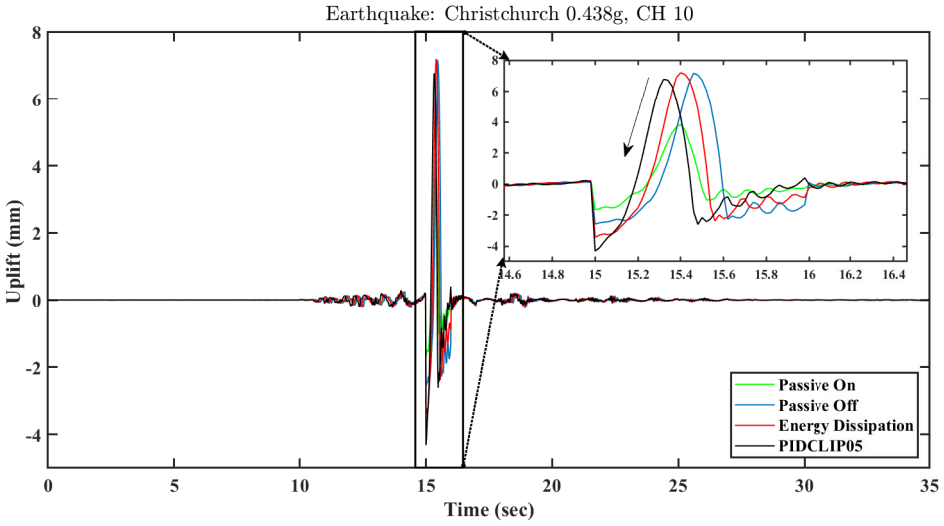

Figure 4.49: Uplift displacement comparison between experimental results of two passive and two semi-active controllers under the Christchurch 2011, 0.438 g

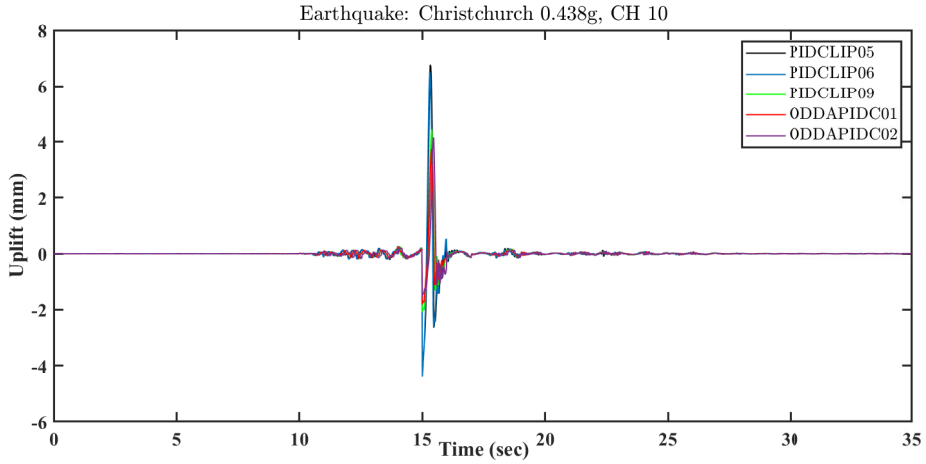

Figure 4.50: Uplift displacement comparison between experimental results of several semi-active model-based and online data-driven adaptive controllers under the Christchurch 2011, 0.438 g

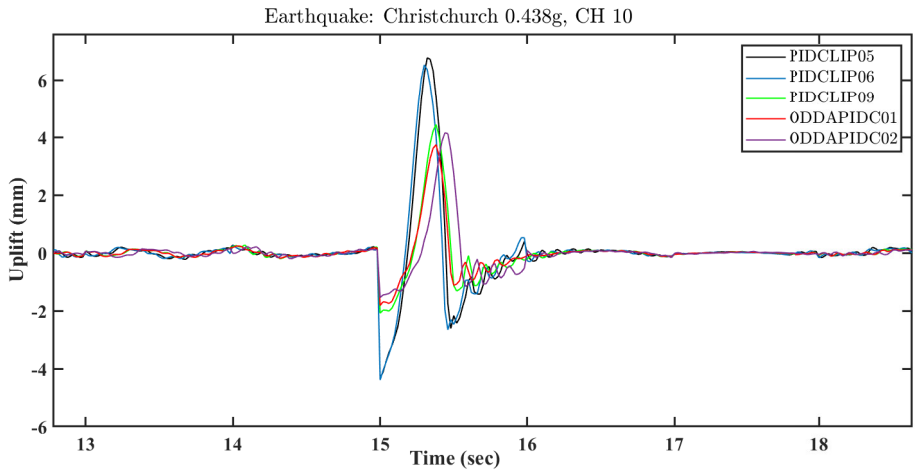

Figure 4.51: Uplift displacement comparison between experimental results of several semi-active model-based and online data-driven adaptive controllers under the Christchurch 2011, 0.438 g – close-up

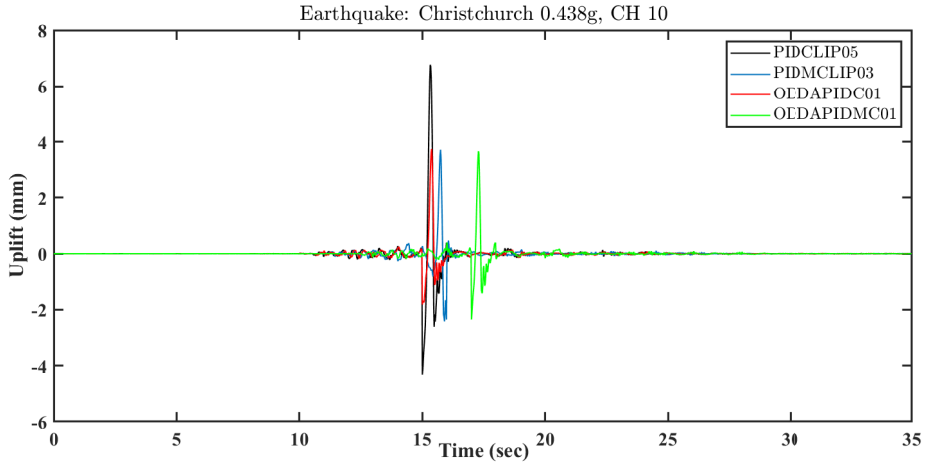

Figure 4.52: Uplift displacement comparison between experimental results of several semi-active model-based and online data-driven adaptive controllers using standard and modified Clipping technique under the Christchurch 2011, 0.438 g

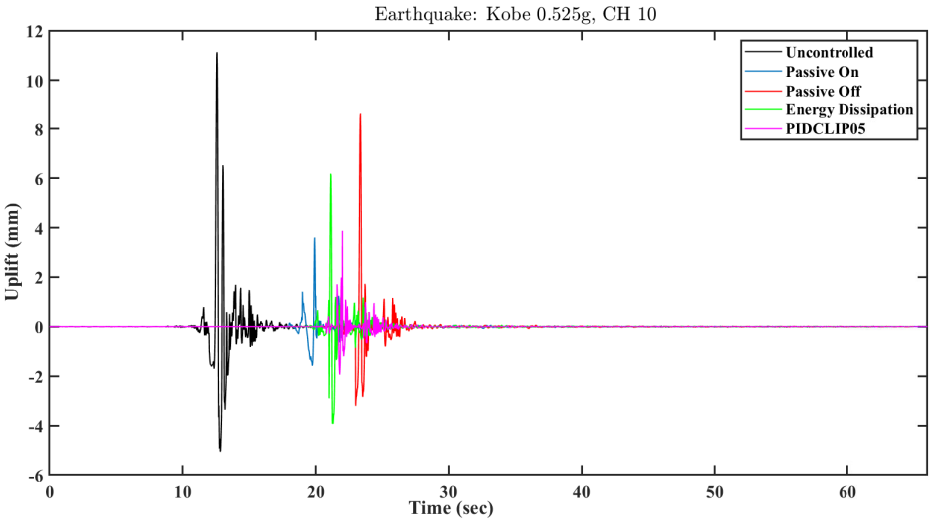

Figure 4.53: Uplift displacement comparison between experimental results of uncontrolled and controlled system by passive and semi-active model-based controllers under the Kobe 1995, 0.525 g

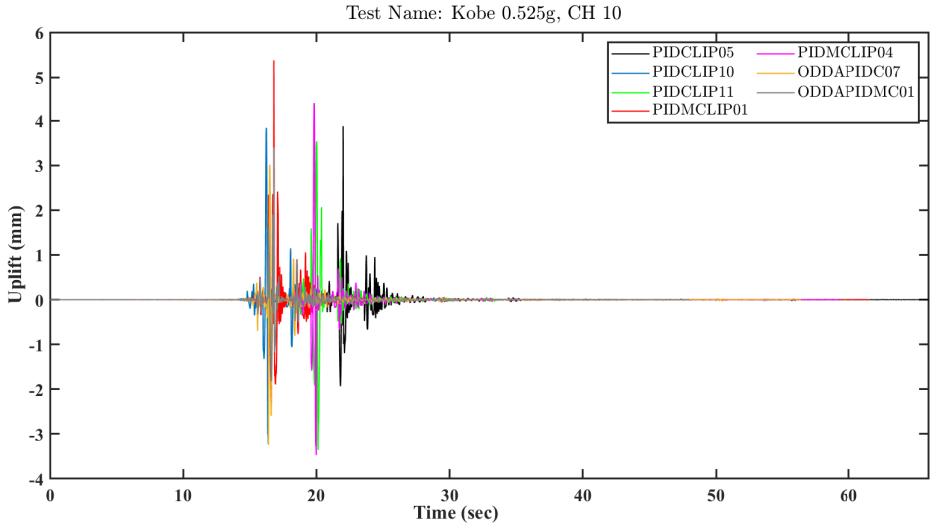

Figure 4.54: Uplift displacement comparison between experimental results of several model-based and online data-driven adaptive controllers using standard and modified Clipping technique under the Kobe 1995, 0.525 g

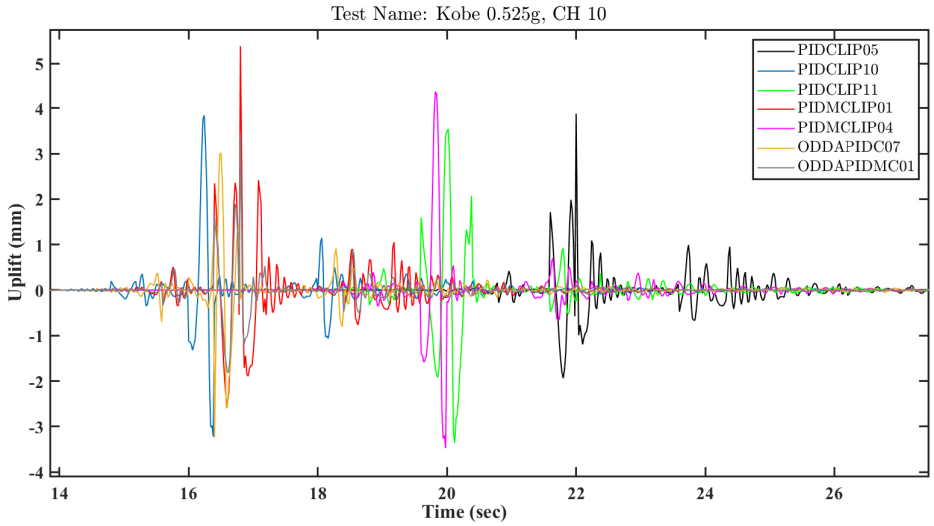

Figure 4.55: Uplift displacement comparison between experimental results of several model-based and online data-driven adaptive controllers using standard and modified Clipping technique under the Kobe 1995, 0.525 g – close-up

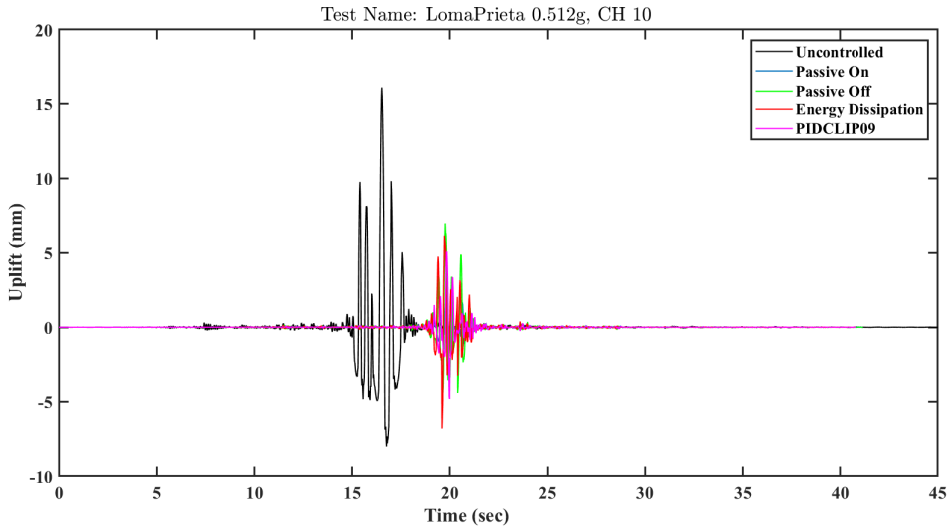

Figure 4.56: Uplift displacement comparison between experimental results of uncontrolled and controlled system with passive and semi-active controllers under the Loma Prieta 1989, 0.512 g

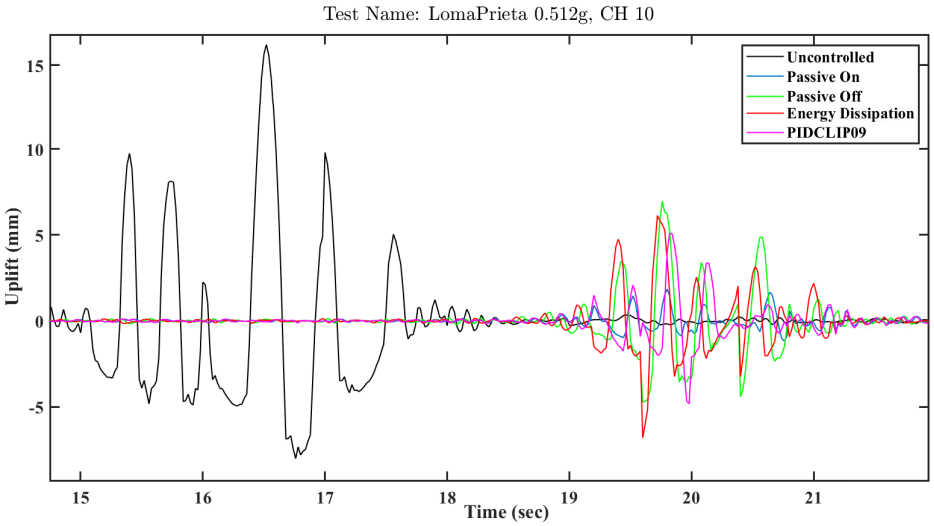

Figure 4.57: Uplift displacement comparison between experimental results of uncontrolled and controlled system with passive and semi-active controllers under the Loma Prieta 1989, 0.512 g – close-up

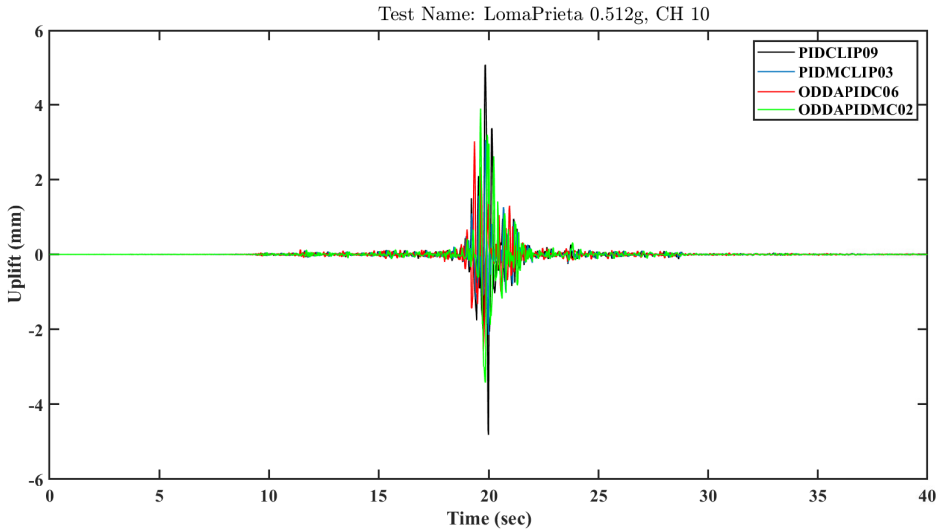

Figure 4.58: Uplift displacement comparison between experimental results of the controlled system with several model-based and online data-driven adaptive semi-active controllers using the standard and modified Clipping technique under the Loma Prieta 1989, 0.512 g

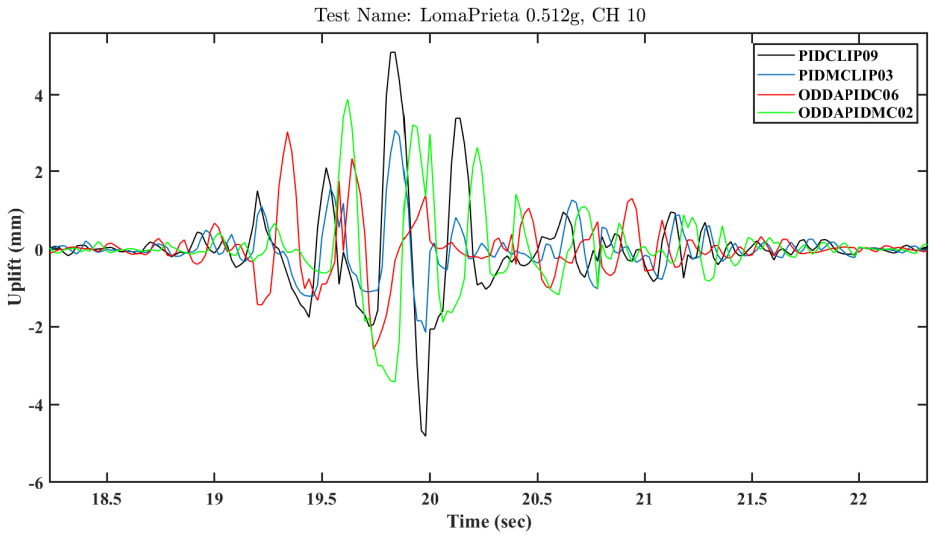

Figure 4.59: Uplift displacement comparison between experimental results of the controlled system with several model-based and online data-driven adaptive semi-active controllers using the standard and modified Clipping technique under the Loma Prieta 1989, 0.512 g – close-up

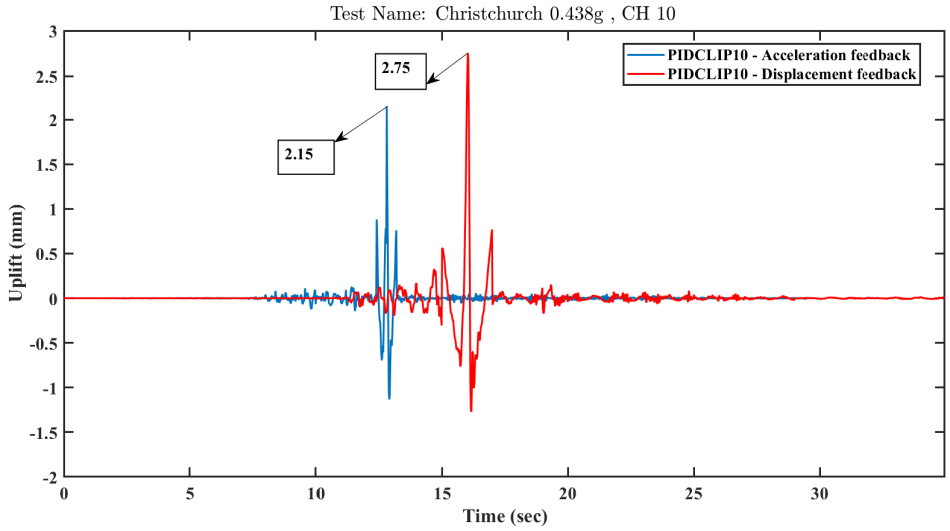

Figure 4.60: Uplift displacement comparison between experimental results of the controlled system using displacement and acceleration feedback semi-active controllers under the Christchurch 2011, 0.438 g

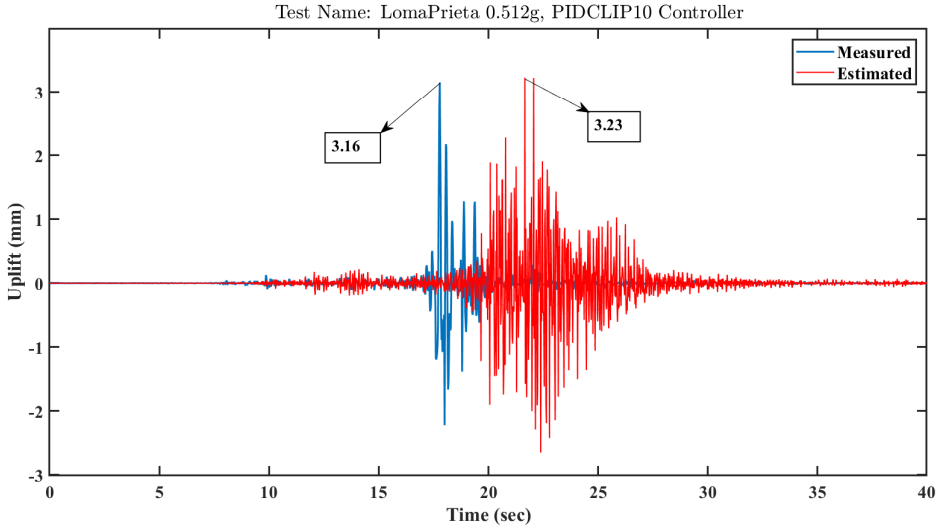

Figure 4.61: The measured experimental and estimated uplift displacements of the controlled system under the Loma Prieta 1989, 0.512 g using PIDCLIP10 controller based on acceleration feedback

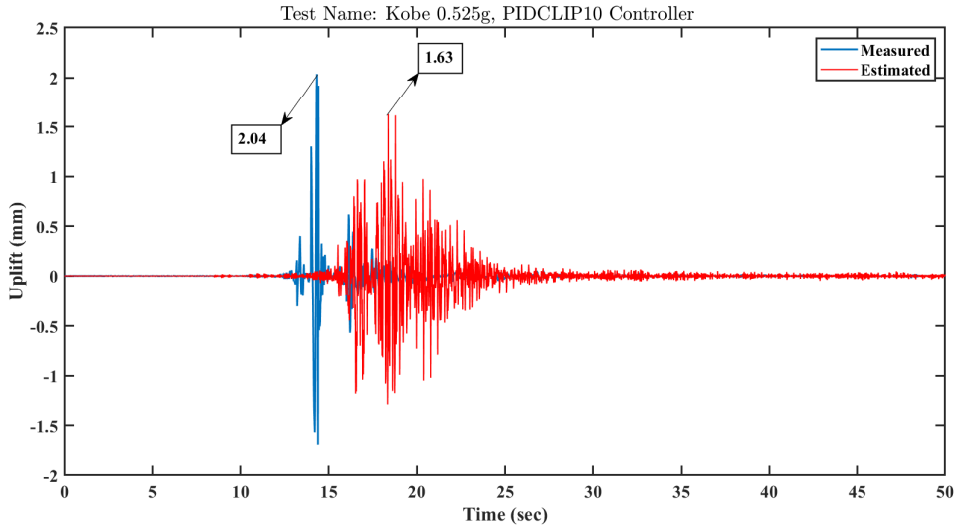

Figure 4.62: The measured experimental and estimated uplift displacements of the controlled system under the Kobe 1995, 0.525 g using PIDCLIP10 controller based on acceleration feedback

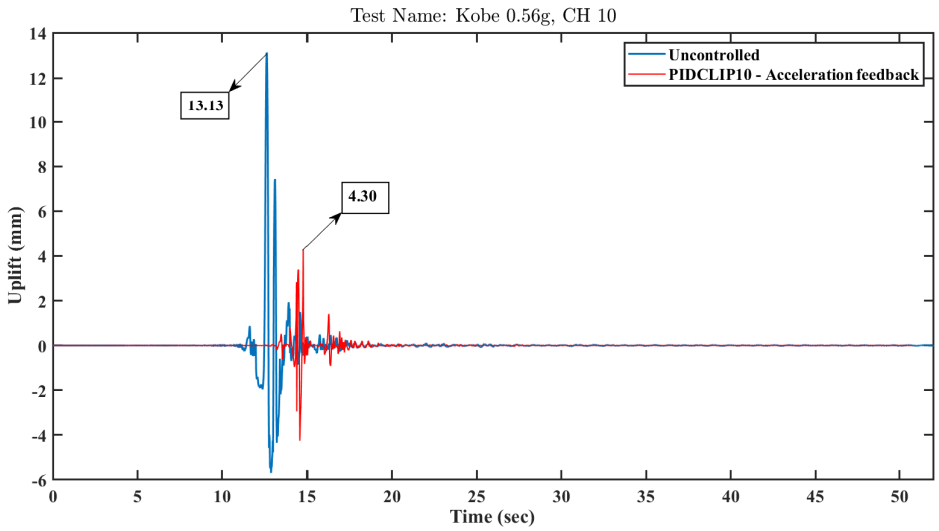

Figure 4.63: Experimental uplift displacements of the uncontrolled and controlled system using semi-active PIDCLIP10 controller based on acceleration feedback under the Kobe 1995, 0.56 g

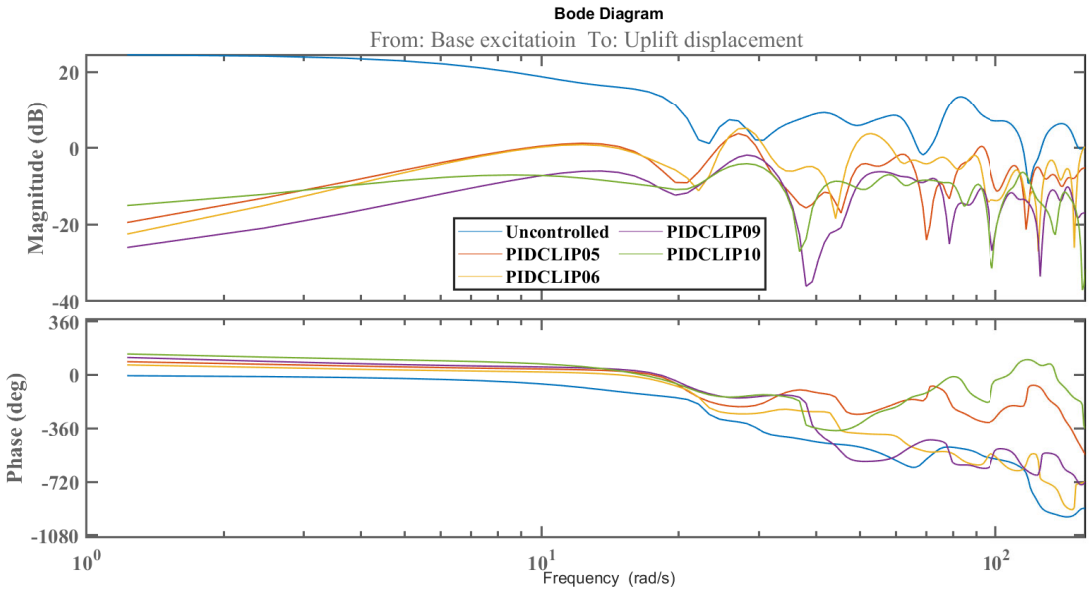

Figure 4.64: Frequency response of the uncontrolled and controlled system using several semi-active controllers under the Christchurch 2011, 0.438 g, from input base excitation to the output uplift displacement of the tank

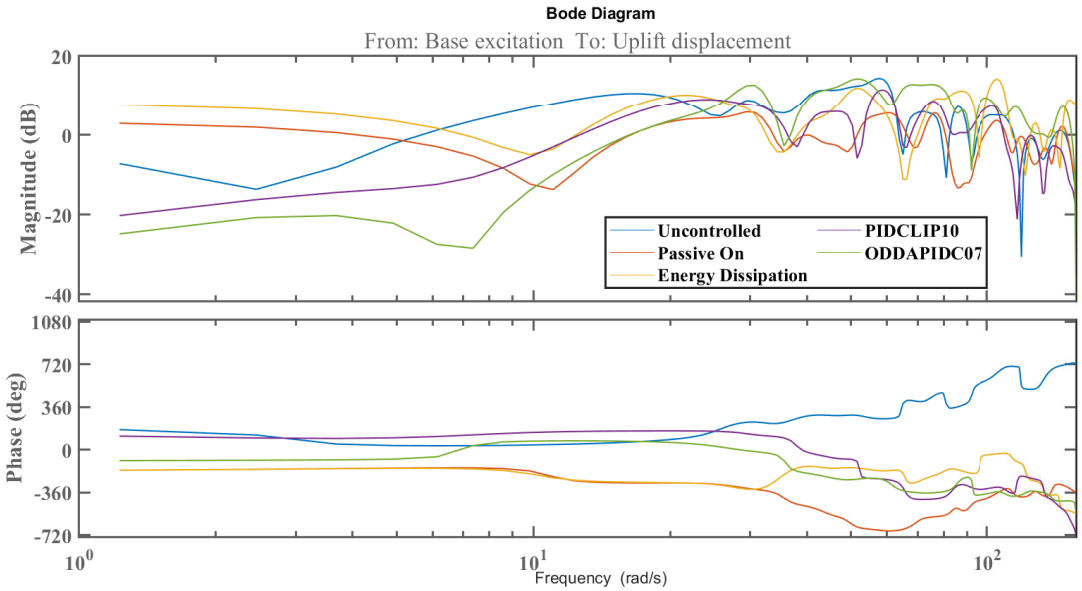

Figure 4.65: Frequency response of the uncontrolled and controlled system using several semi-active controllers under the Kobe 1995, 0.525 g, from input base excitation to the output uplift displacement of the tank

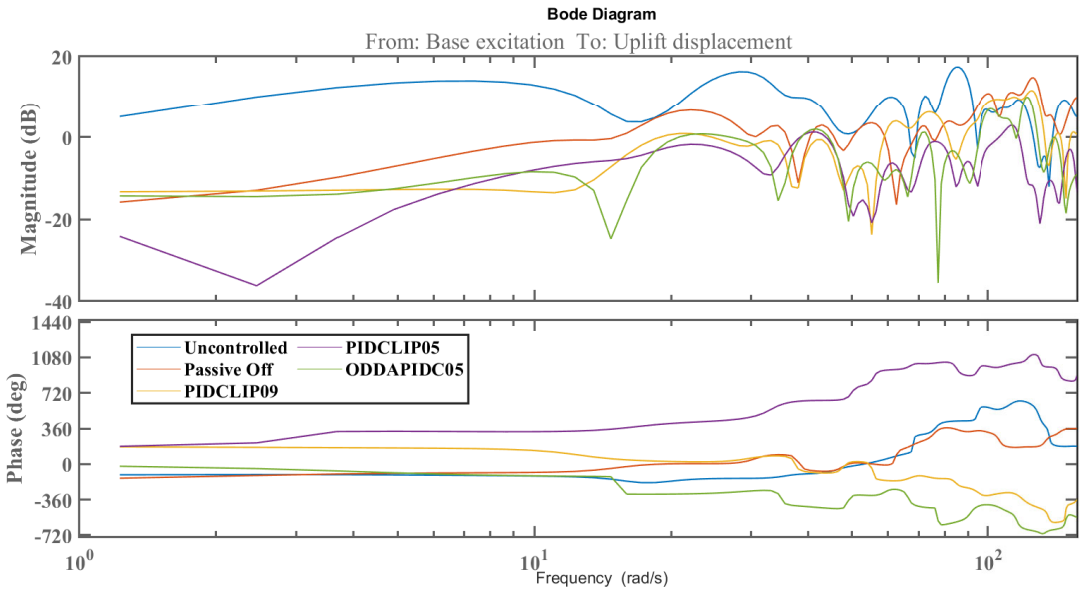

Figure 4.66: Frequency response of the uncontrolled and controlled system using several semi-active controllers under the Loma Prieta 1989, 0.512 g, from input base excitation to the output uplift displacement of the tank

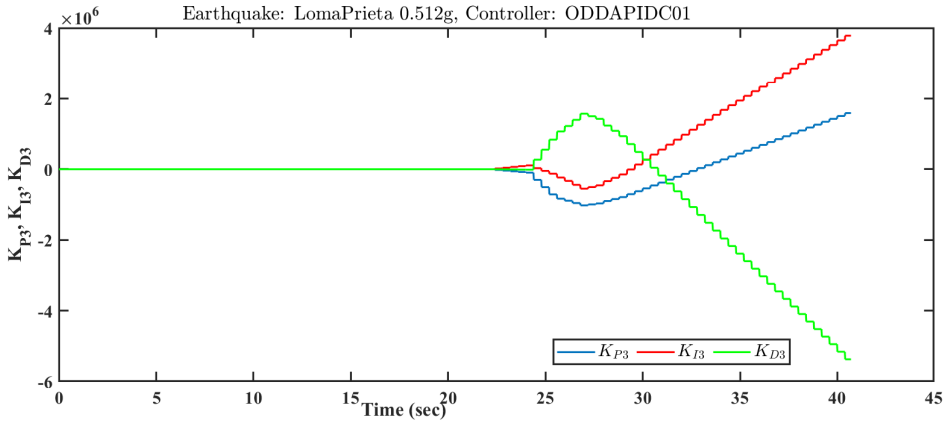

Figure 4.67: Controller's parameters in real-time for the online data-driven adaptive semi-active controller commanding voltage to sensor $[CH11 : LVDT03]$ under the Loma Prieta 1989, 0.512 g

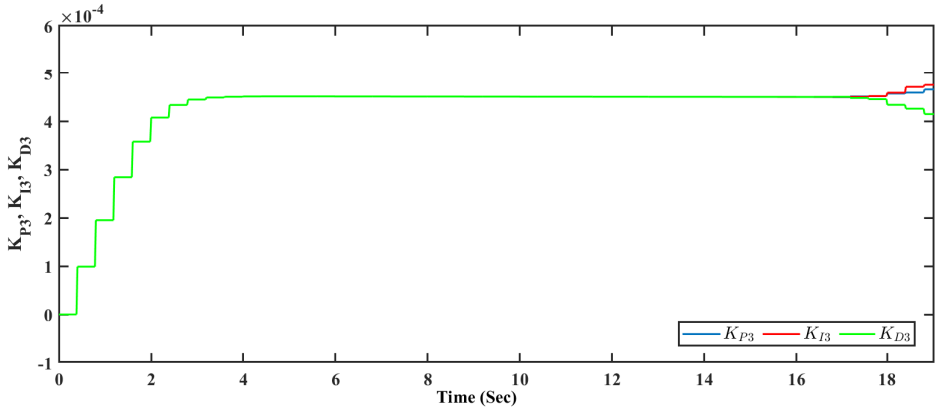

Figure 4.68: Controller's parameters in real-time for the online data-driven adaptive semi-active controller $ODDAPIDC01$, commanding voltage to sensor $[CH11 : LVDT03]$ under the Loma Prieta 1989, 0.512 g – close-up in the range $[0 – 19]\,(s)$

Table 4.14: Experimental and theoretical peak uplift responses of the rigid legged tank-liquid system under different applied ground motion tests

Uplift	**Christchurch 0.438g**	**Kobe 0.525g**	**Kobe 0.56g**	**Loma Prieta 0.512g**
$Theoretical\ (mm)$	15.44	10.66	11.15	11.10
$Experimental\ (mm)$	15.80	11.13	12.83	12.55
$Estimation\ error\ (\%)$	2.33	4.41	15.07	13.06

Table 4.15: Experimental peak uplift responses of the rigid legged tank-liquid-MR damper system under different PGA scales of the Christchurch 2011 earthquake for different control techniques

Uplift Response	**Control technique**	**Christchurch 0.30g**	**Christchurch 0.35g**	**Christchurch 0.38g**	**Christchurch 0.42g**
		Uncontrolled system			
$U_{CH10}(mm)$	Uncontrolled	1.35	4.26	4.51	11.48
		Passive control tests			
$U_{CH10}(mm)$	Passive Off	0.44	0.78	2.00	4.57
	Passive On	0.31	0.55	1.15	2.93
		Semi-active controllers			
$U_{CH10}(mm)$	Energy dissipation	0.42	0.64	1.87	4.88
	PIDCLIP01	0.40	0.70	1.81	4.10
	PIDCLIP02	0.37	0.54	1.02	2.83

Table 4.16: Experimental peak uplift responses of the rigid legged tank-liquid-MR damper system under the selected ground motions for different control techniques

Uplift Response	**Control technique**	**Christchurch 0.438g**	**Kobe 0.525g**	**Kobe 0.56g**	**Loma Prieta 0.512g**
		Uncontrolled system			
$U_{CH10}(mm)$	Uncontrolled	15.80	11.13	13.12	16.32
		Passive control tests			
$U_{CH10}(mm)$	Passive Off	7.51	7.93	–	6.97
	Passive On	3.83	4.19	–	2.19
		Semi – active energy dissipation Clipping controller			
$U_{CH10}(mm)$	Energy dissipation	5.90	6.18	–	6.80
		Semi – active model – based PID standard – Clipping controllers			
$U_{CH10}(mm)$	PIDCLIP01	6.12	–	–	–
	PIDCLIP02	4.75	–	–	–
	PIDCLIP03	5.19	–	–	–
	PIDCLIP04	4.57	–	–	–
	PIDCLIP05	6.77	6.49	–	5.34
	PIDCLIP06	6.53	6.47	–	6.96
	PIDCLIP07	4.85	–	–	–
	PIDCLIP08				
	PIDCLIP09				
	PIDCLIP10				
	PIDCLIP11				
	PIDCLIP12				

Continue on the next page

Table 4.16: Experimental peak uplift responses of the rigid legged tank-liquid-MR damper system under the selected ground motions for different control techniques

Uplift Response	**Control technique**	**Christchurch 0.438g**	**Kobe 0.525g**	**Kobe 0.56g**	**Loma Prieta 0.512g**
		3.62	–	–	–
		3.18	4.05	–	4.58
		2.75	3.84	–	3.28
		2.66	3.54	–	4.60
		7.55	–	–	–
Semi – active model – based PID modified – Clipping controllers					
	PIDMCLIP01	6.64	7.41	–	6.09
	PIDMCLIP02	6.03	6.39	–	–
$U_{CH10}(mm)$	PIDMCLIP03	3.71	4.76	–	3.31
	PIDMCLIP04	2.70	4.40	–	–
	PIDMCLIP05	2.26	4.08	–	4.74
Semi – active online data – driven adaptive PID standard Clipping controllers					
	ODDAPIDC01	2.36	3.55	–	3.52
	ODDAPIDC02	4.15	3.89	–	3.65
	ODDAPIDC03	3.66	–	–	4.63
$U_{CH10}(mm)$	ODDAPIDC04	4.82	–	–	–
	ODDAPIDC05				
	ODDAPIDC06				
	ODDAPIDC07				

Continue on the next page

Table 4.16: Experimental peak uplift responses of the rigid legged tank-liquid-MR damper system under the selected ground motions for different control techniques

Uplift Response	**Control technique**	**Christchurch 0.438g**	**Kobe 0.525g**	**Kobe 0.56g**	**Loma Prieta 0.512g**
		5.44	5.86	–	–
		4.62	4.15	–	3.08
		2.81	3.25	–	–
$Semi-active\ online\ data-driven\ adaptive\ PID\ modified-Clipping\ controllers$					
$U_{CH10}(mm)$	ODDAPIDMC01	2.69	3.40	–	–
	ODDAPIDMC02	2.59	4.42	–	3.89
	ODDAPIDMC03	3.49	4.39	–	4.85
	ODDAPIDMC04	3.32	4.11	–	–
	ODDAPIDMC05	3.35	3.91	–	–
$Semi-active\ acceleration-feedback\ model-based\ PID\ standard-Clipping\ control\ tests$					
$U_{CH10}(mm)$	PIDCLIP10	2.15	2.04	5.70	3.05

Table 4.17: Performance indices of control techniques applied to the experimentally tested rigid legged tank-liquid-MR damper system under the applied ground motion tests

Uplift Response	Control technique	Christchurch 0.438g	Kobe 0.525g	Kobe 0.56g	Loma Prieta 0.512g
		Passive control tests			
PI_{upl}	Passive Off	0.4753	0.7125	–	0.4271
	Passive On	0.2424	0.3765	–	0.1342
		Semi – active energy dissipation Clipping controller			
PI_{upl}	Energy dissipation	0.3734	0.5553	–	0.4167
		Semi – active model – based PID standard – Clipping controllers			
PI_{upl}	PIDCLIP01	0.3873	–	–	–
	PIDCLIP02	0.3006	–	–	–
	PIDCLIP03	0.3285	–	–	–
	PIDCLIP04	0.2892	–	–	–
	PIDCLIP05	0.4285	0.5831	–	0.3272
	PIDCLIP06	0.4133	0.5813	–	0.4265
	PIDCLIP07	0.3070	–	–	–
	PIDCLIP08	0.2291	–	–	–
	PIDCLIP09	0.2013	0.3639	–	0.2806
	PIDCLIP10	0.1741	0.3450	–	0.2010
	PIDCLIP11	0.1684	0.3181	–	0.2819
	PIDCLIP12				

Continue on the next page

Table 4.17: Performance indices of control techniques applied to the experimentally tested rigid legged tank-liquid-MR damper system under the applied ground motion tests

Uplift Response	Control technique	Christchurch 0.438g	Kobe 0.525g	Kobe 0.56g	Loma Prieta 0.512g
		0.4778	–	–	–
		Semi – active model – based PID modified – Clipping controllers			
PI_{upl}	PIDMCLIP01	0.4203	0.6658	–	0.3732
	PIDMCLIP02	0.3816	0.5741	–	–
	PIDMCLIP03	0.2348	0.4277	–	0.2028
	PIDMCLIP04	0.1709	0.3953	–	–
	PIDMCLIP05	0.1430	0.3666	–	0.2904
		Semi – active online data – driven adaptive PID standard Clipping controllers			
PI_{upl}	ODDAPIDC01	0.1494	0.3190	–	0.2157
	ODDAPIDC02	0.2627	0.3495	–	0.2237
	ODDAPIDC03	0.2316	–	–	0.2837
	ODDAPIDC04	0.3051	–	–	–
	ODDAPIDC05	0.3443	0.5265	–	–
	ODDAPIDC06	0.2924	0.3729	–	0.1887
	ODDAPIDC07	0.1778	0.2920	–	–
		Semi – active online data – driven adaptive PID modified – Clipping controllers			
PI_{upl}	ODDAPIDMC01	0.1703	0.3055	–	–
	ODDAPIDMC02				
	ODDAPIDMC03				
	ODDAPIDMC04				
	ODDAPIDMC05				

Continue on the next page

Table 4.17: Performance indices of control techniques applied to the experimentally tested rigid legged tank-liquid-MR damper system under the applied ground motion tests

Uplift Response	**Control technique**	**Christchurch 0.438g**	**Kobe 0.525g**	**Kobe 0.56g**	**Loma Prieta 0.512g**
		0.1639	0.3971	–	0.2384
		0.2209	0.3944	–	0.2972
		0.2101	0.3693	–	–
		0.2120	0.3513	–	–
$Semi-active\ acceleration-feedback\ model-based\ PID\ standard-Clipping\ control\ tests$					
PI_{upl}	PIDCLIP10	0.1361	0.1833	0.4345	0.1869

PSD analysis of the experimental results of swept-sine tests over the rigid legged fluid tank showed three major frequencies of 3.9, 10.2, and 14.2 Hz. Examining the results of analyses shown in Figures 4.46 and 4.47 for experimental and theoretical uplift displacements of the tank under the Christchurch 2011 earthquake in both uncontrolled and controlled cases demonstrates a good level of accuracy in the theoretical formulations developed for the tank. Figure 4.48 shows the amount at which the MR dampers have reduced the uplift displacements in the tank under this earthquake using the $PIDCLIP05$ controller while Figure 4.49 compares the results of the controlled system using two passive controllers, i.e. the Passive On and Passive Off, and two semi-active controllers. It can be stated that under all tested ground motions, the Passive On controller makes the highest reductions in the uplift displacements of the tank versus the Passive Off controller at the other side of this spectrum which results in the lowest. The Energy Dissipation-Clipping controller which has a very simple structure proved efficient in reducing the uplift displacements of the tank. Model-based PID-Clipping controllers have shown the best performance in reducing the uplift displacements of the tank under all the applied ground motions following the Passive On control technique.

Results of the theoretical and experimental evaluations of the uncontrolled tank under applied ground motion tests in this study presented in Table 4.14 show the estimation of the uplift displacements for the rigid legged tank using the formulations developed in Chapter 3 has a maximum evaluation error up to around 15%. Comparisons between the experimental uplift displacements of the controlled system using the $PIDCLIP10$ controller via acceleration feedback and displacement feedback approaches illustrated in Figure 4.60 show that the acceleration feedback technique can effectively follow the performance of the displacement feedback control strategy. Figures 4.61 and 4.62 depict the accuracy of the developed technique in estimating the displacements of the tank to be used in the control design system. It is noteworthy that the developed control design based on the acceleration feedback is stable in the sense that with any level of accuracy in displacement estimations, it continues to reduce the uplift of the tank. Figure 4.63 demonstrates the efficiency of a controller based on acceleration feedback and displacement estimation of the tank in seismic uplift reduction of the system. The

frequency response of both the uncontrolled fluid-tank and the controlled fluid-tank-MR damper system using different control strategies estimated based on the Blackman-Tukey spectral analysis have been presented in Figures 4.64-4.66 which show the effect of the controlled system and different controllers on the frequency response behaviour of the fluid-tank. Examining the experimental results illustrated in Figures 4.49-4.59 and tables 4.16 and 4.17 prove the performance of the online data-driven adaptive PID-Clipping controller strategy in reducing the vibrations and show how closely the data-driven controller follows the performance of the model-based PID controllers. The experimental results of the uncontrolled and controlled fluid tank under different PGA scales of the Christchurch 2011 have been presented in Table 4.15. These results demonstrate the efficiency of the MR dampers and the controllers in reducing the seismic responses of the tank even under low levels of vibrations. However, to examine the potentials of the controlled system under sever vibrations, the main focus of examining the experimental tests was set over large PGA scales of specific ground motions which create large enough vibrations in the system to better pinpoint the performance of the dampers and the controllers. Results of tables 4.16 and 4.17 show that depending on the applied ground motion to the system and control strategy, the added MR dampers were able to reduce the uplift displacements of the tank between 29% - 86%, for which the lowest reduction percentage point is for the Passive Off technique under the Kobe $0.525g$ and the highest reduction belongs to the $PIDCLIP10$ control technique using the acceleration feedback approach for tests under the Christchurch $0.438g$.

Two major categories of semi-active controllers based on PID control strategy were employed to control the fluid-tank-MR damper system including model-based and model-free data-driven control techniques. Each of these techniques was utilised in two sub-categories of PID-Clipping and PID-Modified Clipping techniques. Subsequently, the transfer functions developed for the rigid legged tank in Chapter 3 were used to obtain the parameters of the model-based PID control techniques, hence resulting in different model-based PID-Clipping or PID-Modified Clipping approaches. These transfer functions were used for the model reference in the case of online model-free data-driven adaptive PID-Clipping or PID-Modified Clipping control techniques. Results of tests in Table 4.17

show that semi-active control strategies using standard and modified Clipping approaches result in almost the same level of performance for the controlled system design. There were found some instances for which the standard Clipping technique resulted in lower performance indices which indicates more reductions in the structural responses of the system. The developed online data-driven adaptive controllers were able to follow the same performance indices as that of the model-based controllers and even surpassed them in some cases. These controllers work only based on the online output measurements of the system in real-time which act as the input to the control system design. More importantly, they are stable and robust to inaccuracies in mathematical representations of the system. Therefore, it is expected that they are scalable and applicable to any fluid-tank with different structural characteristics and geometrical shapes. The low computational cost of the developed formulations and control techniques make them deployable on the micro-controllers for developing autonomous systems for making seismic-resilient fluid tanks.

4.5 Summary

In this chapter, the results of numerical and experimental investigations conducted in this research were presented and analysed in three separate parts. First, the experimental results of a full-scale stainless steel thin-walled circular cylindrical fluid tank which was set freely on the shake table were examined. This tank was tested under swept-sine tests of different frequency bands, time lengths, and amplitudes. Using the software platform developed, the system's natural frequencies were extracted and compared with theoretical ones. Moreover, the damping ratios of several detected modes were calculated using the power bandwidth method. There were found discrepancies between the experimentally detected and theoretical natural frequencies of the fluid-tank system. Analysis of the experimental results showed that the experimental and theoretical natural frequencies would be closer together should the aspect ratio be 2.8 and above for the three aspect ratios considered in this study. Moreover, the variations of the tank's body accelerations

from bottom to top of the tank under the applied ground motions were examined. These variations were proved to have a nonlinear trend and descended from the bottom to the mid-height of the tank body and then ascended from that point towards the fluid surface. Measurements of axial strains in the tank shell demonstrated maximum strain values around the base plate with a bilinear decreasing trend towards higher levels of the shell.

In the second part of this chapter, the results of numerical investigations over a flexible thin-walled stainless steel legged circular cylindrical fluid tank equipped with one MR damper at the base in a horizontal configuration were examined. The equations of the controlled system which were developed in section 3.3.3 and the controlled techniques described in chapter 3 were employed to investigate the efficacy of the added one damper to the tank in reducing the most important structural responses of the tank under different Near-Fault and Far-Fault earthquakes with different frequency contents. Peak responses of the uncontrolled and controlled fluid tank with the MR damper and the performance indices of the applied controllers were studied. It was shown that even a small-scale MR damper with a capacity of 2.45 kN could substantially decrease the lateral displacements and absolute accelerations of the tank shell which play a crucial role in causing damage to tanks including the elephant foot and diamond shape buckling failures. It was also shown that the frequency content of the base excitation and the aspect ratio of the tank are the two important factors affecting the percentage point to which the structural responses of the system could be mitigated by the damper.

In the last part of this chapter, the numerical and experimental investigations of a rigid legged stainless steel circular cylindrical fluid tank were presented and studied. This tank was considered freely set on the ground which undergoes rocking motions under the base excitations. This system was examined numerically based on the developed dynamic equation of motion in the section 3.3.4 using SIMULINK - MATLAB platform for different passive and semi-active controllers. In the next step, a full-scale rigid legged stainless steel fluid tank representing the same tank that was examined numerically was tested experimentally via shake table tests. First, this tank was tested for a series of swept-sine excitations to understand its dynamic performance and detect its natural frequencies. Then the tank was tested without dampers under different ground motions

to study the most important structural responses of such a tank which are the uplift displacements. A software platform was developed based on SIMULINK-MATLAB platform for the data acquisition, visualization, and real-time output saving of the signal data from the sensory system.

In the next phase, the four MR dampers were connected to the tank each damper beside one of the legs in a vertical configuration. The developed data-acquisition software was equipped with the control design techniques and this system was tested again using MR dampers. In the case of semi-active controllers, different techniques including Energy Dissipation - Clipping, model-based PID-Clipping, and online data-driven adaptive PID-Clipping controllers were applied to the system. Comparisons between the numerical and experimental results of the uncontrolled and controlled systems were made to show the accuracy of the developed equations for the legged rigid tank. Also, comparative studies in the form of figures and tables were presented to investigate the efficacy of MR dampers and the different control techniques in seismic response mitigation of such tanks. Results of studies showed that MR dampers reduced the uplift displacements of the tank under the base excitations substantially. Different applied controlled techniques caused different reduction percentage points of the uplift displacements of the tank under different ground motions. The applied online data-driven adaptive PID-Clipping controller which only works based on the online measurements of the system proved successful in reducing the uplift displacements of the tank and followed the same reduction percentage points as the model-based PID-Clipping controller and even surpassed it in some cases. A control system design that was developed to work based on the sole acceleration data making an acceleration feedback control system was tested over the fluid-tank-MR system. This controller also proved successful in reducing the uplift displacements of the tank and achieved performance indices as low as that of other semi-active controllers and even lower in some cases. The developed equations and techniques for controlling the investigated fluid-tank-MR system have a low computational cost making them possible to be deployed over the micro-controllers for developing an autonomous control system for application for such tanks to protect them against seismic vibrations.

Chapter 5

Conclusion

5.1 Introduction

This Chapter is dedicated to the summary of all the achievements obtained in this study which are described below in three separate parts.

5.2 Conclusions part I:

Experimental tests over the thin-walled flexible flat-based cylindrical stainless steel liquid tank

A thin-walled stainless steel fluid storage tank freely set over a shake table was subjected to different unidirectional base excitations. The structural responses of the fluid-tank system under swept-sine input with different frequency bands, amplitudes, and durations were examined. The fundamental natural frequencies of the fluid-tank system were extracted using time-frequency domain analysis based on Power Spectral Density (PSD) analysis and the results were compared with the simplified mathematical formulations widely used in the literature and standards for structural analysis and design of these

structures.

Examining the experimental results demonstrated that the closest match between the theoretical and experimental convective frequency could be attributed to the aspect ratio of 2.1 which resulted in a frequency of 1.85 Hz which matches the second convective mode frequency. For the theoretical impulsive mode of the coupled system, the best matches were found for the aspect ratios of 2.8 and 3.5 for the experimentally detected natural frequencies of 56.30 and 41.66 Hz, respectively. Other observed frequencies from the experimental results were 2.85 Hz for the aspect ratio of 2.1, and 73.30 Hz for the aspect ratio of 3.5. It may be concluded that for the impulsive mode of the system, the higher the aspect ratio the closer the theoretical value to the experimental results. This could be attributed to the fact that the high values of the aspect ratio cause the system to behave more like a flexural beam which corresponds to the theory used for formulating the mathematical model. The discrepancies found between the theoretical and experimentally detected natural frequencies of the coupled fluid-tank system could be attributed to the chaotic, rotational, and highly nonlinear vibrations of the fluid in the tank that violate the simplified hypotheses considered when formulating the SMM of these structures.

Damping ratios of 0.5% and 3% have been widely used in literature and seismic design codes of fluid storage tanks for the convective and impulsive modes, respectively. The half-power bandwidth analysis conducted over power amplitude graphs of signal measurements at different natural frequencies detected different damping ratios mostly in the range of 0.3%-3%. Based on the obtained experimental results for the natural frequencies of the fluid-tank system, it seems consideration of higher sloshing modes will result in more exact calculations for the analysis and design of fluid storage tanks.

The effects of the input excitation frequency content over the structural responses of the system were studied. For the swept-sine excitations which were originally used for the detection of the natural frequencies of the system, each frequency band of the input can activate certain natural frequencies of the system. The higher the range of the frequency band of the input excitation the higher the values of the PSD diagrams at the studied resonant frequencies and the stronger rays reflected in the spectrograms in

the frequency range of interest. Experimental results of the system were examined for five ground motions with different PGA levels, frequency content, and different fault mechanisms.

The acceleration amplification factor which shows how the input excitation is transferred to the system body at different heights was calculated for different scales of the Manjil 1990 earthquake at different PGA scales at different heights. Also, a comparative study in this regard under different earthquakes all at the same PGA level of $0.1G$ was conducted. Variations of this factor through the height of the tank showed a nonlinear behavior with a descending trend from the base of the tank up to the mid-height and then an ascending trend up to the fluid surface. The highest acceleration amplification factor for all earthquakes was calculated at the fluid surface. This factor again starts decreasing at heights above the fluid surface. The highest acceleration amplification factors at almost all heights of the tank were calculated for the Manjil earthquake. Frequency domain analysis of the acceleration time history of this earthquake showed it possesses the dominant frequency content over the whole frequency components compared to other studied ground motions. The maximum axial strain values occurred around the base of the tank and decreased in an almost bilinear behavior at higher levels from the base. Response time histories of strain gauge sensors around the base and the one at a higher level showed high compressive strain values with an unsymmetrical behavior around the base of the tank (70 mm from the base) and symmetrical tensile-compressive strain values at the strain gauge sensor at a height of 320 mm from the base. The absolute strain values developed in the shell under the Manjil ground motion are the highest at almost all considered levels.

Based on the analyzed experimental results, it is concluded that,

- The first fundamental convective natural frequency of the tank-water system has a high discrepancy from the theoretical one.
- For higher aspect ratios (close to 3 and higher) the calculated theoretical fundamental impulsive frequency of the tank-water system approaches the obtained experimental one, very well. This result can verify the impulsive mode frequency

of the fluid-tank system represented by Haroun and Housner (Haroun & Housner, 1981b) based on the flexural beam-like behavior of the system.

- It is regarded as more conservative to include higher modes of vibration, specifically higher convective modes, in the analysis and design of fluid-tank systems.
- Accelerations transmitted from the base to the shell non-linearly decrease from the base up to mid-hight and then increase towards higher levels. The maximum acceleration amplification factor always occurs at the fluid surface.
- Maximum axial strain values occurred around the base of the tank which showed an unsymmetrical behavior with higher values of compressive strains. Axial strain in the shell decreases towards higher levels from the base.
- Frequency content of the input excitation has a considerable effect on the structural responses of the system including accelerations and axial strains.
- Considering the damping ratios of 0.5% for the convective mass and 3% for the impulsive mass for steel fluid storage tanks may not necessarily reflect the practical damping ratios of these modes. Even though the experimental results of the current study showed damping ratios mostly in the range above, some discrepancies were found, too.

5.3 Conclusions part II:

Numerical investigations on a legged flexible cylindrical liquid tank equipped with one MR damper in a horizontal configuration

Various seismic energy-dissipating devices have been introduced in the literature for seismic retrofitting and vibration mitigation of fluid tanks. Most of these devices are passive systems which their characteristics cannot be adapted during future unknown

excitations. On the other hand, active control mechanisms rely on huge external energy resources which can throw them out of the loop and make them unreliable during severe seismic events. In this research, the application of an MR damper as a smart semi-active mechanism that combines features of both active and passive systems while removing their drawbacks has been examined. The dynamic behaviour of the coupled fluid-tank system was modeled using the simplified mechanical model which forms the basis of analysis and design for these structures in seismic design codes around the world. Further, aspect ratio as an operational condition has been regarded in simulations for examining the effectiveness of the damper on the system. The coupled fluid-tank-MR damper system has been investigated under Far-Fault and Near-Fault ground motions with different frequency contents. Three different control scenarios including H2/LQG, PID, and FOPID, and two passive approaches including the Passive-off and Passive-on were considered to examine the structural responses of the controlled structure. For the three applied semi-active control techniques and for each aspect ratio and ground motion, the deciding parameters of each controller are optimally designed using the HGS optimisation approach which has proved promising features in the literature compared to other methods. Passive control strategies show the efficiency of the damper as a passive device as this mechanism can turn into a passive mechanism in two off (no command voltage) and on (constant voltage commanded) modes. In the semi-active control scenario, the voltage is decided based on a combined control technique. Accelerations of the system which can easily be measured through accelerometers in practical applications were used for the feedback in the control design. For the nature of the damper, a secondary control technique, namely the Clipping algorithm has been used to decide the voltage to be commanded to the damper at each time step. Four performance indices which show the performance of each controller in attenuating the lateral displacements and absolute accelerations of the rigid and impulsive masses have been calculated and compared for each controller, aspect ratio, and ground motion. Based on the conducted numerical investigations the below conclusions can be reached,

- MR damper has shown to be a promising semi-active mechanism in reducing the

structural responses of legged fluid storage tanks under the base excitations. By reducing the accelerations of the impulsive and rigid mass, these dampers can mitigate the base shear and overturning moment, and hence protect these structures against damage to the legs and elephant foot buckling.

- MR damper has reduced the lateral displacements and absolute accelerations of the impulsive and rigid mass. As the frequency and stiffness of the first convective mode are much farther away from that of the rigid and impulsive mass, this damper did not show much effect on this mode in the current configuration.

- The amount of reduction percentage points of the structural responses of the fluid tank and the performance indices of the controllers depend on the aspect ratio of the tank and the frequency content of the base excitation.

- By increasing the aspect ratio of the tank from 1 to 3, substantial changes in the frequency of the first impulsive mode are observed, however, the frequency of the first convective mode is not affected considerably. Starting from the aspect ratio 2, the reduction percentage points in the structural responses tend to become closer together under all the applied ground motions with different frequency contents. Under most of the considered ground motions and control techniques, for the aspect ratio of 3 with a first impulsive frequency much closer to the dominant frequencies in the applied ground motions, reduction percentage points become the closest together.

- Considering the four performance indices defined to evaluate the applied controllers, the PID-COC-HGS and FOPID-COC-HGS contributed to the seismic response attenuation of the fluid tank the most for all aspect ratios and under all ground motions.

5.4 Conclusions part III:

Numerical and experimental investigations on a rigid legged stainless steel cylindrical tank equipped with MR dampers in the vertical mode under base excitations

Numerical and experimental investigations for the uncontrolled and controlled rigid legged stainless steel fluid tank were conducted using SIMULINK-MATLAB and the developed software platforms. First, a series of swept-sine tests with different frequency bands, durations, and amplitudes were conducted over the tank to extract its natural frequencies. The data acquisition was implemented using a software platform based on SIMULINK for real-time data acquisition, visualisation, and output saving of the results. Post-processing analyses were conducted using another developed software based on MATLAB and signal processing tools. Three main frequencies including 3.9, 10.2, and 14.2 Hz were detected for the tank. In the next phase of tests, the tank was tested under different ground motions with many different PGA scales. Preliminary analysis of results showed that specific earthquakes with certain PGA scales create enough uplift displacement for the freely set tank over the shake table. Therefore, the rest of the experiments were narrowed and focused on these ground motion tests. A comparison between the results of numerical evaluations using the developed equations for the rigid legged circular cylindrical tank under rocking motions developed in Chapter 3 with that of experimental results for different ground motions showed estimation errors in the range of 2–15%.

In the third step of tests over the legged rigid fluid tank, four MR dampers were connected to the tank in a vertical configuration, one damper beside each leg, and tests using the developed control techniques were conducted to evaluate the performance of the controlled system and the control techniques in reducing the uplift displacement of such a tank as its most important structural response under the base excitations. Another software platform was developed for simultaneous data acquisition and control of the system. In one approach, uplift displacement of the system was considered as the feedback to the control system design to achieve the control objective being

minimisation of the response of the fluid tank. Different model-based and data-driven control procedures were tested for the fluid-tank-MR system. In another approach, a technique was used based on discrete-time integration, offset and trend removing, and designing specific High Pass Filters to estimate the displacements from acceleration data in real-time. The estimated displacement was then used in the control process to achieve the control objective. Comparisons between the estimations and measurements of the displacements showed errors between 2% - 25%. Evaluation of results using the $PIDCLIP10$ control strategy using acceleration feedback obtained the least possible uplift displacement for the controlled system.

Examining different passive and semi-active controllers to the experimentally tested fluid-tank-MR damper system demonstrated that depending on the ground motion and the controller technique, responses of the system can be reduced between 29% - 86%. In the worst-case scenario that the dampers are working in a Passive Off mode, they have reduced the uplift displacements of the tank between 29% under the Kobe $0.525g$ to 57% under the Loma Prieta $0.512g$. In Passive On mode, uplift responses of the tank have been reduced between 62% - 86%. Finally, in the case of applying semi-active controllers, uplift responses of the tank have been attenuated in the range of 52% - 86%.

The MR damper and the control strategies are robust in the sense that even with the inaccuracies in the mathematical representation of the model and estimation errors, and even in the case of the damper behaving as a passive system, considerable reductions in the uplift displacement of the tank are achievable. The low computation cost of the developed techniques and approaches makes them possible to be deployed on micro-controllers to develop autonomous control systems for making seismic-resilient fluid tanks.

5.5 Highlights

This thesis has highlighted the dynamic behaviour of thin-walled fluid storage unanchored flat-based tanks as well as developing a smart vibration control technique for developing

seismic-resilient rigid legged cylindrical fluid tanks:

- According to the review conducted in this thesis, fluid tanks are the lifeline to strategic industries. Damages occurred to these structures during past earthquakes have inflicted huge economic losses and jeopardised environmental safety in different countries around the world.

- A software platform based on MATLAB was developed for post-processing of data acquisition data measurements using the sensory system in time and frequency domains using signal processing procedures.

- Dynamic performance evaluations of a full-scale thin-walled stainless steel circular cylindrical unanchored flat-based tank using shake table tests showed discrepancies between the theoretical and experimentally detected natural frequencies of the system. Results would match better for high aspect ratios of 2.8 and above. Moreover, lower damping ratios than 0.5% for the convective mode and 3% for the impulsive mode, as have been advised in the literature and design codes, were calculated for the detected natural frequencies.

- Numerical evaluations of the application of one MR damper in a horizontal configuration under a legged flexible circular cylindrical stainless steel fluid tank under different earthquakes with different frequency contents proved that these dampers could be a promising candidate for reducing the seismic effects in such tanks. Examinations showed that depending on the aspect ratio of the tank and applied ground motion, the peak absolute acceleration and relative displacements of the rigid and impulsive masses can be reduced up to 67% and 72%, respectively.

- Numerical and experimental investigations of a rigid legged circular cylindrical stainless steel fluid tank equipped with MR dampers beside legs in a vertical configuration demonstrated that these dampers can mitigate the uplift displacements of such tanks up to 86%.

- A software platform was developed for simultaneous data acquisition and control of a semi-actively controlled fluid tank in real-time.
- A series of dynamic equations of motion were developed for the rocking motion of legged rigid circular cylindrical fluid tanks. A comparison of numerical and experimental evaluations showed a maximum error percentage point up to 15%.
- Developed equations and control techniques possess a low computational cost making them possible to be deployed over micro-controllers for making autonomous control systems for seismic retrofitting applications and seismic-resilient tanks.

5.6 Future Recommendations

This thesis covered broad research topics including the dynamics of the rigid and flexible fluid tanks and vibration control of these structural systems using MR dampers, among others. A comprehensive literature review, numerical simulations, and experimental investigations were conducted to examine the dynamic behaviour of these systems and the efficacy of MR dampers in seismic vibration control of these structures. However, some recommendations are put forward herein for future research works as presented in subsections below.

5.6.1 Enhanced dynamic modelling of fluid tanks

Experimental investigations of a flat-based highly flexible unanchored fluid storage tank conducted in this research proved discrepancies between the theoretical and experimental structural characteristics of these systems. Nonlinear, rotational, and chaotic fluid surface vibrations were observed during base excitations. Moreover, the literature review showed that assumptions made for developing the dynamic equation of motion and the simplified mechanical model of tanks are far from reality. Even though highly capable commercial FE software platforms are available for advanced analysis of structures like fluid tanks that involve multi-physics dynamics, employing such analyses is computationally heavily expensive, rendering them substantially challenging for online real-time control procedures. Therefore, it is suggested that a new set of modified equations that reflect the behaviour of these structural systems in action be developed. Enhanced representation of the dynamic equation of motion, natural frequencies, and damping ratios for fluid tanks will pave the way for improved analysis and design of these structures, and vibration control designs, too. Such a representation could further be incorporated to develop seismic-resilient fluid tanks that could withstand earthquakes more efficiently.

5.6.2 Perforamnce of MR dampers for flat-based tanks

Experimental tests were conducted to study the dynamic behaviour of flexible unanchored flat-based tanks. In the literature, different energy-dissipating devices have been proposed for seismic protection of such tanks. MR dampers as smart devices have proved highly efficient in a variety of industries, civil structures and infrastructures, among others, for vibration control. The potential of these dampers for seismic protection of fluid tanks had not been investigated before. Due to limitations, conducting experimental tests for examining the performance of MR dampers for vibration mitigation of such tanks was not possible. However, these dampers demonstrated a high level of performance for reducing the uplift displacement of a legged unanchored fluid tank. Considering the features of MR dampers and their capability in mitigating vibrations of structures, it is suggested that the possibility and potential of employing them for protecting flat-based unanchored circular cylindrical fluid tanks be investigated, numerically and experimentally.

5.6.3 Performance of MR dampers in horizontal configurations

Dynamic equation of motion for a legged flexible anchored fluid tank equipped with an MR damper in a horizontal configuration was presented and numerical investigations were conducted to evaluate the efficacy of these dampers for vibration control of such systems. It is recommended that a series of experimental investigations be conducted to further verify and prove the application of MR dampers and their potential in reducing the lateral displacements and absolute accelerations of flexible legged circular cylindrical fluid tanks in such a configuration.

5.6.4 Developing autonomous control systems

In this study, extensive numerical and experimental investigations were conducted to examine the efficiency of MR dampers for seismic vibration control of fluid tanks. However, in a practical application, connecting the dampers and accelerometers to a data acquisition system and usage of a computer in the field is not feasible and efficient.

Thus, it is recommended that using the developed equations and control techniques in this research, an autonomous control system based on micro-controllers be developed, constructed, and tested experimentally, to evaluate the efficacy of these techniques for embedded data acquisition, monitoring, and control systems for fluid tanks.

References

Abdeddaim, M., Djerouni, S., Ounis, A., Athamnia, B. & Farsangi, E. N. (2022). Optimal design of magnetorheological damper for seismic response reduction of base-isolated structures considering soil-structure interaction. In *Structures* (Vol. 38, pp. 733–752).

Abir, J., Longo, S., Morantz, P. & Shore, P. (2016). Optimized estimator for real-time dynamic displacement measurement using accelerometers. *Mechatronics*, *39*, 1–11.

Aboel-Hassan, A., Arafa, M. & Nassef, A. (2009). Design and optimization of input shapers for liquid slosh suppression. *Journal of Sound and Vibration*, *320*(1-2), 1-15. doi: 10.1016/J.JSV.2008.07.015

Acarman, T. & Ozguner, U. (2003). Rollover prevention for heavy trucks using frequency shaped sliding mode control. In (Vol. 1, p. 7-12). IEEE.

ACI. (2009). Seismic design of liquid-containing concrete structures (ACI 350.3-06) and commentary (ACI 350.3r-06).

Adler, J. M., Lee, M. S. & Saugen, J. D. (1991). Adaptive control of propellant slosh for launch vehicles. *Sensors and sensor integration*, *1480*, 11-22.

Ahamed, R., Choi, S.-B. & Ferdaus, M. M. (2018). A state of art on magneto-rheological materials and their potential applications. *Journal of Intelligent material Systems and structures*, *29*(10), 2051–2095.

Ahari, M. N., Eshghi, S. & Ashtiany, M. G. (2009). The tapered beam model for bottom plate uplift analysis of unanchored cylindrical steel storage tanks. *Engineering Structures*, *31*(3), 623–632.

Al-Bargothi, S. N., Qaryouti, G. M. & Jaber, Q. M. (2019). Speed control of dc motor using conventional and adaptive pid controllers. *Indonesian Journal of Electrical Engineering and Computer Science*, *16*(3), 1221–1228.

Almahmoud, S., Shiryayev, O., Vahdati, N. & Rostron, P. (2018). Detection of internal metal loss in steel pipes and storage tanks via magnetic-based fiber optic sensor. *Sensors*, *18*(3), 815. doi: 10.3390/s18030815

Almazán, J. L., Cerda, F. A., Juan, C. & López-García, D. (2007). Linear isolation of stainless steel legged thin-walled tanks. *Engineering structures*, *29*(7), 1596-1611.

Alsalah, A., Holloway, D. & Ghazijahani, T. G. (2017). Recovery of capacity lost due to

openings in cylindrical shells under compression. *Journal of Constructional Steel Research*, *137*, 169–179.

Amabili, M. (1997). Ritz method and substructuring in the study of vibration with strong fluid-structure interaction. *Journal of Fluids and Structures*, *11*(5), 507-523. doi: 10.1006/jfls.1997.0089

Amabili, M. (1998). Rayleigh quotient, Ritz method and substructuring to study vibrations of structures coupled to heavy fluids: Potential of the artificial spring method. *Flow, Turbulence and Combustion*, *61*(1), 21-30. doi: 10.1023/a:1026432717204

Ancheta, T. D., Darragh, R. B., Stewart, J. P., Seyhan, E., Silva, W. J., Chiou, B. S.-J., ... others (2014). Nga-west2 database. *Earthquake Spectra*, *30*(3), 989–1005.

Aoki, D., Bando, Y., Watanabe, N. & Suzuki, M. (2019). Development of seismic device for stainless steel rectangular water tank at short period earthquake. *Ce/Papers*, *3*(3-4), 475-480. doi: 10.1002/cepa.1086

API. (2005). Standard API 650: Welded steel tanks for oil storage. *American Petroleum Institute, Addendum 4*.

Aquelet, N., Souli, M., Gabrys, J. & Olovson, L. (2003). A new ale formulation for sloshing analysis. *Structural Engineering and Mechanics*, *16*(4), 423–440.

Asadi, Y., Farsangi, M. M., Bijami, E., Amani, A. M. & Lee, K. Y. (2021). Data-driven adaptive control of wide-area non-linear systems with input and output saturation: A power system application. *International Journal of Electrical Power & Energy Systems*, *133*, 107225.

ASCE. (2017). Seismic analysis of safety-related nuclear structures. *American Society of Civil Engineers*.

Askari, E., Daneshmand, F. & Amabili, M. (2011). Coupled vibrations of a partially fluid-filled cylindrical container with an internal body including the effect of free surface waves coupled vibrations of a partially fluid-filled cylindrical container with an internal body including the effect of free s. (April 2020). doi: 10.1016/j.jfluidstructs.2011.04.010

AWWA. (2011). Welded carbon steel tanks for water storage (AWWA d100-11).

Baek, E. R., Choi, H. S., Park, D. U., Kim, N. S. & Kim, J. M. (2017). Shake table test db of the liquid storage tank for fluid sloshing analysis. *Transactions of the Korean Society for Noise and Vibration Engineering, KSNVE*, *27*(5), 545-554.

Bakalis, K., Fragiadakis, M. & Vamvatsikos, D. (2017). Surrogate modeling for the seismic performance assessment of liquid storage tanks. *Journal of Structural Engineering*, *143*(4), 4016199-4016199.

Baltieri, M. & Buckley, C. L. (2020). On kalman-bucy filters, linear quadratic control and active inference. *arXiv preprint arXiv:2005.06269*.

Bandyopadhyay, B., Gandhi, P. S. & Kurode, S. (2009). Sliding mode observer based sliding mode controller for slosh-free motion through pid scheme. *IEEE Transactions on Industrial Electronics*, *56*(9), 3432-3442.

Bielak, J. (1978). Dynamic response of non-linear building-foundation systems. *Earthquake Engineering and Structural Dynamics*, *6*(1), 17-30.

Boashash, B. (2016). Time-frequency signal analysis and processing: a comprehensive reference.

Brandão, F. D. S. & Miguel, L. F. F. (2023). A new methodology for optimal design of hybrid vibration control systems (mr+ tmd) for buildings under seismic excitation. *Shock and Vibration*, *2023*(1), 8159716.

Brunesi, E. & Nascimbene, R. (2018). Effects of structural openings on the buckling strength of cylindrical shells. *Advances in Structural Engineering*, *21*(16), 2466–2482.

Brunesi, E., Nascimbene, R., Pagani, M. & Beilic, D. (2015). Seismic performance of storage steel tanks during the may 2012 emilia, italy, earthquakes. *Journal of Performance of Constructed Facilities*, *29*(5), 04014137.

Brunton, S. L. & Noack, B. R. (2015). Closed-loop turbulence control: Progress and challenges. *Applied Mechanics Reviews*, *67*(5), 050801.

Bu, X., Wang, Q., Hou, Z. & Qian, W. (2018). Data driven control for a class of nonlinear systems with output saturation. *ISA transactions*, *81*, 1–7.

Butterworth, J. (2000). Ductile concentrically braced frames using slotted bolted joints. *J Struct Eng Society of New Zealand*, *13*(1), 39-48.

Casapulla, C., Giresini, L. & Lourenço, P. B. (2017). Rocking and kinematic approaches for rigid block analysis of masonry walls: State of the art and recent developments. *Buildings*, *7*(3), 69.

Casiano, M. (2016). *Extracting damping ratio from dynamic data and numerical solutions* (Tech. Rep.).

Chatterjee, P. & Basu, B. (2004). Wavelet-based non-stationary seismic rocking response of flexibly supported tanks. *Wiley Online Library*, *33*(2), 157-181. doi: 10.1002/eqe.340

Chatterjee, P. & Basu, B. (2006). Nonstationary seismic response of a tank on a bilinear hysteretic soil using wavelet transform. *Probabilistic engineering mechanics*, *21*(1), 54-63.

Chen, P.-C., Tsai, K.-C. & Lin, P.-Y. (2014). Real-time hybrid testing of a smart base isolation system. *Earthquake engineering & structural dynamics*, *43*(1), 139–158.

Chen, S. J., Hein, B. & Worn, H. (2007). Using acceleration compensation to reduce liquid surface oscillation during a high speed transfer. In (p. 2951-2956). IEEE. Retrieved from `https://ieeexplore.ieee.org/abstract/document/4209538/`

Chen, W., Haroun, M. A. & Liu, F. (1996). Large amplitude liquid sloshing in seismically excited tanks. *Earthquake engineering and structural dynamics*, *25*(7), 653-669.

Chen, X. & Li, C. (2020). Seismic performance of tall pier bridges retrofitted with lead rubber bearings and rocking foundation. *Engineering structures*, *212*, 110529.

Cheng, X., Jing, W. & Gong, L. (2017). Simplified model and energy dissipation characteristics of a rectangular liquid-storage structure controlled with sliding base isolation and displacement-limiting devices. *Journal of Performance of Constructed Facilities*, *31*(5), 04017071-04017071. doi: 10.1061/(asce)cf.1943 -5509.0001066

Chiba, M. (1993). Experimental studies on a nonlinear hydroelastic vibration of a clamped cylindrical tank partially filled with liquid.

Chopra, A. K. (2001). *Dynamics of structures: Theory and applications to earthquake engineering* (Second Eidtion ed.). Prentice Hall.

Colombo, J. & Almazán, J. (2017). Experimental investigation on the seismic isolation for a legged wine storage tank. *Journal of Constructional Steel Research*, *133*, 167-180.

Colombo, J. & Almazán, J. (2019). Simplified 3d model for the uplift analysis of liquid storage tanks. *Engineering Structures*, *196*, 109278.

Colombo, J., Wilches, J. & Leon, R. (2022). Seismic fragility of legged liquid storage tanks based on soil type classifications. *Journal of Constructional Steel Research*, *192*, 107212.

Colombo, J. I. & Almazán, J. L. (2015). Seismic reliability of continuously supported steel wine storage tanks retrofitted with energy dissipation devices. *Engineering Structures*, *98*, 201-211. doi: 10.1016/j.engstruct.2015.04.037

Compagnoni, M. E. & Curadelli, O. (2018). Experimental and numerical study of the response of cylindrical steel tanks under seismic excitation. *International Journal of Civil Engineering*, *16*(7), 793-805. doi: 10.1007/s40999-017-0218-3

Cortes, G., Nussbaumer, A., Berger, C. & Lattion, E. (2011). Experimental determination of the rotational capacity of wall-to-base connections in storage tanks. *Journal of Constructional Steel Research*, *67*(7), 1174–1184.

Cortes, G. & Prinz, G. S. (2017). Seismic fragility analysis of large unanchored steel tanks considering local instability and fatigue damage. *Bulletin of Earthquake Engineering*, *15*(3), 1279-1295. doi: 10.1007/S10518-016-9984-6

Council, B. S. S. (1997). NEHRP commentary on the guidelines for the seismic rehabilitation of buildings (FEMA publication 274). *ATC-33 Project, Washington, DC*.

Cruz, A. M. & Krausmann, E. (2013). Vulnerability of the oil and gas sector to climate change and extreme weather events. *Climatic change*, *121*(1), 41–53.

Cruz, E. F. & Valdivia, D. (2011). Performance of industrial facilities in the chilean earthquake of 27 february 2010. *The Structural Design of Tall and Special Buildings*, *20*(1), 83-101. doi: 10.1002/tal.679

Curadelli, O. (2013). Equivalent linear stochastic seismic analysis of cylindrical base-isolated liquid storage tanks. *Journal of constructional steel research*, *83*, 166-176.

Curadelli, O. & Ambrosini, D. (2011). Damage detection in elevated spherical containers

partially filled with liquid. *Engineering Structures*, *33*(9), 2708-2715.

Daful, A. G. (2018). Comparative study of pid tuning methods for processes with large & small delay times. In *2018 advances in science and engineering technology international conferences (aset)* (pp. 1–7).

De Angelis, M., Giannini, R. & Paolacci, F. (2010). Experimental investigation on the seismic response of a steel liquid storage tank equipped with floating roof by shaking table tests. *Earthquake Engineering and Structural Dynamics*, *39*(4), 377-396.

Decuyper, J., De Troyer, T., Tiels, K., Schoukens, J. & Runacres, M. C. (2020). A nonlinear model of vortex-induced forces on an oscillating cylinder in a fluid flow. *Journal of Fluids and Structures*, *96*, 103029.

Demirol, E. & Ayoub, A. S. (2017). Inelastic displacement ratios of ssi systems. *Soil Dynamics and Earthquake Engineering*, *96*, 104-114.

Demirol, E., Fragkos, A., Arulanantham, S. & Ayoub, A. (2018). Inelastic displacement ratios of ssi systems under repeated earthquakes. In *Structures congress 2018: Buildings and disaster management* (p. 379-387). American Society of Civil Engineers Reston, VA.

Dizhur, D., Simkin, G., Giaretton, M., Loporcaro, G., Palermo, A. & Ingham, J. (2017). Performance of winery facilities during the 14 november 2016 kaikōura earthquake. *Bulletin of the New Zealand Society for Earthquake Engineering*, *50*(2), 206-224. doi: 10.5459/bnzsee.50.2.206-224

Dominguez, A., Sedaghati, R. & Stiharu, I. (2008). Modeling and application of mr dampers in semi-adaptive structures. *Computers & structures*, *86*(3-5), 407–415.

Dubey, V., Goud, H. & Sharma, P. C. (2022). Role of pid control techniques in process control system: a review. *Data Engineering for Smart Systems: Proceedings of SSIC 2021*, 659–670.

Dyke, S. J., Spencer Jr, B., Sain, M. & Carlson, J. (1996). Modeling and control of magnetorheological dampers for seismic response reduction. *Smart materials and structures*, *5*(5), 565.

Ebrahimian, M., Noorian, M. A. & Haddadpour, H. (2014). Equivalent mechanical model of liquid sloshing in multi-baffled containers. *Engineering Analysis with Boundary Elements*, *47*, 82-95.

el Mezaini, N. (2006). Effects of soil-structure interaction on the analysis of cylindrical tanks. *Practice periodical on structural design and construction*, *11*(1), 50-57.

EN, B. (2004). 14015-2004, specification for the design and manufacture of site built, vertical, cylindrical, flat-bottomed, above ground, welded, steel tanks for the storage of liquids at ambient temperature and above. *British standard*, *14015*.

EN, B. (2006). *Eurocode 8: Design of structures for earthquake resistance- part 4: Silos, tanks and pipelines.* European Committee for Standardization Brussels, Belgium.

Erkmen, B. (2017). Evaluation of code provisions for seismic performance of unanchored

liquid storage tanks. In *Proceedings of the 6th eccomas thematic conference on computational methods in structural dynamics and earthquake engineering (compdyn 2017), rhodes island.*

Estekanchi, H. E. & Alembagheri, M. (2012). Seismic analysis of steel liquid storage tanks by endurance time method. *Elsevier*, *50*(1), 14-23.

Fahmy, R. A., Badr, R. I. & Rahman, F. A. (2014). Adaptive pid controller using rls for siso stable and unstable systems. *Advances in Power Electronics*, *2014*(1), 507142.

Fahmy, R. A., Badr, R. I. & Rahman, F. A. (2018). Alternative approach to use rls algorithm in multivariable online adaptive pid controllers for mimo systems. *IETE Journal of Research*, *64*(1), 27–35.

Falcone, R., Lima, C. & Martinelli, E. (2020). Soft computing techniques in structural and earthquake engineering: a literature review. *Engineering Structures*, *207*, 110269.

Fallah, A. Y. & Taghikhany, T. (2013). Time-delayed decentralized h2/lqg controller for cable-stayed bridge under seismic loading. *Structural Control and Health Monitoring*, *20*(3), 354–372.

Fan, M., Wu, G., Cao, B., Sarkodie-Gyan, T., Li, Z. & Tian, G. (2019). Uncertainty metric in model-based eddy current inversion using the adaptive monte carlo method. *Measurement*, *137*, 323–331.

Fang, Z., Chen, Z., Yan, S., Cao, G. & Wang, J. (2013). Dynamic experimental investigation on the uplift response of liquid storage tanks under seismic excitations with different characteristics. *Proceedings of the Institution of Mechanical Engineers, Part C: Journal of Mechanical Engineering Science*, *227*(7), 1525–1534.

Farajian, M., Khodakarami, M. & Kontoni, D.-P. (2017). Evaluation of soil-structure interaction on the seismic response of liquid storage tanks under earthquake ground motions. *Computation*, *5*(4), 17. doi: 10.3390/computation5010017

Feddema, J. T., Dohrmann, C. R., Parker, G. G., Robinett, R. D., Romero, V. J. & Schmitt, D. J. (1997). Control for slosh-free motion of an open container. *IEEE Control Systems Magazine*, *7*(1), 29-36.

Fischer, E. C., Liu, J. & Varma, A. H. (2016). Investigation of cylindrical steel tank damage at wineries during earthquakes : Lessons learned and mitigation opportunities. *Practice Periodical on Structural Design and Construction*, *21*(3), 04016004-04016004. doi: 10.1061/(ASCE)SC.1943-5576.0000283

Flah, M., Nunez, I., Ben Chaabene, W. & Nehdi, M. L. (2021). Machine learning algorithms in civil structural health monitoring: a systematic review. *Archives of computational methods in engineering*, *28*(4), 2621–2643.

Frandsen, J. B. (2004). *Sloshing motions in excited tanks* (Vol. 196) [Book]. doi: 10.1016/j.jcp.2003.10.031

Gabbianelli, G., Perrone, D., Brunesi, E. & Monteiro, R. (2022). Seismic acceleration

demand and fragility assessment of storage tanks installed in industrial steel moment-resisting frame structures. *Soil Dynamics and Earthquake Engineering*, *152*, 107016.

Gates, W. (1980). Elevated and ground-supported steel storage tanks. reconnaissance report, imperial county, california earthquake of october 15, 1979. *Earthquake Engineering Research Institute, Oakland*.

Gazetas, G. (1983). Analysis of machine foundation vibrations: state of the art. *International Journal of soil dynamics and earthquake engineering*, *2*(1), 2-42.

Gazetas, G. & Tassios, T. P. (1978). Elastic-plastic slabs on elastic foundation. *Journal of the Structural Division*, *104*(4), 621-636.

Ghaemmaghami, A. R. & Kianoush, M. R. (2010). Effect of wall flexibility on dynamic response of concrete rectangular liquid storage tanks under horizontal and vertical ground motions. *Journal of structural engineering*, *136*(4), 441-451. doi: 10.1061/ASCEST.1943-541X.0000123

Ghamari, S. M., Mollaee, H. & Khavari, F. (2021). Robust self-tuning regressive adaptive controller design for a dc–dc buck converter. *Measurement*, *174*, 109071.

Ghannad, M. & Jahankhah, H. (2007). Site-dependent strength reduction factors for soil-structure systems. *Soil Dynamics and Earthquake Engineering*, *27*(2), 99-110.

Ghazijahani, T. G., Jiao, H. & Holloway, D. (2015). Fatigue experiments on circular hollow sections with cfrp reinforced cutouts. *Journal of Constructional Steel Research*, *106*, 322–328.

Glickman, S., Kulessky, R. & Nudelman, G. (2004). Identification-based pid control tuning for power station processes. *IEEE transactions on control systems technology*, *12*(1), 123–132.

Glisic, B. & Inaudi, D. (2004). Health monitoring of full composite cng tanks using long-gauge fiber optic sensors. In (Vol. 5384, p. 44-53). doi: 10.1117/12.544943

Godderidge, B., Tan, M., Earl, C. & Turnock, S. (2007). Grid resolution for the simulation of sloshing using cfd.. Retrieved from `https://eprints.soton.ac.uk/48789/1/nuttspaper_bg.pdf`

González, E., Almazán, J., Beltrán, J., Herrera, R. & Sandoval, V. (2013). Performance of stainless steel winery tanks during the 02/27/2010 maule earthquake. *Engineering Structures*, *56*, 1402-1418.

Goodwin, G. C. & Sin, K. S. (2014). *Adaptive filtering prediction and control*. Courier Corporation.

Goudarzi, M. A. & Danesh, P. N. (2016). Numerical investigation of a vertically baffled rectangular tank under seismic excitation. *Journal of Fluids and Structures*, *61*, 450-460. doi: 10.1016/J.JFLUIDSTRUCTS.2016.01.001

Goudarzi, M. A. & Sabagh, Y. S. R. (2009). Numerical investigation on accuracy of mass spring models for cylindrical tanks under seismic excitation. *International Journal of Civil Engineering*.

Goudarzi, M. A. & Sabbagh-Yazdi, S. R. (2012). Investigation of nonlinear sloshing effects in seismically excited tanks. *Soil Dynamics and Earthquake Engineering*, *43*, 355–365.

Govindharaj, A. & Mariappan, A. (2020). Real-time implementation of chebyshev neural adaptive controller for boost converter. *International Transactions on Electrical Energy Systems*, *30*(6), e12394.

Gradinscak, M., Semercigil, S. & Turan, Ö. (2011). A sloshing absorber with a flexible container [Book Section]. In (p. 315-322). Springer.

Graham, E. W. & Rodriguez, A. M. (1952). The characteristics of fuel motion which affect airplane dynamics.

Habenberger, J. (2015). Fluid damping of cylindrical liquid storage tanks. *SpringerPlus*, *4*(1). doi: 10.1186/s40064-015-1302-2

Halabian, A. M. & El Naggar, M. H. (2002). Effect of non-linear soil–structure interaction on seismic response of tall slender structures. *Soil Dynamics and Earthquake Engineering*, *22*(8), 639-658.

Hall, J. F., Holmes, W. T. & Somers, P. (1995). *Northridge earthquake of january 17, 1994: reconnaissance report* (Vol. 11) [Book]. Earthquake Engineering Research Institute.

Hallquist, J. O. et al. (2007). Ls-dyna keyword user's manual. *Livermore Software Technology Corporation*, *970*, 299–800.

Hanson, R. D. (1973). Behavior of liquid-storage tanks, the great alaska earthquake of 1964. *Proceedings of the National Academy of Science, Washington*, *7*, 331-339.

Hara, F. (1994). Refined active control of sloshing by intermittent air-bubble injection. *JSME international journal. Ser. C, Dynamics, control, robotics, design and manufacturing*, *37*(3), 595-600.

Harirchian, E., Hosseini, S. E. A., Jadhav, K., Kumari, V., Rasulzade, S., Işık, E., ... Lahmer, T. (2021). A review on application of soft computing techniques for the rapid visual safety evaluation and damage classification of existing buildings. *Journal of Building Engineering*, *43*, 102536.

Haroun, M. A. (1980). Dynamic analyses of liquid storage tanks.

Haroun, M. A. (1983). Vibration studies and tests of liquid storage tanks. *Earthquake Engineering and Structural Dynamics*, *11*(2), 179-206.

Haroun, M. A. & Abou-Izzeddine, W. (1992a). Parametric study of seismic soil-tank interaction. i: Horizontal excitation. *Journal of structural Engineering*, *118*(3), 783-797.

Haroun, M. A. & Abou-Izzeddine, W. (1992b). Parametric study of seismic soil-tank interaction. ii: Vertical excitation. *Journal of Structural Engineering*, *118*(3), 798-811.

Haroun, M. A. & Ellaithy, H. M. (1985a). Model for flexible tanks undergoing rocking. *Journal of engineering mechanics*, *111*(2), 143-157.

Haroun, M. A. & Ellaithy, H. M. (1985b). Model for flexible tanks undergoing rocking. *Journal of engineering mechanics*, *111*(2), 143–157.

Haroun, M. A. & Housner, G. W. (1981a). Earthquake response of deformable liquid storage tanks. Retrieved from https://asmedigitalcollection.asme.org/appliedmechanics/article-abstract/48/2/411/423034

Haroun, M. A. & Housner, G. W. (1981b). Seismic design of liquid storage tanks. *Journal of the Technical Councils of ASCE*, *107*(1), 191-207.

Haroun, M. A. & Housner, G. W. (1982a). Complications in free vibration analysis of tanks. *Journal of the Engineering Mechanics Division*, *108*(5), 801-818.

Haroun, M. A. & Housner, G. W. (1982b). Dynamic characteristics of liquid storage tanks. *Journal of the Engineering Mechanics Division*, *108*(5), 783-800.

Haroun, M. A. & Tayel, M. A. (1985). Response of tanks to vertical seismic excitations. *Earthquake engineering and structural dynamics*, *13*(5), 583-595.

Hashemi, S., Saadatpour, M. & Kianoush, M. (2013). Dynamic behavior of flexible rectangular fluid containers. *Thin-Walled Structures*, *66*, 23–38.

Hasheminejad, S. M. & Mohammadi, M. M. (2016). Active sloshing control in a smart flexible cylindrical floating roof tank. *Journal of Fluids and Structures*, *66*, 350-381. doi: 10.1016/j.jfluidstructs.2016.07.022

Hasheminejad, S. M., Mohammadi, M. M. & Jamalpoor, A. (2020). Hydroelastic modeling and active control of transient sloshing in a three dimensional rectangular floating roof tank. *Journal of Sound and Vibration*, *470*, 115146-115146. doi: 10.1016/j.jsv.2019.115146

Hasheminejad, S. M., Mohammadi, M. M. & Jarrahi, M. (2014). Liquid sloshing in partly-filled laterally-excited circular tanks equipped with baffles. *Journal of Fluids and Structures*, *44*, 97-114.

Hassani, N., Bararnia, M. & Amiri, G. G. (2018). Effect of soil-structure interaction on inelastic displacement ratios of degrading structures. *Soil Dynamics and Earthquake Engineering*, *104*, 75-87.

Hatayama, K. (2008). Lessons from the 2003 tokachi-oki, japan, earthquake for prediction of long-period strong ground motions and sloshing damage to oil storage tanks. *Journal of seismology*, *12*(2), 255–263.

Heidari, A. A., Mirjalili, S., Faris, H., Aljarah, I., Mafarja, M. & Chen, H. (2019). Harris hawks optimization: Algorithm and applications. *Future generation computer systems*, *97*, 849–872.

Hernandez-Hernandez, D., Larkin, T. & Chouw, N. (2021a). Evaluation of the adequacy of a spring-mass model in analyses of liquid sloshing in anchored storage tanks. *Earthquake Engineering & Structural Dynamics*, *50*(14), 3916–3935.

Hernandez-Hernandez, D., Larkin, T. & Chouw, N. (2021b). Shake table investigation of nonlinear soil–structure–fluid interaction of a thin-walled storage tank under

earthquake load. *Thin-Walled Structures*, *167*, 108143.

Hernandez-Hernandez, D., Larkin, T. & Chouw, N. (2022). Lid induced sloshing suppression and evaluation of wall stresses in a liquid storage tank including seismic soil-structure interaction. *Earthquake Engineering & Structural Dynamics*, *51*(11), 2708–2729.

Hernandez-Hernandez, D., Larkin, T., Chouw, N. & Banide, Y. (2020a). Experimental findings of the suppression of rotary sloshing on the dynamic response of a liquid storage tank. *Journal of Fluids and Structures*, *96*, 103007.

Hernandez-Hernandez, D., Larkin, T., Chouw, N. & Banide, Y. (2020b). Experimental findings of the suppression of rotary sloshing on the dynamic response of a liquid storage tank. *Journal of Fluids and Structures*, *96*, 103007.

Hernández, E. & Santamarina, D. (2012). Active control of sloshing in containers with elastic baffle plates. *International journal for numerical methods in engineering*, *91*(6), 604-621. doi: 10.1002/nme.4283

Hilburger, M. W. & Starnes Jr, J. H. (2005). Buckling behavior of compression-loaded composite cylindrical shells with reinforced cutouts. *International Journal of Non-Linear Mechanics*, *40*(7), 1005–1021.

Hogan, S. (1992). The effect of damping on rigid block motion under harmonic forcing. *Proceedings of the Royal Society of London. Series A: Mathematical and Physical Sciences*, *437*(1899), 97–108.

Hoskins, L. M. & Jacobsen, L. S. (1934). Water pressure in a tank caused by a simulated earthquake. *Bulletin of the seismological society of America*, *24*(1), 1-32.

Hosseini, S. E. A. & Beskhyroun, S. (2023). Fluid storage tanks: A review on dynamic behaviour modelling, seismic energy-dissipating devices, structural control, and structural health monitoring techniques. In *Structures* (Vol. 49, pp. 537–556).

Hou, Z.-S. & Wang, Z. (2013). From model-based control to data-driven control: Survey, classification and perspective. *Information Sciences*, *235*, 3–35.

Housner, G. W. (1954). Earthquake pressures on fluid containers. *In: 8th technical report under office of naval research*.

Housner, G. W. (1957a). Dynamic pressures on accelerated fluid containers. *Bulletin of the seismological society of America*, *47*(1), 15–35.

Housner, G. W. (1957b). Dynamic pressures on accelerated fluid containers. *Bulletin of the seismological society of America*, *47*(1), 15-35.

Housner, G. W. (1963a). The behavior of inverted pendulum structures during earthquakes. *Bulletin of the seismological society of America*, *53*(2), 403–417.

Housner, G. W. (1963b). The dynamic behavior of water tanks. *Bulletin of the seismological society of America*, *53*(2), 381-387.

Ibrahim, R. A. (2005). *Liquid sloshing dynamics: theory and applications* [Book]. Cambridge University Press.

Iemura, H., Igarashi, A. & Kalantari, A. (2004). Enhancing dynamic performance of

liquid storage tanks by semi-active controlled dampers. In *13th world conference on earthquake engineering, vancouver, bc, canada.*

IITK-GSDMA. (2007). Guidelines for seismic design of liquid storage tanks—provisions with commentary and explanatory examples. *Indian Institute of Technology Kanpur, Kanpur, India*.

Ikeda, T. & Ibrahim, R. A. (2014). Passive vibration control of structures subjected to random ground excitation utilizing sloshing in rectangular tanks. *Journal of Pressure Vessel Technology*, *136*(1). doi: 10.1115/1.4025083

Inc, A. (2016). *Ansys cfx-17 user's guide* [Book].

Ishida, K. & Kobayashi, N. (1988). An effective method of analyzing rocking motion for unanchored cylindrical tanks including uplift.

Jacobsen, L. S. (1949). Impulsive hydrodynamics of fluid inside a cylindrical tank and of fluid surrounding a cylindrical pier. *Bulletin of the Seismological Society of America*, *39*(3), 189-204.

Jain, S. K., LETTIS, W. R., MURTY, C. R. & Bardet, J.-P. (2002). Bhuj, india earthquake of january 26, 2001, reconnaissance report. *Earthquake Spectra*, *18*.

Jansen, L. M. & Dyke, S. J. (2000). Semiactive control strategies for mr dampers: comparative study. *Journal of engineering mechanics*, *126*(8), 795–803.

Japan, A. (2010). Design recommendation for storage tanks and their supports with emphasis on seismic design. *AIJ: Architectural Institute of Japan. AIJ, Japan*.

Jennings, P. C. & Bielak, J. (1973). Dynamics of building-soil interaction. *Bulletin of the Seismological Society of America*, *63*(1), 9-48. doi: 10.1785/bssa0630010009

Ji, M., Lyu, Y., Pan, Q., Wei, G. & Wei, D. (2022). Adaptive control of uncertain systems with input delay based on active inference. In *International conference on autonomous unmanned systems* (pp. 2810–2822).

Joseph, S. B., Dada, E. G., Abidemi, A., Oyewola, D. O. & Khammas, B. M. (2022). Metaheuristic algorithms for pid controller parameters tuning: Review, approaches and open problems. *Heliyon*, *8*(5).

Kalantari, A. (2017). Seismic response reduction in liquid storage tanks by simple smart base isolation systems. *Iranian Journal of Science and Technology - Transactions of Civil Engineering*, *41*(2), 121-133. doi: 10.1007/s40996-017-0048-1

Kalogerakou, M. E., Maniatakis, C. A., Spyrakos, C. C. & Psarropoulos, P. N. (2017). Seismic response of liquid-containing tanks with emphasis on the hydrodynamic response and near-fault phenomena. *Engineering Structures*, *153*, 383–403.

Kamalzare, M., Johnson, E. A. & Wojtkiewicz, S. F. (2015). Computationally efficient design of optimal strategies for controllable damping devices. *Structural Control and Health Monitoring*, *22*(1), 1–18.

Kamarroudi, S. H., Hosseini, M. & Hosseini, K. (2021a). Influence of earthquake vertical excitations on sloshing-created p-δ effect in elevated water tanks: Experimental validation, numerical simulation and proposing a modification for housner model.

Engineering Structures, *246*, 112995.

Kamarroudi, S. H., Hosseini, M. & Hosseini, K. (2021b). Influence of earthquake vertical excitations on sloshing-created p- effect in elevated water tanks: Experimental validation, numerical simulation and proposing a modification for housner model. *Engineering Structures*, *246*, 112995.

Kana, D. D. (1979). Seismic response of flexible cylindrical liquid storage tanks. *Nuclear Engineering and Design*, *52*(1), 185-199. doi: 10.1016/0029-5493(79)90020-7

Kang, T.-W., Yang, H.-I. & Jeon, J.-S. (2019). Earthquake-induced sloshing effects on the hydrodynamic pressure response of rigid cylindrical liquid storage tanks using cfd simulation. *Engineering Structures*, *197*, 109376-109376.

Kataria, N. P. & Jangid, R. (2016). Seismic protection of the horizontally curved bridge with semi-active variable stiffness damper and isolation system. *Advances in Structural Engineering*, *19*(7), 1103–1117.

Katoch, S., Chauhan, S. S. & Kumar, V. (2021). A review on genetic algorithm: past, present, and future. *Multimedia tools and applications*, *80*, 8091–8126.

Kazemiyan, M. et al. (2019). A formula for calculating fundamental natural frequency of partially-filled tanks. *Ocean Engineering*, *191*, 106400.

Khayat, M., Baghlani, A. & Dehghan, S. M. (2022). A hybrid algorithm for studying the effects of various uncertainties on the nonlinear dynamic responses of steel storage tanks subjected to seismic base excitation. In *Structures* (Vol. 45, pp. 598–628).

Khoshnoudian, F. & Ahmadi, E. (2015). Effects of inertial soil–structure interaction on inelastic displacement ratios of sdof oscillators subjected to pulse-like ground motions. *Bulletin of Earthquake Engineering*, *13*(6), 1809-1833. doi: 10.1007/s10518-014-9693-y

Khoshnoudian, F., Ahmadi, E. & Nik, F. A. (2013). Inelastic displacement ratios for soil-structure systems. *Engineering Structures*, *57*, 453-464.

Kianoush, M. R. & Chen, J. Z. (2006). Effect of vertical acceleration on response of concrete rectangular liquid storage tanks. *Engineering structures*, *28*(5), 704-715.

Kim, J. K., Koh, H. M. & Kwahk, I. J. (1996). Dynamic response of rectangular flexible fluid containers. *Journal of Engineering Mechanics*, *122*(9), 807-817.

Kim, Y. W. & Lee, Y. S. (2005). Coupled vibration analysis of liquid-filled rigid cylindrical storage tank with an annular plate cover. *Journal of Sound and Vibration*, *279*(1-2), 217-235. doi: 10.1016/j.jsv.2003.10.032

Kirtas, E., Rovithis, E. & Makra, K. (2020). On the modal response of an instrumented steel water-storage tank including soil-structure interaction. *Soil Dynamics and Earthquake Engineering*, *135*, 106198.

Kobayashi, N. & Koyama, Y. (2010). Semi-active sloshing suppression control of liquid in vessel with bulkhead. *Journal of pressure vessel technology*, *132*(5). doi: 10.1115/1.4001194

Konar, T. & Ghosh, A. (2021). Development of a novel tuned liquid damper with floating

base for converting deep tanks into effective vibration control devices. *Advances in Structural Engineering*, *24*(2), 401-407. doi: 10.1177/1369433220953539

Krausmann, E. & Cruz, A. (2017). Chapter 2 - past natech events. In E. Krausmann, A. M. Cruz & E. Salzano (Eds.), *Natech risk assessment and management* (p. 3-31). Elsevier. doi: https://doi.org/10.1016/B978-0-12-803807-9.00002-4

Krausmann, E., Cruz, A. M. & Affeltranger, B. (2010). The impact of the 12 may 2008 wenchuan earthquake on industrial facilities. *Journal of Loss Prevention in the Process Industries*, *23*(2), 242–248.

Kumar, V. B., Sampath, D., Praneeth, V. S. & Kumar, Y. P. (2021). Error performance index based pid tuning methods for temperature control of heat exchanger system. In *2021 ieee international iot, electronics and mechatronics conference (iemtronics)* (pp. 1–6).

Kurode, S., Spurgeon, S. K., Bandyopadhyay, B. & Gandhi, P. S. (2012). Sliding mode control for slosh-free motion using a nonlinear sliding surface. *IEEE/ASME Transactions on Mechatronics*, *18*(2), 714-724.

Lakis, A., Bursuc, G. & Toorani, M. (2009). Sloshing effect on the dynamic behavior of horizontal cylindrical shells. *Nuclear Engineering and Design*, *239*(7), 1193–1206.

Lavassani, S. H. H., Shangapour, S., Homami, P., Gharehbaghi, V., Farsangi, E. N. & Yang, T. (2022). An innovative methodology for hybrid vibration control (mr+ tmd) of buildings under seismic excitations. *Soil Dynamics and Earthquake Engineering*, *155*, 107175.

Lee, D. & Constantinou, M. C. (2016). Quintuple friction pendulum isolator: Behavior, modeling, and validation. *Earthquake Spectra*, *32*(3), 1607–1626.

Li, J., Chen, H.-M. & Chen, J.-B. (2007). Studies on seismic performances of the prestressed egg-shaped digester with shaking table test. *Engineering structures*, *29*(4), 552–566.

Li, W., Hancock, C., Yang, Y., Wang, J. & Meng, X. (2022). Dynamic deformation monitoring of an offshore platform structure with accelerometers. *Journal of Civil Structural Health Monitoring*, *12*(2), 275–287.

Li, Y. & Hou, Z. (2014). Data-driven asymptotic stabilization for discrete-time nonlinear systems. *Systems & Control Letters*, *64*, 79–85.

Li, Y.-C. & Gou, H.-L. (2018). Modeling problem of equivalent mechanical models of a sloshing fluid. *Shock and Vibration*, *2018*.

Lin, G., Liu, J., Li, J. & Hu, Z. (2015). A scaled boundary finite element approach for sloshing analysis of liquid storage tanks. *Engineering Analysis with Boundary Elements*, *56*, 70-80. doi: 10.1016/J.ENGANABOUND.2015.02.006

Liu, F., Gao, S. & Chang, S. (2021). Displacement estimation from measured acceleration for fixed offshore structures. *Applied Ocean Research*, *113*, 102741.

Liu, W., Xiao, C., Zhou, H. & Wang, C. (2023). Experimental investigation of liquid-tank

interaction effects on full containment lng storage tanks through shaking table tests. *Thin-Walled Structures*, 111527.

Liu, Y., Páez Chávez, J., Brzeski, P. & Perlikowski, P. (2021). Dynamical response of a rocking rigid block. *Chaos: An Interdisciplinary Journal of Nonlinear Science*, *31*(7).

Livaoglu, R. & Dogangun, A. (2007). Effect of foundation embedment on seismic behavior of elevated tanks considering fluid–structure-soil interaction. *Soil Dynamics and Earthquake Engineering*, *27*(9), 855-863.

Ljung, L. (1998). System identification. In *Signal analysis and prediction* (pp. 163–173). Springer.

Longatte, E., Bendjeddou, Z. & Souli, M. (2003). Application of arbitrary lagrange euler formulations to flow-induced vibration problems. *J. Pressure Vessel Technol.*, *125*(4), 411-417.

Luco, J. E. (1976). Vibrations of a rigid disc on a layered viscoelastic medium. *Nuclear Engineering and Design*, *36*(3), 325-340.

Luo, H., Zhang, R. & Weng, D. (2016). Mitigation of liquid sloshing in storage tanks by using a hybrid control method. *Soil Dynamics and Earthquake Engineering*, *90*, 183-195. doi: 10.1016/j.soildyn.2016.08.037

Lysmer, J. & Kuhlemeyer, R. L. (1969). Finite dynamic model for infinite media. *Journal of the engineering mechanics division*, *95*(4), 859-877.

Lyu, Y., Sun, J., Sun, Z., Cui, L. & Wang, Z. (2020). Simplified mechanical model for seismic design of horizontal storage tank considering soil-tank-liquid interaction. *Ocean Engineering*, *198*, 106953.

Ma, L. & Chang, C. S. (1993). Pressures exerted on soil due to rocking of liquid storage tanks. *Journal of geotechnical engineering*, *119*(11), 1679-1695.

Madhekar, S. N. & Jangid, R. S. (2009, sep). Variable dampers for earthquake protection of benchmark highway bridges. *Smart Materials and Structures*, *18*(11), 115011. doi: 10.1088/0964-1726/18/11/115011

Maheri, M. R., Karbaschi, M. & Mahzoon, M. (2016). Analytical evaluation of dynamic characteristics of unanchored circular ground-based steel tanks. *Thin-Walled Structures*, *109*, 251–259.

Maiti, D., Acharya, A., Chakraborty, M., Konar, A. & Janarthanan, R. (2008). Tuning pid and pi/λ d δ controllers using the integral time absolute error criterion. In *2008 4th international conference on information and automation for sustainability* (pp. 457–462).

Malhotra, P., Veletsos, A. & Tang, H. (1993). Seismic response of unanchored liquid storage tanks.

Malhotra, P. K. (1997). Seismic response of soil-supported unanchored liquid-storage tanks. *Journal of Structural Engineering-American Society of Civil Engineers*, *123*(4), 440-450. doi: 10.1061/(ASCE)0733-9445(1997)123:4(440)

Malhotra, P. K. & Veletsos, A. S. (1994a). Beam model for base-uplifting analysis of cylindrical tanks. *Journal of Structural Engineering*, *120*(12), 3471-3488. doi: 10.1061/(ASCE)0733-9445(1994)120:12(3471)

Malhotra, P. K. & Veletsos, A. S. (1994b). Uplifting analysis of base plates in cylindrical tanks. *Journal of Structural Engineering*, *120*(12), 3489-3505. doi: 10.1061/(ASCE)0733-9445(1994)120:12(3489)

Malhotra, P. K. & Veletsos, A. S. (1994c). Uplifting response of unanchored liquid-storage tanks. *Journal of Structural Engineering*, *120*(12), 3525-3547. doi: 10.1061/(ASCE)0733-9445(1994)120:12(3525)

Malhotra, P. K., Wenk, T. & Wieland, M. (2000). Simple procedure for seismic analysis of liquid-storage tanks. *Structural engineering international*, *10*(3), 197-201.

Manos, G. C. (1991). Evaluation of the earthquake performance of anchored wine tanks during the san juan, argentina, 1977 earthquakexs. *Earthquake engineering and structural dynamics*, *20*(12), 1099-1114.

Manos, G. C. & Clough, R. W. (1982). *Further study of the earthquake response of a broad cylindrical liquid-storage tank model* [Book].

Manos, G. C. & Clough, R. W. (1983). The measured and predicted shaking table response of a broad tank model.

Manos, G. C. & Clough, R. W. (1985). Tank damage during the may 1983 coalinga earthquake. *Earthquake Engineering and Structural Dynamics*, *13*(4), 449-466.

Mansour, T. (2011). *Pid control: implementation and tuning*. BoD–Books on Demand.

Marchetti, G., Barolo, M., Jovanovic, L., Zisser, H. & Seborg, D. E. (2008). An improved pid switching control strategy for type 1 diabetes. *ieee transactions on biomedical engineering*, *55*(3), 857–865.

Markovsky, I., Huang, L. & Dörfler, F. (2023). Data-driven control based on the behavioral approach: From theory to applications in power systems. *IEEE Control Systems Magazine*, *43*(5), 28–68.

McKenna, F., Fenves, G. L. & Scott, M. H. (2006). Opensees: Open system for earthquake engineering simulation. *Pacific Earthquake Engineering Research Center, University of California, Berkeley, CA., http://opensees. berkeley. edu*.

Mehrvarz, A., Najafi Ardekani, A., Khodaei, M. J. & Jalili, N. (2019). Vibration analysis and control of fluid containers using piezoelectrically-excited side wall. *Journal of Vibration and Control*, *25*(7), 1393-1408. doi: 10.1177/1077546318822374

Meng, F., Liu, S. & Liu, K. (2020). Design of an optimal fractional order pid for constant tension control system. *IEEE Access*, *8*, 58933–58939.

Meng, X., Li, X., Xu, X., Zhang, J., Zhou, W. & Zhou, D. (2019). Earthquake response of cylindrical storage tanks on an elastic soil. *Journal of Vibration Engineering and Technologies*, *7*(5), 433-444. doi: 10.1007/s42417-019-00141-0

Merino, R. J., Brunesi, E. & Nascimbene, R. (2020). Probabilistic evaluation of earthquake-induced sloshing wave height in above-ground liquid storage tanks.

Engineering Structures, *202*, 109870-109870.

Merino Vela, R. J., Brunesi, E. & Nascimbene, R. (2019a). Floor spectra estimates for an industrial special concentrically braced frame structure. *Journal of Pressure Vessel Technology*, *141*(1).

Merino Vela, R. J., Brunesi, E. & Nascimbene, R. (2019b). Seismic assessment of an industrial frame-tank system: development of fragility functions. *Bulletin of Earthquake Engineering*, *17*(5), 2569–2602.

Mesa-Gómez, A., Casal, J. & Muñoz, F. (2020). Risk analysis in natech events: State of the art. *Journal of Loss Prevention in the Process Industries*, *64*, 104071.

Mir, F. U. H., Yu, C.-C. & Whittaker, A. S. (2021). Rocking response of liquid-filled cylindrical tanks. *Earthquake Spectra*, *37*(3), 1698–1709.

Miranda, E. & Bertero, V. V. (1994). Evaluation of strength reduction factors for earthquake-resistant design. *Earthquake spectra*, *10*(2), 357-379.

Mirjalili, S., Mirjalili, S. M. & Lewis, A. (2014). Grey wolf optimizer. *Advances in engineering software*, *69*, 46–61.

Mitropoulou, C. C., Kostopanagiotis, C., Kopanos, M., Ioakim, D. & Lagaros, N. D. (2016). Influence of soil–structure interaction on fragility assessment of building structures. In *Structures* (Vol. 6, p. 85-98). Elsevier.

Mittal, V., Chakraborty, T. & Matsagar, V. (2014). Dynamic analysis of liquid storage tank under blast using coupled euler–lagrange formulation. *Thin-Walled Structures*, *84*, 91–111.

Mituletu, I. C., Gillich, G.-R. & Maia, N. M. (2019). A method for an accurate estimation of natural frequencies using swept-sine acoustic excitation. *Mechanical Systems and Signal Processing*, *116*, 693–709.

Modi, V. J. & Munshi, S. R. (1998). An efficient liquid sloshing damper for vibration control..

Moeindarbari, H., Malekzadeh, M. & Taghikhany, T. (2014). Probabilistic analysis of seismically isolated elevated liquid storage tank using multi-phase friction bearing. *Earthquakes and Structures*, *6*(1), 111–125.

Mohamed, A. A., Metwally, H., El-Sayed, A. & Selem, S. (2019). Predictive neural network based adaptive controller for grid-connected pv systems supplying pulse-load. *Solar Energy*, *193*, 139–147.

Mohebbi, M., Dadkhah, H. & Rasouli Dabbagh, H. (2018). Modified h2/lqg control algorithm for designing a multi-objective semi-active base isolation system. *Journal of Vibration and Control*, *24*(23), 5693–5704.

Moradi, R., Behnamfar, F. & Hashemi, S. (2018). Mechanical model for cylindrical flexible concrete tanks undergoing lateral excitation. *Soil Dynamics and Earthquake Engineering*, *106*, 148-162.

Morris, G. J., Bradley, B. A., Walker, A. & Matuschka, T. (2013). Ground motions and damage observations in the marlborough region from the 2013 lake grassmere

earthquake. *Bulletin of the New Zealand Society for Earthquake Engineering*, *46*(4), 169-187.

Muto, K., Kasai, Y. & Nakahara, M. (1988). Experimental tests for suppression effects of water restraint plates on sloshing of a water pool. *Journal of Pressure Vessel Technologoy*, *110*(3), 240-246.

Naik, K. A., Gupta, C. P. & Fernandez, E. (2020). Design and implementation of interval type-2 fuzzy logic-pi based adaptive controller for dfig based wind energy system. *International Journal of Electrical Power & Energy Systems*, *115*, 105468.

Nayar, N., Gautam, S., Singh, P. & Mehta, G. (2021). Ant colony optimization: A review of literature and application in feature selection. *Inventive Computation and Information Technologies: Proceedings of ICICIT 2020*, 285–297.

Nicolici, S. & Bilegan, R. (2013). Fluid structure interaction modeling of liquid sloshing phenomena in flexible tanks. *Nuclear Engineering and design*, *258*, 51-56.

Nikoomanesh, M. R., Moeini, M. & Goudarzi, M. A. (2019). An innovative isolation system for improving the seismic behaviour of liquid storage tanks. *International Journal of Pressure Vessels and Piping*, *173*(April), 1-10. doi: 10.1016/j.ijpvp .2019.04.012

Niwa, A. & Clough, R. W. (1982). Buckling of cylindrical liquid-storage tanks under earthquake loading. *Earthquake Engineering & Structural Dynamics*, *10*(1), 107–122.

NZSEE. (2009). Seismic design of storage tanks. New Zealand National Society for Earthquake Engineering.

Ogunmakinde, O. E., Egbelakin, T., Omotayo, T. & Sojobi, A. (2023). Seismic vulnerability and inventory of at-risk elements in the wine industry: Auckland region case study. In *Structures* (Vol. 58, p. 105346).

Oh, S.-H., Song, S.-H., Lee, S.-H. & Kim, H.-J. (2012). Seismic response of base isolating systems with U-shaped hysteretic dampers. *International Journal of Steel Structures*, *12*(2), 285-298.

Oh, S.-H., Song, S.-H., Lee, S.-H. & Kim, H.-J. (2013). Experimental study of seismic performance of base-isolated frames with U-shaped hysteretic energy-dissipating devices. *Engineering structures*, *56*, 2014-2027.

Ormeño, M., Larkin, T. & Chouw, N. (2012). Influence of uplift on liquid storage tanks during earthquakes. *Coupled systems mechanics*, *1*(4), 311–324.

Ormeño, M., Larkin, T. & Chouw, N. (2015). The effect of seismic uplift on the shell stresses of liquid-storage tanks. *Earthquake Engineering & Structural Dynamics*, *44*(12), 1979–1996.

Ormeño, M., Larkin, T. & Chouw, N. (2019). Experimental study of the effect of a flexible base on the seismic response of a liquid storage tank. *Thin-Walled Structures*, *139*, 334–346.

Ormeño, M., Geddes, M., Larkin, T. & Chouw, N. (2015). Experimental study of

slip-friction connectors for controlling the maximum seismic demand on a liquid storage tank. *Engineering Structures*, *103*, 134-146.

Oustaloup, A., Sabatier, J. & Moreau, X. (1998). From fractal robustness to the crone approach. In *Proc., esaim* (Vol. 5, pp. 177–192).

Ozdemir, Z., Souli, M. & Fahjan, Y. M. (2010). Application of nonlinear fluid-structure interaction methods to seismic analysis of anchored and unanchored tanks. *Engineering Structures*, *32*(2), 409-423. doi: 10.1016/J.ENGSTRUCT.2009.10.004

Ozsarac, V., Brunesi, E. & Nascimbene, R. (2021). Earthquake-induced nonlinear sloshing response of above-ground steel tanks with damped or undamped floating roof. *Soil Dynamics and Earthquake Engineering*, *144*, 106673.

Öztürk, S. & Kahraman, M. F. (2019). Modeling and optimization of machining parameters during grinding of flat glass using response surface methodology and probabilistic uncertainty analysis based on monte carlo simulation. *Measurement*, *145*, 274–291.

Panchal, V. & Jangid, R. (2008). Variable friction pendulum system for seismic isolation of liquid storage tanks. *Nuclear Engineering and Design*, *238*(6), 1304-1315.

Paolacci, F. (2015). On the effectiveness of two isolation systems for the seismic protection of elevated tanks. *Journal of Pressure Vessel Technology*, *137*(3).

Paolacci, F., Giannini, R. & De Angelis, M. (2013). Seismic response mitigation of chemical plant components by passive control techniques. *Journal of loss prevention in the process industries*, *26*(5), 924–935.

Paolacci, F., Quinci, G., Nardin, C., Vezzari, V., Marino, A. & Ciucci, M. (2021). Bolted flange joints equipped with fbg sensors in industrial piping systems subjected to seismic loads. *Journal of Loss Prevention in the Process Industries*, *72*, 104576.

Paolacci, F., Reza, M. S. & Bursi, O. S. (2011). Seismic analysis and component design of refinery piping systems. In *3rd international conference on computational methods in structural dynamics and earthquake engineering, compdyn* (pp. 25–28).

Paolacci, F., Reza, M. S., Bursi, O. S., Gresnigt, A. M. & Kumar, A. (2013). Main issues on the seismic design of industrial piping systems and components. In *Pressure vessels and piping conference* (Vol. 55744, p. V008T08A018).

Papagiannopoulos, G. A. & Hatzigeorgiou, G. D. (2011). On the use of the half-power bandwidth method to estimate damping in building structures. *Soil Dynamics and Earthquake Engineering*, *31*(7), 1075–1079.

Park, S. W., Kang, D. H., Bang, H. J., Park, S. O. & Kim, C. G. (2006). Strain monitoring and damage detection of a filament wound composite pressure tank using embedded fiber bragg grating sensors. *Key Engineering Materials*, *321-323*, 182-185. doi: 10.4028/www.scientific.net/kem.321-323.182

Pei, P., Peng, Y. & Qiu, C. (2022). An improved semi-active structural control combining optimized fuzzy controller with inverse modeling technique of mr damper. *Structural and Multidisciplinary Optimization*, *65*(9), 272.

Peña, F., Prieto, F., Lourenço, P. B., Campos Costa, A. & Lemos, J. V. (2007). On the dynamics of rocking motion of single rigid-block structures. *Earthquake Engineering & Structural Dynamics*, *36*(15), 2383–2399.

Phan, H., Paolacci, F., Corritore, D., Akbas, B., Uckan, E. & Shen, J. (2016). Seismic vulnerability mitigation of liquefied gas tanks using concave sliding bearings. *Bulletin of Earthquake Engineering*, *14*(11), 3283–3299. doi: 10.1007/s10518-016-9939-y

Podlubny, I. (1999). Fractional-order systems and pi/sup/spl lambda//d/sup/spl mu//-controllers. *IEEE Transactions on automatic control*, *44*(1), 208–214.

Pohoryles, D. A. & Duffour, P. (2015). Adaptive control of structures under dynamic excitation using magnetorheological dampers: an improved clipped-optimal control algorithm. *Journal of Vibration and Control*, *21*(13), 2569–2582.

Pommier Budinger, V., Richelot, J. & Bordeneuve-Guibe, J. (2006). Active control of a structure with sloshing phenomena. *IFAC Proceedings Volumes*, *39*(16), 644-649. doi: 10.3182/20060912-3-DE-2911.00112

Prakash, S. & Jangid, R. (2022). Seismic response of isolated structures with an improved model of the ufrei. In *Structures* (Vol. 42, pp. 434–448).

Pridgen, B., Bai, K. & Singhose, W. (2013). Shaping container motion for multimode and robust slosh suppression. *American Institute of Aeronautics and Astronautics*, *50*(2), 440-448. doi: 10.2514/1.A32137

Priestley, M. J. N. (1986). Seismic design of storage tanks: Recommendations of a study group of the new zealand national society for earthquake engineering. *New Zealand National Society for Earthquake Engineering*.

Prinz, G. S. & Nussbaumer, A. (2012a). Fatigue analysis of liquid-storage tank shell-to-base connections under multi-axial loading. *Engineering Structures*, *40*, 75–82.

Prinz, G. S. & Nussbaumer, A. (2012b). On the low-cycle fatigue capacity of unanchored steel liquid storage tank shell-to-base connections. *Bulletin of Earthquake Engineering*, *10*(6), 1943–1958.

Rainieri, C., Gargaro, D., Reynders, E. & Fabbrocino, G. (2020). A study on the concurrent influence of liquid content and damage on the dynamic properties of a tank for the development of a modal-based shm system. *Journal of Civil Structural Health Monitoring*, *10*(1), 57-68.

Rao, C. S., Santosh, S. et al. (2020). Tuning optimal pid controllers for open loop unstable first order plus time delay systems by minimizing itae criterion. *IFAC-PapersOnLine*, *53*(1), 123–128.

Rawat, A. & Matsagar, V. (2022). An oblate spheroid base isolator and floating surface diaphragm for seismic protection of liquid storage tank. *Journal of Earthquake Engineering*, *26*(10), 5447–5475.

Rawat, A., Mittal, V., Chakraborty, T. & Matsagar, V. (2019). Earthquake induced sloshing and hydrodynamic pressures in rigid liquid storage tanks analyzed by

coupled acoustic-structural and euler-lagrange methods. *Thin-Walled Structures*, *134*(July 2017), 333-346. doi: 10.1016/j.tws.2018.10.016

Reid, R. M. & Russell, D. L. (1985). Boundary control and stability of linear water waves. *SIAM journal on control and optimization*, *23*(1), 111-121.

Reyes, S. I., Almazán, J. L., Vassiliou, M. F., Tapia, N. F., Colombo, J. I. & de la Llera, J. C. (2022). Full-scale shaking table test and numerical modeling of a 3000-liter legged storage tank isolated with a vertical rocking isolation system. *Earthquake Engineering & Structural Dynamics*, *51*(6), 1563–1585.

Reyhanoglu, M. & Hervas, J. R. (2012). Nonlinear dynamics and control of space vehicles with multiple fuel slosh modes. *Control Engineering Practice*, *20*(9), 912-918. doi: 10.1016/J.CONENGPRAC.2012.05.011

Reyhanoglu, M. & Hervas, J. R. (2013a). Nonlinear modeling and control of slosh in liquid container transfer via a ppr robot. *Communications in Nonlinear Science and Numerical Simulation*, *18*(6), 1481-1490. doi: 10.1016/J.CNSNS.2012.10.006

Reyhanoglu, M. & Hervas, J. R. (2013b). Robotically controlled sloshing suppression in point-to-point liquid container transfer. *JVC/Journal of Vibration and Control*, *19*(14), 2137-2144. doi: 10.1177/1077546312456865

Rezaiee-Pajand, M., Mirjalili, Z. & Kazemiyan, M. S. (2023). Analytical 2d model for the liquid storage rectangular tank. *Engineering Structures*, *289*, 116215.

Ribeiro, J. G. T., de Castro, J. T. P. & Meggiolaro, M. A. (2021). An algorithm to minimize errors in displacement measurements via double integration of noisy acceleration signals. *Journal of the Brazilian Society of Mechanical Sciences and Engineering*, *43*, 1–21.

Richter, H. (2010). Motion control of a container with slosh: Constrained sliding mode approach. *Journal of dynamic systems, measurement, and control*, *132*(3). doi: 10.1115/1.4001329

Robinson, W. & Tucker, A. (1977). A lead-rubber shear damper. *Bulletin of the New Zealand Society for Earthquake Engineering*, *10*(3), 151–153.

Robu, B., Baudouin, L., Prieur, C. & Arzelier, D. (2012). Simultaneous h vibration control of fluid/plate system via reduced-order controller. *IEEE Transactions on Control Systems Technology*, *20*(3), 700-711.

Rosewitz, J. & Kahanek, C. (2014). Performance of wine storage tanks: Lessons from the earthquakes near marlborough. In *Australasian structural engineering conference (asec)*.

Safari, S. & Tarinejad, R. (2018). Parametric study of stochastic seismic responses of base-isolated liquid storage tanks under near-fault and far-fault ground motions. *Journal of Vibration and Control*, *24*(24), 5747-5764. doi: 10.1177/1077546316647576

Saha, S., Sepahvand, K., Matsagar, V., Jain, A. & Marburg, S. (2013). Stochastic analysis of base-isolated liquid storage tanks with uncertain isolator parameters

under random excitation. *Engineering Structures*, *57*, 465-474.

Saha, S. K., Matsagar, V. A. & Jain, A. K. (2016). Seismic fragility of base-isolated water storage tanks under non-stationary earthquakes. *Bulletin of Earthquake Engineering*, *14*(4), 1153-1175. doi: 10.1007/S10518-016-9874-Y

Sahami, K., Zarnani, P. & Quenneville, P. (2020). Earthquake-resilience of storage tanks: using an innovative anchorage system.

Sahami, K., Zarnani, P. & Quenneville, P. (2021). Using a self-centring friction damper as anchorage system for industrial tanks and vessels.

Şahin, Ö., Adar, N. G., Kemerli, M., Caglar, N., Şahin, İ., Parlak, Z., ... Engin, T. (2021). A comparative evaluation of semi-active control algorithms for real-time seismic protection of buildings via magnetorheological fluid dampers. *Journal of Building Engineering*, *42*, 102795.

Salimbeni, M., De Angelis, M., Vezzari, V. & Ciucci, M. (2022). Earthquake natech risk assessment, monitoring and management of cylindrical liquid storage tanks with floating roof in major-hazard industrial plants. In *Pressure vessels and piping conference* (Vol. 86199, p. V005T08A018).

Scharf, K. (1993). Beitrage zur erfassung des verhaltens von erdbebenerregten, oberirdischen tankbauwerken.

Seismosoft. (2022). Seismosignal – signal processing of strong-motion data. (accessed on 20 June 2022). Retrieved from `https://seismosoft.com/products/seismosignal/`

Sepahvand, K., Marburg, S. & Hardtke, H.-J. (2010). Uncertainty quantification in stochastic systems using polynomial chaos expansion. *International Journal of Applied Mechanics*, *2*(02), 305-353.

Sepahvand, K., Marburg, S. & Hardtke, H.-J. (2012). Stochastic free vibration of orthotropic plates using generalized polynomial chaos expansion. *Journal of Sound and Vibration*, *331*(1), 167-179.

Sezen, H., Livaoglu, R. & Dogangun, A. (2008). Dynamic analysis and seismic performance evaluation of above-ground liquid-containing tanks. *Engineering Structures*, *30*(3), 794–803.

Shaban, E., Sayed, H. & Abdelhamid, A. (2019). A novel discrete pid+ controller applied to higher order/time delayed nonlinear systems with practical implementation. *International Journal of Dynamics and Control*, *7*, 888–900.

Shaheen, Y. B., Eltaly, B. A. & Abd-Alla, M. K. (2013). Damage detection of ferrocement tanks using experimental modal analysis and finite element analysis. *Concr. Res. Lett*, *4*(2), 598-598.

Shami, T. M., El-Saleh, A. A., Alswaitti, M., Al-Tashi, Q., Summakieh, M. A. & Mirjalili, S. (2022). Particle swarm optimization: A comprehensive survey. *Ieee Access*, *10*, 10031–10061.

Shekari, M. R. (2018). A coupled BE-FE-BE study for investigating the effect of

earthquake frequency content and predominant period on seismic behavior of base-isolated concrete rectangular liquid tanks. *Journal of Fluids and Structures*, *77*, 19-35.

Shekari, M. R., Khaji, N. & Ahmadi, M. (2009). A coupled BE–FE study for evaluation of seismically isolated cylindrical liquid storage tanks considering fluid–structure interaction. *Elsevier*.

Shi, X., Song, L.-L., Guo, T. & Pan, Z.-H. (2022). Seismic design of self-centering bridge piers considering soil-structure interaction. In *Structures* (Vol. 43, p. 1819-1833).

Shrimali, M. & Jangid, R. (2004). Seismic analysis of base-isolated liquid storage tanks. *Journal of Sound and Vibration*, *275*(1-2), 59-75.

Shrimali, M. K. & Jangid, R. S. (2002). A comparative study of performance of various isolation systems for liquid storage tanks. *International Journal of Structural Stability and Dynamics*, *2*(04), 573-591.

Shrimali, M. K. & Kasar, A. A. (2012). Seismic response of connected liquid tanks with MR dampers. *15th World Conference on Earthquake Engineering, Lisbon, Portugal*.

Silvestri, S., Mansour, S., Marra, M., Distl, J., Furinghetti, M., Lanese, I., ... others (2022). Shaking table tests of a full-scale flat-bottom manufactured steel silo filled with wheat: Main results on the fixed-base configuration. *Earthquake Engineering & Structural Dynamics*, *51*(1), 169–190.

Singhose, W., Eloundou, R. & Lawrence, J. (2010). Command generation for flexible systems by input shaping and command smoothing. *Journal of guidance, control, and dynamics*, *33*(6), 1697-1707. doi: 10.2514/1.50270

Sira-Ramirez, H. (2002). A flatness based generalized pi control approach to liquid sloshing regulation in a moving container. In (Vol. 4, p. 2909-2914). IEEE.

Slate, J. & Sheppard, L. (1982). Automatic control of blood pressure by drug infusion. *IEE Proceedings A (Physical Science, Measurement and Instrumentation, Management and Education, Reviews)*, *129*(9), 639–645.

Sohn, H., Lim, H. J., DeSimio, M. P., Brown, K. & Derriso, M. (2014). Nonlinear ultrasonic wave modulation for online fatigue crack detection. *Journal of Sound and Vibration*, *333*(5), 1473–1484.

Solvang, P. S. (2019). *State space model based pid controller tuning* (Unpublished master's thesis). University of South-Eastern Norway.

Sorenson, H. W. (1966). Kalman filtering techniques. In *Advances in control systems* (Vol. 3, pp. 219–292). Elsevier.

Souli, M. & Zolesio, J. P. (2001). Arbitrary Lagrangian–Eulerian and free surface methods in fluid mechanics. *Computer methods in applied mechanics and engineering*, *191*(3-5), 451-466.

Souto-Iglesias, A., Delorme, L., Pérez-Rojas, L. & Abril-Pérez, S. (2006). Liquid moment amplitude assessment in sloshing type problems with smooth particle

hydrodynamics. *Ocean Engineering*, *33*(11-12), 1462–1484.

Spencer Jr, B., Dyke, S. & Deoskar, H. (1998). Benchmark problems in structural control: Part i—active mass driver system. *Earthquake Engineering & Structural Dynamics*, *27*(11), 1127–1139.

Spencer Jr, B., Dyke, S., Sain, M. & Carlson, J. (1997). Phenomenological model for magnetorheological dampers. *Journal of engineering mechanics*, *123*(3), 230–238.

Sreenivasappa, B. & Udaykumar, R. (2010). Analysis and implementation of discrete time pid controllers using fpga. *International journal of electrical and computer engineering*, *2*(1), 71–82.

Steinbrugge, K. V. & Flores A, R. (1963). The chilean earthquakes of may, 1960: A structural engineering viewpoint. *Bulletin of the Seismological Society of America*, *53*(2), 225-307.

Sun, J., Cui, L., Li, X., Wang, Z., Liu, W. & Lv, Y. (2018). Vibration mode decomposition response analysis of large floating roof tank isolation considering swing effect. *Earthquakes and Structures*, *15*(4), 411-417.

Sun, Y., Zhou, D. & Wang, J. (2019). An equivalent mechanical model for fluid sloshing in a rigid cylindrical tank equipped with a rigid annular baffle. *Applied Mathematical Modelling*, *72*, 569-587. doi: 10.1016/j.apm.2019.03.024

Sun, Y., Zhou, D., Wang, J. & Han, H. (2021). Lumped parameter model for liquid sloshing in a cylindrical tank equipped with multiple annular baffles. *Journal of Structural Engineering*, *147*(5), 04021042-04021042. doi: 10.1061/(asce)st.1943-541x.0002972

Suzuki, K. (2002). Report on damage to industrial facilities in the 1999 kocaeli earthquake, turkey. *Journal of Earthquake Engineering*, *6*(2), 275–296.

Swan, S. W., Miller, D. D. & Yanev, P. I. (1985). The morgan hill earthquake of april 24, 1984—effects on industrial facilities, buildings, and other facilities. *Earthquake spectra*, *1*(3), 457–568.

Tang, W. & Daoutidis, P. (2022). Data-driven control: Overview and perspectives. In *2022 american control conference (acc)* (pp. 1048–1064).

Team, E. et al. (1990). Loma prieta earthquake reconnaissance report. *Earthquake Spectra*, 127–149.

Tepljakov, A., Vunder, V., Petlenkov, E., Nakshatharan, S. S., Punning, A., Kaparin, V., ... Aabloo, A. (2019). Fractional-order modeling and control of ionic polymer-metal composite actuator. *Smart Materials and Structures*, *28*(8), 084008.

Terashima, K., Hamaguchi, M. & Yamaura, K. (1996). Modeling and input shaping control of liquid vibration for an automatic pouring system. In (Vol. 4, p. 4844-4850). IEEE. Retrieved from `https://ieeexplore.ieee.org/abstract/document/577707/`

Terashima, K. & Schmidt, G. (1994). Motion control of a cart-based container considering suppression of liquid oscillations. In (p. 275-280). IEEE. Retrieved from

https://ieeexplore.ieee.org/abstract/document/333105/

Terashima, K. & Yano, K. (2001). Sloshing analysis and suppression control of tilting-type automatic pouring machine. *Control Engineering Practice*, *9*(6), 607-620. doi: 10.1016/S0967-0661(01)00023-5

Thomson, W. & Dahleh, M. (1997). *Theory of vibration with applications* (Fifth edition ed.). Prentice Hall.

Thong, Y., Woolfson, M., Crowe, J., Hayes-Gill, B. & Jones, D. (2004). Numerical double integration of acceleration measurements in noise. *Measurement*, *36*(1), 73–92.

Tsai, C., Lin, Y. & Su, H. (2010). Characterization and modeling of multiple friction pendulum isolation system with numerous sliding interfaces. *Earthquake engineering & structural dynamics*, *39*(13), 1463–1491.

Tsipianitis, A. & Tsompanakis, Y. (2018a). Optimizing the dynamic performance of friction pendulum isolators in liquid fuels tanks. In *16th european conference on earthquake engineering* (p. 18-21).

Tsipianitis, A. & Tsompanakis, Y. (2018b). Seismic vulnerability assessment of liquid storage tanks isolated by sliding-based systems. *Advances in Civil Engineering*, *2018*.

Tsipianitis, A. & Tsompanakis, Y. (2021). Optimizing the seismic response of base-isolated liquid storage tanks using swarm intelligence algorithms. *Computers and Structures*, *243*, 106407.

Tsipianitis, A., Tsompanakis, Y. & Psarropoulos, P. N. (2020). Impact of dynamic soil–structure interaction on the response of liquid-storage tanks. *Frontiers in Built Environment*, *6*, 140.

Uckan, E., Umut, Ö., Sisman, F. N., Karimzadeh, S. & Askan, A. (2018). Seismic response of base isolated liquid storage tanks to real and simulated near fault pulse type ground motions. *Soil Dynamics and Earthquake Engineering*, *112*, 58–68.

Vakilaadsarabi, A., Miyajima, M. & Murata, K. (2012). Study of the sloshing of water reservoirs and tanks due to long period and long duration seismic motions. In *Procerdings of the 15th world conference on earthquake engineering. lisbon, portugal.*

Vathi, M. & Karamanos, S. A. (2014a). Liquid storage tanks: Seismic analysis [Book Section]. In *Encyclopedia of earthquake engineering* (p. 1-27). Springer Berlin Heidelberg. doi: 10.1007/978-3-642-36197-5_144-1

Vathi, M. & Karamanos, S. A. (2014b). Modeling of uplifting mechanism in unanchored liquid storage tanks subjected to seismic loading. In (p. 24-29). Retrieved from http://www.eaee.org/Media/Default/2ECCES/2ecces_ss/2385.pdf

Vathi, M. & Karamanos, S. A. (2015). Simplified model for the seismic performance of unanchored liquid storage tanks. In *Pressure vessels and piping conference* (Vol.

56987, p. V005T09A014). doi: https://doi.org/10.1115/PVP2015-45695

Vathi, M. & Karamanos, S. A. (2018). A simple and efficient model for seismic response and low-cycle fatigue assessment of uplifting liquid storage tanks. *Journal of Loss Prevention in the Process Industries*, *53*, 29-44. doi: 10.1016/j.jlp.2017.08.003

Vela, R. M., Brunesi, E. & Nascimbene, R. (2018). Derivation of floor acceleration spectra for an industrial liquid tank supporting structure with braced frame systems. *Engineering Structures*, *171*, 105–122.

Veletsos, A. (1974). Seismic effects in flexible liquid storage tanks. In *Proceedings of the 5th world conference on earthquake engineering* (Vol. 1, pp. 630–639).

Veletsos, A. (1976). Dynamic of fixed-based liquid-storage tanks. In *Us-japan seminar for earthquake engineering research with emphasis on lifeline systems, 1976.*

Veletsos, A. (1984). Seismic response and design of liquid storage tanks. *Guidelines for the seismic design of oil and gas pipeline systems*, 255–370.

Veletsos, A. S. (1974). Seismic effects in flexible liquid storage tanks. In (Vol. 1, p. 630-639).

Veletsos, A. S. (1984). Seismic response and design of liquid storage tanks. guidelines for the seismic design of oil and gas pipeline systems. , 255-370.

Veletsos, A. S. & Meek, J. W. (1974). Dynamic behaviour of building-foundation systems. *Earthquake Engineering and Structural Dynamics*, *3*(2), 121-138.

Veletsos, A. S. & Nair, V. D. (1975). Seismic interaction of structures on hysteretic foundations. *Journal of the Structural Division*, *101*(1), 109-129.

Veletsos, A. S., Shivakumar, P., Tang, Y. & Tang, H. T. (1990). Seismic response of anchored steel tanks. In (p. 2-15).

Veletsos, A. S. & Tang, Y. (1987a). Rocking response of liquid storage tanks. *Journal of Engineering Mechanics*, *113*(11), 1774-1792. doi: 10.1061/(ASCE)0733 -9399(1987)113:11(1774)

Veletsos, A. S. & Tang, Y. (1987b). Rocking vibration of rigid ring foundations. *Journal of geotechnical engineering*, *113*(9), 1019-1032.

Veletsos, A. S. & Wei, Y. T. (1971). Lateral and rocking vibration of footings. *Journal of the Soil Mechanics and Foundations Division*, *97*(9), 1227-1248.

Venugopal, R. & Bernstein, D. S. (1996). State space modeling and active control of slosh. In *Proceeding of the 1996 ieee international conference on control applications ieee international conference on control applications held together with ieee international symposium on intelligent control ieee international symposium on computer-aided contro* (p. 1072-1077). IEEE. doi: 10.1109/cca.1996.559074

Vesenjak, M., Mullerschon, H., Hummel, A. & Ren, Z. (2004). Simulation of fuel sloshing-comparative study. *LS-DYNA Anwenderforum*, 1–8.

Virella, J. C., Godoy, L. A. & Suárez, L. E. (2006). Fundamental modes of tank-liquid systems under horizontal motions. *Engineering Structures*, *28*(10), 1450–1461.

Vlachakis, G., Giouvanidis, A. I., Mehrotra, A. & Lourenço, P. B. (2021). Numerical

block-based simulation of rocking structures using a novel universal viscous damping model. *Journal of Engineering Mechanics*, *147*(11), 04021089.

Wang, F. & Song, G. (2019). Bolt early looseness monitoring using modified vibro-acoustic modulation by time-reversal. *Mechanical Systems and Signal Processing*, *130*, 349–360.

Wang, J., Lo, S. & Zhou, D. (2012). Liquid sloshing in rigid cylindrical container with multiple rigid annular baffles: Free vibration. *Journal of Fluids and Structures*, *34*, 138-156.

Wang, W., Peng, Y., Zhou, Y. & Zhang, Q. (2016). Liquid sloshing in partly-filled laterally-excited cylindrical tanks equipped with multi baffles. *Applied Ocean Research*, *59*, 543-563.

Wang, Y. & Dyke, S. J. (2006). A comparative study of the base isolation benchmark problem using h2/lqg and smart dampers. In *Structures congress 2006: 17th analysis and computation specialty conference* (pp. 1–16).

Wani, Z. R. & Tantray, M. (2022). Study on integrated response-based adaptive strategies for control and placement optimization of multiple magneto-rheological dampers-controlled structure under seismic excitations. *Journal of Vibration and Control*, *28*(13-14), 1712–1726.

Welch, P. (1967). The use of fast fourier transform for the estimation of power spectra: a method based on time averaging over short, modified periodograms. *IEEE Transactions on audio and electroacoustics*, *15*(2), 70–73.

Wu, J.-Y., Yu, Q.-Q. & Gu, X.-L. (2023). A modified analytical model for predicting seismic behaviors of unanchored liquid storage tanks. *Journal of Constructional Steel Research*, *208*, 108018.

Xiu, D. & Karniadakis, G. E. (2002). The Wiener–Askey polynomial chaos for stochastic differential equations. *SIAM journal on scientific computing*, *24*(2), 619-644.

Xiu, D. & Karniadakis, G. E. (2003). Modeling uncertainty in flow simulations via generalized polynomial chaos. *Journal of computational physics*, *187*(1), 137-167.

Yamada, Y., Iemura, H., Noda, S. & Shimada, S. (1987). Long-period response spectra from nonlinear sloshing analysis under horizontal and vertical excitations. *Natural disaster science*, *9*(2), 39-54.

Yang, Y., Chen, H., Heidari, A. A. & Gandomi, A. H. (2021). Hunger games search: Visions, conception, implementation, deep analysis, perspectives, and towards performance shifts. *Expert Systems with Applications*, *177*, 114864.

Yano, K. & Terashima, K. (2001). Robust liquid container transfer control for complete sloshing suppression. *IEEE Transactions on Control Systems Technology*, *9*(3), 483-493.

Yano, K. & Terashima, K. (2005). Sloshing suppression control of liquid transfer systems considering a 3-d transfer path. *IEEE/ASME Transactions on Mechatronics*, *10*(1), 8-16.

Yano, K., Toda, T. & Terashima, K. (2001). Sloshing suppression control of automatic pouring robot by hybrid shape approach. In (Vol. 2, p. 1328-1333). IEEE. Retrieved from https://ieeexplore.ieee.org/abstract/document/981074/

Yazdanian, M., Firouzsalari, S., Ingham, J. & Dizhur, D. (2021). Shake table testing of full scale 22 kl legged liquid storage tank [NZSEE Annual Conference].

Yazdanian, M., Ingham, J. & Dizhur, D. (2019). A conspectus of wine storage tank damage data following the 2013 and 2016 new zealand earthquakes..

Yazdanian, M., Ingham, J. & Dizhur, D. (2020). Damage to flat-based wine storage tanks in the 2013 and 2016 new zealand earthquakes. *Journal of Constructional Steel Research*, *168*(May), 105983-105983. doi: 10.1016/j.jcsr.2020.105983

Yazdanian, M., Ingham, J., Kahanek, C., Cradock, N., Fountain, J. & Dizhur, D. (2020). Analysis of damage data collected for wine storage tanks following the 2013 and 2016 new zealand earthquakes. (June). doi: 10.5459/bnzsee.53.2.83-100

Yazdanian, M., Ingham, J., Sadashiva, V., Cutfield, M., Kahanek, C. & Dizhur, D. (2021). Seismic fragility curves for stainless-steel wine storage tanks. In *Structures* (Vol. 33, p. 4766-4780). Elsevier.

Yazdanian, M., Ingham, J. M., Lomax, W., Wood, R. & Dizhur, D. (2020). Damage observations and remedial options for approximately 1500 legged and flat-based liquid storage tanks following the 2016 kaikōura earthquake. *Structures*, *24*(February), 357–376. doi: 10.1016/j.istruc.2020.01.024

Yazici, G. & Cili, F. (2008). Evaluation of the liquid storage tank failures in the 1999 kocaeli earthquake. In *Proceedings of the 14th world conference on earthquake engineering, beijing, china* (pp. 12–17).

Yoshida, O. & Dyke, S. J. (2004). Seismic control of a nonlinear benchmark building using smart dampers. *Journal of engineering mechanics*, *130*(4), 386–392.

Yu, C.-C. & Whittaker, A. S. (2021). Review of analytical studies on seismic fluid-structure interaction of base-supported cylindrical tanks. *Engineering Structures*, *233*, 111589.

Zafarani, M. M. & Halabian, A. M. (2018). Supervisory adaptive nonlinear control for seismic alleviation of inelastic asymmetric buildings equipped with mr dampers. *Engineering Structures*, *176*, 849–858.

Zafarani, M. M. & Halabian, A. M. (2020). A new supervisory adaptive strategy for the control of hysteretic multi-story irregular buildings equipped with mr-dampers. *Engineering Structures*, *217*, 110786.

Zama, S., Nishi, H., Hatayama, K., Yamada, M., Yoshihara, H. & Ogawa, Y. (2012). On damage of oil storage tanks due to the 2011 off the pacific coast of tohoku earthquake (mw9. 0), japan. In *Proceedings of the 15th world conference on earthquake engineering (wcee)* (Vol. 2428, pp. 1–10).

Zand, J. P., Sabouri, J., Katebi, J. & Nouri, M. (2021). A new time-domain robust

anti-windup pid control scheme for vibration suppression of building structure. *Engineering Structures*, *244*, 112819.

Zang, Q. & Huang, J. (2014). Dynamics and control of three-dimensional slosh in a moving rectangular liquid container undergoing planar excitations. *IEEE Transactions on Industrial Electronics*, *62*(4), 2309-2318.

Zareian, F., Sampere, C., Sandoval, V., McCormick, D. L., Moehle, J. & Leon, R. (2012). Reconnaissance of the chilean wine industry affected by the 2010 chile offshore maule earthquake. *Earthquake Spectra*, *28*(1_suppl1), 503–512.

Zhai, X. W. H. & Feng, F. (2014). Multi-physics coupling method and applications of fluid-structure interaction on LNG storage tanks..

Zhang, D.-Y. & Wu, J.-Y. (2024). Experimentally validated numerical analyses on the seismic responses of extra-large lng storage structures. *Thin-Walled Structures*, *195*, 111407.

Zhang, D.-Y., Wu, J.-Y., Zhou, H. & Gong, M.-S. (2023). A benchmark shaking table test on the seismic responses of an extra-large lng storage tank. *Earthquake Engineering & Structural Dynamics*, *52*(2), 439–459.

Zhang, H., Trott, G. & Paul, R. (1990). Minimum delay pid control of interpolated joint trajectories of robot manipulators. *IEEE Transactions on Industrial Electronics*, *37*(5), 358–364.

Zhang, R., Zhao, Z. & Pan, C. (2018). Influence of mechanical layout of inerter systems on seismic mitigation of storage tanks. *Soil Dynamics and Earthquake Engineering*, *114*, 639-649.

Zhang, Y., Xu, W., Du, D. & Wang, S. (2023). Stochastic optimization of dissipation structures based on lyapunov differential equations and the full stress design method. *Buildings*, *13*(3), 665.

Zhang, Z. & Peng, Y. (2020). Dynamic physical model for mr damper considering chain deflection in preyield stage. *Journal of Engineering Mechanics*, *146*(11), 04020122.

Zheng, W., Dan, D., Cheng, W. & Xia, Y. (2019). Real-time dynamic displacement monitoring with double integration of acceleration based on recursive least squares method. *Measurement*, *141*, 460–471.

Zhou, W., Wu, Z. & Mevel, L. (2010). Vibration-based damage detection to the composite tank filled with fluid. *Structural Health Monitoring*, *9*(5), 433-445. doi: 10.1177/1475921710361329

Zhu, H., Tang, Z. & Luo, H. (2023). Seismic performance of a base-isolated flexible liquid storage tank equipped with a novel rate-independent damping device. In *Structures* (Vol. 51, pp. 215–225).

Ziegler, J. G. & Nichols, N. B. (1942). Optimum settings for automatic controllers. *Transactions of the American society of mechanical engineers*, *64*(8), 759–765.

Zingoni, A. (2015). Liquid-containment shells of revolution: A review of recent studies

on strength, stability and dynamics. *Thin-Walled Structures*, *87*, 102-114.

Appendix A

Glossary

ACI American concrete institute

ADC Active damping control

AI Artificial Intelligence

API American petroleum institute

APID Adaptive PID

AVC Active vibration control

AWWA American water works association

BE Boundary Element

CAS Coupled Acoustic-Structural

CEL Coupled Eulerian-Lagrangian

CFD Computational fluid dynamics

COC Clipped optimal control

CPSD Cross Power Spectral Density

DDC Data-driven control

DF Dominant frequency

DFPB Double friction pendulum bearing

DFT Discrete Fourier Transform

FBG Fiber Bragg grating

FD Finite difference

FE Finite Element

FFT Fast Fourier Transform

FOPID Fractional order proportional-integral-derivative

FOS Fiber optic sensor

FPS Friction pendulum system

FRF Frequency Response Function

HGS Hunger game search

HPF High pass filter

IFT Iterative feedback tuning

ILC Iterative learning control

LFSP Liquid fuel storage pool

LNG Liquefied natural gas

LPF Low pass filter

LQG Linear Quadratic Gaussian

LRB Lead Rubber Bearing

MC Monte Carlo

MFAC Model-free adaptive control

MOPSO Multi-objective particle swarm optimization

NSGA Non-dominated sorting genetic algorithm

NZSEE New Zealand National Society for Earthquake Engineering

PD Proportional-derivative

PDE Partial differential equation

PGA Peak Ground Acceleration

PI Proportional-integral

PID Proportional-Integral-Derivative

PIS Parallel inerter system

PNS Pseudo negative stiffness

PSD Power Spectral Density

PSO Particle swarm intelligence

RLS Recursive least squares

RSFD Resilience slip friction damper

SFPB Single friction pendulum bearing

SHM Structural Health Monitoring

SIS Series inerter system

SPH Smooth particle hydrodynamics

SSFI Soil-structure-fluid interaction

SSI Soil-structure interaction

STFT Short-time Fourier Transform

TFPB Triple friction pendulum bearing

VFPS Variable friction pendulum system

VMD Viscous mass damper

VOF Volume of fluid

VRF Virtual reference tuning

VRI Vertical-rocking isolation

Appendix B

Control procedures and digital filters

B.1 Digital filters

Low Pass Filter (LPF) transfer function over the RLS estimation parameters:

$$H_{LPF}(z) = \frac{0.0001}{z - 0.9999} \tag{B.1}$$

Recursive IIR digital High Pass Filter (HPF) over acceleration data to estimate dynamic displacement and velocity.

Filter method: butterworth

Filter order: 2

Normalised frequency: $f_n = 0.152$

$$f_n = \frac{f_{cut-off}}{f_{Nyquist}} \tag{B.2}$$

$f_{cut-off}$ and $f_{Nyquist}$ are the cut-off and Nyquist frequencies, respectively. The filter

transfer function for this HPF in z-domain is considered as follows,

$$H_{HPF}(z) = \frac{0.7125 - 1.425Z^{-1} + 0.7125Z^{-2}}{1 - 1.3406 + 0.5095Z^{-2}} \tag{B.3}$$

First-order filter over the voltage signal,

$$u(z) = \frac{0.6988}{z - 0.3012} \tag{B.4}$$

Low Pass Filter (LPF) over displacement measurements to estimate velocity:

Filter method: Recursive IIR digital filter

Filter order: 6

Passband edge frequency: 20 Hz

Maximum passband ripple: 0.1 dB

Minimum stopband attenuation: 80 dB

B.2 Control techniques, transfer functions, parameters

Model and model reference transfer functions:

$$H_1(z) = \frac{0.0003943z + 0.0003937}{z^2 - 1.988z + 0.9953} \tag{B.5}$$

$$H_2(z) = \frac{2.187e - 6z + 2.184e - 6}{z^2 - 1.988z + 0.9953} \tag{B.6}$$

$$H_3(z) = \frac{0.0002421z + 0.0002419}{z^2 - 1.997z + 0.9978} \tag{B.7}$$

$$H_4(z) = \frac{2.469e-5z+2.468e-5}{z^2-1.998z+0.9988} \tag{B.8}$$

$$H_5(z) = \frac{1.37e-7z+1.369e-7}{z^2-1.998z+0.9988} \tag{B.9}$$

$$H_6(z) = \frac{0.004234z+0.004221}{z^2-1.982z+0.9908} \tag{B.10}$$

PIDCLIP01: PID + Clipping algorithm,

$$Controller\ parameters: \begin{cases} K_P = 100 \\ K_I = 10 \\ K_D = 0.0 \\ N = 100 \end{cases} \tag{B.11}$$

PIDCLIP02: PID + Clipping algorithm,

$$Controller\ parameters: \begin{cases} K_P = 100 \\ K_I = 0.0 \\ K_D = 10 \\ N = 100 \end{cases} \tag{B.12}$$

PIDCLIP03: PID + Clipping algorithm,

$$Controller\ parameters: \begin{cases} K_P = 150 \\ K_I = 0.0 \\ K_D = 10 \\ N = 100 \end{cases} \tag{B.13}$$

PIDCLIP04: PID + Clipping algorithm:

$$Controller\ parameters: \begin{cases} K_P = 150 \\ K_I = 5 \\ K_D = 50 \\ N = 100 \end{cases} \tag{B.14}$$

PIDCLIP05: PID + Clipping algorithm,

Model transfer function: $H_1(z)$

$$Controller\ parameters: \begin{cases} K_P = 0.042862 \\ K_I = 1.3035 \\ K_D = 0 \\ N = 100 \end{cases} \tag{B.15}$$

PIDCLIP06: PID + Clipping algorithm,

Model transfer function: $H_2(z)$

$$Controller\ parameters: \begin{cases} K_P = 1.4169 \\ K_I = 141.6933 \\ K_D = 0 \\ N = 100 \end{cases} \tag{B.16}$$

PIDCLIP07: PID + Clipping algorithm,

$$Controller\ parameters: \begin{cases} K_P = 19.205 \\ K_I = 11.398 \\ K_D = 7.071 \\ N = 91.829 \end{cases} \tag{B.17}$$

PIDCLIP08: PID + Clipping algorithm,

Model transfer function: $H_3(z)$

$$Controller\ parameters: \begin{cases} K_P = 111.8761 \\ K_I = 107.7379 \\ K_D = 5.6681 \\ N = 388.3171 \end{cases} \tag{B.18}$$

PIDCLIP09: PID + Clipping algorithm,

Model transfer function: $H_4(z)$

$$Controller\ parameters: \begin{cases} K_P = 187.0527 \\ K_I = 421.0758 \\ K_D = 18.092 \\ N = 365.9331 \end{cases} \tag{B.19}$$

PIDCLIP10: PID + Clipping algorithm,

Model transfer function: $H_4(z)$

$$Controller\ parameters: \begin{cases} K_P = 731.9133 \\ K_I = 1161.545 \\ K_D = 55.7802 \\ N = 301.251 \end{cases} \tag{B.20}$$

PIDCLIP11: PID + Clipping algorithm,

Model transfer function: $H_5(z)$

$$Controller\ parameters: \begin{cases} K_P = 194778.884 \\ K_I = 574910.9104 \\ K_D = 11556.8737 \\ N = 389.8736 \end{cases} \tag{B.21}$$

PIDCLIP12: PID + Clipping algorithm,

$$Controller\ parameters: \begin{cases} K_P = 111.8761 \\ K_I = 11.18761 \\ K_D = 0.0 \\ N = 388.3171 \end{cases} \tag{B.22}$$

ODDAPIDC01: Online data-driven adaptive PID + Clipping algorithm,

Model reference transfer function: $H_1(z)$

LPF transfer function: $H_{LPF}(z)$

ODDAPIDC02: Online data-driven adaptive PID + Clipping algorithm,

Model reference transfer function: $H_2(z)$

LPF transfer function: $H_{LPF}(z)$

ODDAPIDC03: Online data-driven adaptive PID + Clipping algorithm,

Model reference transfer function: $H_3(z)$

LPF transfer function: $H_{LPF}(z)$

ODDAPIDC04: Online data-driven adaptive PID + Clipping algorithm,

Model reference transfer function: $H_6(z)$

LPF transfer function: $H_{LPF}(z)$

$$Controller\ parameters\ for\ model\ reference: \begin{cases} K_P = 0.002357 \\ K_I = 0.2357 \\ K_D = 0 \\ N = 100 \end{cases} \tag{B.23}$$

ODDAPIDC05: Online data-driven adaptive PID + Clipping algorithm,

Model reference transfer function: $H_5(z)$

LPF transfer function: $H_{LPF}(z)$

PIDMCLIP01: PID + Modified Clipping algorithm,

Model reference transfer function: $H_1(z)$

$$Controller\ parameters: \begin{cases} K_P = 0.042862 \\ K_I = 1.3035 \\ K_D = 0 \\ N = 100 \end{cases} \tag{B.24}$$

PIDMCLIP02: PID + Modified Clipping algorithm,

Model reference transfer function: $H_2(z)$

$$Controller\ parameters: \begin{cases} K_P = 1.4169 \\ K_I = 141.6933 \\ K_D = 0 \\ N = 100 \end{cases} \tag{B.25}$$

PIDMCLIP03: PID + Modified Clipping algorithm,

Model reference transfer function: $H_4(z)$

$$Controller\ parameters: \begin{cases} K_P = 731.9133 \\ K_I = 1161.545 \\ K_D = 55.7802 \\ N = 301.251 \end{cases} \tag{B.26}$$

PIDMCLIP04: PID + Modified Clipping algorithm,

Model transfer function: $H_4(z)$

$$Controller\ parameters: \begin{cases} K_P = 187.0527 \\ K_I = 421.0758 \\ K_D = 18.092 \\ N = 365.9331 \end{cases} \tag{B.27}$$

PIDMCLIP05 = PID + Modified Clipping algorithm:

Model transfer function: $H_5(z)$

$$Controller\ parameters: \begin{cases} K_P = 194778.884 \\ K_I = 574910.9104 \\ K_D = 11556.8737 \\ N = 389.8736 \end{cases} \tag{B.28}$$

ODDAPIDC06: Online data-driven adaptive PID + Clipping algorithm,

Model reference transfer function: $H_4(z)$

LPF transfer function: $H_{LPF}(z)$

$$Controller\ parameters\ for\ model\ reference: \begin{cases} K_P = 731.9133 \\ K_I = 1161.545 \\ K_D = 55.7802 \\ N = 301.251 \end{cases} \tag{B.29}$$

ODDAPIDC07: Online data-driven adaptive PID + Clipping algorithm,

Model reference transfer function: $H_4(z)$

LPF transfer function: $H_{LPF}(z)$

$$Controller\ parameters\ for\ model\ reference: \begin{cases} K_P = 187.0527 \\ K_I = 421.0758 \\ K_D = 18.092 \\ N = 365.9331 \end{cases} \tag{B.30}$$

ODDAPIDMC01: Online data-driven adaptive PID + Modified Clipping algorithm,

Model reference transfer function: $H_4(z)$

LPF transfer function: $H_{LPF}(z)$

$$Controller\ parameters\ for\ model\ reference: \begin{cases} K_P = 187.0527 \\ K_I = 421.0758 \\ K_D = 18.092 \\ N = 365.9331 \end{cases} \tag{B.31}$$

ODDAPIDMC02: Online data-driven adaptive PID + Modified Clipping algorithm,

Model reference transfer function: $H_4(z)$

LPF transfer function: $H_{LPF}(z)$

$$Controller\ parameters\ for\ model\ reference: \begin{cases} K_P = 731.9133 \\ K_I = 1161.545 \\ K_D = 55.7802 \\ N = 301.251 \end{cases} \quad \text{(B.32)}$$

ODDAPIDMC03: Online data-driven adaptive PID + Modified Clipping algorithm,

Model reference transfer function: $H_5(z)$

LPF transfer function: $H_{LPF}(z)$

ODDAPIDMC04: Online data-driven adaptive PID + Modified Clipping algorithm,

Model reference transfer function: $H_2(z)$

LPF transfer function: $H_{LPF}(z)$

ODDAPIDMC05: Online data-driven adaptive PID + Modified Clipping algorithm,

Model reference transfer function: $H_1(z)$

LPF transfer function: $H_{LPF}(z)$